

AN ORAL GHOST DELIVERY DEVICE FOR MACROMOLECULES

Angus Rolland Hibbins

A thesis submitted to the Faculty of Health Sciences, University of the Witwatersrand, in fulfilment of the requirements a Doctorate of Philosophy.



Supervisor:

Professor Viness Pillay, Department of Pharmacy and Pharmacology, University of the Witwatersrand, South Africa

Co-Supervisor:

Associate Professor Yahya Essop Choonara, Department of Pharmacy and Pharmacology, University of the Witwatersrand, South Africa

Co-Supervisor:

Dr. Lisa Clare du Toit, Department of Pharmacy and Pharmacology, University of the Witwatersrand, South Africa

Johannesburg, 2014

DECLARATION

I, Angus Rolland Hibbins declare that this thesis is my own work and has been submitted for the degree of Doctorate in Philosophy in the field of Pharmaceutics at the Faculty of Health Sciences, University of the Witwatersrand (Johannesburg, South Africa). It has not been submitted before for any degree or examination at this or any other University.

.....

Signature

.....

Date

PUBLICATIONS

Orally Administered Therapeutic Peptide Delivery: Enhanced Absorption Through the Small Intestine Using Permeation Enhancers (Review). Viness Pillay, Angus R. Hibbins, Yahya E. Choonara, Lisa C. du Toit, Pradeep Kumar, Valance M.K. Ndesendo. International Journal of Peptide Research and Therapeutics, Volume 18, Issue 3, Pages 259-280, April 2012.

Physicomechanical Characterisation and Optimization of EDTA-mPEG and Avicel®-EDTA-mPEG *In Situ* Melt Dispersion Mini-Pellets (Research). Angus R. Hibbins, Yahya E. Choonara, Lisa C. du Toit, Viness Pillay. AAPS PharmSciTech, Volume 14, Issue 3, Pages 935-949, September 2013.

pH Responsive Hydrogel Formulations for Oral Drug Delivery Applications: From Synthesis to Physicomechanical and Physicochemical Evaluation Within the Physiologically Representative *In Vitro* Environments and *Ex Vivo* Performance in Isolated Porcine Gastrointestinal Fluids (Research). Angus R. Hibbins, Yahya E. Choonara, Lisa C. du Toit, Viness Pillay. Prepared.

The Box-Behnken Design of Optimized Eudragit® Coated Insulin Loaded Trimethyl Chitosan mPEG-EDTA mini-pellet: From Synthesized Excipient Characterization to Performance Analysis Within Biorelevant Dissolution Media and Isolated Porcine Gastrointestinal Fluids (Research). Angus R. Hibbins, Yahya E. Choonara, Lisa C. du Toit, Pradeep Kumar, Viness Pillay. Prepared.

PODIUM PRESENTATIONS

A Novel Ghost Drug Delivery Device for the Injection Free Administration of Salmon Calcitonin. Angus R. Hibbins, Viness Pillay, Yahya E. Choonara, Lisa C. du Toit, Pradeep Kumar. School of Therapeutic Sciences Research Day, University of the Witwatersrand, August 2011.

POSTER PRESENTATIONS

Improving New Chemical Entity Predications in Rat and Canine *In Vitro* Models – Development of Biorelevant Media. Angus R. Hibbins, Giancarlo Francese, Frank H. Seiler. Next Generation Scientist Internship Program 2012, Basel, Switzerland, September 2012.

Improving New Chemical Entity Predications in Rat and Canine *In Vitro* Models: Comparison of Solubilities within Biorelevant Media. Angus R. Hibbins, Giancarlo Francese, Frank H. Seiler. Science Forum, Basel, Switzerland, October 2012 (Closed Industrial Conference).

PATENTS ARISING FROM THIS WORK

An Oral Ghost Delivery Device for the administration of macromolecules, patent reference
PTC:P63226PC00

INTERNSHIP

Next Generation Scientist Internship 2012

Program Director: Colin (Goonaseelan) Pillai, PhD

Leadership Mentor: Marcelo Gutierrez, PhD

Scientific Mentors: Giancarlo Francese, PhD

Frank H. Seiler, PhD

Time Period: 3 months

Scientific project: Developing dissolution media that is representative of the canine and rat model

“This 3-month internship forms part of a Novartis program to build the next generation of scientific leaders. Candidates in the program completed a drug discovery or clinical development research project under the mentorship of a Novartis scientist, and presented their research findings as a scientific poster during the Novartis Next Generation Scientist Research Day event. Their skills development training included ≥70 hours of: presentation and scientific event organisation. Each candidate was an active participant in structured, interactive learning sessions on Pharmaceutical Research and Development topics, including: Ethics, Social Responsibility, Intellectual Property, Drug Targets, Drug Regulation, Technical Drug Development, Safety, Modeling and Simulation and Clinical Trials”

Colin Pillai (PhD) – Pharma Development (Basel, Switzerland)

Brigitta Tadmor (PhD) – NIBR (Cambridge, USA)

23 August 2012

ABSTRACT

Recently, there has been an explosion of interest in developing biopharmaceutical therapeutics for the treatment of life altering conditions. The main issue with the utilization of biopharmaceutical therapeutics is the mode of administration. The Oral Ghost Drug Delivery (OGDD) device could potentially enable the administration of these peptide therapeutics via the oral route and significantly extend the application of these advanced therapeutic compounds.

The OGDD device is a drug delivery platform that can permits the oral administration of peptide therapeutics at a targeted location within the gastrointestinal tract. The OGDD is composed of four entities: the non-responsive shell component, peptide therapeutic loaded EDTA-mPEG trimethyl chitosan mini-pellet, Avicel®-EDTA-mPEG *in situ* hot melt dispersion mini-pellet, pH responsive acrylamide-methacrylic acid hydrogel trigger mechanism. The peptide therapeutic loaded EDTA-mPEG trimethyl chitosan was optimized with a Box-Behnken design with the peptide insulin. For ethical and moral reasons, salmon calcitonin was substituted for insulin during the *in vivo* assessment of the OGDD. The Avicel®-EDTA-mPEG *in situ* hot melt dispersion mini-pellet and the pH responsive acrylamide-methylacrylic acid hydrogel trigger mechanism was characterized with a textual analyzer with respect to swelling properties in biorelevant dissolution fluid, USP dissolution fluid and isolated gastrointestinal fluid. This analysis illustrates the impact of physiologically similar dissolution fluid will not only impact the release or solubilisation of drug compounds but also the physical behaviour of the drug containing matrix. In addition small molecular weight drug compounds from biopharmaceutical classification system (BCS) I, II and III. The release of these compounds from the hydrogel is not only impacted by the BSC class but also the physical response of the drug matrix to these environments. Differential scanning calorimetry was utilized for both the hydrogel and hot melt dispersion components of this device.

The oral administration of salmon calcitonin from the OGDD device was assessed in the porcine model. The *in vitro-in vivo* correlation for the oral administration of salmon calcitonin within different dissolution fluids and isolated porcine gastrointestinal fluids was conducted. The biorelevant dissolution fluid of the canine model generated a closer *in vivo-in vitro* correlation in comparison with USP and human biorelevant dissolution fluids. The utilization of the OGDD device as a platform for the oral administration of peptide therapeutics was achieved and the device is extremely customizable in a mathematically deterministic manner.

ACKNOWLEDEMENTS

Many individuals have contributed to the successful completion of this research and to them I thank sincerely:

To my parents, Mrs. J.R. Hibbins and Mr. A.W. Hibbins, I thank you for the support, care and love that if absent, the present research would not have been achieved.

To Mr. Pradeep Kumar, who assisted me greatly with some of the finer technical aspects of my research and patient understanding of issues which occurred during development.

To Ms. Oluwatoyin A. Kolawole and Mr. Pius Fasinu for their insight and assistance with general technical aspects of my research during the initial stages.

To my fellow students, Mr. Mpho Ngoepe, Mr. Felix Mashingaidze, Mr. Pierre Kondiah, Ms. Teboho Kgesa, Ms. Martina Manikana, Mr. Maluta Mufamadi, Ms. Ameena Wadee, Mr. Miles Braithwaite, Ms. Raeesa Moosa, Mr. Mershen Govender, Ms. Nonhlanhla Masina, and Dr. Lomus Kumar Tomar, thank you for your assistance during my studies.

To Prof. Yahya E. Choonara and Ms. Lisa C. du Toit, thank you for your time, effort and assistance throughout my research.

To the Central Animal Service staff at the University of Witwatersrand, Ms. Kershnee Chetty, Ms. Lorraine Setimo, Ms. Amelia Ramakawwa, Ms. Mary-Anne Costello, Mr. Patrick Selahle and Dr. Leith Meyer, my thanks for your assistance with my animal studies.

To my supervisor, Prof. Viness Pillay, for your vision, passion and understanding which shaped and enhanced this research throughout my studies.

To the National Research Foundation (NRF), the Witwatersrand Financial Aid office and the Department of Education (DEO) for the funding that enabled this research to be completed.

DEDICATION

I dedicate this work to my parents, Ms. J.R. Hibbins and Mr. A.W. Hibbins, as they are the sunlight which focuses my efforts.

ANIMAL ETHICS DECLARATION

I, Angus Rolland Hibbins hereby confirm that the study entitled “An Oral Ghost Delivery Device for Macromolecules” received approval from the Animal Ethics Committee of the University of Witwatersrand with Ethics Clearance Number 2011/33/03 (Appendix 1).

TABLE OF CONTENTS

	Page
CHAPTER 1	
An Oral Ghost Delivery Device for Macromolecules	
1.1. Introduction	1
1.2. Currently describe strategies for oral delivery of macromolecular therapeutics	2
1.3. Rationale and motivation for this study	4
1.4. The Oral Ghost Delivery Device	5
1.5. Aim and Objectives of this study	8
1.6. Overview of the thesis	9
CHAPTER 2	
Orally Administered Therapeutic Peptide Delivery: Enhanced Absorption Through Small Intestine Using Permeation Enhancers	
2.1. Introduction	11
2.1.1. Macromolecular therapeutics	11
2.1.2. Parenteral administration of peptide therapeutics	14
2.1.3. Potential problems associated with the administration of peptide therapeutics via the oral route and potential solutions	17
2.2. The biochemical, anatomical and physiological makeup of the small intestine	17
2.2.1. The importance of intestinal mucus in the design of an oral peptide therapeutic drug delivery system	20
2.2.2. Tight junctions: a barrier as well as a target	23
2.2.3. Main components of tight junctions	25
2.2.4. Structure and components of tight junctions	27
2.3. Permeation enhancers employed in the small intestine	28
2.3.1. Ethylenediamine-<i>N.N.N'</i>-tetraacetic acid	29
2.3.2. Sodium carprate	29
2.3.3. Bile salts	30
2.3.4. Occuldin peptides	30
2.3.5. Clostridium perfringens enterotoxin	31
2.3.6. Zonula occludens toxin	32
2.4. Chitosan and its derivatives as permeation enhancers	32

2.4.1.	The rationale for consideration of chitosan and its derivatives for orally administered drug delivery systems	33
2.4.2.	The chemistry of chitosan and its derivatives	34
2.4.3	Trimethyl chitosan	34
2.4.4.	Food and Drug Administration approval of chitosan and chitosan derivatives	40
2.5.	Concluding remarks	41

CHAPTER 3

Physicomechanical Characterization and Optimization of EDTA-mPEG and Avicel®-EDTA-mPEG *In Situ* Hot Melt Dispersion Mini-pellets

3.1.	Introduction	42
3.2.	Materials and Methods	43
3.3.	Materials	43
3.4.	Methods	43
3.4.1.	Synthesis of EDTA-mPEG <i>in situ</i> hot melt dispersion powder formulations	43
3.4.2.	Attenuated Total Reflectance-Fourier Transform Infrared Quantification of EDTA and Avicel®	44
3.4.3.	Determination of EDTA loading using physical separation within deionized water	45
3.4.4.	Polydispersal index analysis of EDTA <i>in situ</i> hot melt dispersion	46
3.4.5.	Differential Scanning Calorimetry of EDTA-mPEG <i>in situ</i> hot melt dispersion/Avicel®-EDTA-mPEG formulations	46
3.4.6.	Mini-pellet manufacture of EDTA-mPEG <i>in situ</i> hot melt dispersion powder formulation and Avicel®-EDTA-mPEG powder formulations	47
3.4.7.	Physicomechanical properties of EDTA-mPEG <i>in situ</i> hot melt dispersion mini-pellet formulations and Avicel®-EDTA-mPEG <i>in situ</i> hot melt dispersion mini-pellet formulations	48
3.4.8.	Scanning Electron Microscopy imaging of EDTA-mPEG <i>in situ</i> hot melt dispersion mini-pellet formulations and Avicel®-EDTA-mPEG <i>in situ</i> hot melt dispersion mini-pellet formulations	48
3.4.9.	Statistical regression analysis of obtained data measurements	49
3.5.	Results and Discussion	50
3.5.1.	Determination of entrapped EDTA from EDTA-mPEG <i>in situ</i> hot melt dispersion powder formulations	50

3.5.3.	Differential Scanning Calorimetry of EDTA-mPEG <i>in situ</i> hot melt dispersion/Avicel®-EDTA-mPEG formulations	52
3.5.4.	Physicochemical properties of EDTA-mPEG <i>in situ</i> hot melt dispersion/Avicel®-EDTA-mPEG <i>in situ</i> hot melt dispersion mini-pellets	55
3.5.4.1.	Matrix Hardness, Matrix resilience and deformation energies studies	55
3.5.4.2.	Disintegration of EDTA-mPEG <i>in situ</i> hot melt dispersion mini-pellet and Avicel®-EDTA-mPEG <i>in situ</i> hot melt dispersion mini-pellets	58
3.5.5.	Scanning Electron Microscopy Imaging of EDTA-mPEG <i>in situ</i> hot melt dispersion and Avicel®-EDTA-mPEG <i>in situ</i> hot melt dispersion mini-pellet formulations	61
3.5.6.	The customization of EDTA-mPEG <i>in situ</i> hot melt dispersion mini-pellet formulations and Avicel®-EDTA-mPEG <i>in situ</i> hot melt dispersion mini-pellet formulations	62
3.6.	Concluding remarks	64

CHAPTER 4

pH Responsive Hydrogel Formulations For The Oral Ghost Drug Delivery Device: From Synthesis To Physicomechanical And Physicochemical Evaluation Within The Physiologically Representative *In Vitro* Environments And *Ex Vivo* Performance In Isolated Porcine Gastrointestinal Fluids

4.1.	Introduction	65
4.2.	Materials and Methods	66
4.3.	Materials	74
4.4.	Methods	66
4.4.1.	Synthesis of the pH responsive hydrogel to be implemented in the oral ghost drug delivery device	66
4.4.2.	Chemical structure analysis of the crosslinked AAm-MAA hydrogel formulations	68
4.4.3.	Thermal characterization of crosslinked AAm-MAA hydrogel formulations	68
4.4.4.	Viscosity analysis of the polymerizing crosslinked AAm-MAA formulation hydrogels	68
4.4.5.	Determination of the gel fraction of the crosslinked AAm-MAA hydrogel formulations	69
4.4.6.	Powdered X-ray Diffraction to determine the crystallinity of the hydrogel	70

	formulations	
4.4.7.	Isolation of porcine small intestinal tissue and gastrointestinal fluids	70
4.4.8.	USP 35 and biorelevant dissolution media utilized for the gravimetric swelling analysis and distance-time analysis	70
4.4.9.	Gravimetric swelling analysis of the crosslinked AAm-MAA hydrogel in United States Pharmacopeia simulated gastrointestinal fluids and biorelevant fluids	71
4.4.10.	Distance-time studies of the crosslinked AAm-MAA formulation hydrogels	71
4.4.11.	The porositometric characteristics of crosslinked AAm-MAA hydrogel formulation 6	73
4.4.12.	UPLC analysis of the drug compounds utilized in this within the pH responsive hydrogel	75
4.4.13.	Loading drug within crosslinked AAm-MAA hydrogel F6	75
4.4.14.	Determination of drug entrapment efficiency	76
4.4.15.	Dissolution studies from crosslinked AAm-MAA hydrogel formulation 6 within dissolution fluids and isolated porcine gastrointestinal fluids	76
4.4.16.	Drug release mechanism	77
4.4.17.	Morphological analysis images of crosslinked AAm-MAA formulation hydrogel 6	77
4.4.18.	Magnetic Resonance Imaging of crosslinked AAm-MAA formulation hydrogel 6	78
4.5.	Results and Discussion	78
4.5.1.	Synthesis of hydrogel	78
4.5.2.	Viscosity analysis of the polymerizing crosslinked AAm-MAA formulation hydrogels	79
4.5.3.	Determination of the gel fraction percent of the crosslinked AAm-MAA hydrogel formulations	82
4.5.4.	Attenuated Total-Reflectance-Fourier Transform Infrared analysis of crosslinked AAm-MAA formulation hydrogels	84
4.5.5.	The powder X-ray diffraction of the hydrogel formulations and the percentage of crystallinity	85
4.5.6.	Thermal analysis of crosslinked AAm-MAA hydrogel formulation	86
4.5.7.	Gravimetric swelling analysis of the crosslinked AAm-MAA hydrogel formulation 2, 6 and 8	86
4.5.8.	Distance-time studies of the crosslinked AAm-MAA formulation	89

	hydrogels	
4.5.9.	The porositometric characteristics of crosslinked AAm-MAA formulation hydrogel 6	92
4.5.10.	UPLC detection of drug compounds	98
4.5.11.	Determination of drug entrapment efficiency within pH responsive hydrogel F6	100
4.5.12.	Dissolution analysis of crosslinked AAm-MAA hydrogel F6	100
4.5.14.	Magnetic Resonance Imaging of crosslinked AAm-MAA formulation hydrogel 6	105
4.6.	Concluding remarks	107

CHAPTER 5

The Box-Behnken Design of Optimized Eudragit® Coated Insulin Loaded Trimethyl Chitosan mPEG-EDTA Mini-pellet

5.1.	Introduction	108
5.2.	Materials and Methods	109
5.3.	Materials	109
5.4.	Methods	110
5.4.1.	Synthesis of mini-pellet components	110
5.4.1.1.	Preparation and characterization of trimethyl chitosan chloride	110
5.4.1.2.	Preparation of EDTA-mPEG <i>in situ</i> hot melt dispersion powder (a component of the trimethyl chitosan mini-pellet formulation)	110
5.4.2.	Characterisation of trimethyl chitosan and chitosan	111
5.4.2.1.	Attenuated Total Reflectance-Fourier Transform Infrared analysis	111
5.4.2.2.	Thermal Gravimetric Analysis of trimethyl chitosan and chitosan for the temperature at which maximal degradation occurs	112
5.4.2.3.	Differential Scanning Calorimetry analysis to determine the unique heat capacities of trimethyl chitosan and chitosan	112
5.4.2.4.	Powdered X-ray Diffraction for the determination of crystallinity in trimethyl chitosan and amorphism in chitosan	112
5.4.2.5.	Morphological analysis of trimethyl chitosan and chitosan	112
5.4.3.	Isolation of porcine small intestinal tissue and gastrointestinal fluids	113
5.4.4.	USP 35 and biorelevant dissolution fluid utilized for rheological, dissolution and disintegration experimentation	113
5.4.5.	Viscosity analysis of the trimethyl chitosan chloride within dissolution media and isolated gastrointestinal fluids of the porcine model	114

5.4.6.	Box-Behnken Design of insulin loaded trimethyl chitosan chloride mini-pellet formulations	114
5.4.7.	Preparation of insulin loaded trimethyl chitosan chloride mini-pellet formulations	115
5.4.7.1.	High Performance Liquid Chromatography of insulin	115
5.4.7.2.	Insulin incorporation and entrapment studies of insulin within trimethyl chitosan chloride powder	116
5.4.7.3.	Direct compression of mini-pellets formulations	117
5.4.8.	Textual analysis of insulin loaded trimethyl chitosan chloride mini-pellet formulations	117
5.4.8.1.	Physicomechanical analysis	117
5.4.8.2.	<i>Ex vivo</i> mucoadhesive analysis	118
5.4.9.	Dissolution studies and dissolution fitting analysis of mini-pellet formulations	119
5.4.10.	<i>In vitro</i> and <i>ex vivo</i> characterization of the optimized Eudragit® insulin loaded mini-pellet formulation within biorelevant dissolution fluid and isolated porcine gastrointestinal fluids	120
5.4.10.1.	Physicomechanical characterization of the optimized insulin loaded trimethyl mini-pellet formulation	120
5.4.10.2.	Disintegration analysis	120
5.4.10.3.	Dissolution of optimized Eudragit® coated insulin loaded trimethyl chitosan mini-pellet formulation	121
5.4.11.	Statistical regression analysis of obtained data measurements	121
5.5.	Results and Discussion	121
5.5.1.	Characterization of trimethyl chitosan chloride and chitosan	122
5.5.1.1.	Attenuated Total Reflectance-Fourier Transform infrared analysis	122
5.5.1.2.	Thermal gravimetric analysis of trimethyl chitosan chloride and chitosan	124
5.5.1.3.	Dynamic Scanning Calorimetry analysis	126
5.5.1.4.	Scanning Electron Microscopy images of trimethyl chitosan and chitosan	129
5.5.1.5.	Powdered X-ray Diffraction analysis of trimethyl chitosan chloride and chitosan	129
5.5.2.	Viscosity analysis of fluids and mini-pellet components	131
5.5.3.	Box-Behnken Design of insulin loaded trimethyl chitosan chloride mini-pellet formulations	132

5.5.4.	Physicomechanical and <i>ex vivo</i> mucoadhesive analysis of insulin loaded trimethyl chitosan chloride mini-pellet formulations	135
5.5.5.	Insulin entrapment studies, dissolution studies and dissolution fitting analysis of optimized Eudragit® coated insulin loaded trimethyl chitosan chloride mini-pellet formulation	138
5.5.6.	The statistical analysis of the experimental results obtained from the Box-Behnken design formulations	139
5.5.7.	<i>In vitro</i> and <i>ex vivo</i> characterisation of the optimized Eudragit® insulin loaded mini-pellet formulation within biorelevant dissolution fluid and isolated porcine gastrointestinal fluids	140
5.5.7.1.	Physicomechanical characterisation of the optimized insulin loaded trimethyl chitosan chloride mini-pellet formulation	140
5.5.7.2.	Disintegration analysis of the optimized Eudragit® coated insulin loaded trimethyl chitosan mini-pellet formulation	142
5.5.7.3.	Dissolution of the optimized Eudragit® coated insulin loaded trimethyl chitosan chloride mini-pellet formulation	144
5.6	Concluding remarks	145

CHAPTER 6

***In Vitro-In Vivo* Correlation of the Optimised Oral Ghost Drug Delivery Device in the Porcine Model**

6.1.	Introduction	147
6.2.	Materials and Methods	148
6.3.	Materials	158
6.4.	Methods	149
6.4.1.	Preparation of the optimised Oral Ghost Delivery Device	149
6.4.2.	Manufacture of non-responsive non-degradable shell component	149
6.4.3.	Synthesis of the stimuli responsive hydrogel as the trigger mechanism of the Oral Ghost Delivery Device	150
6.4.4.	Manufacture of erodible methyl cellulose disc	151
6.4.5.	Manufacture of Avicel®-EDTA-mPEG <i>in situ</i> hot melt dispersion mini-pellet	151
6.4.6.	Synthesis of trimethyl chitosan	152
6.4.7.	Manufacture of salmon calcitonin loaded trimethyl chitosan mini-pellet	153
6.4.8.	Assembly of the Oral Ghost Drug Delivery device and spray Eudragit® coating	153

4.4.9.	Isolation of porcine gastrointestinal fluids	155
6.4.10.	Dissolution of salmon calcitonin form the Oral Ghost Drug Delivery device	155
6.4.11.	Standard market product for 100% bioavailability comparison	156
6.4.12.	<i>In vivo</i> studies in the pig model utilising the optimised Oral Ghost Drug Delivery device	156
6.4.12.1.	Animal studies design for the <i>in vivo</i> assessment of the salmon calcitonin bioavailability from the Oral Ghost Delivery Device in comparison to the marketed product Macalcin [®]	156
6.4.12.2.	Development of a blood sampling protocol through the insertion of a resident catheter for the accurate analysis of plasma samples	157
6.4.12.3.	Dosing procedure for the Oral Ghost Drug Delivery device and Intramuscular Administration of Salmon Calcitonin	158
6.4.12.4.	Blood Withdrawal Protocol	158
6.4.13.	Procedure of utilizing the enzyme immunoassay kit for the determination of salmon	159
6.4.14.	Pharmacokinetic analysis of <i>in vivo</i> drug concentration profiles	160
6.4.15.	<i>In vitro-In Vivo</i> Correlation	160
6.4.15.1.	The <i>in vitro</i> dissolution of salmon calcitonin within USP and biorelevant dissolution fluids	161
6.4.15.2.	<i>In vivo</i> administration of salmon calcitonin	161
6.4.15.3.	Deconvolution of the Unit Impulse Response	161
6.4.15.4.	Correlation of predicted salmon calcitonin release observations and fitted release model profiles	164
6.4.15.5.	Correlation validation	164
6.5.	Results and Discussion	164
6.5.1.	The insertion of a chronic catheter for chronic withdrawal of blood samples	164
6.5.2.	Isolation of the porcine gastrointestinal fluids in the fasted state	165
6.5.3.	Dissolution of the salmon calcitonin loaded Oral Ghost Drug Delivery device	167
6.5.4.	Pharmacokinetic analysis of <i>in vivo</i> drug concentration profiles	169
6.5.4.1.	Noncompartmental analysis	172
6.5.4.2.	Compartmental analysis	175
6.5.5.	Unit Impulse Response	178
6.5.6.	<i>In vitro-in vivo</i> correlation	178

6.5.7.	<i>In vitro-in vivo</i> correlation validation	181
6.6.	Concluding remarks	186

CHAPTER 7

Conclusions and Recommendations

7.1.	Conclusions	187
7.2.	Recommendations	188
7.3.	Future Outlook	190

REFERENCES	191
-------------------	-----

APPENDICES

Appendix 1	217
Appendix 2	218
Appendix 3	222
Appendix 4	225
Appendix 5	227
Appendix 6	229
Appendix 7	237
Appendix 8	242
Appendix 9	245
Appendix 10	254

LIST OF FIGURES

	Page
CHAPTER 1	
Figure 1.1	Schematic of the Oral Ghost Delivery Device (OGDD) 7
Figure 1.2	The assembly of the Oral Ghost Delivery Device with size dimensions 8
CHAPTER 2	
Figure 2.1	Graphical illustration theoretical profile of ideal location within the gastrointestinal tract to target peptide therapeutic delivery 21
Figure 2.2	Three dimensional representations of two cysteine amino acids. 23
Figure 2.3	A schematic representation of some anatomical and biochemical elements that form the small intestinal epidermis layer depicting the five transport mechanisms that are currently known to occur in the small intestine 27
Figure 2.4	Localisation of occludin peptides in confluent T84 cell monolayers 31
Figure 2.5	Three dimensional representation of chitosan which gives an indication of the optimised ring structure of each chitosan unit. 34
Figure 2.6	Three dimensional representation of trimethyl chitosan with functional groups highlighted in red rings. 35
Figure 2.7	Schematic chemical process diagram of trimethyl chitosan using sodium hydroxide. 37
CHAPTER 3	
Figure 3.1	ATR-FTIR spectra of different standard EDTA concentrations 50
Figure 3.2	Scatter plot of ethylenediaminetetraacetic concentration, Avicel [®] RC/CL type R-591 concentration and EDTA weight recovery 52
Figure 3.3	Differential Scanning Calorimetry of Formulation 1 (EDTA-mPEG (10:90) <i>in situ</i> hot melt dispersion powder and Formulation 5 (Avicel [®] -EDTA-mPEG (33:6.7:60.3) <i>in situ</i> hot melt dispersion powder. 54
Figure 3.4	Differential Scanning Calorimetry of Formulation 6 (EDTA-mPEG (50:50)) <i>in situ</i> hot melt dispersion powder and Formulation 10 (Avicel [®] -EDTA-mPEG (33:33.5:33.5)) <i>in situ</i> hot melt dispersion powder. 55

Figure 3.5	The scatter plot of matrix, deformation and matrix resilience for formulations 1 to 5.	56
Figure 3.6	The scatter plot of matrix, deformation and matrix resilience for formulations 6 to 10.	57
Figure 3.7	The scatter plot of total disintegration time, primary disintegration rate, secondary disintegration rate and pellet thickness for formulations 1 to 5.	59
Figure 3.8	The scatter plot of total disintegration time, primary disintegration rate, secondary disintegration rate and pellet thickness for formulations 6 to 10.	60
Figure 3.9	Scanning Electron images of the EDTA-mPEG <i>in situ</i> hot melt dispersion mini-pellet formulations and Avicel®-EDTA-mPEG <i>in situ</i> hot melt dispersion mini-pellet formulations	63

CHAPTER 4

Figure 4.1	The viscosity analysis of AAm-MAA hydrogel formulation for formulation 2 to 6	80
Figure 4.2	The viscosity analysis of AAm-MAA hydrogel formulation for formulation 7 to 11	81
Figure 4.3	Bar graph representing the gel fraction percent for each of the AAm-MAA hydrogel formulations.	83
Figure 4.4	The ATR-FTIR spectra represent crosslinked AAm-MAA hydrogel formulation 1 to 11	84
Figure 4.5	The PXRD profile of formulation 6 and a bar graph of the percentage of crystallinity for each hydrogel formulation.	85
Figure 4.6	Differential Scanning Calorimetry of crosslinked AAm-MAA hydrogel formulations	87
Figure 4.7	The gravimetric swelling profile of AAm-MAA hydrogel formulation 6 and the area under curve for the gravimetric swelling profiles for AAm-MAA hydrogel formulation 2, 6 and 8.	89
Figure 4.8	The swelling velocity of AAm-MAA hydrogel formulation 2, 6 and 8 within biorelevant media and USP simulated fluids and within isolated porcine fluids with respect to sequential time points.	91
Figure 4.9	The porositometric surface area analysis with respect to time of AAm-MAA hydrogel formulation 6 within United States Pharmacopeia simulated gastric fluid United States	93

	Pharmacopeia simulated intestinal fluid and Millipore® water.	
Figure 4.10	The porositometric pore volume and pore diameter analysis with respect to time of AAm-MAA hydrogel formulation 6	94
Figure 4.11	Scanning Electron Microscopy images of AAm-MAA hydrogel	97
Figure 4.12	Ultra Performance Liquid Chromatography chromatograms of theophylline, caffeine, ciprofloxacin, indomethacin, metronidazole, sulfamethoxazole and sulpiride, zidovudine, 4-aminosalicylic acid and naprozen.	99
Figure 4.13	The <i>in vitro</i> dissolution of theophylline within United States Pharmacopeia simulated gastric fluid, United States Pharmacopeia simulated intestinal fluid, Fasted State Simulated Gastric Fluid pH 1.6 and Fasted State Simulated Intestinal Fluid Version 2 pH 6.5.	101
Figure 4.14	Fed State Simulated Intestinal Fluid pH 5.0 and Fasted State Simulated Gastric Fluid canine pH 1.5, Fasted State Simulated Gastric Fluid canine pH 6.5 and Fasted Stated Simulated Intestinal Fluid canine pH 7.5.	102
Figure 4.15	The <i>ex vivo</i> dissolution of theophylline and ciprofloxacin within isolated fasted gastric fluids and isolated fasted intestinal fluids of the porcine model.	103
Figure 4.16	Magnetic Resonance Imaging of AAm-MAA hydrogel formulation 6.	106

CHAPTER 5

Figure 5.1	Schematic representation of the steps utilized for the synthesis of trimethyl chitosan chloride from chitosan.	111
Figure 5.2	ATR-FTIR spectra of trimethyl chitosan chloride, insulin-loaded trimethyl chitosan chloride powder and medium molecular weight chitosan.	123
Figure 5.3:	Thermogravitational Analysis profiles of trimethyl chitosan chloride and chitosan.	124
Figure 5.4	Dynamic Scanning Calorimetry of trimethyl chitosan chloride and chitosan.	127
Figure 5.5	Scanning Electron Microscopy images of trimethyl chitosan chloride and chitosan.	129
Figure 5.6	Powdered X-ray Diffraction profiles of trimethyl chitosan chloride	130

	and medium molecular weight chitosan (77% deacetylation).	
Figure 5.7	The viscosity analysis of biorelevant media and isolated gastrointestinal fluids of the porcine model (fasted state). Trimethyl chitosan (0.1% w/v) was dissolved in the respective solvents.	132
Figure 5.8	Residual Plots of Fractional Release after 8 hours, Mean Dissolution Time after 2.5 hours and Matrix Hardness determined from the Box-Behnken design of insulin-TMC:Cl mini-pellets.	135
Figure 5.9	Three dimensional scatter plots of the matrix hardness against dissolution analysis and mucoadhesive analysis, respectively, for the Box-Behnken mini-pellet formulations (F1-F15) and chitosan mini-pellet formulation (Chit). Mucin-coated porcine intestinal epithelium samples and non-mucin-coated porcine intestinal epithelium samples were utilized to determine mucoadhesive properties of the mini-pellet formulations.	136
Figure 5.10	Release profile of insulin for Formulation 1 of insulin-loaded trimethyl chitosan chloride mini-pellet which conforms to a Makoid-Banakar with Tlag regression fitted scatter plot. The High Performance Liquid Chromatography analysis of the market available Intramuscular insulin formulation and insulin released from trimethyl chitosan formulation 1.	138
Figure 5.11	Three dimensional surface plots of the insulin-loaded trimethyl chitosan chloride mini-pellet components.	139
Figure 5.12	Optimized insulin-loaded trimethyl chitosan chloride mini-pellet formulation output from Box-Behnken Design.	140
Figure 5.13	A graphical representation of the three responses (mean dissolution time after 2.5 hours [1.3959 hours], fractional release after 8 hours [94.06%] and matrix hardness [94.22 N/mm]) for the optimized insulin-loaded trimethyl chitosan chloride mini-pellet formulation.	141
Figure 5.14	The textual analysis force distance profile of 3% w/v mucin coated porcine small intestine epithelium tissue, none mucin coated porcine small intestine epithelium tissue and matrix hardness of the optimized insulin loaded Box-Behnken mini-pellet formulation.	142
Figure 5.15	Three dimensional bar graph of the disintegration profile of the optimized Eudragit® coated insulin loaded trimethyl chitosan mini-	143

pellet.

Figure 5.16	The dissolution profiles of Eudragit® coated insulin loaded trimethyl chitosan mini-pellets.	145
--------------------	--	-----

CHAPTER 6

Figure 6.1	Schematic representation of the non-responsive non-degradable shell component of the Oral Ghost Drug Delivery device manufacture process.	150
Figure 6.2	A schematic representation of the Oral Ghost Drug Delivery device assembly.	154
Figure 6.3	Animal study design which contains three groups.	157
Figure 6.4	Photographs of the surgical preparative measures utilised for the pigs in this study.	165
Figure 6.5	Photographs of the insertion of the intrajugular catheter surgery utilised for the pigs in this study.	166
Figure 6.6	Isolation of the gastrointestinal fluid from the porcine model and the filtered porcine gastrointestinal fluid.	167
Figure 6.7	The <i>in vitro</i> dissolution modeling of salmon calcitonin from the Oral Ghost Drug Delivery device within biorelevant dissolution fluid FaSSGF-FeSSIF V2 set and isolated porcine gastric-isolated intestinal set.	168
Figure 6.8	The <i>in vivo</i> plasma salmon calcitonin concentration-time profile for the intramuscular administration of salmon calcitonin and the orally administered salmon calcitonin-time profile for the Oral Ghost Drug Delivery device.	170
Figure 6.9	The AUC and AUMC derived from <i>in vivo</i> plasma salmon calcitonin concentration-time profile for the intramuscular administration of salmon calcitonin.	172
Figure 6.10	The one compartment IV-bolus, no lag time, 1 st order elimination of intramuscular administration of salmon calcitonin.	176
Figure 6.11	The one compartment 1 st order, initial lag time, 1 st order elimination of oral administration of salmon calcitonin in the Oral Ghost Drug Delivery device.	176
Figure 6.12	The generation of a Unit Impulse Response (UIR).	179
Figure 6.13	The <i>in vitro-in vivo</i> correlation generated from the dissolution of salmon calcitonin from the Oral Ghost Drug Delivery device within	180

isolated porcine gastrointestinal fluids (fasted state).

Figure 6.14 The *in vitro-in vivo* correlation generated from the dissolution of salmon calcitonin from the Oral Ghost Drug Delivery device within FaSSGF-FeSSIF V2 dissolution set. 181

Figure 6.15 The *in vitro-in vivo* correlation validation generated from the dissolution of salmon calcitonin from the Oral Ghost Drug Delivery device within isolated porcine gastrointestinal fluids (fasted state). 183

Figure 6.16 The *in vitro-in vivo* correlation validation generated from the dissolution of salmon calcitonin from the Oral Ghost Drug Delivery device within the FaSSGF-FeSSIF V2 set. 184

LIST OF TABLES

	Page
CHAPTER 1	
Table 1.1	Summary of drug delivery systems for the oral administration of insulin 3
CHAPTER 2	
Table 2.1	Advantages and disadvantages of peptide therapeutics over recombinant proteins, small drug molecules and antibodies 13
Table 2.2	Permeation enhancers that have been tested in the small intestine to facilitate therapeutic absorption 29
CHAPTER 3	
Table 3.1	Component concentrations (in percent w/w) comprising each formulation 44
Table 3.2	Textural profiling parameters employed for physicochemical characterization of EDTA-mPEG <i>in situ</i> hot melt dispersion mini-pellet formulations and Avicel®-EDTA-mPEG <i>in situ</i> hot melt dispersion mini-pellet formulations 47
Table 3.3	Textual parameters settings employed for disintegration characterization of EDTA-mPEG <i>in situ</i> hot melt dispersion mini-pellet formulations and Avicel®-EDTA-mPEG <i>in situ</i> hot melt dispersion mini-pellet formulations 49
Table 3.4	The calculated total disintegration time, primary rate of disintegration, secondary rate of disintegration and pellet thickness of formulation 1 pellets, formulation 5 pellets, formulation 6 pellets and formulation 10 pellets at the optimal harness weight of each pellet formulation. The optimal pellet weight, optimal pellet hardness, and EDTA weight within formulation 1, 5, 6 and 10 64
CHAPTER 4	
Table 4.1	The composition of the crosslinked acrylamide-methacrylic acid hydrogel formulations 67
Table 4.2	Rheological parameters utilized for the analysis of gelation 69

initiation within the crosslinked acrylamide-methacrylic acid hydrogel formulations

Table 4.3	Parameters utilized to obtain the swelling distance-time profiles for crosslinked acrylamide-methacrylic acid hydrogel formulations	72
Table 4.4	Parameters utilized for the porositometric analysis of crosslinked acrylamide-methacrylic acid hydrogel formulations	74

CHAPTER 5

Table 5.1	Rheological parameters utilized for the analysis of trimethyl chitosan chloride within dissolution media and isolated gastrointestinal fluids of the porcine model	114
Table 5.2	The 3-factor, 3-level Box-Behnken Design variables utilizing MINITAB V15 software	115
Table 5.3	Textual profiling parameters settings employed for physicochemical, mucoadhesive and disintegration characterisation of the mini-pellet formulations	118
Table 5.4	ATR-FTIR of trimethyl chitosan chloride, insulin-loaded trimethyl chitosan chloride powder and medium molecular weight chitosan	123
Table 5.5	Thermogravimetric analysis of trimethyl chitosan chloride and chitosan	125
Table 5.6	Dynamic Scanning Calorimetry (DSC) analysis of trimethyl chitosan chloride and chitosan at heating rate 10°C/min, 5°C/min and 2°C/min	128
Table 5.7	The formulation of the mini-pellets were completed according to a Box-Behnken design	134

CHAPTER 6

Table 6.1	The concentrations of sequentially added chemical components whilst constantly stirring, in order to form the AAm-MAA stimuli responsive hydrogel	151
Table 6.2	The noncompartmental pharmacokinetic parameters determined from the intramuscular (I.M.) administration of salmon calcitonin and the oral administration of salmon calcitonin from the Oral Ghost Drug Delivery device	174
Table 6.3	The statistical analysis of the compartmental pharmacokinetic parameters determined from the intramuscular (I.M.)	177

administration of salmon calcitonin and the oral administration of salmon calcitonin from the Oral Ghost Drug Delivery device for each pig utilized

Table 6.4	The compartmental pharmacokinetic parameters determined from the intramuscular (I.M.) administration of salmon calcitonin and the oral administration of salmon calcitonin from the Oral Ghost Drug Delivery device	178
------------------	---	-----

Table 6.5	The noncompartmental pharmacokinetic parameters determined from the <i>in vitro-in vivo</i> correlation generated from the dissolution analysis of salmon calcitonin from the Oral Ghost Drug Delivery device in isolated porcine gastrointestinal fluids (fasted state) and the FaSSGF-FeSSIF V2 dissolution set.	185
------------------	--	-----

LIST OF ABBREVIATIONS

Å	Angstrom units
°C	Degree Centigrade
%	Percent
\$	United States Dollar
µm	Micrometer
AAm	Acrylamide
ACE	Angiotension Converting Enzyme
ACTH	Adrenocorticotrophic Hormone
ADS	Ac-Di-Sol®
AbsScale-time	Absorbance scale-time
AESC	Animal Screening Committee
API	Active Pharmaceutical Ingredient
aPKC	atypical Protein Kinase C
APS	Ammonium Persulfate
AUC	Area Under Curve
AUMC	Area Under Moment Curve
ATR	Attenuated Total Reflectance
ATR-FTIR	Attenuated Total Reflectance-Fourier Transform Infrared
BET	Brunauer, Emmett, and Teller method
BIS	<i>N-N'</i> -Methylenebisacrylamide
BJH	Barrett-Joyner-Halenda method
BS	Sodium Deoxycholate
CAMs	Cell Adhesion Protein Molecules
C-CPE	C terminal of <i>Clostridium perfringens</i> Enterotoxin
cm	Centimeter
Cmax	Maximum concentration
CPE	<i>Clostridium perfringens</i> Enterotoxin
DDS	Drug Delivery System
DE	Deformation Energy
DEH	Dynamic Equilibrating Hydrogel
DSC	Differential Scanning Calorimetry
DTG	Differential Thermal Analysis
<i>E.coli</i>	<i>Escherichia coli</i>
EDTA	Ethylenediaminetetraacetic Acid

EGTA	Ethyleneglycoltetraacetic Acid
EIA	Enzyme Immunoassay
EMA	European Medicines Agency
F127	Pluronic F-127
FAbs	Fractional absorption
FaSSGF	Fasted State Simulated Gastric Fluid
FaSSGFc pH 1.5	Fasted State Simulated Gastric Fluid canine pH 1.5
FaSSGFc pH 6.5	Fasted State Simulated Gastric Fluid canine pH 6.5
FaSSIFc pH 7.5	Fasted State Simulated Intestinal Fluid canine pH 7.5
FaSSIF V2	Fasted State Simulated Intestinal Fluid Version 2
FDA	United States Food and Drug Administration
Fdiss	Fractional dissolution
FeSSIF V2	Fed State Simulated Intestinal Fluid Version 2
g/mol	Grams Per Mole
GIT	Gastrointestinal Tract
HIV	Human Immunodeficiency Virus
HPLC	High Performance Liquid Chromatography
HSS	High Strength Silica
IgG	Immunoglobulin G
I.M.	Intramuscular
I.V.	Intravenous
IU	International Unit
J	Joule
JAMs	Junctional Adhesion Molecules
K	Kelvin
Kg	Kilogram
MAA	Methacrylic Acid
MDF	Maximum Detachment Force
MDT	Mean Dissolution Time
MH	Matrix Hardness
Min	Minutes
mL	Millilitre
mm	Millimeter
mPEG	Methoxy Polyethylene Glycol
MR	Matrix Resilience
MRI	Magnetic Resonance Imaging

MTT	Maximum Transit Time
MUPP1	Multi-PDZ domain protein-1
NCE	New Chemical Entity
nm	Nanometer
NMP	N-methyl-2-pyrrolidone
OGDD	Oral Ghost Delivery Device
PDI	Polydispersion Index
PEG	Polyethylene Glycol
pH	Power of Hydrogen
PI3K	Phosphatidylinositol 3-kinase
PKC	Protein Kinase C
Pressure per Square	PSI
PTs	Peptide Therapeutics
PXRD	Powder X-ray Diffraction
RPM	Revolutions Per Minute
RT	Retention Time
S.C.	Subcutaneous
SEM	Scanning Electron Microscopy
SNR	Signal to Noise Ratio
SPH	Superporous Hydrogel
TEER	Trans-epithelial Electrical Resistance
TEMED	Tetramethylenediamine
TGA	Thermogravimetric Analysis
Tscale-time	Time scale-time
TJ	Tight Junction
TMC	Trimethyl Chitosan Chloride
TMC:CI MiPe	Trimethyl Chitosan Chloride Mini-Pellet
TNBS	Trinitro Benzene Sulfonic
UPLC	Ultra Performamance Liquid Chromatography
UHMW-PE	Ultra High Molecular Weight Polyethylene
UIR	Unit Impulse Response
USP pH 1.2	United States Pharmacopeia simulated gastric fluid
USP pH 6.8	United States Pharmacopeia simulated intestinal fluid
v/v	Volume in volume
V	Volume
Vd	Volume of distribution

Vs	Volume of system
w/v	Weight in volume
w/w	Water-in-water
WA	Work of Adhesion
ZO	Zolin Plague Proteins
Zot	Zolin Occuling Toxin

LIST OF EQUATIONS

CHAPTER 2

Equation 2.1

$$\text{Absolute bioavailability (\%)} = \left(\frac{\text{AUC}_{\text{EV}}}{\text{AUC}_{\text{IV}}} \right) - \left(\frac{\text{Dose}_{\text{IV}}}{\text{Dose}_{\text{EV}}} \right) \times 100$$

Where:

AUC_{EV}: Area Under Curve Extravenous

AUC_{IV}: Area Under Curve Intravenous

Dose_{IV}: Dosage of Intravenous

Dose_{EV}: Dosage of Extravenous

CHAPTER 3

Equation 3.1

$$A = \epsilon lc$$

Where:

A: Absorbance

ϵ : Absorptivity

l: Path length

c: Concentration

Equation 3.2

$$m = \epsilon l$$

Where:

m: Gradient of calibration curve

ϵ : Absorptivity

l: Pathlength

Equation 3.3

$$C_{\text{unknown}} = \frac{A_{\text{unknown}}}{m}$$

Where:

C_{unknown}: Unknown concentration

A_{unknown}: Absorbance of unknown sample at specific peak

m: Gradient calibration curve

Equation 3.4

$$W_{\text{ETDA}} = W_{\text{ETDA filter}} - W_{\text{filter}}$$

Where:

W_{EDTA}: Weight of EDTA dry mass

W_{EDTA filter}: Weight of the dry filter after EDTA has been retained in the filter

W_{filter} : Weight of the dry filter before EDTA was retained within the filter

CHAPTER 4

Equation 4.1

$$\text{Gel Fraction percent (\%)} = \frac{W_e}{W_0} \times 100$$

Where:

W_0 : Weight of sample at time 0

W_e : Weight of sample at time x

Equation 4.2

$$\text{SP\%} = \frac{W_{T_x} - W_{T_0}}{W_{T_0}} \times 100$$

Where:

SP%: Swelling percentage

W_{T_x} : Weight at time X

W_{T_0} : Weight at time 0

Equation 4.3

$$SV = \frac{D_x - D_0}{T_x - T_0}$$

Where:

SV: Swelling Velocity

D_0 : Distance moved at time 0

D_x : Distance moved at time X

T_0 : Time 0

T_x : Time X

Equation 4.4

$$\frac{p}{n^a (p - p)} = \frac{1}{n_m^a \times C} + \frac{(C - 1)p}{n_m^a C p^0}$$

Where:

n_a : Quantity of N₂ absorbed at the relative pressure $\frac{P}{P_0}$

n_m^a : The monolayer capacity

C: Exponentially related to the enthalpy of absorption in the first absorption layer

Equation 4.5

$$A_s(\text{BET}) = n_m^a \times L \times a_m$$

Where:

$A_s(\text{BET})$: Total specific surface area of the adsorbent (of mass m)

$a_s(\text{BET})$: Specific surface area of the adsorbent (of mass m)

L : Avogadro constant ($6.0221415 \times 10^{23} \text{ mol}^{-1}$)

Equation 4.6

$$a_s(\text{BET}) = \frac{A_s(\text{BET})}{m}$$

Where:

$A_s(\text{BET})$: Total specific surface area of the adsorbent (of mass m)

$a_s(\text{BET})$: Specific surface area of the adsorbent (of mass m)

L : Avogadro constant ($6.0221415 \times 10^{23} \text{ mol}^{-1}$)

Equation 4.7

$$\text{Drug entrapment efficiency (\%)} = \left(\frac{\text{Actual drug content}}{\text{theoretical drug content}} \right) \times 100$$

Equation 4.8

$$MDT = \sum_{i=1}^n \tau_i \frac{M_t}{M_\infty}$$

Where:

MDT: Mean Dissolution Time

M : The fraction of drug dose release

τ_i : $(t_i - t_{i-1})/2$

M_∞ : Loading dose

Equation 4.9

$$S = M_0 \times \exp \frac{-TE}{T_2} \times \left(1 - \exp \frac{-TR}{T_1} \right)$$

Where:

M_0 : Magnetisation

T_1 and T_2 : Relaxation times

TR: Prepetition time

TE: Echo time

CHAPTER 5

Equation 5.1

$$y = b_0 + b_1(m\text{PEG}) + b_2(\text{ADS}) + b_3(\text{BS}) + b_4(m\text{PEG})^2 + b_5(\text{ADS})^2 + b_6(\text{BS})^2 \\ + b_7(m\text{PEG})(\text{ADS}) + b_8(m\text{PEG})(\text{BS}) + b_9(\text{ADS})(\text{BS})$$

Where:

y : Measured response

mPEG: Methoxy polyethylene glycol 2000

ADS: Ac-Di-Sol[®]

BS: Sodium deoxycholate

b_0 to b_9 : Regression coefficient

Equation 5.2

$$HEE = \frac{C_{t3}(\text{measured})}{C_{\text{loaded dose}}} \times 100$$

Where:

HEE: Homogenous Entrapment Efficiency

C_{t3} : Concentration of insulin measured at 3 hours

$C_{\text{loaded dose}}$: Amount of insulin originally loaded

Equation 5.3

$$MDT = \sum_{i=1}^n \tau_i \frac{M_t}{M_{\infty}}$$

Where

MDT: Mean dissolution time

M : Fraction of dose released in time $\tau_i = (t_i - t_{i-1})/2$

M_{∞} : Loading dose

Equation 5.4

$$FR_{t8} = \frac{C_{t8}}{C_{TD}}$$

Where:

FR_{t8} : Fractional Release after 8 hours

C_{t8} : Concentration of insulin after 8 hours

C_{TD} : Total dose of insulin

CHAPTER 6**Equation 6.1**

$$\Pr(t_a \geq t) = \int_0^t h(u) du$$

Where:

$h(u)$: Probability function

Equation 6.2

$$\bar{g}(t) = \int_0^t g(t - t_A) \times h(t_A) dt_A$$

Where:

$\bar{g}(t)$: Average time of the movement of drug molecule from point A to point B

$h(t_A)$: Probability of drug molecule having time A

Equation 6.3

$$N_B(t) = N\bar{g}(t) = N \int_0^t g(t - t_A) \times h(t_A) dt_A = \int_0^t g(t - t_A) \times N'_A(t_A) dt_A$$

Where:

$N_B(t)$: Drug molecules at point B with respect to time

$N\bar{g}(t)$: Drug molecules have average time of movement from point A to point B

Equation 6.4

$$M_B(t) = \int_0^t g(t - t_A) \times f(t_A) dt_A$$

Where:

$M_B(t)$: Mass of drug molecules at point B with respect to time

Equation 6.5

$$c(t) = \int_0^t f(t - u) \times c_\delta(u) du \equiv f(t) \times c_\delta(t)$$

Where:

$c(t)$: Concentration of drug molecules with respect to time

c_δ : Function of drug molecule movement with respect to time divided by the volume of the system

Equation 6.6

$$AUC_{t_0}^{t_\infty} = \frac{C_{p \text{ last}}}{\lambda} \text{ or } AUMC_{t_0}^{t_\infty} = \left(\left(\frac{C_{p \text{ last.t last}}}{\lambda} \right) + \left(\frac{C_{p \text{ last}}}{\lambda^2} \right) \right)$$

Where:

$AUC_{t_0}^{t_\infty}$: The Area Under Curve from time 0 to time infinity

$C_{p \text{ last}}$: Plasma drug concentration that was last measured

λ : Terminal elimination rate constant

$AUMC_{t_0}^{t_\infty}$: Area Under the Moment Curve from time 0 to time infinity

$C_{p \text{ last.t last}}$: Plasma drug concentration measured against the last time point

Equation 6.7

$$MRT = \frac{AUMC}{AUC}$$

Where:

MRT: Mean Residence Time

AUMC: Area Under Moment Curve

AUC: Area Under Curve

Equation 6.8

$$MTT = MRT + MAT$$

Where MTT: Mean Transit Time

MRT: Mean Residence Time

MAT: Mean Absorption Time

Equation 6.9

$$MTT = \frac{AUMC}{AUC}$$

Where:

MTT: Mean Transit Time

AUMC: Area Under Moment Curve

AUC: Area Under Curve

DEFINITIONS OF PHARMACOKINETIC ANALYSIS

AUC: Area Under a Concentration of analyte vs time curve. If $C(t)$ denotes the concentration of analyte at time t , then:

$$AUC_a^b = \int_a^b c(t)dt$$

AUC %Extra: Area Under Curve percent extrapolated from the drug concentration measurements

AUCall: computed from time zero to the time of the last Y value

AUCINF: AUC from time zero extrapolated to infinity

AUCINF D: The Area Under Curve to infinity divided by dose

AUCINF Predicted: Area Under Curve to infinity from predicted drug concentration measurements

AUClast: AUC computed from time zero to the time of the last positive Y value

AUMC: Area Under the Moment Curve

$$AUMC_a^b = \int_a^b c(t)tdt$$

AUMCINF: Area Under the Moment Curve when the time concentration curve is extrapolated to infinity

$$AUMCINF = AUMC_0^\infty$$

AUMClast: Area Under the Moment Curve computed to the last observation

$$AUMClast = AUMC_0^{t_{last}}$$

CL: The body clearance

$$CL = \frac{Dose}{AUC}$$

CL F: For extravascular models the fraction of dose absorbed cannot be estimated, therefore Clearance for these models is actually Clearance Fraction where F is the fraction of dose absorbed

$$CL F = \frac{Dose}{AUC_0^t}$$

Clast: Drug concentration at last time point

Cmax: The peak or maximum concentration

Cmax D: The peak or maximum drug concentration divided by dose

MRT: Mean Residence Time is the average amount of time a particle remains in a compartment or system, equal to $AUMC/AUC$

MRT_{last}: Mean Residence Time when the drug concentration profile is not extrapolated to infinity, but rather is based on values up to and including the last measured concentration ($MRT_{last} = AUMC_{last} / AUC_{last}$)

MRT_{INF}: Mean Residence Time when the drug concentration profile is extrapolated to infinity. This can be estimated from single dose data or steady state data

T_{max}: Time at maximum drug concentration

T_{lag}: Time lag (time period before observable drug concentration can be observed)

T_{last}: Time of last measured drug concentration

V_Z: Volume of distribution based on the terminal phase

V_Z F: The volume of distribution for the extravascular models, the fraction of dose absorbed cannot be estimated. Therefore, Volume for these models is actually Volume/F, where F is the fraction of dose absorbed

CHAPTER ONE

An Oral Ghost Delivery Device for Macromolecules

1.1. An introduction to macromolecules and their application as therapeutic agents

Macromolecules, such as peptides and proteins, are any relatively large compounds that are composed of uniquely distinct monomers (Brander et al., 2009; Bennet et al., 2009; Amidi et al., 2010; Karsdal et al., 2011). These monomers can be substituted with alternative monomer types to form an entirely new macromolecule. Proteins and peptides can be considered the most elegant examples of macromolecule compounds that contain uniquely combinations of amino acid monomers. Nucleic acids that form the DNA macromolecule is often considered the blue print to life but it is the peptide and protein macromolecules that imbues purpose and function to these blueprints. Medical and biological scientists have progressively unlocked the unique function of proteins and peptides which has lead to the exploitation of these macromolecules for medical intervention purposes.

Over many years, proteins and peptides have been exposed to selective pressures that optimize the functionality and robustness of these compounds to generate some of the most potent compounds. An extreme example of this is botulism toxin from the bacterium *Clostridium botulinum* (Montecucco and Molgó, 2005; Kukreja and Singh, 2009). Botulism toxin is a protein that is extremely efficient at blocking acetylcholine release between neurons and is the most potent acute toxin described. It has been shown to have a human median lethal dose of 1.3-2.1ng/kg (intravenous administration) and 10-13ng/kg (inhalation administration) (Arnon et al., 2001). Ironically, this toxin is utilized as a protein therapeutic for US Food and Drug Administration (FDA) approved treatments of cervical dystonia, strabismus, severe primary auxiliary hyperhidrosis, blepharospasm, achalasia, migraine, bruxism and hemifacial spasm (Brin et al., 1999; Eisenach et al., 2005; Shukla and Sharma, 2005; Felber, 2006; Naumann et al., 2008; Ranoux et al., 2008). Peptides have also been exploited for the treatment of chronic conditions such as type I diabetes (insulin) and osteoporosis (calcitonin) (Cui et al., 2009; du Plessis et al., 2010; Cheng and Lim, 2010; Chaudhury and Das, 2011). Protein or peptide macromolecules that have been exploited for medical intervention purposes are often referred to as peptide or protein therapeutics as an indication that the specific function of the macromolecule has been determined and is effective at the treatment of a specific ailment. An issue arising in tandem with the progressive development of peptide or protein therapeutics is the delivery of these large molecules in a manner that is accommodating for the patient.

1.2. Currently described strategies for oral delivery of macromolecular therapeutics

The oral administration of macromolecular therapeutics is most preferable by patients because of the convenience and comfort associated with this mode of drug delivery (Chen et al., 2013). In addition, for some macromolecular therapeutics such as insulin, oral absorption within the small intestine has been suggested to be more representative of the natural physiological distribution of the therapeutic within the systemic circulation than subcutaneous administration (Rekha and Sharma, 2013). Insulin is secreted into the hepatic portal vein in response to an increase in blood glucose levels and transported to the liver (Rekha and Shama, 2013). Parenteral administration of insulin will initially bypass the liver which may negatively impact the body's natural response to insulin (Still, 2002; Federwisch et al., 2002; Rekha and Shama, 2013). The administration of insulin that more closely represents the innate physiologically means of distributing insulin to the liver may enhance the effectiveness of auxiliary biochemical pathways that can control blood glucose levels. The main challenges of orally administering peptide therapeutics is (i) by-passing the acidic gastric environment, (ii) circumventing the gastric peptidase enzymes, (iii) mucus barriers that exist within the gastrointestinal tract (GIT) and (iv) permeating intact peptide therapeutics through the GIT epidermis and into the systemic circulation (Torres-Lugo et al., 2002; Cui et al., 2009; Sajeesh et al., 2010a; Huang et al., 2011; Rekha and Sharma, 2013). There are three main formulation approaches that have been employed to achieve an effective oral administration of peptide therapeutics.

The first approach is the development of nanoparticle based systems that enhances oral delivery of peptide therapeutics by possessing a high surface area to volume ratio (Rekha and Shama, 2013). An example of this approach can be reviewed in Foss et al. (2004) whereby the researched utilized methacrylic acid grafted poly(ethylene glycol) to generate nanospheres that were pH responsive. The nanospheres were administered to rats and to lower blood glucose levels for 6 hours (Foss et al., 2004). The main issue with this study was that the dosage form was administered in gelatine capsules to a 200g rat which has a very low representation with respect to a human model. There are many other examples of this approach which can be reviewed in Reis et al. (2008), Cui et al. (2009), Sonaje et al. (2009) and Makhlof et al. (2011). The second approach is the administration of microparticles that may convey increased functionality with respect to drug delivery applications (Rekha and Shama, 2013). For instance, Lowman and co-workers, administered insulin loaded in polymethacrylic grafted polyethylene glycol microparticles that prevented the release of insulin within the gastric environment but also facilitates the effective penetration within the mucosal layer in the intestinal environment (Lowman et al., 1999). A major drawback was

once again the microparticles were administered to 200 g rats in a gelatine capsule which rapidly degrades in the stomach (Lowman et al., 1999). The stomach of the human model has a far greater volume than the rat model and the stomach has an extremely thick mucus layer (Kerss et al., 1982; Copeman et al., 1994; Jordan et al., 1998; Lowman et al., 1999). The thick mucus layer of the stomach may easily entrap microparticles and reduce the effective absorbed dosage. A further example of the microparticle approach can be reviewed in Sajeesh and co-workers, whereby two functional groups were utilized to achieve an effective oral insulin absorption (Sajeesh et al., 2010a,b). Lastly, lipid based approaches have been attempted because it has been indicated that these systems have low acute toxicity and high biocompatibility properties (Torchilin, 2005; Almeida and Souto, 2007; Rekha and Shama, 2013). An example of this approach is where solid lipid nanoparticles were administered to rats and achieved *in vivo* absorption of orally administered insulin (Zhang et al., 2006). Additional examples of oral administration of insulin can be reviewed in **Table 1.1**. This table contains some examples of drug delivery systems that were assessed *in vivo*. The gap is that of upscaling to a larger *in vivo* model as many of these drug delivery solutions were suspensions. A suspension may not achieve the desired response in larger animal models due to the increased volume of distribution.

Table 1.1 Summary of drug delivery systems for the oral administration of insulin

Authors	Year Published	Drug delivery system	Status	Significant results	Specific further steps required
Sarmiento et al.	2007	Insulin loaded alginate/chitosan nanoparticles	Further development is required	Particles had a mean size of 750nm Lowered basal glucose levels by more than 40% over 18 hours in diabetic rats	Upscaling of the dosing into larger <i>in vivo</i> models
Lin et al.	2007	Insuline loaded chitosan/poly(γ -glutamic acid) nanoparticles	Further development is required	Particles had a mean size of 110-150nm Transiently opens tight junctions Lowered basal glucose levels for 10 hours in rats	Upscaling of the dosing into larger <i>in vivo</i> models
Yin et al.	2009	Insulin loaded trimethyl chitosan-cysteine nanoparticles	Further development is required	Particle size 100-200nm Trimethyl chitosan-cysteine increased transport of insulin and resulted in a 35% decrease in glucose level after 8	Upscaling of the dosing into larger <i>in vivo</i> models

He et al.	2012	Insulin loaded Poly(ester amide) microspheres	Further development is required	hours within rats Reduce basal glucose level by 49.4% within 5 hours until an 8 hour period had elapsed within rats	Upscaling of the dosing into larger <i>in vivo</i> models
Xong et al.	2013	Insulin loaded Pluronic P85/ poly(lactic acid) vesicles	Further development is required	Vesicle diameter was 178nm Basal glucose level decreased after 2.5 hours following oral administration in mice Basal glucose level remained stable at 31.8% of initial blood glucose level for 14 hours	Upscaling of the dosing into larger <i>in vivo</i> models
Chuang et al.	2013	Insulin loaded EGTA-conjugated poly(γ glutamic acid) and chitosan nanoparticles	Further development is required	Significantly increased paracellular permeability Insulin present in heart, aorta, renal cortex, renal pelvis and liver after administration to rats	Upscaling of the dosing into larger <i>in vivo</i> models
Mukhopadhyay et al.	2014	Insulin loaded <i>N</i> -succinyl chitosan grafted polyarylamide hydrogel	Further development is required	pH sensitive with respected to the tested USP gastric and USP intestinal dissolution media. Bioavailability of insulin was ~4.43%	Upscaling of the dosing into larger <i>in vivo</i> models
Nielsen et al.	2014	Insulin coadministered with penetratin	Further development is required	Half-life of insulin increased from 24.9min to 90.5min in the presence of L-penetratin and D-penetratin	Upscaling of the dosing into larger <i>in vivo</i> models

1.3. Rationale and motivation for this study

An innovative small intestinal targeted drug delivery device may overcome the limitations of the oral delivery of peptide therapeutic, therefore enhancing patient compliance, efficacy and reducing toxicity. This may be achieved with a combination of strategies that limits presystemic enzymatic degradation, site specific targeting within the small intestine, the use of permeation enhancers and mucoadhesives across a synergistic platform. Chronic administration of peptide therapeutics (such as calcitonin and insulin) is usually delivered as subcutaneous or intramuscular injections at a high dosing frequency (three times a week

to three times a day). Some of these macromolecules often require daily dosing which is painful and inconvenient for the patient. The proposed Oral Ghost Drug Delivery (OGDD) device may be taken orally once or twice a day, depending on the type of peptide therapeutic and the condition that is being treated. The OGDD protects the peptide therapeutic from the harsh gastric environment and releases the peptide therapeutic at a targeted location within the small intestine. In addition, the OGDD device provides a platform for the oral administration of peptide therapeutics in a manner that promotes successful absorption in a multi-approach strategy without the utilization of highly variable suspensions and within a large animal model.

The comparison between isolated fasted state fluids from the GIT tract of Large White the pig model would aid significantly in generating a tighter correlation between the pig model, human biorelevant fluids and USP dissolution fluids. Acquired data from these comparisons, correlations and basic chemical profiling could be used in future for *in vitro* oral drug dissolution studies that would reduce development time and reduce the potential *in vivo* failure of an oral drug delivery system. In addition, the *in silico* analysis of the dissolution and disintegration behaviours could be used to generate disintegration kinetics of novel excipients that would assist in formulating enhanced *in vivo* relevant mechanisms.

1.4. The Oral Ghost Delivery Device for the delivery of macromolecules within the therapeutic peptide class of drugs

The Oral Ghost Drug Delivery (OGDD) device comprises a non-responsive non-degradable shell component was produced from United States Food and Drug Administration (FDA) approved plastic, Polystone® M. Polystone® M is a very hard plastic with low water retention and is utilized within surgical implants during knee and hip operations. This plastic has demonstrated a biocompatibility that can be maintained within the body for an extended period of time. Due to these properties, Polystone® M is an ideal material as it provides structure to the OGDD and has previously demonstrated biocompatibility. A dynamically equilibrating stimuli responsive hydrogel was placed within the base of the shell component. The stimuli responsive hydrogel was utilised to displace the peptide-loaded trimethyl chitosan chloride mini-pellet and the ethylenediaminetetraacetic acid (EDTA) *in situ* hot melt dispersion mini-pellet from the OGDD device. A peptide-loaded trimethyl chitosan chloride mini-pellet (TMC:Cl MiPe) was utilised as the drug carrier within the drug delivery system. An EDTA *in-situ* suspension mini-pellet was utilised to release EDTA within the targeted delivery site to transiently inhibit zinc-peptidase enzymes and reduce mucus viscosity by chelating zinc and calcium divalent ions respectively. A Eudragit® cap was utilised to facilitate the

release of the mini-pellets within the target location and to facilitate the generation of a positive pressure within the OGDD device. The positive pressure enabled the mini-pellets to be released within the small intestine at approximately the same time and at relatively the same location (through the synergistic degradation of the Eudragit® cap and the displacing force of the pH sensitive hydrogel). The design of the OGDD device is shown in **Figure 1.1**.

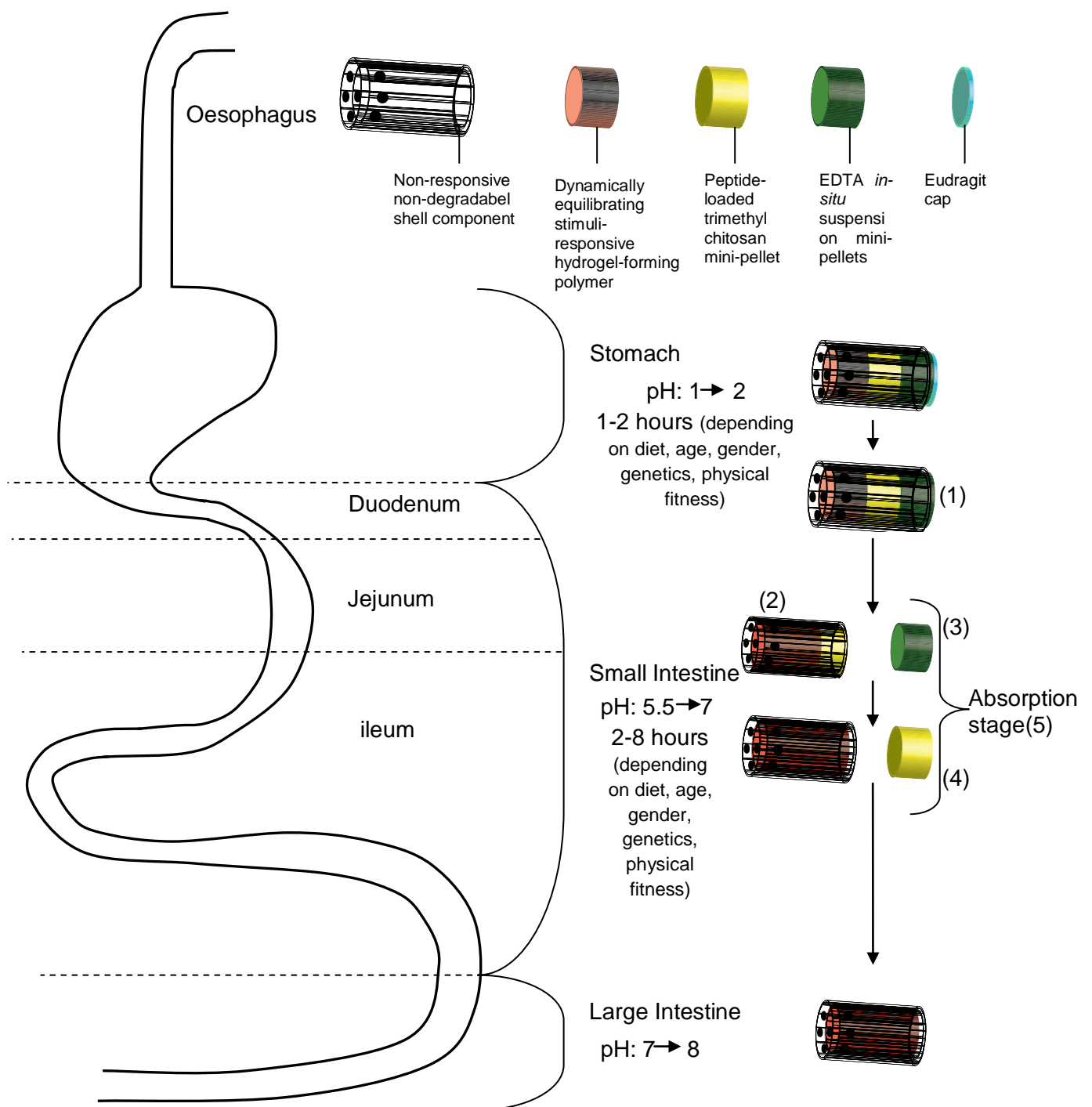


Figure 1.1: Schematic of the Oral Ghost Delivery Device (OGDD) components and mechanism of action within the GIT. The Eudragit[®] cap (1) becomes soluble as the pH increases within the GIT tract. The dynamically equilibrating hydrogel (2) dramatically increases in volume in response to increasing pH of the GIT tract. The increase in volume of the dynamically equilibrating hydrogel displaces the EDTA *in situ* suspension mini-pellet (3) and the peptide-loaded trimethyl chitosan mini-pellet (4) at close relative position along the small intestine. EDTA is released from the mini-pellet and the peptide therapeutic is released from the trimethyl chitosan mini-pellet, thereafter absorption takes place in the jejunum-ileum region of the small intestine (5).

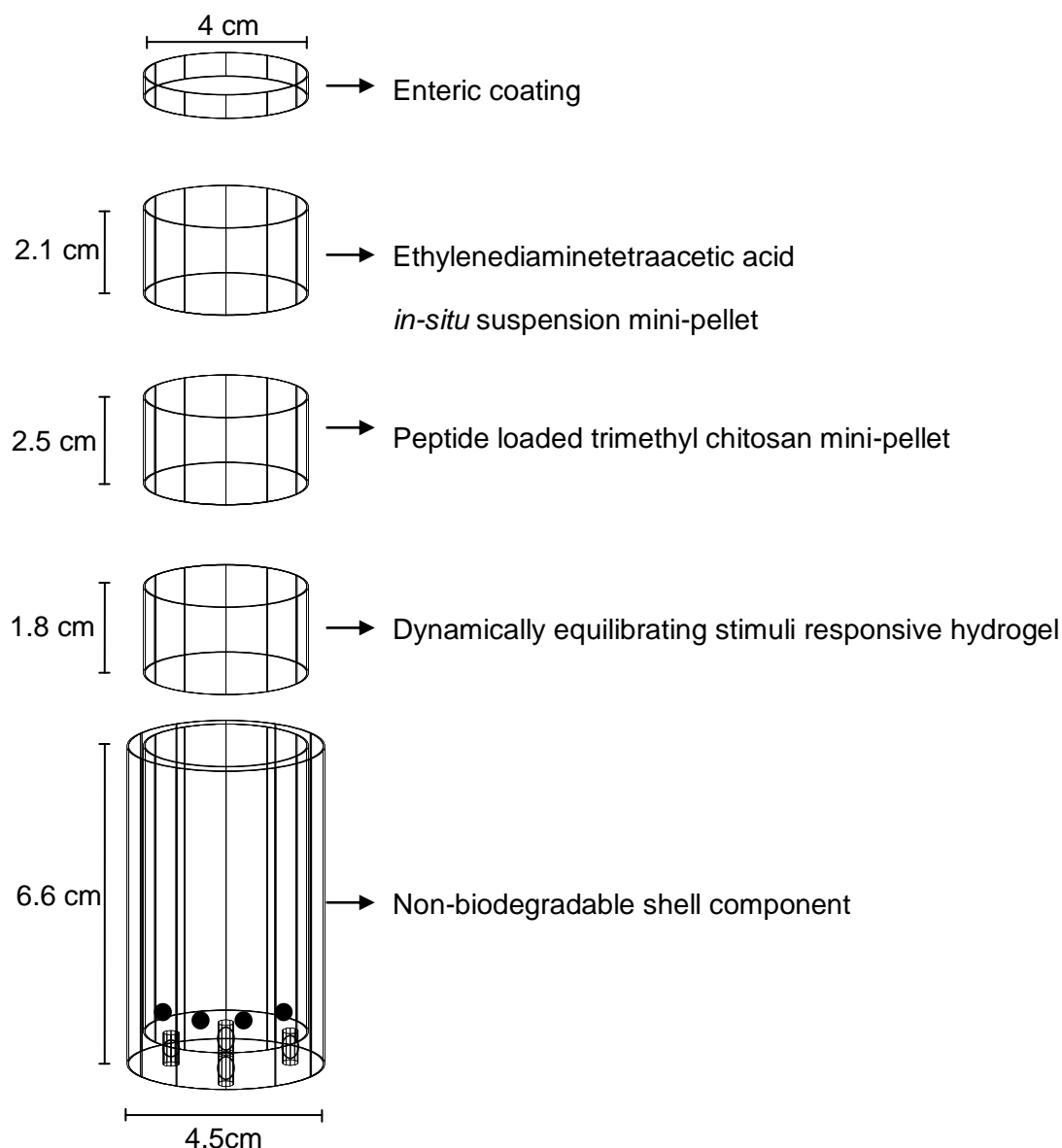


Figure 1.2: The assembly of the Oral Ghost Delivery Device with size dimensions

1.5. Aim and Objectives of this study

The aim of this study was to develop an Oral Ghost Drug Delivery (OGDD) device that enabled effective targeted oral delivery of macromolar therapeutic, which are primarily peptide therapeutics. Additionally, an *in vitro/ex vivo/in vivo* correlation of orally administered peptides namely salmon calcitonin will be evaluated with respect to USP dissolution fluid, biorelevant dissolution fluid and isolated gastrointestinal fluids from large White Pig model.

The following objectives are outlined for the aim:

- 1) Synthesis and characterization of a pH responsive superporous hydrogel
- 2) Conduct release studies with a number of drugs for BCS I, II, III from hydrogel
- 3) Synthesis and characterization of methoxypolyethylene glycol-ethylenediaminetetraacetic acid-Avicel[®] *in situ* hot melt dispersion mini-pellets
- 4) Synthesis and characterization of therapeutic peptide loaded EDTA-mPEG trimethyl chitosan mini-pellets utilizing a Box-Behnken design and formulation characterization
- 5) Engineer a non-biodegradable non-responsive shell component from FDA approved food-grade plastic to facilitate the release of the mini-pellet dosage forms at the desired GIT location
- 6) Assemble and conduct *in vitro* analysis of the Oral Ghost Drug Delivery device
- 7) Conduct preclinical animal studies within Large White pigs for *in vitro/ex vivo/in vivo* pharmacokinetic analysis

1.6. Overview of the thesis

Chapter 1 introduces the issues associated with the current mode of administration of macromolecular therapeutics and the rationale for the study. A brief background and introduction of the Oral Ghost Delivery Device design and conception is summarised. The aims and objectives of the study are outlined.

Chapter 2 is an extension of Chapter 1 whereby an in-depth literature review focuses on the currently known aspects of orally administered therapeutic peptide delivery through the utilization of permeation enhancers to achieve enhanced absorption within the small intestine. The in-depth literature analysis of the permeation enhancers and strategies utilised for this drug delivery system is reviewed.

Chapter 3 describes the development of the metal chelator component of the OGDD device that overcomes some of the zinc-dependent peptidase and mucus viscosity issues associated with the oral administration of peptide therapeutics. A number of EDTA-mPEG *in situ* hot melt dispersion mini-pellet formulations are investigated in order to achieve the most desirable formulation properties.

Chapter 4 describes the development of the pH responsive hydrogel that facilitates the displacement of loaded mini-pellet solid dosage forms from the Oral Ghost Drug Delivery

device within the targeted small intestinal environment. An indepth physicochemical and physicomechanical characterisation of the pH responsive hydrogel within representative dissolution fluids and *ex vivo* performance was evaluated.

Chapter 5 describes the development of the peptide-loaded trimethyl chitosan mini-pellet formulations that are loaded into the Oral Ghost Delivery Device. A Box-Behnken factorial design coupled with physicomechanical and dissolution studies was utilised to generate an optimised formulation for the peptide drug carrier. This formulation overcame additional issues associated with oral administration of peptide therapeutics such as intraluminal loss of peptide from peptidase enzymes and non-specific targeting within the GIT.

Chapter 6 describes the development of the final components, the non-responsive non-degradable shell component and the Eudragit[®] cap. A finalised OGDD device was assembled and administered to the Large White pig model. A comparative *in vivo* study of the orally administered Oral Ghost Delivery Device with respect to intramuscular administration of salmon calcitonin was undertaken and descibed. These components facilitate the engineered mechanism for the delivery of the mini-pellet solid dosage forms to the targeted location of the jejunum and ileum of the small intestine.

Chapter 7 provides the conclusions and recommendations of the study. These conclusions and recommendations describe the scientific direction that could be utilized to further enhance the OGDD device for therapeutic applications.

CHAPTER 2

Orally Administered Therapeutic Peptide Delivery: Enhanced Absorption Through the Small Intestinal Wall Utilising Permeation Enhancers

2.1. Introduction

Peptide therapeutics are relatively small molecules (fifty or less amino acids or a maximum molecular weight of 5000Da) which may contain a specific sequence of amino acids joined together by peptide bonds resulting in a highly specific secondary structure, but absent of tertiary structure, that induces a rapid and highly specific beneficial response (Johnson, 2005; Sato et al., 2006; Giuliani et al., 2007; Oyston et al., 2009; Tshala-Katumbay, 2010). Peptide therapeutics are currently one of the most advanced pharmacologically active compounds which may replace many traditional small molecule drug compounds as technological advances and economically feasible production methodologies are implemented within the industrial setting. Additionally, innovative and novel means that allow peptide therapeutics to be conveniently administered to patients in an acceptable manner need to be sought after in order to achieve an optimal pharmaceutical product that would significantly enhance medical treatment. The main focus of this review is therefore to provide a critical overview of peptide therapeutics and the means by which they may be desirably administered orally.

2.1.1. Macromolecular therapeutics

Presently, over 60 peptide therapeutics (PTs) are available and hundreds are in clinical development (Degim and Celebi, 2007; Vlieghe et al., 2010; Agyei and Danquah, 2011). The contemplation of the extraordinary amount of research and development invested into PTs, highlights their assured existence within the market place (Loffet, 2002; Bray, 2003; Guzman et al., 2007; Stevenson, 2009; Vlieghe et al., 2010). This is evidenced by an estimated PTs market value of US\$15.7 billion in the year 2013 (Pichereau and Allary, 2005). Moreover, in the year 2004, peptides, proteins, and antibodies had an estimated sales value of US\$40 billion which accounted for 10% of the total pharmaceutical sales in that year (Decaffmeyer et al., 2008; Vlieghe et al., 2010). PTs are tremendously valuable therapeutic agents which are composed of a very specific sequence of amino acids. The composing amino acid sequence within PTs determines the three dimensional structure of these compounds and therefore influences the specific extracellular receptor that the peptide therapeutic physically interacts with (Oyston et al., 2009). The composing amino acid sequence also determines the charge that the peptide therapeutic exerts, thus influences the extracellular receptor that

the peptide therapeutic chemically interacts with (Yeaman and Yount, 2003). The charge and the three dimensional structure of PTs is extremely crucial for a desired therapeutic outcome to transpire. Any interference with the sensitive make-up of a peptide therapeutic will render the entire macromolecule inactive. PTs are considered to have many advantages over established small molecule therapeutics but also have many distinctive disadvantages (Vlieghe et al., 2010).

The core issues surrounding the use of PTs in daily treatment is the prohibitive expense of these agents, their availability and sensitivity to degradation. The price of PTs and the availability of PTs can be considered as related issues since even readily available therapeutic agents may be expensive due to the unrefined material requirements or vast processing measures. PTs may clearly be prohibitively expensive if their availability is restrictive. A classical example is the production of recombinant human insulin by *Escherichia coli* (*E. Coli*) (insulin was firstly *commercially* available as animal insulin) in 1982 under the trade names Humulin® in USA and Humuline® in Europe (Ferrer-Miralles et al., 2009). Insulin was originally acquired from the pancreas of pigs and cattle in abattoirs but since 1982, diabetics have progressively purchased recombinant human insulin derived from *E. Coli* (Ferrer-Miralles et al., 2009). A 3mL vial of Humuline® with a concentration of 100IU/mL can cost between US\$40 and US\$70 as of July 2010, which is considerably less expensive when compared to the difficulty incurred in acquiring insulin derived from the pancreas of cattle or pigs. Even though infinite potential amounts of recombinant human insulin can be produced from *E. coli*, the purification and isolation processes from massive vats of *E. coli*, adds some substantial overheads. Another example is enfuvirtide that took up to 8 months to synthesise and 106 steps to increase the scale of its production to a multi-tonne per year operation (Bray, 2003; Vlieghe et al., 2010). Enfuvirtide has been used as a drug model to reduce the large scale production cost of peptides to less than US\$1 per amino acid residue, therefore the potential cost of peptide drugs could be decreased significantly in the future (Bray, 2003; Vlieghe et al., 2010). This is a demonstration of the biotechnology industry filling the ever growing need for a peptide therapeutic at an economical feasible level. The advantages and disadvantages of peptide therapeutics with respect to recombinant proteins, small drug molecules and antibodies are shown in **Table 2.1**.

Table 2.1 Advantages and disadvantages of peptide therapeutics over recombinant proteins, small drug molecules and antibodies.

Advantages	Reference
Deeper infiltration into tissues Reduced immunogenic profile	McGregor, 2008; Vlieghe et al., 2010
Less cost of manufacture Higher activity ratio (activity per unit mass) than antibodies Reduced upstream patents which downstream firms have to acquire due to reduced intellectual property rigidity Greater stability than recombinant proteins and antibodies	Ladner et al., 2004; Vlieghe et al., 2010
Peptide therapeutics are the smallest functional element of a protein therapeutic macromolecule, therefore peptide therapeutics have greater efficacy, selectivity and specificity than small drug molecules.	Hummel et al., 2006; Vlieghe et al., 2010
Peptide therapeutics degrade to amino acids hence reduces the probability for drug-drug interactions which limits adverse effects.	Loffet, 2002; Vlieghe et al., 2010
Less potential to amass in tissues and organs due to short half life thereby limiting the adverse effects.	Vlieghe et al., 2010
Small quantities of agonistic peptides are required to activate targeted receptors.	Hruby, 2002; Vlieghe et al., 2010
Disadvantages	Reference
Potential of immunogenic reactions due to an extensive period of exposure or poor peptide therapeutic design.	Guichard, 2004; Pichereau and Allary, 2005; Vlieghe et al., 2010
Restricted systemic transport in contrast to small drug molecules.	
Inadequate movement through biological membranes due to the general hydrophilic nature of peptide drugs.	
Rapidly cleared from the systemic circulation rapidly through hepatic and renal clearance.	
Extensively metabolised by excessive protease enzyme concentrations within the stomach, intestinal lumen and intestinal brush boarder.	
Limited absorption in the gastrointestinal tract therefore parenteral administration is often required.	
Peptide therapeutics has the potential to have distorted three dimensional structures due to pH variation, protease activity or ionic stress that may activate alternative receptors resulting in adverse effects.	
Incredibly expensive to synthesise and/or produce depending on the molecular weight of the peptide drug.	Guichard, 2004; Pichereau and Allary, 2005; Bray, 2003; Vlieghe et al., 2010

Parenteral administration of peptide therapeutics is extremely expensive with respect to orally administered therapeutic compounds. The injection needles, injection plungers and saline solution each require thorough sterilisation to prevent infections at the injection site or systemically. With the increase in PTs availability, a Drug Delivery System (DDS) which can administer these therapeutics without the experience of needle injections will become extremely important. An essential consideration for a DDS is to diminish the quantity of peptide therapeutic which is lost during the administration process so that the cost of the DDS can be minimised, thus allowing patients financial access to the DDS. A demonstration of the encompassing capacity in which PTs have been employed in diseased states and diagnostic purposes can be seen in the six examples listed under **Section 2.1.2**.

2.1.2. Parenteral administration of peptide therapeutics

PTs are currently administered primarily by the parenteral route though modes such as intramuscular injections (I.M.), subcutaneous injections (S.C.) and intravenous administration (I.V.). These modes of administration are used for PTs for the following reasons:

- Guarantee that the complete PTs dose is delivered to the systemic circulation therefore ensuring that the therapeutic index is achieved.
- Circumvent first pass metabolism so that the lowest amount of PTs is required, which reduces the cost of the therapeutic to the patient.
- Circumvent pre-systemic metabolism in the stomach and intestine which also ensures that the lowest quantity of PTs is administered to attain the desirable therapeutic level.

These reasons are extremely valid for administration of expensive PTs but as with any route of administration there are certain disadvantages as listed below:

- Pain coupled with parenteral administration reduces patient compliance.
- Inconvenience of using injections and I.V.'s.
- Expenditure encompassed in using sterilised needles, injection plungers, I.V. bags, saline and catheters.

The advantages and disadvantages of parenteral administration have to be weighted carefully, especially if the PTs are intended for an extended period of time or even over a life time. This is often encountered in disease conditions such as osteoporosis, human

immunodeficiency virus (HIV) or type 1 diabetes. These diseased states necessitate frequent administration of PTs ranging from three times a week to three times daily. More than 80% of the most lucrative pharmaceuticals are administered via the oral route (Lennernäs and Abrahamson, 2005).

One approach to augment the oral bioavailability of PTs is to modify the biologically synthesised peptide, such as salmon calcitonin, by adding functional groups or molecules that reduce proteolytic enzymes activity on a specific peptide (Cheng and Lim, 2010). Modification of these PTs may occur by PEGylation where specific amino acids within the backbone of the peptide, are modified by the addition of polyethylene glycol (PEG) and this reduces the activity of proteolytic enzymes (Cheng and Lim, 2010). These engineered macromolecule therapeutics are often considered synthetic as they are manufactured in the laboratory. Below is a list of some interesting peptide therapeutics that demonstrates their wide activity:

- 1) Corticorelin trifluoroacetate, known by the trade name Acthrel[®], is a potent stimulator of adrenocorticotrophic hormone (ACTH) which is released from the anterior pituitary. This synthetic peptide contains a 41 amino acid sequence and induces ACTH to stimulate cortisol production in the adrenal cortex. Acthrel[®] is produced by both Ferring Pharms and Biovail Pharms and is used in the diagnosis of ACTH-dependent Cushing's syndrome as well as in the treatment of hypertension.
- 2) Enalapril maleate, known by the trade name Vasotec[®], is considered a long-acting angiotension converting enzyme (ACE) inhibitor drug. Vasotec[®], a prodrug, is unique as this peptide therapeutic is administered orally and dependent on activation (via hydrolysis) in the gastrointestinal tract. In addition, Vasotec[®] has a sequence of 3 amino acids only but it is still capable of exerting a significant biological response.
- 3) Enfuvirtide, known by the trade name Fuzeon[®], is a fusion inhibitor peptide drug against the HIV-1 virus. Fuzeon[®] binds to the gp120 receptor on the HIV-1 protein coat which prevents the HIV-1 virus from fusing with CD4 receptors on mammalian cells. Fuzeon[®] has a 36 amino acid sequence and is produced by Roche. Enfuvirtide is used together with HAART therapy to further reduce the viral load in HIV-1/Aids.
- 4) Human calcitonin, known by the trade name Cibacalcin[®], is a polypeptide hormone drug. Human calcitonin is used to reduce osteoclastic osteolysis in the bone and to reduce mineral removal from bone. Human calcitonin also promotes renal excretion of calcium thus contributing to the reduction of pain symptoms in skeleton joints. Human calcitonin has a 32 amino acid sequence and is primarily administered via intramuscular or

subcutaneous injections. Cibacalcin[®] is produced by Novartis Pharma and is used in adults for postmenopausal osteoporosis, Paget's disease and hypercalcaemia.

- 5) Bivalirudin trifluoroacetate hydrate, known by the trade name Angiomax[®], is an intravenously administered synthetic peptide drug. Bivalirudin trifluoroacetate hydrate works in the cardiovascular system by specifically and reversibly inhibiting thrombin activity, thus acting as an anticoagulant. Angiomax[®] has a 20 amino acids sequence and is produced by Nycomed Pharma. Bivalirudin trifluoroacetate is used in patients with unstable angina undergoing percutaneous transluminal coronary angioplasty or percutaneous coronary intervention.
- 6) Ziconotide acetate, known by the trade name Prialt[®], is an intrathecal administered synthetic peptide. Ziconotide acetate is a central nervous system drug which has a 25 amino acids sequence. Ziconotide acetate is an interesting peptide drug because it is administered using a programmable implantable micro-infusion device with a variable rate of dosing. Ziconotide is produced by Elan Pharm and is used in patients to elicit relief of severe chronic pain which is refractory to other treatment methods.

Recently "bioidentical" hormones, which can also be modified in laboratories, have entered the marketplace. Bioidentical hormones are plant derivatives that have been chemically modified to have the same three dimensional structures as naturally synthesised hormones (Chervenak, 2009). A large number of these bioidentical hormones are not FDA approved but many women are using them with the hope that they may avoid the potential side effects of FDA approved hormonal therapeutics (Boothby et al., 2004; Hickey et al., 2005; MacLennan, 2008). Any further discussion on the "bioidentical" hormones falls outside of the latitude of this literature review but it should be appreciated that these "bioidentical" compounds do not count towards an FDA approved peptide therapeutic market.

The exploitation of polymers (such as chitosan, polyacrylic acid, poly(methyl acrylic) acid, cellulose, and many more) is another approach that has been demonstrated to be a budding solution to this quandary. Polymers, according to many researchers, are exceedingly adaptable with unique influence over biological membranes and in biological environments. An elaborate description of chitosan and trimethyl chitosan will be provided in detail as these polymers not only demonstrate mucoadhesive properties but also permeation enhancing activities (Mourya and Inamdar, 2009). Drug delivery systems using polymers have been shown to enhance the therapeutic outcome significantly but presently drug delivery systems which are based on chitosan polymers have not been approved by the FDA. Currently there are only two chitosan products namely Celox and Bandage, that have been approved for use in humans but they are not under the drug delivery systems category (Baldrick, 2010). Celox

is a chitosan based device which is used for the treatment of bleeding (Ranfeild, 2006) while Bandage, under the trade name HemCon® and QuikClot® (available in the USA and Europe), are devices which rapidly clot blood in open wounds (Barnard and Millner, 2009).

2.1.3. Potential problems associated with the administration of peptide therapeutics via the oral route and possible solutions

There are many potential problems with the oral administration of peptide therapeutics which can be unique to the PT itself or PTs in general which are separate from pharmaceutical excipients. The delivery of PTs via the oral route requires a number of important considerations that will be discussed fully throughout this literature review for which major focus will be within a pharmaceutical scientist's perspective. The first factor that all pharmaceutical scientists should generally consider is the absorption of PTs from gastrointestinal tract. The second factor is the movement of PTs through the mucus layer that lines the gastrointestinal tract. The third factor that should be under consideration is the potential means to circumvent the proteolytic enzymes that exist in the stomach and the small intestine. A pharmaceutical scientist must also choose the animal model that most closely represents a human system in order to obtain data that closely predicts the behaviour of a PT delivery system in the human gastrointestinal tract. Finally a pharmaceutical scientist should consider approval bodies such as the United States Food and Drug Agency (FDA) and the European Medicines Agency (EMA) by designing a drug delivery system with components that have a well established toxicity profile. Each of these considerations will be discussed and potential solutions suggested.

2.2. The biochemical, anatomical and physiological makeup of the small intestine

The small intestine is habitually depicted as a continuous tube-like organ that is divided into three distinct regions namely duodenum, jejunum and ileum. The primary function of the small intestine is the uptake of nutrients (fat, monosaccharides, amino acids, di and tri peptides and vitamins), whereas the colon is the major site for fluid and electrolyte absorption (Paranjpe and Sinko, 2002). The total surface area of the small intestine is approximately 200m², including the columnar epithelial cell layer (Deli, 2009). The lower parts of the small intestine i.e. jejunum and ileum, are considered to be the major locations of drug absorption, because of the leaky paracellular tight junctions reflected by the low transepithelial electrical resistance, as compared to the other parts of the gastrointestinal tract (Ward et al., 2000).

The digestive role of the small intestines is one of the central factors which considerably reduce the oral bioavailability of PTs. This occurs principally in the small intestine lumen fluid. An in-depth comprehension of the small intestine lumen fluid would allow pharmaceutical scientists to design drug delivery systems that function more cost-effectively in the small intestines. A pharmaceutical scientist should contemplate that the physiological nature of the small intestine is highly reliant on the diet of an individual, the age, disease state and the genetic input of that individual. A typical example is where it has been reported that a change in pH within the small intestines of an individual was measured a week apart and found to diverge extensively, even though the diet of that individual had not changed within that week (Ibekwe et al., 2008). The intestinal lumen fluid was considered to be ubiquitous in the small intestines until magnetic resonance imagery was used to demonstrate that the intestinal lumen fluid exists in what has been referred to as "fluid pockets" (Schiller et al., 2005). The average volume of fluid in the small intestines is 319mL but each fluid pocket contained a volume of 12mL in the fasted state (Schiller et al., 2005). The average volume during the fed state was 156mL where each fluid pocket contained a volume of 4mL only (Schiller et al., 2005). This is exceptionally important for researchers who intend to design DDS whilst considering the volume of fluid in the small intestine or the pH environment of the small intestine. Preferably, a DDS should be able to perform in the intestinal fluid volume found within fluid pockets, therefore preventing sporadic drug release from a DDS as the DDS moves through the small intestine, thus reducing peptide therapeutic absorption and causing the plasma levels of the peptide therapeutic to fluctuate.

A pressing issue that has been reported is the inaccurate global representation of all the components in the small intestinal lumen fluid during *in vitro* dissolution testing (McConnell et al., 2008). Hank's bicarbonate buffer has been demonstrated to model the ionic composition of the jejunal lumen fluid and Kreb's bicarbonate buffer has been demonstrated to model the ionic composition of the ileal lumen fluid (Fadda and Basit, 2005; Ibekwe et al., 2006). Drug dissolution profiles for Eudragit® S-coated mesalazine tablets were evaluated in phosphate buffer medium, Hank's bicarbonate buffer and Kreb's bicarbonate buffer (Fadda and Basit, 2005). The drug dissolution profiles that were generated from these medium types showed that Eudragit® S-coated mesalazine tablets release drug much more rapidly in phosphate buffer than in Hank's bicarbonate buffer or Kreb's bicarbonate buffer (Fadda and Basit, 2005). Hank's and Kreb's buffer medium also demonstrated to have the same buffering capacity as the small intestinal lumen fluid and consequently was concluded to be a more accurate representation of *in vivo* drug dissolution profiles (Ibekwe et al., 2006; Fadda and Basit, 2007). An accurate correlation between *in vitro* data and *in vivo* data

should be obtained in order for *in vitro* data to be used as a prediction of *in vivo* outcomes. Therefore, a pharmaceutical scientist should choose the medium in which a DDS has the highest degree of representation with respect to *in vivo* conditions. Phosphate buffers are used by a pharmaceutical scientist as a rapid means of obtaining a drug dissolution profile that is characteristic of the average intestinal pH environment. Phosphate buffers should therefore be used primarily as a screening tool when an optimised DDS is in the progress of being developed. Hank's and Kerb's bicarbonate buffers should then be used on the optimised DDS to generate a drug dissolution profile that is a closer representation of *in vivo* conditions.

A novel or innovative DDS is often compared to a market gold standard or the leading market competitor. Phosphate buffers simulating physiological conditions are analysed for the market gold standard to generate a drug dissolution profile rapidly and then used again to compare the novel or innovative DDS. The drug dissolution profile of the innovative DDS can then be optimised with respect to the marketed gold standard. Both the market gold standard and the innovative DDS should then be tested in alternative buffers that model the intestinal lumen fluid more closely. Furthermore the volume of buffer available to the marketed gold standard or the novel DDS should be limited during dissolution studies, so that *in vivo* behaviour within fluid pockets may be characterised (McConnell et al., 2008). The pharmaceutical scientist can then decide how to change the DDS if intestinal fluid pocket volumes do not achieve the desired output.

The simulated intestine lumen fluid for *in vitro* testing can be further refined for the fasted state and the fed state (Jantratid et al., 2008). The fasted state may correspond to a medium known as Fasted State Simulated Intestinal Fluid (FaSSIF) whereas the fed state can be represented by a medium known as Fed State Simulated Intestinal Fluid (FeSSIF) (Jantratid et al., 2008). FaSSIF and FeSSIF which have bile salts and phospholipids incorporated into the medium gives a superior representation of *in vivo* conditions with respect to Hank's or Kerb's bicarbonate buffer (Vertzoni et al., 2005; Jantratid et al., 2008). An assessment of the fasted and fed state should also be conducted since the volume and composition of the intestinal fluid during the fed and fasted state have been shown to differ (Schiller et al., 2005). Currently there is no piece of lab equipment or methodology that will predict the behaviour of a DDS *in vitro* with an accuracy that can correlate well with *in vivo* behaviours (McConnell et al., 2008; Jones and Grainger, 2009; Hsiao, 2011). Therefore a pharmaceutical scientist should try conducting a number of drug dissolution procedures using different medium volumes, pH conditions and compositions. This may characterise as fully as possible the *in vivo* behaviour of a DDS targeted at the small intestine.

The small intestine is one of the most active sites in the body for biochemical processes. The small intestine is composed of six different cell types in the epithelium layer that enhance the exchange of nutrients and mediate immunological processes. Protease enzymes secreted from the pancreas into the small intestine has a paramount influence on the bioavailability of PTs (Vlieghe et al., 2010). The total proteolytic enzyme load in the luminal fluid of the small intestine can reach gram quantities (Vlieghe et al., 2010). These proteolytic enzymes are secreted by the pancreas and include enzyme species such as α -chymotrypsin, trypsin, pancreatic elastase, carboxypeptidases A, B, D, N and U (Woodley, 1994). The brush border along the intestinal epithelium also contains a high number of proteolytic enzymes that rapidly degrade PTs (Vlieghe et al., 2010). The brush border secretes a great number of different peptidase species that include dipeptidyl-peptidase IV, prolyl tripeptidyl-peptidase, angiotensin-converting enzyme, leucyl-aminopeptidase, aminopeptidase M, aminopeptidase A, and neprilysin (Woodley et al., 1994). Should PTs manage to escape all of these peptidase species but then be endocytosed by the epithelia cells that line the small intestine, the PTs will get degraded by lysosomal enzyme species such as leukocyte elastase, cathepsins B and cathepsins D (Vlieghe et al., 2010).

2.2.1. The importance of intestinal mucus in the design of an oral peptide therapeutic drug delivery system

Mucus is a semi-permeable barrier that lines the small intestine as well as other organs along the gastrointestinal tract (Cone et al., 2009). Mucus permits an exchange of nutrients, water, gases and other compounds between the intestinal lumen and the blood stream through the small intestine epithelium layer (Cone et al., 2009). Notably the small intestine is covered in the thinnest mucus layer along the gastrointestinal tract which is exceptionally important for the proper functioning of the small intestine and a very attractive factor for a pharmaceutical scientist to consider (Varum et al., 2010). Mucus is constantly secreted by specialised epithelial cells (Goblet cells) which prevent many bacteria and fungi from gaining access to the intestinal epithelium wall (Cone et al., 2009). Due to nearly 10L of mucus secreted each day into the gastrointestinal tract, PTs absorption through the gastrointestinal tract is highly restricted (Powell, 1987; Cone et al., 2009). In addition, mucus is an extremely viscous material (non-Newtonian property), therefore causing further retardation in peptide diffusion through the mucus layer. Mucoadhesive polymers are used to concentrate a drug load at a relatively small portion of the gastrointestinal tract and allow a concentration gradient to form in the localised area. With a higher concentration of localised drug, the pharmaceutical scientist aims to overcome the mucus release per second gradient. A

graphical illustration of the ideal location within the gastrointestinal tract to target peptide therapeutic delivery is shown in **Figure 2.1**.

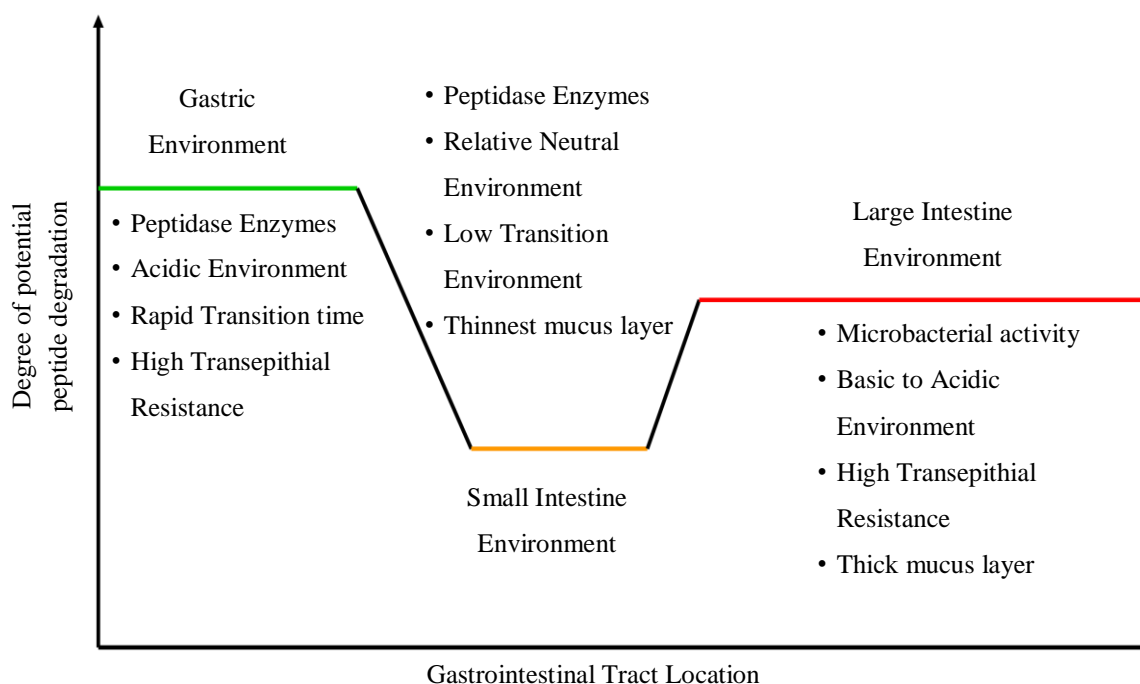


Figure 2.1: Graphical illustration theoretical profile of ideal location within the gastrointestinal tract to target peptide therapeutic delivery (adapted from Cone, 2009).

The mucus secretion in the gastrointestinal tract has been estimated to be at an average rate of between 1 μ m and 100 μ m per second (Powell et al., 1987; Cone, 2009). Within an individual in good health, the average thickness of mucus should remain consistent but vast ranges have been observed from 0 μ m to 300 μ m along the gastrointestinal tract (Powell et al., 1987; Cone, 2009). This is a substantial issue with respect to oral drug delivery systems based on mucoadhesive polymers because of the following aspects:

- If the oral DDS does not encompass an extremely refined and accurate target location within the gastrointestinal tract, the oral DDS will fail to deliver the drug load efficiently.
- If the oral DDS releases the drug load in a region where the mucus layer is too thick for the design, the drug load will not penetrate the mucus layer efficiently.
- If the oral DDS releases the drug load in a region where the mucus layer is too thin for the design, the coadhesion between the DDS, the intestinal epithelium and the mucus layer could be too weak causing the DDS to fail.

The stomach offers the least desirable target for the delivery of PTs. The mucus thickness, from the epithelium layer, in the human stomach has been estimated to be on average

180µm (range 50-450µm) (Kerss et al., 1982; Sandzen et al., 1988; Coperman et al., 1994; Cone 2009) and the gastric pH is as low as 1.2 to 1.7. Since the mucus layer is so thick, it is problematic for peptide therapeutics to move through this semi-permeable layer and reach the epithelium layer of the stomach. Furthermore, the low pH of the stomach causes PTs to undergo acidic catabolism and therefore their breakage to amino acids.

The small intestine has the thinnest layer of mucus throughout the entire human gastrointestinal tract, which appeals to many pharmaceutical researchers as the target site for most oral peptide drug delivery systems (Varum et al., 2010). The thinner mucus layer in the small intestine permits the most effective opportunity for second generation mucoadhesive polymers that not only adhere to the mucus layer but also to the epithelium of the small intestine (Serra et al., 2009). Thus, providing the most prolonged direct interaction with the small intestine epithelium that may afford a more effective application of permeation enhancers. The colon has the second most thick mucus layer of 110-160µm (Kerss et al., 1982; Sandzen et al., 1988; Coperman et al., 1994; Cone, 2009; Varum et al., 2010) but also an astronomical population of enteric bacteria live on the mucus layer. The combination of the thick mucus layer and the presence of enteric bacteria make the colon an undesirable target for delivery of PTs.

The assembly of the peptide therapeutic delivery system should also take into consideration that a reserve of unhydrated mucus is stored in Goblet cells which can be rapidly released in the case of toxic or irritating elements that makes contact with the intestine (Cone et al., 2009). Therefore the DDS should use the least toxic components possible to prevent the rapid release of mucus that will obstruct the movement of the PTs from the intestine lumen through the mucus layer to the epithelium. A unique property of the mucus structure is the unstirred layer, also known as the glycocalyx, which adheres tightly to the surface of the epithelium layer. This layer is between 10nm to 500nm in the gastrointestinal tract and remains present on the epithelium layer even when the mucus layer is removed by chyme (Szentkuti and Lorenz, 1995; Strugala et al., 2003; Cone et al., 2009). This unstirred layer is a considerable challenge to the dispersion of PTs as this layer is more compacted in comparison to rest of the mucus layer. The effect this layer has on the movement of PTs must be minimised, so as to allow PTs to diffuse towards the epithelium surface of the intestine more rapidly. A pharmaceutical scientist could consider a chemical means to reduce the viscosity of the glycocalyx since physical means (the presence of chyme) do not seem to have a significant effect on this layer of mucus.

Mucus contains two main negatively charged functional groups which are carboxyl and sulphate groups (Cone et al., 2009). The sulphate groups form disulphide bonds which causes mucin to fold into its three dimensional structures. The sulphate groups have become a recent target in the design of thiolated polymers (Cevher et al., 2008). The thiolated polymer interacts covalently with sulphate functional groups on mucin which prolongs the mucoadhesiveness of the thiolated polymer. The potential problem with this thiolated polymer is that the polymer could interact with the cysteine amino acids in PTs which could result in PTs becoming inactive or worse immunogenic. Sulphate functional groups are generally incorporated into proteins and peptides to facilitate the formation of covalent disulphide bonds that link peptide strands together or to the peptide strand itself (**Figure 2.2**). An example of this potential interaction can be seen in salmon calcitonin which has 32 amino acids, two of which are cysteine amino acids that forms a disulfide bridge (Cheng et al., 2008). Therefore thiolated polymers may not only interact with the mucin proteins within mucus but also with PTs, potentially resulting in misfolding of these PTs. A pharmaceutical scientist should consider a polymer that has the least potential to interact with PTs but maintains balanced mucoadhesion (a polymer should adhere to the mucus layer but not reinforce the mucus layer).

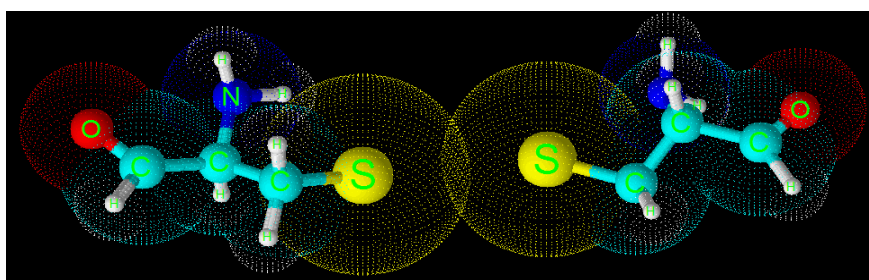


Figure 2.2: Three dimensional representations of two cysteine amino acids. There is a sulphur bond present between the cysteine amino acids.

2.2.2. Tight junctions: a barrier as well as a target

Tight junctions (TJ) are highly regulated orifices that limit toxic substance absorption and regulate the passage of ions between epithelial cells through a process known as paracellular transport (Brandner, 2009). Pharmaceutical scientists that wish to use paracellular transport should consider the dimensions of the peptide therapeutic because the diameter of tight junction orifices range between 30-50Å (Rubas et al., 1996; Morishita and Peppas, 2006). Tight junctions are often considered ridged structures with two functions: a barrier function and a fence function (Brander, 2009). Evidence is increasing being discovered that implicates tight junctions as dynamic structures that are responsive to many stimuli (Kondoh et al., 2008; Steed et al., 2010). Paracellular transport of PTs is very

important because presently this transport mechanism is the only means by which PTs can be absorbed in an undigested state (Kavimandan and Peppas, 2008). Pharmaceutical scientists use permeation enhancers (i.e. β -cyclodextrin) and recently polymers (i.e. chitosan) to increase the bioavailability of drug molecules therefore lessen the amount of drug required to achieve a desired therapeutic index (Ammar et al., 2008). Permeation enhancers are substances that facilitate the transient breakdown of the barrier function within tight junctions (Furuse and Tsukita, 2006). Furthermore, the small intestinal epithelium has the lowest trans-epithelial electrical resistance (TEER) throughout the body that can be practically observed by the highest absorption of salmon calcitonin from the jejunum and ileum in comparison to the stomach or large intestine (Shah and Khan, 2004).

PTs, such as insulin, may be transported intracellular from the small intestinal lumen to the systemic circulation via the epithelial cells but will likely undergo degradation due to exposure to intracellular metalloproteinase enzymes (Bennett et al., 2009). The intracellular degradation of therapeutic agents has led to the development of pro-drugs. Pro-drugs are engineered therapeutic agents that become biologically activated after being exposed to the gastrointestinal tract (Vlieghe et al., 2010). Large PTs that are engineered to be administered as pro-drugs are difficult to develop and expensive to manufacture. Large peptide pro-drug therapeutics has a great number of cleavage sites for proteolytic enzyme activity when exposed to the highly variable gastrointestinal environment. Peptide pro-drug therapeutics may also be lost, because the absorption of these large macromolecules may be challenging to achieve at a therapeutically relevant level. Thus, large PTs that are administered in their native form within a DDS may offer more potential to be effective than the development of large peptide pro-drug therapeutics.

Tight junctions serve as exceptionally beneficial targets for facilitating the oral absorption of native PTs because they act as a direct link between the lumen of the intestine and the systemic circulation. The structural components within tight junctions function dynamically within the cytoplasm of cell, the external environment of the cell and other extracellular proteins (Brander, 2009). The central components that make up tight junction membrane proteins are claudins, occludins and junctional adhesion molecules (JAMs). These components are coupled to the cytoskeleton of the cell through tight junction plaque proteins (Brandner, 2009). Tight junction plaque proteins (ZO-1, ZO-2, ZO-3, cingulin, symplekin, aPKC, Par3, and Par6) mediate the connection between the tight junction membrane proteins and the cell cytoskeleton (Brandner, 2009). In order to open these tight junctions and allow PTs to permeate through these orifices, an appreciation of the tight junction

biological function as well as the extensive intracellular signalling biochemistry and structure is essential.

2.2.3. Main components of tight junctions

The main components of tight junctions are highlighted in **Figure 2.3**. Occludin was the first transmembrane proteins within tight junctions to be identified (Furuse et al., 1993). These proteins have been demonstrated to regulate the permeability properties of tight junctions and in particular the regulation of size-selective diffusion (Balda et al., 1996; McCarthy et al., 1996; Balda et al., 2000). Occludins have been characterised as integral membrane protein that loops four times through the phospholipid layer of the epithelial cell (Furuse et al., 1993; Paris et al., 2008). The two extracellular domains of one occludin protein within a cell interact with two extracellular domains of one occludin protein in an adjacent cell (**Figure 2.3**). Tight-junction plaque proteins ZO-1 (Furuse et al., 1994), ZO-2 (Itoh et al., 1999), ZO-3 (Haskins et al., 1998) and actin (Paris et al., 2008) interact with occludins as well as the cytoskeleton. Cingulin which interacts with actin and myosin also interact with occludin (Cordenonsi et al., 1999). Phosphorylation of occludin on tyrosine using non-receptor kinase c-Yes, has been thought to maintain tight junction integrity (Paris et al., 2008). Occludin is also phosphorylated on serine/threonine residues which may be linked to some signalling cascades (Sakakibara et al., 1997).

The disassembly of occludin from kinase c-Yes due to extracellular reduction of calcium causes the disassembly of the tight junction (Chen et al., 2002). The reduction of calcium from the tight junction with calcium chelation agents such as ethyleneglycoltetraacetic acid (EGTA) or ethylenediaminetetraacetic acid (EDTA) will be discussed as first generation permeation enhancers. Occludin which is phosphorylated on to the serine/threonine amino acids by casein kinase-2 (Andreeva et al., 2001; Smales et al., 2003) and atypical protein kinase C (aPKC) has a significant impact on the core polarity complex (Paris et al., 2008). It has been suggested that phosphorylation of serine/threonine on occludin maintains tight junction integrity (Paris et al., 2008). Therefore a possible permeation enhancer may be a reversible inhibitor of casein kinase-2 or aPKC that may reversibly decrease the tight junction integrity. Occludin is dephosphorylated by protein phosphatase 2A which inhibits the over phosphorylation of occludin (Paris et al., 2008). Thus an alternative tactic for opening tight junctions for peptide therapeutic delivery would be inducing dephosphorylation of occludin, by indentifying a substance which reversibly enhances the activity of protein phosphatase 2A.

Occludin has also been observed to interact with lipid kinases, such as phosphatidylinositol 3-kinase (PI3K) (Sheth et al., 2003). Occludin associates with the p85 regulatory subunit of PI3K and during oxidative stress, PI3K-mediated tight junction disassembly may be induced (Sheth et al., 2003). Another permeation enhancer strategy could be suggested whereby oxidative stress is induced in the epithelial cell, thereby causing the tight junction to open but it should also be understood that many studies have reported that oxidative stress may induce the formation of oncogenes and therefore precancerous cells may form. These are just some of the examples of intracellular regulation mechanisms of occludin.

Claudins are considered to be the major component of tight junctions with over 20 protein isotypes each having four transmembrane domains (Morita et al., 1999). Based on the charge on the two extracellular domains, Claudins have been reported to act as paracellular ion channels or paracellular ion barriers (Simon et al., 1999; Amasheh et al., 2002; Yu et al., 2003). The different isotypes of claudins have been noted to be associated with a specific tissue type (Claudin 3, 4 and 7 are found in the small intestine), therefore a substance which can interact with these claudins transiently, could be incorporated into a drug delivery formulation and therefore aid in the absorption of therapeutic macromolecules (Gonzalez-Mariscal et al., 2008). Claudins interact with tight junction plaque proteins ZO-1, ZO-1, multi-PDZ domain protein-1 (MUPP1), and PATJ (Hamazaki et al., 2002). Each of these plaque proteins have the potential to mediate tight junction opening from within the cell. A schematic representation of the anatomical and biochemical elements at the small intestinal epidermis layer is shown in **Figure 2.3**.

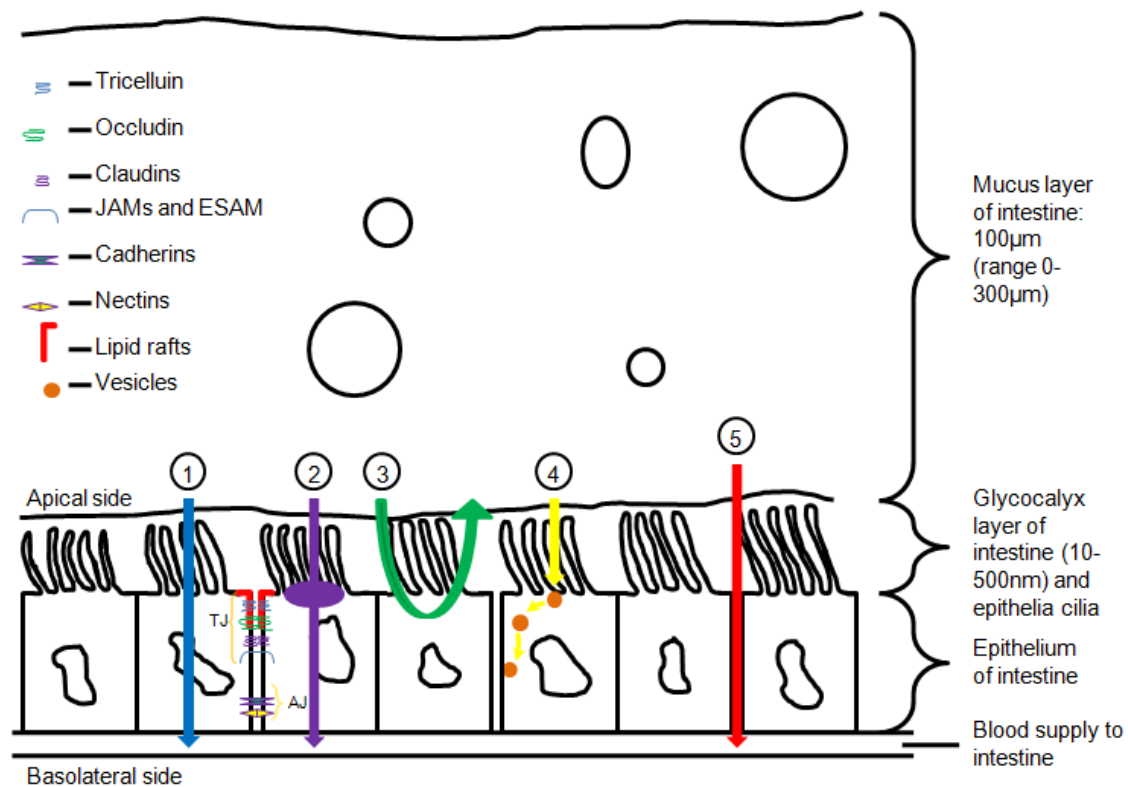


Figure 2.3: A schematic representation of some anatomical and biochemical elements that form the small intestinal epidermis layer depicting the five transport mechanisms that are currently known to occur in the small intestine as: 1) passive diffusion transcellular transport (represented by a blue arrow); 2) active transcellular transport (represented by a purple arrow); 3) carrier mediated efflux which results in the absorption of a compound from the intestinal lumen and its secretion into the intestinal lumen (represented as a green arrow); 4) active vesicle mediated transcellular transport (represented by a yellow line); and passive paracellular transport (represented by a red arrow) which is the most important transport mechanism for the absorption of peptide therapeutics in the oral route (Adapted from Gonzalez-Mariscal et al., 2008; Paris et al., 2008).

2.2.4. Structure and components of tight junctions

The contraction of the perijunctional actinomyosin ring and the protein kinase or phosphatase mediated changes during tight junction protein phosphorylation (Hochman and Artursson, 1994). Intracellular tight junctions (**Figure 2.3**) serve as the rate-limiting barrier for solutes crossing columnar epithelial cells by means of the route between the cells. As bridges, the gap junctions (**Figure 2.3**) regulate solute movement from the inside part of one cell to another. As gates, the tight junctions regulate solute movement from the luminal solution directly into the lateral intercellular spaces, bypassing the cells. As fences, the tight junctions or associated structures presumably also regulate the movement of membrane constituents from the apical cell membrane to the basolateral cell membrane. The cell-cell contact is mediated by cell adhesion protein molecules (CAMs) that participate in spatial organisation and establishment of cell polarity. Tight junctions seal adjacent epithelial cells in a narrow band just beneath their apical surface. Adherens junctions provide strong

mechanical attachments between adjacent cells. Gap junctions are intercellular channels (1.5-2nm diameter) (**Figure 2.3**). These permit the free passage between the cells of ions and small molecules (up to a molecular weight of about 1000Da). They are constructed from 4 (sometimes 6) copies of a family of transmembrane proteins called connexions. Because ions can flow through them, gap junctions permit changes in membrane potential to pass from cell to cell. Desmosomes are localised patches that hold two cells tightly together. They are common in epithelia (i.e. skin). Desmosomes are associated with intermediate filaments in the cytoplasm.

2.3. Permeation enhancers employed in the small intestine

Permeation enhancers are substances that are used to aid the transport of substances (e.g. PTs) through a biological membrane such as the small intestinal epithelia by opening tight junctions. The efficiency of permeation enhancers is often measured as a reduction of transepithelial electrical resistance (TEER). The more effective a permeation enhancer is the more tight junctions or for a longer time period tight junctions are opened, thus the ions flux is increased through the biological membrane due to less resistance (Kondoh et al., 2008). An ideal permeation enhancer is a substance that reversibly opens tight junctions within a definite time period, precisely at a tissue layer, in an instantaneous and unidirectional way (Fasano, 2008). The permeation enhancer should not be toxic (e.g. irritate or damage the biological membrane), but should decompose quickly and be excreted rapidly when absorbed systemically (Fasano et al., 2008). The permeation enhancer should act as a “universal key” which can open tight junctions for a variety of PTs. Currently there are important disadvantages with many of the known permeation enhancers, especially first generation permeation enhancers, such as: low specificity with regard to the tight junction components or the epithelium layer, an influx into the systemic circulation of toxic metabolites or contaminants from the intestinal lumen may occur; and damage to the epithelial lumen may occur resulting in malabsorption of nutrients (Kondoh et al., 2008). **Table 2.2** depicts permeation enhancers that have been tested in the small intestine to facilitate therapeutics absorption which have been divided into first and second generation TJ permeation enhancers. The first generation TJ permeation enhancers are those that do not target specific TJ components whereas second generation TJ permeation enhancers are the ones that target specific components in tight junctions (Kondo et al., 2008).

Table 2.2 Permeation enhancers that have been tested in the small intestine to facilitate therapeutic absorption.

Permeation enhancer	Generation	Location of activity	Reference
ΔG (Zot fragment; 12 kDa)	Second	Duodenum	Salama et al. 2005
AT-1002	Second	Duodenum	Song et al. 2008
Zot (45kDa)	Second	Jejunum and ileum	Fasano et al. 1997; Fasano and Uzzau 1997; Fasano et al. 1995
Zonulin (47kDa)	Second	Jejunum and ileum	Wang et al. 2000
C-CPE	Second	Jejunum	Masuyama et al. 2005; Kondo et al. 2005; Kondoh et al. 2008
Sodium caprate	First	Jejunum and ileum	Kondo et al. 2005; Soderholm et al. 1998; Kondoh et al. 2008
Dimethyl-β-cyclodextrin	First	Jejunum	Shao et al. 1994
NO donors (NOC5, NOC12 and SNAP)		Jejunum and ileum	Yamamoto et al. 2001; Kondoh et al. 2008;
Oleic acid	First	Through out	Fetih et al. 2005, Fetih et al. 2006
EDTA	First	Through out	Kondo et al. 2008
Occludin peptide	Second	Through out	Kondo et al. 2008
FSH-fusion occludin peptide	Second	Through out	Kondo et al. 2008
Trimethyl chitosan	First	Jejunum	Du Plessis et al. 2010
Bile Salts	First	Through out	Kondo et al. 2008

2.3.1. Ethylenediaminetetraacetic acid

Ethylenediaminetetraacetic acid (EDTA) is classified as a zinc and calcium chelator (Bernkop-Schnürch and Krajicek, 1998; Deli, 2009). The reduction of calcium by EDTA leads to the activation of protein kinase C (PKC) thus increasing paracellular transport through tight junctions and adhesion junctions (Citi, 1992; Tomita et al., 1996). Since both tight junctions and adhesion junctions are opened, the diffusion of PTs would be significantly enhanced. EDTA has been reported to increase the transport of polyethylene glycol 4000 (average molecular weight between 3400-4500g/mol) through Caco-2 monolayers (Tomita et al., 1994). Additionally EDTA may augment the swelling and distribution of mucus by chelating calcium ions that crosslink mucin peptides (Chen et al., 2009). This may aid the diffusion of PTs through the mucus layer, towards the epidermal layer of the small intestine.

2.3.2. Sodium caprate

Sodium caprate is a 10 carbon medium chain fatty acid (Deli, 2009). Sodium caprate activates phospholipase C by inducing the contraction of calmodulin-dependent actin-myosin filaments (Aungst, 2000; Kondoh et al., 2008). The contraction of calmodulin-dependent actin-myosin filaments causes the plaque protein ZO-1 and transmembrane protein occludin

to dissociate from the tight junction, thus allowing substances such as mannitol to access the paracellular permeation pathway (Lindmark et al., 1995; Lindmark et al., 1998).

2.3.3. Bile salts

Bile acids are included into pharmaceutical formulations by binding these compounds to sodium to form salts or by mixing with polyoxyethylated hydrogenated castor oil (Muranishi, 1990). The exact mechanism in which bile salts increase the absorption of compounds such as polyethylene glycol 4000 is not known but it has been suggested to be most likely through paracellular transport (Meaney and O'Driscoll, 2000).

2.3.4. Occludin peptides

Occludin peptides are synthetic peptides that bind the extracellular domain of transmembrane protein occludin, thus inhibiting the interaction of occludin molecules on each side of the lateral membrane within tight junctions (Wong and Gumbiner, 1997). This induces the tight junction to open and does not affect other tight junction components such as ZO-1, ZO-2 and cingulin (Wong and Gumbiner, 1997). A short peptide of 14 amino acids that binds to the extracellular loop region of occludin could be a prototype for a new class of TJ modulators in intestinal epithelium (Tavelin et al., 2003). Occludin peptides may be digested in the stomach due to proteolytic enzymes and harsh pH environment before reaching the small intestine. Thus a DDS that has been designed to deliver PTs and use occludin peptides as permeation enhancer will have to protect both peptides. The DDS will also have to ensure that both peptides are co-localised, within a small region of the intestinal wall to ensure that a peptide therapeutic concentration gradient is set up at the same time when occludin peptide is opening the tight junction. The localised occludin peptides are depicted in **Figure 2.4**.

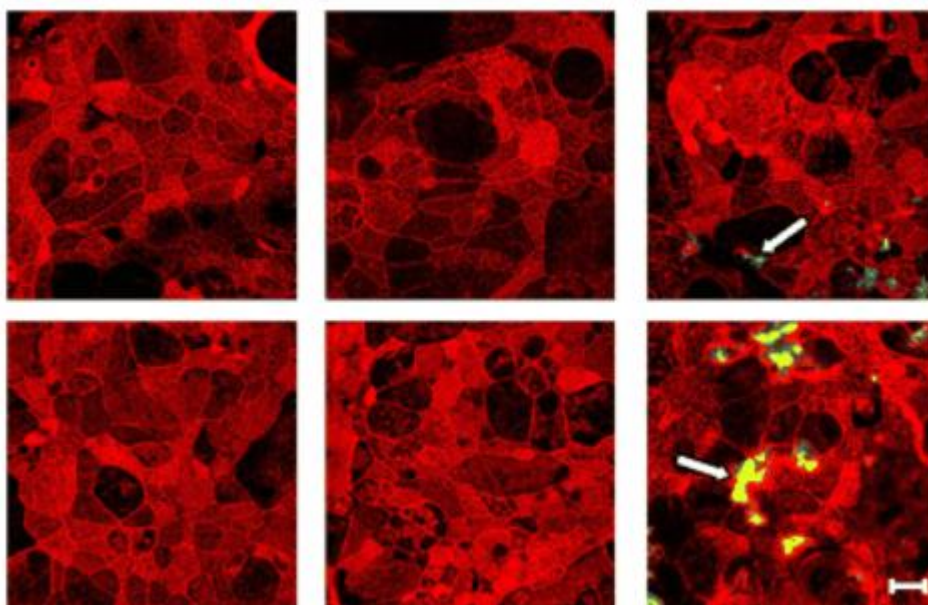


Figure 2.4: Localisation of occludin peptides in confluent T84 cell monolayers which has undergone cation (Ca^{2+}) depletion and elucidation using fluorescence microscopy (adopted from Nusrat et al., 2006). FITC-conjugated streptavidin (green fluorescence) was used to determine the distribution of BAIT peptides after cation repletion and F-actin architecture (red fluorescence) was determined using Alexa 568-phalloidin.

2.3.5. *Clostridium perfringens* enterotoxin

Clostridium perfringens enterotoxin (CPE) is a toxin secreted by the gastrointestinal pathogen *Clostridium perfringens* (Hanna et al., 1992). CPE has been modified to act as a tight junction permeation enhancer by removing the cytotoxic *N*-terminal domain and manufacturing the receptor binding C-terminal (C-CPE) (Hanna et al., 1992). The receptor binding C-terminal has been reported to interact with the second claudin extracellular loop domain, therefore preventing two claudin proteins from adjacent cells interacting with one another (Fujita et al., 2000). The ability of C-CPE to reversibly enhance paracellular transport has been demonstrated to be 400 times greater than sodium caprate in the jejunum (currently used in pharmaceutical formulations) (Kondoh et al., 2005). Even though C-CPE is extremely efficient at decreasing tight junction integrity, this permeation enhancer is a peptide sequence and may be susceptible to extensive acid catabolism within the stomach (Sonoda et al., 1999). Furthermore, C-CPE is not readily available commercially and has not currently received FDA approval in any drug formulations with intent to deliver PTs orally.

2.3.6. Zonula occludens toxin

Zonula occludin toxin (Zot) is a toxin secreted by the pathogenic bacterium species *Vibrio cholera* (Fasano et al., 1991). Zot is a peptide that reversibly opens tight junctions within the small intestine (Fasano et al., 2008). Zot activates protein kinase C α -dependent polymerisation of actin microfilaments that induces the opening of tight junctions (Fasano et al., 2008). Insulin and immunoglobulin G (IgG) have been administered with Zot on excised rabbit ileum and demonstrated significant absorption of these macromolecules (Fasano and Uzzau, 1997). Some of the benefits of Zot as a permeation enhancer are as follows (Fasano et al., 2008):

- Zot is not cytotoxic and therefore does not negatively impact the viability of the intestinal epithelium.
- Zot does not completely inhibit TEER, thus potential toxins may be limited from entering the systemic circulation.
- Zot is a generation 2 permeation enhancer and interacts with specific intestinal receptors.
- Zot does not have activity in tight junctions located in the small intestine which prevents harmful enteric bacterium from entering the systemic circulation and causing sepsis.
- Zot has not been reported to cause systemic side effects when administered orally.
- Zot is a rapid and reversible permeation enhancer within the small intestine that has a half life of 60 minutes.

Zot, like occludin peptide and C-CPE, is a peptide that has not currently received FDA approval as a permeation enhancer for orally administered PTs. Zot peptides may also be significantly degraded within the stomach due to proteolytic enzymes and harsh pH conditions. For any DDS using Zot as a permeation enhancer, there will be a need to protect it from degradation.

2.4. Chitosan and its derivatives as permeation enhancers

Chitosan is a cationic polymer which is derived from chitin through three distinct chemical processes (George and Abraham, 2006). The most common commercially available chitin is derived from crab and shrimp (Roberts, 1992; Shepherd et al., 1997). The shells from crabs and shrimp were the first to be ground to produce chitin powder (George and Abraham, 2005). The ground chitin was then deproteinised by treatment with alkali followed by demineralisation with an acid. Finally the deproteinised and demineralised chitin was deacetylated at high temperatures with an alkali solution to form α -chitosan (George and

Abraham, 2005). The average molecular weight and the degree of acetylation (percentage of primary amino groups in the chitosan backbone) are dependent on the length of duration of the chemical process (Roberts, 1992). Chitosan has been reported to be an extremely effective mucoadhesive agent *in vitro* (Gåserød et al., 1998). Mucoadhesivity of chitosan is a very important property with respect to drug delivery devices. The mucoadhesiveness of chitosan has been reported to improve its residence time thus improving the bioavailability of a loaded macromolecule therapeutic agent by providing an increased time window which the macromolecule therapeutic agent may achieve optimal absorption.

2.4.1. The rationale for consideration of chitosan and its derivatives for orally administered drug delivery systems

A great amount of interest has been shown in chitosan for drug delivery applications because of its reported potential for biocompatibility and biodegradability (Kean and Thanou, 2010). Commercially available chitosan is said to be highly customisable since its average molecular weight can range between 10kDa to 1000kDa and the degree of deacetylation can range between 70% to 95% (George and Abraham, 2005). For this reason, chitosan can be refined to create novel drug delivery systems with very specific properties. The degree of deacetylation and molecular weight determines the solubility of chitosan within an aqueous environment at pH 7 (neutral pH that is relatively similar the pH of the small intestine). It has been observed that increased acetylation of the chitosan crystal structure increases its solubility with neutral aqueous environments hence chitosan in its native form will not dissolve at pH 7 whereas chitosan that has been half acetylated can easily dissolve at pH 7 (Zhang et al., 2006; Sogias et al., 2010). One of the main properties which attract medical researchers to chitosan is the biological activity of chitosan. Chitosan has been reported to open tight junctions in the epidermal layer when the pH of the environment is under 6.5 (Thanou et al., 2001; Yeh et al., 2011). Chitosan therefore can act as a functional component in environments such as the stomach and ocular fluid but presents a problem for the small intestine. The small intestine has a pH of 6.8 which is above the generally accepted pH of chitosan solubility hence chitosan cannot act as a permeation enhancer in the small intestine. In order to make chitosan soluble within neutral aqueous medium derivatives which can dissolve at higher pH values were synthesised such as trimethyl chitosan. **Figure 2.5** and **Figure 2.6** are three dimensional representations of chitosan and trimethyl chitosan, respectively.

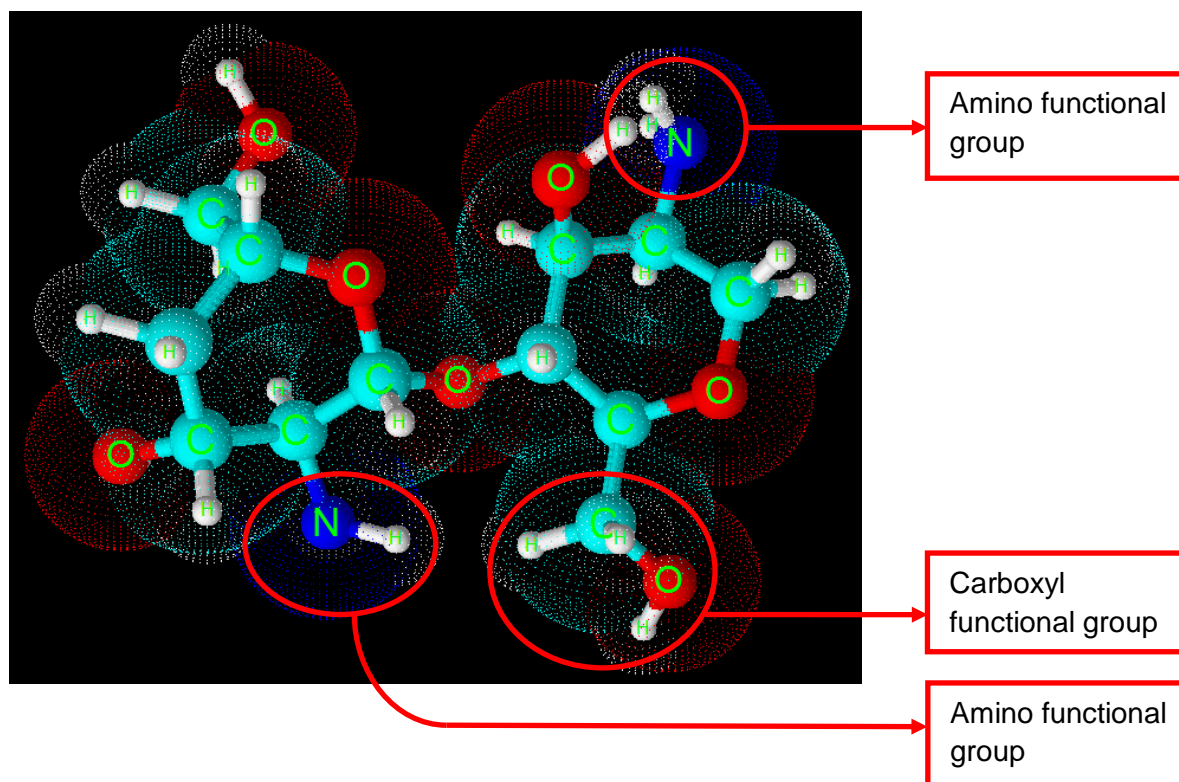


Figure 2.5: Three dimensional representation of chitosan which gives an indication of the optimised ring structure of each chitosan unit. Each functional group in the chitosan back bone is highlighted with a red ring. The functional groups include: a carboxyl and an amino group attached to a ring structure. The atomic radii of each atom in the chemical structure are represented as dotted spheres in the same colour as the source atom. The amino functional group has a positive charge (pKa ~6.5) and is the main functional group that lends chitosan its cationic property.

2.4.2. The chemistry of chitosan and its derivatives

Chitosan contains two units linked by a β 1 to 4 carbon bond; the first unit being 2-amino-2-deoxy-*D*-glucose (*D*-glucosamine) and the second one being 2-acetamido-2-deoxy-*D*-glucose (*N*-acetyl-glucose) (**Figure 2.5**). Chitosan contains many amino functional groups which causes chitosan to swell in response to decreasing pH (more acidic). Therefore chitosan would be a very good functional polymer in environments such as the stomach. But for the use of chitosan in the small intestine where the pH is 6.8, the amount of amino groups needs to be reduced; such that the pH at which chitosan swells is increased.

2.4.3. Trimethyl Chitosan

Trimethyl chitosan (TMC) is a chitosan derivative which has been partially quaternised at the 2-carbon position, in order to make the chitosan backbone soluble in solutions with a pH greater than 6.5 (Verheul et al., 2009). **Figure 2.6** shows a three dimensional representation of trimethyl chitosan. It has been reported in several *in vitro* and *in vivo* models that TMC has

limited toxicity, possesses mucoadhesive properties and can increase the uptake of small drug molecules as well as proteins at various mucosal locations such as the small intestine, nasal passages and in the rectum (Thanou et al., 2000; Hamman et al., 2002; Van der Lubben et al., 2002; Di Colo et al., 2004; Amidi et al., 2006; Boonyo et al., 2007; Chen et al., 2007; Chen et al., 2008; Sayin et al., 2008).

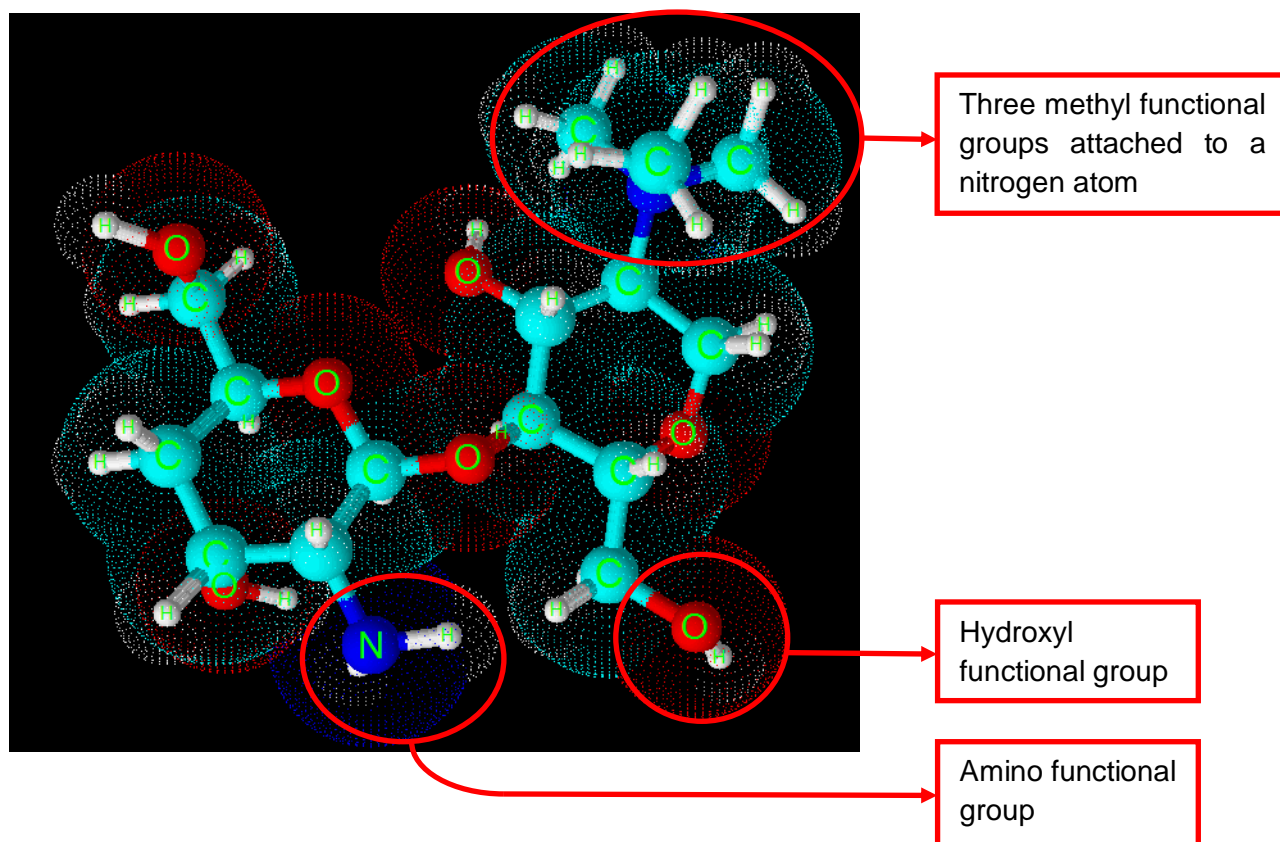


Figure 2.6: Three dimensional representation of trimethyl chitosan with functional groups highlighted in red rings. The atomic radii of each atom in the chemical structure are represented as dotted spheres in the same colour as the source atom.

TMC has recently been formulated in many pharmaceutical forms that range from nanoparticle to macroscopic forms that aim to deliver peptide therapeutics or gene therapeutics and chemotherapeutic compounds (Cafaggi et al., 2011; Guo et al., 2011; Martins et al., 2011; Vongchan et al., 2011). TMC has also been demonstrated in rats to be a potent intestinal absorption enhancer of PTs at neutral environments therefore an oral formulation of trimethyl chitosan that could be tested in humans may be relatively close to finalisation (Thanou et al., 2000; Thanou et al., 2001). TMC facilitates peptide therapeutic absorption by opening tight junctions thereby facilitating paracellular reversible diffusion of PTs from the intestinal lumen into the blood stream (Thanou et al., 2001). The advantage of reversible paracellular diffusion is that after the removal of the polymer from the epithelium surface paracellular orifices close, therefore reducing the potential for toxic metabolites or

pathogens from entering the systemic circulation (Thanou et al., 2001). The degree of quarterisation which has been shown to optimally enhance peptide absorption across epithelium cells is 46%. This is partially important for an optimised oral pharmaceutical formulation that intends to use trimethyl chitosan since this degree of quarterisation reduces the requirement to determine the effect of variant degrees of quarterisation of trimethyl chitosan that would be used in pharmaceutical formulations (Hamman et al., 2003).

Trimethyl chitosan has been reported by different authors to have contradictory properties (Jintapattabakit et al., 2008). An example is the TMC toxicity profile, where some authors have concluded that TMC is non-toxic (Thanou et al., 1999; Amidi et al., 2006; Florea et al., 2006), whereas others have concluded that TMC is a toxic chitosan derivative (Kean et al., 2005; Mao et al., 2005).

Furthermore some authors have reported TMC as having enhanced mucoadhesion capacity with respect to the parent compound chitosan (Sandri et al., 2005) while other authors have reported reduced mucoadhesive properties (Synman et al., 2003; Synman et al., 2004). The contradictory variability of TMC may be due to the procedure of synthesis and the resulting unique TMC properties (i.e. chain length and degree of quarterisation). The mucoadhesivity and cytotoxicity of trimethyl chitosan have been thought to be the result of the interaction between the positively charged methyl groups and the negatively charged groups in mucin (Mao et al., 2005). Thus, a standardised fully described trimethyl chitosan should be developed so that other authors can accurately compare the properties of trimethyl chitosan and refine the chemical nature of this polymer to a form which has optimal functionality but minimal side effects. A standardised means to synthesis trimethyl chitosan could be based on Polnok and coworkers' synthesis which is shown in **Figure 2.7** whereby the methodology is relatively easy to perform and the degrees of deacetylation can be controlled through the various indicated steps (Polnok et al., 2004). In addition, the synthesis of trimethyl chitosan through this methodology could be optimised to produce a product that can be accepted by the FDA as a safe excipient.

The charge density of TMC (as determined by the degree of quarterisation) is an important property with respect to effective absorption enhancement (Kotzé et al., 1999). During synthesis of TMC, the number of positive charges on the TMC backbone is increased by increasing the duration of the alkaline reaction or the strength of the alkaline used (Polnok et al., 2004). The expansion of TMC in alkaline solution is caused by the repelling force between the positive methyl functional groups (Domard et al., 1986). In addition, the thermal

stability of trimethyl chitosan with respect to native chitosan molecule and different counter ions that may be used in the synthesis of trimethyl chitosan has been compared.

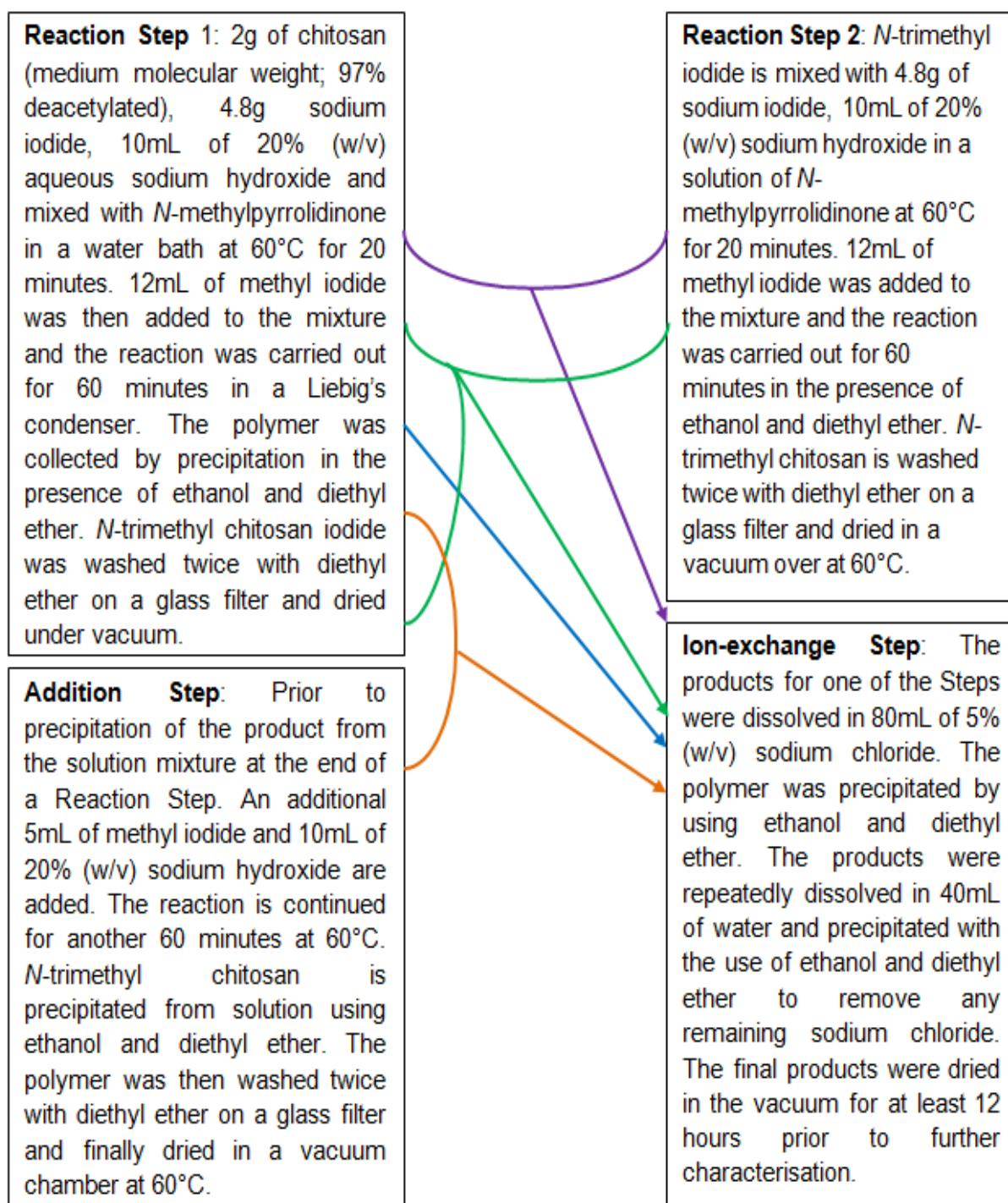


Figure 2.7: Schematic chemical process diagram of trimethyl chitosan using sodium hydroxide. Each coloured line represents a reaction process of 1 to 3 steps.

The differential thermal analysis (DTG) has been determined for a series of different counter ions used in the synthesis of trimethyl chitosan and found to occur at lower DTG peak

temperatures (trimethyl chitosan chloride has a DTG peak of 238.2°C) compared to chitosan which has had a higher DTG peak of 306.4°C thus concluding that trimethyl chitosan variant has a lower thermal stability in comparison to chitosan (de Britto et al., 2011). The stability of trimethyl chitosan variants is an extremely important factor to consider with respect to pharmaceutical products since this stability is a general indication of the shelf life of that variant and therefore an indicator of how long it can remain intact as an active excipient in a pharmaceutical formulation.

The methylation of the primary amine to the quaternary stage is accomplished by using a base to bind the acid that is being generated during the reaction and to avoid the protonation of the unreacted primary amino groups (Polnok et al., 2004). The increased degree of O-methylation at hydroxyl groups has been reported to decrease the solubility of TMC in neutral solutions; therefore methodologies which minimise the degree of O-methylation are highly desired by researchers and pharmaceutical scientists (Snyman et al., 2002; Polnok et al., 2004). High levels of trimethyl substitution at amino groups (above 70%) has led to high levels of methyl substitution on hydroxyl groups found at position 3 and 6 on the chitosan backbone structure (Polnok et al., 2004). The degree of methylation will determine how often nitrogen will be bound to three methyl groups. An example is 60% trimethyl chitosan which indicates that six out of ten nitrogen atoms will be bound to three methyl groups instead to two hydrogen groups. The methyl groups are used to increase the overall positive charge of chitosan and therefore allow trimethyl chitosan to be soluble over a wider pH range. The methylation of chitosan enhances the mucoadhesivity of chitosan.

Polnok and co-workers (2004) attempted to decrease the degree of O-methylation by using dimethylaminopyridine, a weaker alkaline solution (i.e. in comparison to sodium hydroxide). The degree of O-methylation at 3rd and 6th hydroxyl groups was found to have been significantly decreased in some instances but the degree of trimethylation was significantly decreased as well (Polnok et al., 2004). Therefore the use of dimethylaminopyridine would not have produced a degree of trimethylation at the amino group that would significantly enhance peptide absorption from the small intestinal lumen. Formulation scientists should continue the search for nucleophilic catalyst that will enhance trimethylation but reduce O-methylation of chitosan so that synthesised trimethyl chitosan will have optimised peptide therapeutic delivery potential.

The standard methods that have been used by these authors to produce TMC with sodium hydroxide are shown in **Figure 2.7**. The degree of quarterisation was reported to increase significantly with the number of reaction steps when using sodium hydroxide as the base

(Polnok et al., 2004). The green line in **Figure 2.7** represents the three reaction steps which resulted in 77.6% degree of quarterisation whereas the blue line represents one reaction step which resulted in a 29.7% degree of quarterisation. The degrees of O-methylation at 3- and 6- hydroxyl groups also increased with the number of reaction steps (Polnok et al., 2004). The green line in **Figure 2.7** represents three reaction steps which resulted in degrees of O-methylation at 3- and 6- hydroxyl groups as 62.2% and 62.4%, respectively, whereas the blue line represents one reaction step which resulted in degrees of O-methylation at 3- and 6- hydroxyl groups as 17.9% and 25.5%, respectively (Polnok et al., 2004).

Trimethyl chitosan has been used for the oral delivery of salmon calcitonin in the rat model (du Plessis et al., 2010). Trimethyl chitosan was compared to a novel patented DDS Pheroid™ (composed of essential and fatty acids of plant origin which has been emulsified in nitrous oxide saturated water). Salmon calcitonin was administered to the jejunum of the small intestine of rats at a concentration of 500IU/Kg, and then determining the absolute bioavailability using **Equation 2.1**:

$$\text{Absolute bioavailability (\%)} = \left(\frac{AUC_{EV}}{AUC_{IV}} \right) - \left(\frac{Dose_{IV}}{Dose_{EV}} \right) \times 100 \quad (\text{Eq. 2.1})$$

Where:

AUC_{EV} is the area under the curve for extra vascular administration of salmon calcitonin.

AUC_{IV} is the area under the curve for intravenous administration of salmon calcitonin.

$Dose_{EV}$ is the amount of salmon calcitonin that was administered extravascularly.

$Dose_{IV}$ is the amount of salmon calcitonin that was administered intravenously.

Pheroid™ vesicles and microspheres were able to achieve an absolute bioavailability of 3.87% and 4.18%, respectively (du Plessis et al., 2010). TMC at a concentration of 0.5% (w/v) was able to achieve an absolute bioavailability of 6.52%, even though the authors did not indicate the molecular weight, the degree of quarterisation or the degree of O-methylation at the 3- and 6- hydroxyl residues (du Plessis et al., 2010). It should be noted that TMC was injected directly into the jejunum of Sprague Dawley rats; therefore a limited amount of pre-systemic metabolism in the stomach and in the small intestine did not occur. Salmon calcitonin has also been reported to be absorbed most efficiently in the ileum and jejunum region of the small intestine (Shah and Khan., 2004). Noteworthy is that the rat model that has been used is a poor representative model for the human gastrointestinal tract. Thus, an absolute bioavailability could present a poor correlation in human subjects

exposed to the same formulation. A formulation scientist should, when possible, use a large model animal such as the pig in order to obtain better *in vitro* and *in vivo* correlations especially when using extremely small amounts of peptide therapeutic.

2.4.4. Food and Drug Administration approval of chitosan and chitosan derivatives

To date chitosan and chitosan derivatives have not been granted Food and Drug Administration (FDA) approval for use in drug delivery systems (Kean and Thanou, 2010). This is mainly due to the wide range of different substances which are collectively referred to as chitosan (different average molecular weights and different degrees of acetylation). The FDA will only approve a DDS composed of chitosan once it has demonstrated limited toxicity in humans. Currently chitosan has not been characterised fully in terms of *in vivo* degradation but chitosan has been reported to have decreased degradation when the degrees of deacetylation are increased (Xu et al., 2007; Yang et al., 2007). *In vivo* degradation of chitosan within humans has been attributed to three enzymes namely acidic mammalian chitinase and di-*N*-acetylchitobiase. In addition, commercially available chitosan that is derived from shelled fish that may present a problem in patients that have seafood sensitivity (Baldrick, 2010). Even though it has been reported throughout literature that chitosan is a non-toxic, biodegradable and biocompatible polymer (Thanou et al., 2001), the FDA has not yet approved the whole chitosan group as being safe (Thanou et al., 2001). The chitosan derivative, trimethyl chitosan, has been reported to decompose similarly to chitosan by lysozyme processes but the degradation of trimethyl chitosan was pH independent (Verheul et al., 2009).

The oral absorption of chitosan from the small intestine to the systemic circulation is not generally characterised well which presents a further issue for the FDA with regards to the approval of drug delivery systems that are based on chitosan (Kean and Thanou, 2010). It has been generally accepted that chitosan cannot be absorbed orally and therefore it is unlikely to demonstrate biodistribution especially when considering its high average molecular weight (Kean and Thanou, 2010). Weight loss products that are based on chitosan are currently used because these products fall within the weight loss supplement classification; thus chitosan does not need to be FDA approved for these uses. The toxicity of chitosan is also classified according to the degree of deacetylation and the average molecular weight (Schipper et al., 1996; Schipper et al., 1999; Kean and Thanou, 2010). With increased degrees of deacetylation and molecular weight, toxicity of chitosan increases and the visa versa is also the case (Schipper et al., 1996; Schipper et al., 1999; Kean and Thanou, 2010).

2.5. Concluding remarks

The optimisation of pharmaceutical formulations which are designed to deliver peptide therapeutics via the oral route should consider the highlighted features of that was discussed. An example of a peptide drug formulation that is an alternative to parental administration is the FDA accepted nasal formulation of salmon calcitonin that has a bioavailability of only 3% relative to a parentally administered salmon calcitonin. Hence, an oral formulation, for example, of salmon calcitonin that can achieve a bioavailability of 10% to 30% would be a significant, economically feasible option and more over, a far more agreeable administration method for the patient. Any particular pharmaceutical formulation should also attempt to overcome each challenge outlined in this chapter as a single unified entity so that a patient will be more inclined to follow the correct dosing schedule in order to achieve a reasonable therapeutic outcome. The journey begins by developing a none-specific metal chelator solid dosage form that can restrict the divalent cation load within a localized site. Ideally, the chelatory ability of the metal chelator should remain intact, so that maximal chelatory ability can occur at the site of action. If the chelator is already occupied by divalent cations, the compound cannot reduce the localized cationic load at the site of delivery. Therefore, cannot assist the process of oral absorption of the peptide therapeutic at the target site.

CHAPTER 3

Physicomechanical Characterization and Optimization of EDTA-mPEG and Avicel®- EDTA-mPEG *In Situ* Hot Melt Dispersion Mini-Pellets

3.1. Introduction

The development of an oral drug delivery device for therapeutic peptides that will allow patients to avoid the parenteral route of administration, will result in increase patient compliance (Amidi et al., 2010; Makhlof et al., 2011; Dünnhaupt et al., 2012; Pillay et al., 2012). The Oral Ghost Drug Delivery (OGDD) device is a single dosage form that contains distinct entities and is administered as a single unit. The metal chelatory mini-pellet formulation assists with the synergistic enhancement of *in vivo* bioavailability of a therapeutic peptide. This Chapter evaluates the physicomechanical properties of the *in situ* melt dispersion of ethylenediaminetetraacetic acid (EDTA) and the effect of including Avicel® RC/CL type R-591 (Avicel®) has on these *in situ* melt dispersions to facilitate the development of a predictably customizable metal chelating containing entity.

Hot melt dispersion is a process whereby a drug entity is homogenously incorporated within a polymeric matrix without the use of solvent. This comprises a polymeric material that can undergo stable melting and a drug that is thermostable at the melting point of the polymeric material. A hot melt dispersion is a single-step process (polymeric material is melted at required temperature and drug mass is added to the molten polymeric material under constant aggregation) and no solvents are required which is an economical advantage (Breitenback, 2002).

A metal chelator such as EDTA has been utilized for oral delivery of peptide therapeutics because it has been proven that EDTA decreases the localized ionic concentration load thereby reducing mucus viscosity and transiently reducing optimal peptidase enzyme (i.e. *N*-aminopeptidase) activity (Bernkop-Schnürch et al., 1997; Peppas and Kavimandan, 2006; Bravo-Osuna et al., 2007; Whitehead and Mlragotri, 2008). In addition, EDTA has been suggested to enhance permeation of peptide therapeutics through the small intestine (Peppas and Kavimandan, 2006). An example of this can be reviewed in the permeation of hexarelin through the rat distal intestine that achieved an apparent permeation of 2.5 (significantly greater than sodium caprate and palmitoylcarnitine) and allowed for 91% of the peptide drug to be recovered from the rat ileum after 60 min in comparison to 55% of the peptide drug without EDTA present (Westberg et al., 2001). Methoxy polyethylene glycol 2000 (mPEG) is known as a waxy polymer with a low melting temperature. mPEG assisted

in the compatibility of EDTA and enhanced the compressibility of EDTA. Avicel[®] functions as a water-dispersible organic hydrocolloid that is primarily used for suspensions and emulsions. Avicel[®] provides an emulsion or suspension with two primary attributes, namely a structured dispersion element and a protective element (Rudraraju and Wyandt, 2005; Zhao et al., 2011). Avicel[®] was incorporated to determine the effect of an additional excipient to facilitate drug release. Avicel[®] is a spray-dried mixture of carboxymethyl cellulose and microcrystalline cellulose (Rudraraju and Wyandt, 2005; Zhao et al., 2011).

The physicochemical properties of each EDTA-mPEG and Avicel[®]-EDTA-mPEG *in situ* hot melt dispersion mini-pellet formulations were statistically analyzed using regression curve fitting to correlate the change of a physicochemical property with that of changing excipient weight concentration in a predictable manner. A specific physicochemical property degree within a specific formulation can be utilized to calculate, from fitted regression curves, the degree of other measured physicochemical properties such as matrix hardness, matrix resilience, primary disintegration rate, secondary disintegration rate, or total disintegration time.

3.2. Material and methods

3.3. Materials

EDTA ($\geq 99\%$ pure) was purchased from Sigma-Aldrich, mPEG 2000 was purchased from Fluka Analytical, Avicel[®] RC/CL type R-591 (co-dried blend of microcrystalline cellulose and sodium carboxymethyl cellulose) was purchased from FMC, hydrochloric acid from CJ Chem, monobasic potassium phosphate (99.99% pure) and sodium hydroxide ($\geq 98\%$ pure) was purchased from Merck Chemicals.

3.4. Methods

3.4.1. Synthesis of EDTA-mPEG *in situ* hot melt dispersion powder formulations

The *in situ* hot melt dispersion powder formulation of EDTA-mPEG were synthesized at the weight concentration ratios shown in **Table 3.1**. Avicel[®] was added to formulations 6-10 at a constant weight concentration of 33%_{w/w}. The mPEG was first melted to 60°C (two thermometers were utilized, one in a 100mL beaker containing 50mL water and another in within the molten mPEG) were by a calibrated hot plate magnetic stirrer. Once the solid mass of mPEG was melted, EDTA was added to the molten mPEG. The EDTA was

homogenously distributed within the molten mPEG. Once The EDTA-mPEG hot melt dispersion was then allowed to cool under constant stirring. The cool solid mass was then passed through a metal sieve with an aperture of 850µm to form a fine powder.

Table 3.1. Component concentrations (in percent ^{w/w}) within the 10 formulations

Formulation Number	EDTA (%^w/_w)	mPEG (%^w/_w)	Avicel[®] RC/CL R-591 (%^w/_w)
1	10	90	0
2	20	80	0
3	30	70	0
4	40	60	0
5	50	50	0
6	6.7	60.3	33
7	13.4	53.6	33
8	20.1	46.9	33
9	26.8	40.2	33
10	33.5	33.5	33

3.4.2. Attenuated Total Reflectance-Fourier Transform Infrared quantification of EDTA and Avicel[®]

Attenuated Total Reflectance-Fourier Transform Infrared (ATR-FTIR) quantification was performed on EDTA and Avicel[®] at different mass concentrations within potassium bromide (KBr) utilizing a Perkin Elmer Spectrum 2000 FTIR spectrometer with a single-reflection diamond MIRTGS detector (PerkinElmer Spectrum 100, Llantrisant, Wales, UK). Samples were prepared and placed on a diamond crystal and processed by universal ATR polarization accessory for the FTIR spectrum series at a resolution of 4cm⁻¹. The samples were subjected to a pressure of 130psi between the scanning range of 4000-600cm⁻¹ and were scanned to obtain a signal to noise ratio of 10. Beer's Law (**Equation 3.1**) was utilized in order to generate a quantitative analysis of the concentration of EDTA and Avicel[®] which had been serial diluted within potassium bromide.

$$A = \epsilon lc \quad \text{(Eqn. 3.1)}$$

Where *A* is absorbance, ϵ is absorptivity, *l* is path length, and *c* is concentration.

A serial dilution of EDTA and Avicel® was prepared using KBr as the diluent. Accurately weighted EDTA and Avicel® samples were ground with KBr to produce uniform white powder samples of increasing weight concentration of each compound. Unique wavenumber peaks for EDTA and Avicel® was determined from the ATR-FTIR spectra. A corresponding absorbance at the respective wavenumber peak, for each serial dilution, was determined for EDTA and Avicel®. The absorbance of wavenumber peaks ($n=3$) were plotted and a linear regression curve was fitted. The curve gradient was used for determining the absorptivity and path-length (**Equation 3.2**) as a single variable. The single variable (m) and the absorbance at the wavenumber peak was used within **Equation 3.3** to determine the concentration of EDTA and Avicel® from a sample.

$$m = \varepsilon l \quad (\text{Eqn. 3.2})$$

Where m is the gradient of calibration curve, ε absorptivity, and l is path-length.

$$C_{unknown} = \frac{A_{unknown}}{m} \quad (\text{Eqn. 3.3})$$

Where $C_{unknown}$ is the unknown concentration, $A_{unknown}$ is the absorbance of unknown sample at a specific peak, and m is the gradient of the calibration curve.

3.4.3. Determination of EDTA loading using physical separation within deionized water

The weight of entrapped EDTA through physical separation was determined and compared to the loaded EDTA weight within each *in situ* melt dispersion powder formulation. The *in situ* hot melt dispersion powder formulations were accurately weighed into three samples of 500 ± 0.5 mg and dissolved with deionized water for a period of 1 hour (to ensure complete removal of mPEG from the solid phase). The solution of each sample was then separated through filtration utilizing glass filters (0.22 μ m pore size) and placed in an oven at 40°C overnight. The quantity of entrapped EDTA within each sample of the *in situ* hot melt dispersion powder formulations was determined by **Equation 3.4**. This was used to determine the relationship between the effective EDTA entrapment and the loaded EDTA concentrations within each *in situ* hot melt dispersion powder formulation.

$$W_{EDTA} = W_{EDTA \text{ filter}} - W_{filter} \quad (\text{Eqn. 3.4})$$

Where, W_{EDTA} is the weight of EDTA dry mass, $W_{EDTA \text{ filter}}$ is the weight of the dry filter after EDTA was retained in the filter, and W_{filter} is the weight of the dry filter before EDTA was retained within the filter.

3.4.4. Thermal characterization of EDTA-mPEG *in situ* hot melt dispersion/Avicel®-EDTA-mPEG formulations

EDTA-mPEG *in situ* hot melt dispersion powder formulations and Avicel®-EDTA-mPEG *in situ* hot melt dispersion powder formulation samples ($n=3$) were subjected to Differential Scanning Calorimetry (DSC) analysis in a similar manner as previously reported (Prodduturi et al., 2005). Accurately weighed samples ($10 \pm 0.4\text{mg}$) were placed in a $40\mu\text{L}$ aluminium crucible pan. An open crucible system was produced by inducing a 0.2mm hole in the lid aluminium crucible pan, which was then hermetically sealed. The thermal profile of each component that makes up the mini-pellets were compared with the formulation powders to determine any change in thermal properties. DSC protocols were ran within a ramping temperature of 2, 5 and $10^\circ\text{C}/\text{min}$ between the temperature range of $25\text{-}110^\circ\text{C}$ (first run), respectively. Each sample was analyzed again at the same respective heating rate but the temperature range was extended from 25 to 270°C (second run). The heat of fusion, onset of melting, melting peak temperatures and crystallization peak temperatures were determined for each EDTA-mPEG *in situ* hot melt dispersion powder formulations and Avicel®-EDTA-mPEG *in situ* hot melt dispersion powder formulations.

3.4.5. Manufacture of EDTA-mPEG and Avicel®-EDTA-mPEG *in situ* hot melt dispersion powder into mini-pellets

The EDTA-mPEG *in situ* hot melt dispersion powder formulations and Avicel®-EDTA-mPEG *in situ* hot melt dispersion powder formulations were accurately weighed into predetermined weight allotments. A modified punch and die tool was utilized to produce cylindrical mini-pellets with a diameter of 4mm under a hydraulic pressure of 3.45MPa from each accurately weighed allotment. The length of the cylindrical mini-pellets varied depending on the amount of powders used and the compressibility of the formulation. Each mini-pellet which had a weight difference of $\pm 0.5\text{mg}$ of the original allotment weight was discarded. The thickness of the minipellets varied according to the physical amount of the excipient that was utilized for each formulation.

3.4.6. Physicomechanical properties of EDTA-mPEG and Avicel®-EDTA-mPEG *in situ* hot melt dispersion mini-pellets

The EDTA-mPEG and Avicel®-EDTA-mPEG *in situ* hot melt dispersion mini-pellets formulations were evaluated with respect to matrix resilience (MR), matrix hardness (MH) and deformation energy (DE). A calibrated textural analyzer (TA.XT *plus*, Stable Microsystems, Surrey, UK) fitted with a cylindrical steel probe (50mm diameter; for MR) and a flat tip steel probe (2mm diameter; for MH and DE) was utilized. The parameters utilised for the analysis is outlined in **Table 3.2**. All studies ($n=3$) were conducted at standard operating procedures (25°C, 1atm pressure).

Table 3.2. Textural profiling parameters employed for physicochemical characterization of EDTA-mPEG and Avicel®-EDTA-mPEG *in situ* hot melt dispersion mini-pellet formulations

Parameters	MR*(%)	MH* (N/mm)	DE* (J)
Pre-test speed	1mm/s	1mm/s	1mm/s
Test speed	0.5mm/s	0.5mm/s	0.5mm/s
Post-test speed	10mm/s	10mm/s	10mm/s
Trigger type	Auto	Auto	Auto
Trigger force	0.05N	0.05N	0.05N
Load cell	5Kg	5KG	5Kg
Compression strain	Variable	N/A	N/A
Target mode	Stain (40%)	Distance	Distance

*MR: matrix resilience

*MH: matrix hardness

*DE: deformation energy

MR (%) was calculated by the percentage of the ratio between the area under the curve (AUC) of the peak to baseline (after the force was removed; AUC₂₋₃) and the baseline to peak (before the force is removed; AUC₁₋₂) from a Force-Time profile (Murphy et al., 2012). MH (in Newton per millimetre), and DE (in Joules) were both determined based on force-distance profiles. In particular, MH was elucidated from the gradient between the initial force and the maximum force attained, and the DE from the AUC (Murphy et al., 2012). The MH, MR, and DE for each EDTA-mPEG and Avicel®-EDTA-mPEG *in situ* hot melt dispersion formulations were determined ($n=3$). The measurements for each formulation were plotted regression curve fitted to each set of formulations with respect to increasing mini-pellet weight.

3.4.7. Disintegration studies determined from EDTA-mPEG *in situ* hot melt dispersion mini-pellet formulations and Avicel®-EDTA-mPEG *in situ* hot melt dispersion mini-pellet formulations

The disintegration studies of the EDTA-mPEG and Avicel®-EDTA-mPEG *in situ* hot melt dispersion mini-pellet formulations were evaluated on a textural analyzer (TA.XT plus, Stable Microsystems). A speciality probe was attached to the textural analyzer which facilitated disintegration testing. Water soluble glue was used to attach the mini-pellet to the probe head. A reservoir of USP 36 simulated intestinal buffer (pH 6.8) was placed under the probe. The mini-pellet was lowered into the reservoir and as the mini-pellet came in contact with a magnetic gridded base plate, the distance from the magnetic gridded base plate to the surface of the probe head was captured. As the *in situ* hot melt dispersion mini-pellet formulation disintegrates within the simulated intestinal buffer, the probe was lowered and the distance moved over time was captured as a disintegration profile.

The disintegration parameters (primary rate of disintegration, secondary rate of disintegration, and total disintegration time) for each EDTA-mPEG *in situ* hot melt dispersion mini-pellet formulation and Avicel®-EDTA-mPEG was evaluated in triplicate. The obtained data points (including standard deviations) were placed within a scatter plot and a regression curve was applied to these scatter points for each formulation with respect to increasing mini-pellet weights. The parameters utilized for textural disintegration analysis is outlined in **Table 3.3**.

3.4.8. Scanning Electron Microscopy imaging of EDTA-MPEG and Avicel®-EDTA-mPEG *in situ* hot melt dispersion mini-pellet formulations

Scanning electron microscopy (SEM) imaging studies were performed ($n=3$) for each *in situ* hot melt dispersion mini-pellet formulation that had a total weight of 60mg. The surface structures at two locations were obtained per *in situ* hot melt mini-pellet formulation for comparative purposes. Each *in situ* hot melt dispersion mini-pellet formulation was mounted on a stub with silicon tape and sputtered coated with gold for 210s. Each mini-pellet was then placed in a FEI Phenom™ Desktop Scanning Electron Microscopy (The Netherlands, Eindhoven) and SEM images were acquired. The first image obtained was the edge of the *in situ* hot melt dispersion mini-pellet formulation and the second image was obtained in the inner central surface of the *in situ* mini-pellet formulation.

Table 3.3. Textural parameters employed for disintegration characterization of EDTA-mPEG *in situ* hot melt dispersion mini-pellet formulations and Avicel®-EDTA-mPEG *in situ* hot melt dispersion mini-pellet formulations

Mode	Measure force in distance-time
Option	Hold until reset
Pre-test speed	2.0mm/s
Test speed	3.0mm/s
Post test speed	10.0mm/s
Force	10g
Trigger type	Auto - 3g
Load cell	5Kg
Tare mode	Auto

3.4.9. Statistical regression analysis

The standard deviation of each obtained data measurement ($n=3$) was determined using Microsoft® Office Excel® 2007 (Build 12.0.4518.1014, Microsoft Corporation, USA). The obtained data measurements and the standard deviations were plotted within scatter plots using SigmaPlot V11.0 (Build 10.0.0.77, Systat Software Inc., Germany). Regression curves were fitted to the scatter plots and R^2 values for each regression curve were determined using SigmaPlot V11.0. A Shapiro-Wilk test was utilized during the calculation of each regression curve to determine if obtained data measurements were normally distributed populations at an alpha level of 0.05 using SigmaPlot V11.0. In addition, a constant variance test ($P=0.05$) for each regression curve was determined to indicate if the dependent variable remained constant despite a dynamically changing value of the independent variable using SigmaPlot V11.0. The 95% confidence interval and 95% predicted confidence interval was determined for linear regression curves in quantitative ATR-FTIR analysis and physical separation of EDTA from *in situ* melt dispersion powder formulations was obtained using SigmaPlot V11.0.

3.5. Results and Discussion

3.5.1. Determination of entrapped EDTA from EDTA-mPEG *in situ* hot melt dispersion powder formulations

Quantitative ATR-FTIR analysis of EDTA and Avicel® was conducted by serial dilution within KBr which generated a linear standard regression curve (Khoshmanesh et al., 2012) (**Figure 3.1**). The quantitative ATR-FTIR analysis was initially utilized as a non-destructive means to determine the entrapped EDTA weight concentration within each *in situ* melt dispersion powder formulation (Khoshmanesh et al., 2012). The absorbencies ($n=3$) of EDTA and Avicel® increased as the concentrations of these compounds increased within KBr.

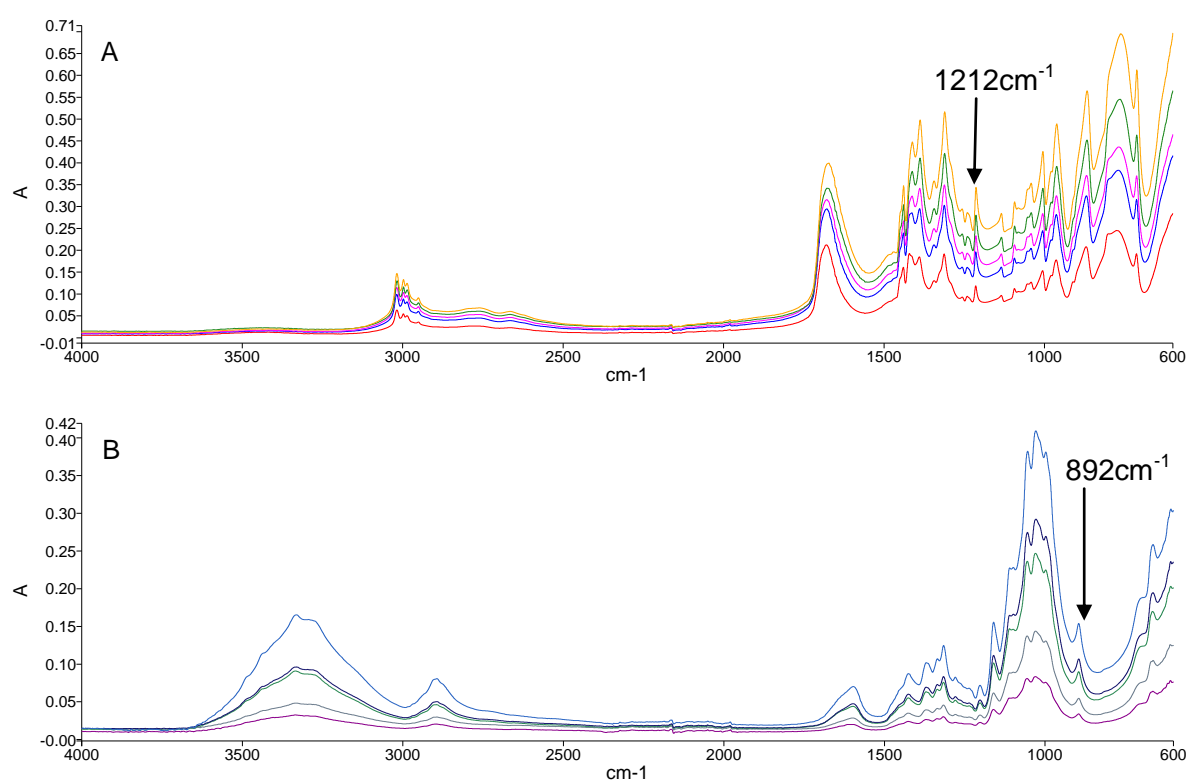


Figure 3.1: ATR-FTIR spectra of different standard EDTA concentrations (A): 10%^{w/w} (red), 20%^{w/w} (blue), 30%^{w/w} (pink), 40%^{w/w} (green) and 50%^{w/w} (orange) used to generate the standard curve. ATR-FTIR spectra of different standard Avicel® RC/CL type R-591 concentrations (B): 10%^{w/w} (light purple), 20%^{w/w} (gray), 30%^{w/w} (green), 40%^{w/w} (dark purple), and 50%^{w/w} (blue) used to generate the standard curve. Each profile was obtained from 100 scans (SNR:10) between a range of 4000-600cm⁻¹ at a constant pressure of 130psi.

The unique wavenumber peak of EDTA and Avicel® was determined at 1212 cm⁻¹ and 892cm⁻¹, respectively. The determined absorbencies ($n=3$) at this wavenumber were plotted and the R^2 adjusted value was determined to be 0.98 for each fitted linear regression curve. The determined absorbencies values remained within the 95% confidence interval and the 95% predicted confidence interval. The fitted linear regression curve passed the normality test

Shapiro-Wilk at an alpha level of 0.05 and the constant variance test ($P=0.05$). The serial dilution of EDTA and Avicel[®] within potassium bromide produced highly predictable absorbencies.

The concentration of EDTA could not be determined accurately because the mPEG had effectively coated EDTA. The ability of ATR-FTIR to detect EDTA within the mPEG melt was restricted because very little surface boundary of EDTA molecule was exposed. An example of this is the entrapment of a drug substance within the core of cyclodextrin (de Sousa et al., 2008). The ability of ATR-FTIR to detect a drug substance within the cyclodextrin core is effectively reduced as the absorption and reflection of infrared light is a surface boundary phenomenon. The infrared light cannot penetrate into the cyclodextrin core or through the mPEG coating of EDTA that allows for the accurate determination of “internalized” compound concentrations. The concentration of Avicel[®] was difficult to determine within the *in situ* melt dispersion powder formulations because this compound is made of methyl cellulose which does not absorb strongly, relatively to EDTA and mPEG.

The loaded concentration of EDTA within *in situ* hot melt dispersion powder formulations were determined by the physical separation of EDTA from the *in situ* hot melt dispersion powder formulations (**Figure 3.2**). The physical separation was conducted within deionized water because EDTA that is not chelated to any metal ion species is highly insoluble within deionized water whereas mPEG is highly soluble within deionized water. The slight predictable deviation, whereby the determined weight of EDTA was higher than the original loaded mass of EDTA, is due to entrapment of mPEG within the filter. The physical separation was conducted within deionized water because EDTA that is not chelated to any metal ion species is highly insoluble within deionized water whereas mPEG is highly soluble within deionized water. The slight predictable deviation, whereby the determined weight of EDTA was higher than the original loaded mass of EDTA, is due to entrapment of mPEG within the filter. The physical separation of EDTA from the *in situ* hot melt dispersion powder formulations allowed for accurate determination of loaded EDTA.

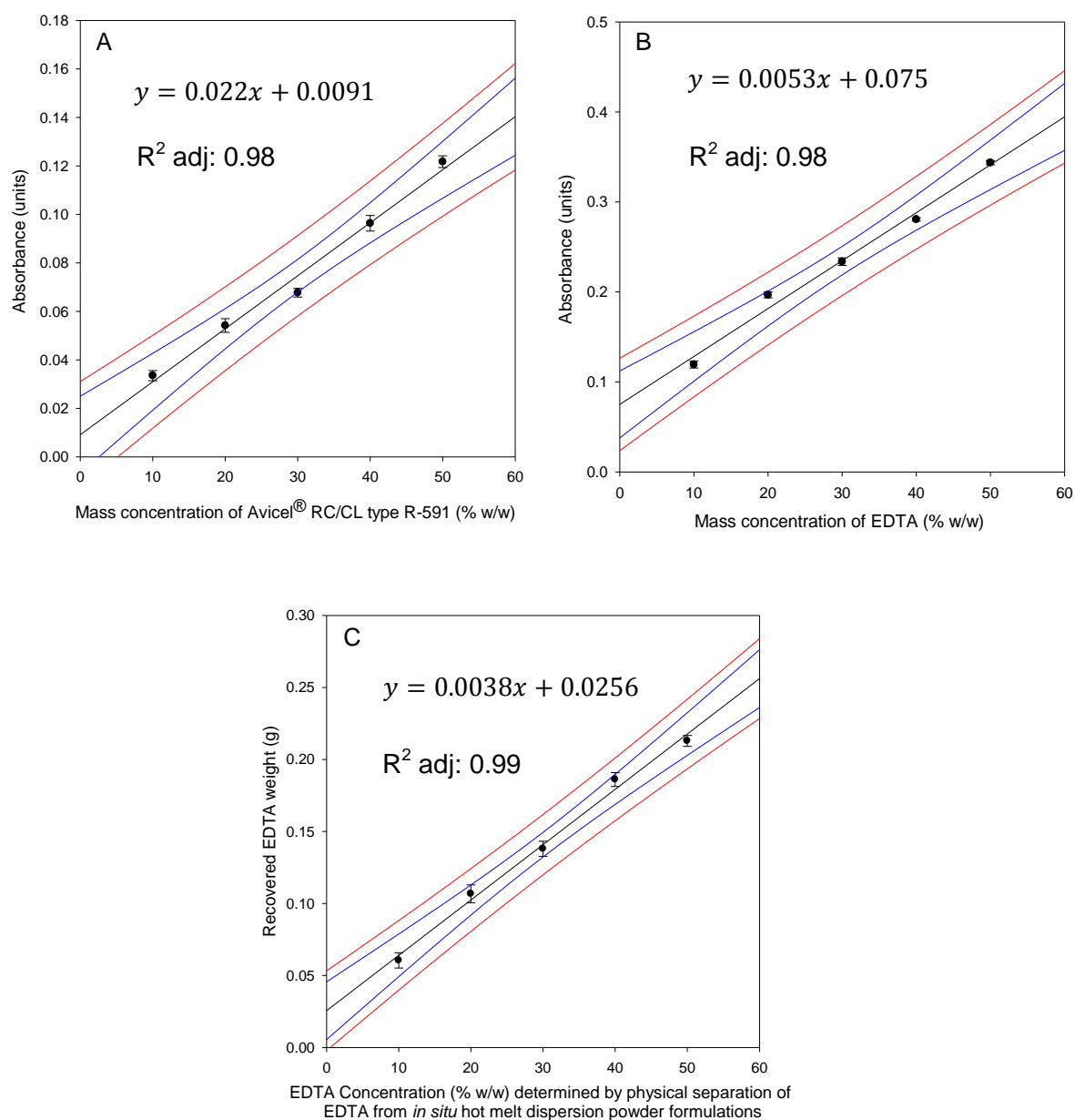


Figure 3.2: Scatter plot of Avicel® RC/CL type R-591 (blue squares) (A) and ethylenediaminetetraacetic acid (B) concentration (in percent w/w) against absorbance units at 892 cm^{-1} and 1212 cm^{-1} , respectively. Scatter plot EDTA weight recovery (C) within increasing EDTA concentration (in $\%w/w$) formulations. A linear regression curve was fitted to each scatter plot and a linear regression curve fitted. Each fitted regression line has an R^2 value, 95% confidence interval (blue line), 95% predicted confidence interval (red line) determined.

3.5.3. Thermal Analysis of EDTA-mPEG *in situ* hot melt dispersion/Avicel®-EDTA-mPEG formulations

The development of an oral pellet dosage form usually requires the homogenous mixing of drug powder excipients and the drug or dissolving the powder excipient within a solvent, the homogeneously mixing powder excipient solutions/suspensions with drug and then removal of

the solvents takes place to generate uniform mixtures (Gu et al., 1990; Breitenback, 2002; Sangnawar et al., 2010). The challenge with mixing drug polymers within a homogenous mixture is the variability that may cause slight deviations in drug concentrations within the powdered excipients but solvent mixing produces industrial pollution and some drugs degrade when exposed to solvents. Melt dispersions allow a reduction in drug loss, a more homogenous distribution with respect to drug, as well eliminating the requirement of solvents.

The heat of fusion, the onset of melting, or crystallization temperature and the peak melting or crystallization temperature for Formulation 1 and 5 in **Figure 3.4** and 6 and 10 in **Figure 3.4**. The crystallization events that occurred during the DSC analysis indicate that amorphous material underwent an enthalpy event to become more ordered in response to heat energy input. Thus, knowing precisely where this may occur can assist formulation processes. The main component that would undergo crystallization within the Avicel[®]-EDTA-mPEG would be Avicel[®] as this component already contains microcrystalline cellulose which may be induced to form additional crystallization upon exposure to heat energy. The DSC results are represented for these formulations because they represent the most extreme weight concentrations of excipients that were utilized in this study. The DSC of the melt of dispersion formulations indicate that EDTA and mPEG formed a physical melt dispersion as the melting points for both compounds did not significantly change. The heating rate of 2°C/min generally obtained the highest heat of fusion and the slower heating rate causes the sample to undergo the process of protracted melting. Interestingly, Formulation 1 which contains EDTA-mPEG (10:90) required 65.34% less heat of fusion energy than Formulation 5 which contains EDTA-mPEG (50:50). The heat of fusion energy required to induce melting in Formulation 6, Avicel[®]-EDTA-mPEG (33:6.7:60.3), was determined to be 66.46% less than Formulation 10, Avicel[®]-EDTA-mPEG (33:33.5:33.5).

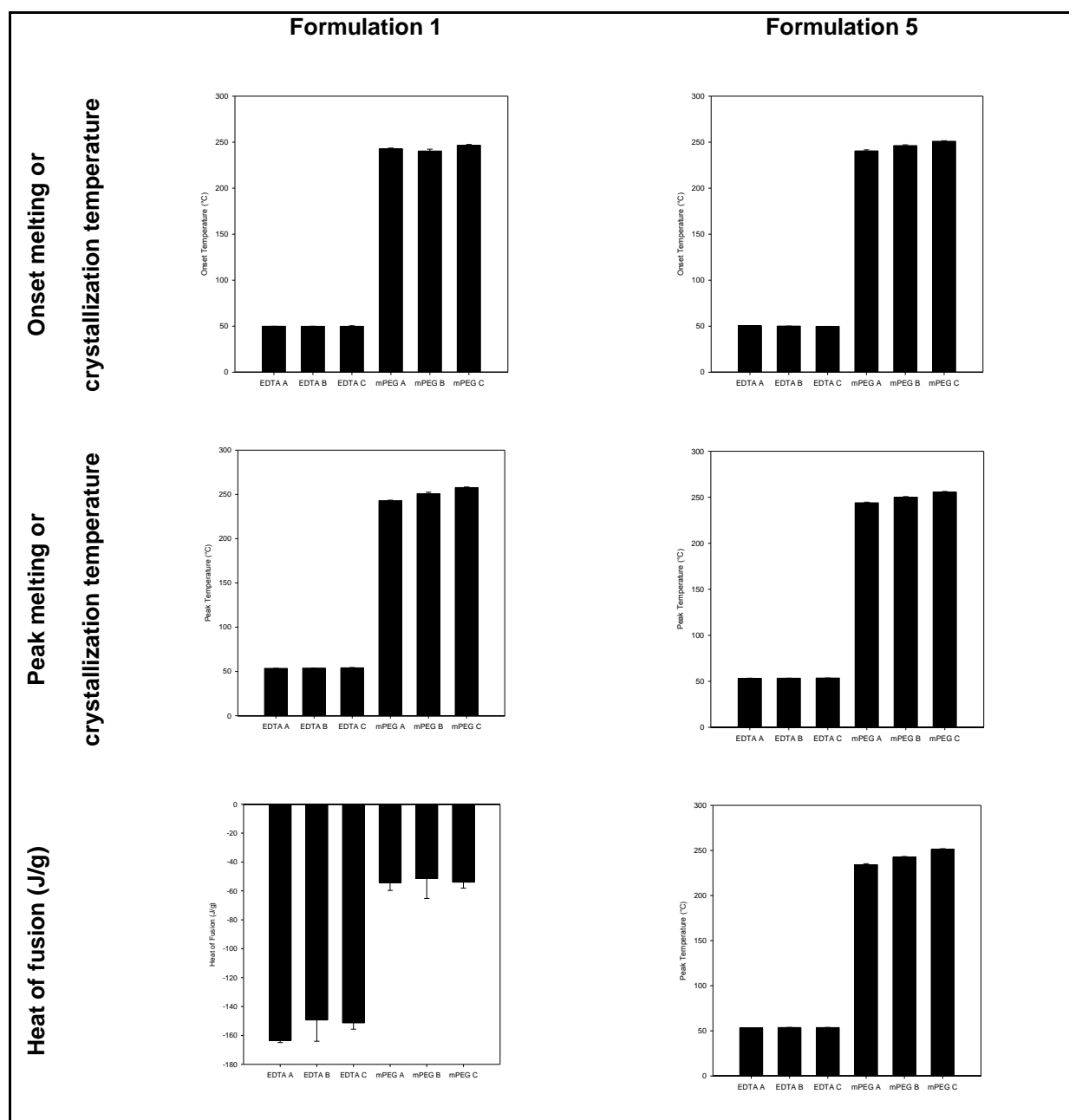


Figure 3.3: Differential Scanning Calorimetry of Formulation 1 (EDTA-mPEG (10:90) *in situ* hot melt dispersion powder and Formulation 5 (Avicel®-EDTA-mPEG (50:50) *in situ* hot melt dispersion powder ($n=3$)).

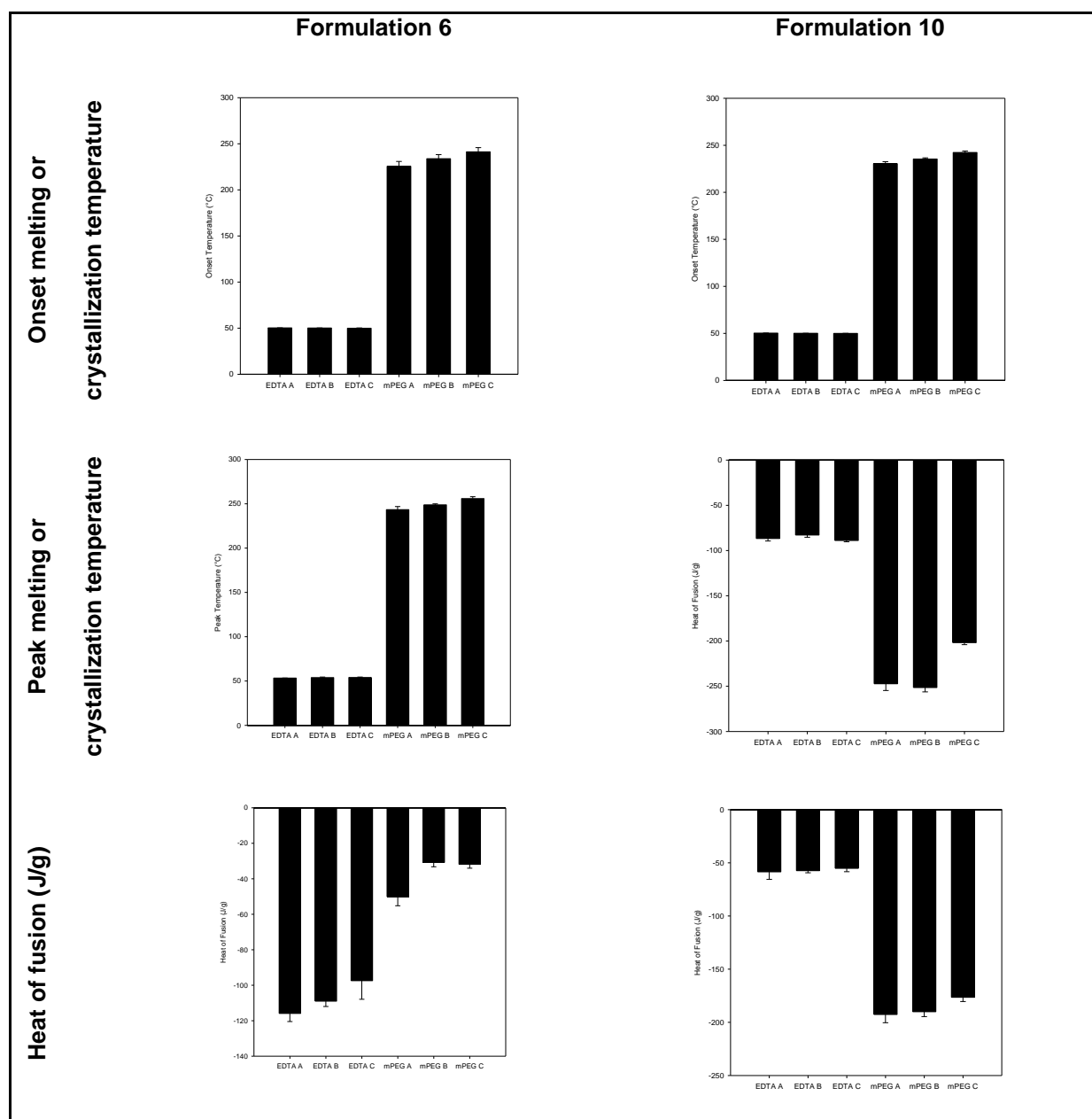


Figure 3.4: Differential Scanning Calorimetry of Formulation 6 (Avicel®-EDTA-mPEG (33:6.7:60.3)) *in situ* hot melt dispersion powder and Formulation 10 (Avicel®-EDTA-mPEG (33:33.5:33.5)) *in situ* hot melt dispersion powder ($n=3$).

3.5.4. Physicochemical properties of the EDTA-mPEG and Avicel®-EDTA-mPEG *in situ* hot melt dispersion mini-pellet formulations

3.5.4.1. Matrix Hardness, Matrix Resilience and Deformation Energies studies

The matrix hardness of a substance is determined at a point of indentation that stresses the local intermolecular bond strength which exists between the powdered granules of the pellet by measuring the amount of force per millimetre required to indent the surface of the pellet.

The greater the force required to cause an indentation within the pellet surface, the greater the bond strength between the powder granules (Ellison et al., 2008). The scatter plots and the fitted regression profile for each formulation are shown in **Figure 3.5** and **Figure 3.6**. The Shapiro-Wilk test passed at an alpha level of 0.05 for each scatter plot and the variance constant test was passed ($P=0.05$) for each regression curve.

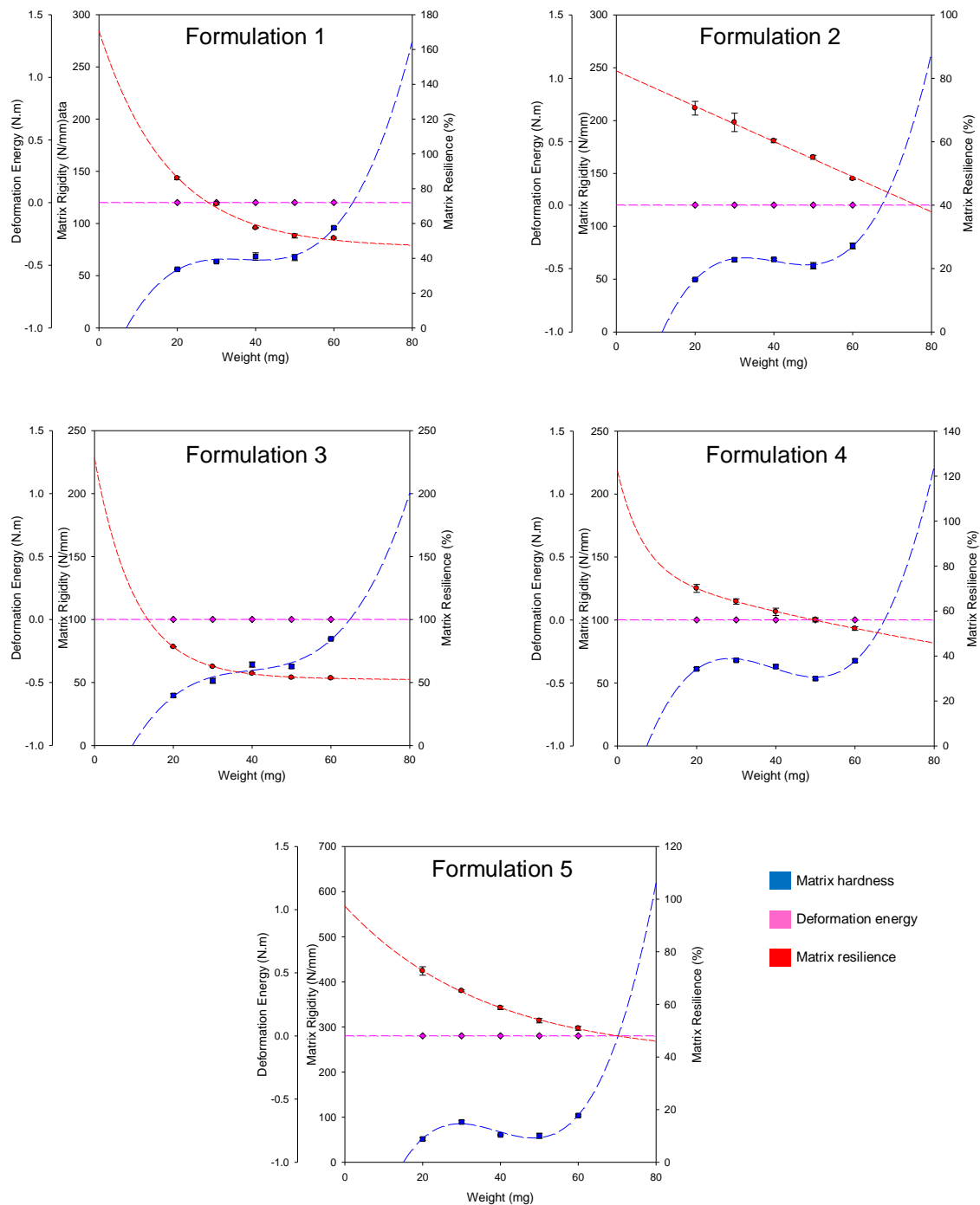


Figure 3.5: Matrix hardness, deformation energy and the matrix resilience regression plots for formulation 1 – 5.

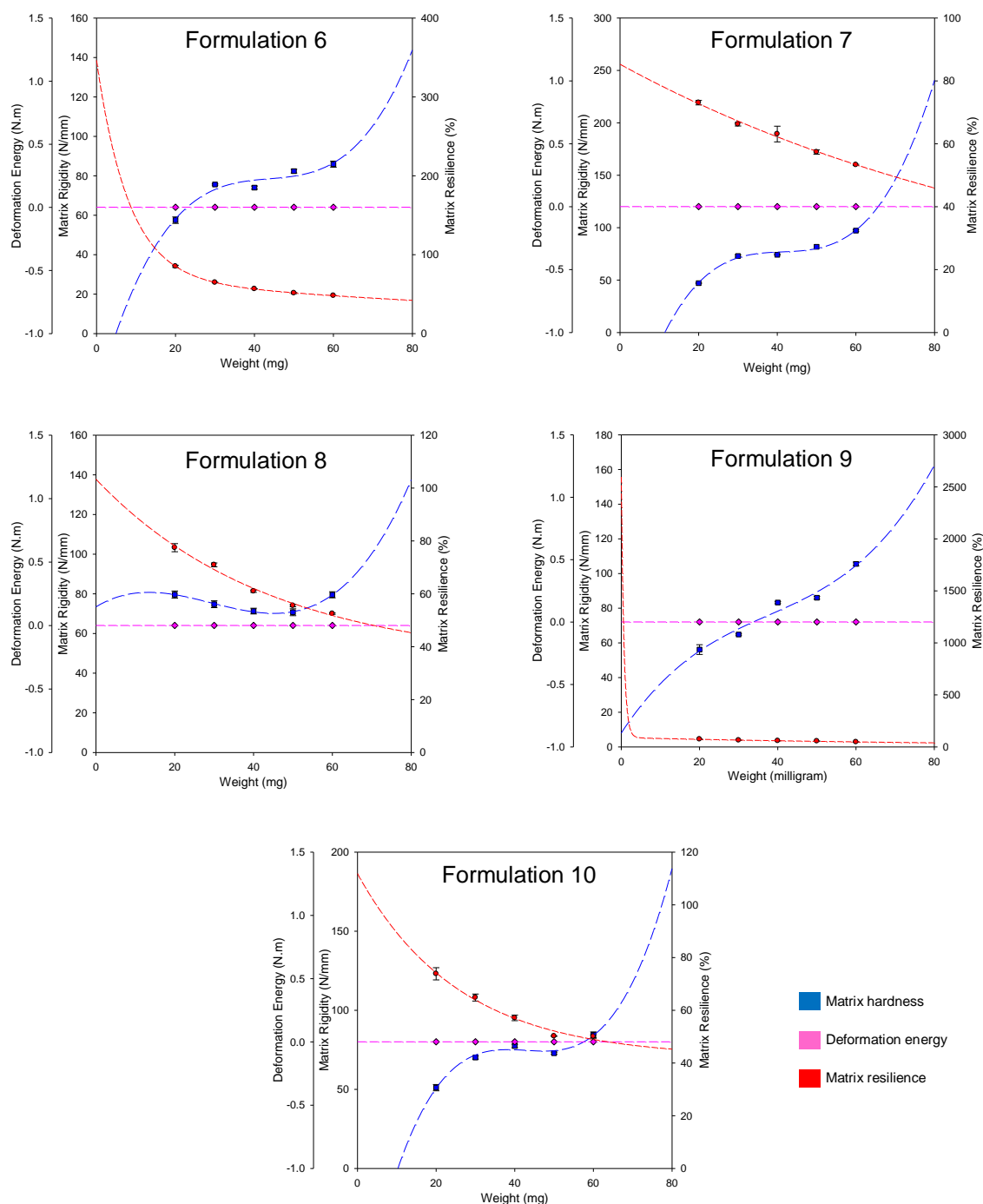


Figure 3.6: Matrix hardness, deformation energy and the matrix resilience regression plots for formulation 6 – 10.

The matrix resilience in these *in situ* hot melt dispersion mini-pellet formulations decreased exponentially since the surface area of void space decreases exponentially as the weight of the mini-pellet for each formulation increased. The exponential decrease in matrix resilience occurred in all formulations that were assessed. The matrix resilience for formulations which contained Avicel® (Formulations 6 and 10) was less than the formulations which did not contain Avicel® (Formulations 1 and 5). Additionally, formulations which had a higher

concentration of EDTA also had reduced matrix resilience. Deformation energy was determined to be constant throughout all the *in situ* melt dispersion formulations than were tested at ~0J. The *in situ* hot melt dispersion mini-pellets were highly resistant to plastic deformation even at high-strain degrees.

3.5.4.2. Disintegration of EDTA-mPEG *in situ* hot melt dispersion mini-pellet and Avicel®-EDTA-mPEG *in situ* hot melt dispersion mini-pellets

The time-distance profile was analyzed and the total time of disintegration, the primary rate of disintegration, the secondary rate of disintegration, and the pellet thickness was determined by the shape of the graph and formulation 1 to 5 in **Figure 3.7** and formulation 6 to 10 in **Figure 3.8** (El-Arini and Clas, 2002). The total disintegration time increased with the increasing concentrations of EDTA within EDTA-mPEG *in situ* hot melt dispersion mini-pellets. Additionally, total disintegration time increased significantly with the addition of Avicel®. Formulation 1 pellets had the fastest disintegration time but the weakest matrix hardness whereas Formulation 10 mini-pellets had the longest disintegration time. The effect that bond strength has on the total disintegration time can be observed when comparing formulations 1 to 5. The weight concentration of EDTA within Formulation 5 was five times greater than in Formulation 1, but the total disintegration time only increased 10 minutes.

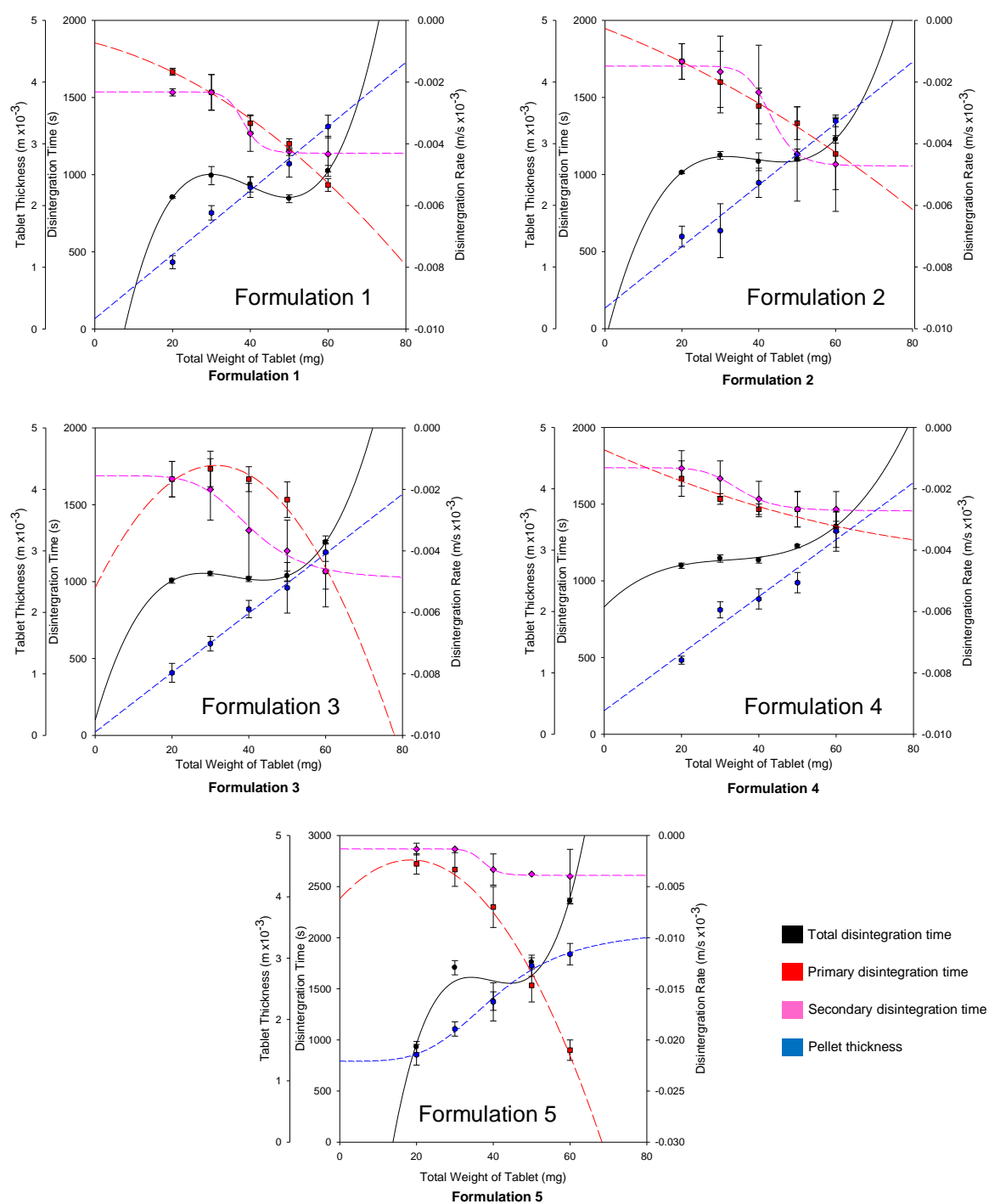


Figure 3.7: Total disintegration time, primary disintegration rate, secondary disintegration rate and mini-pellet thickness regression plots for formulation 1 – 5.

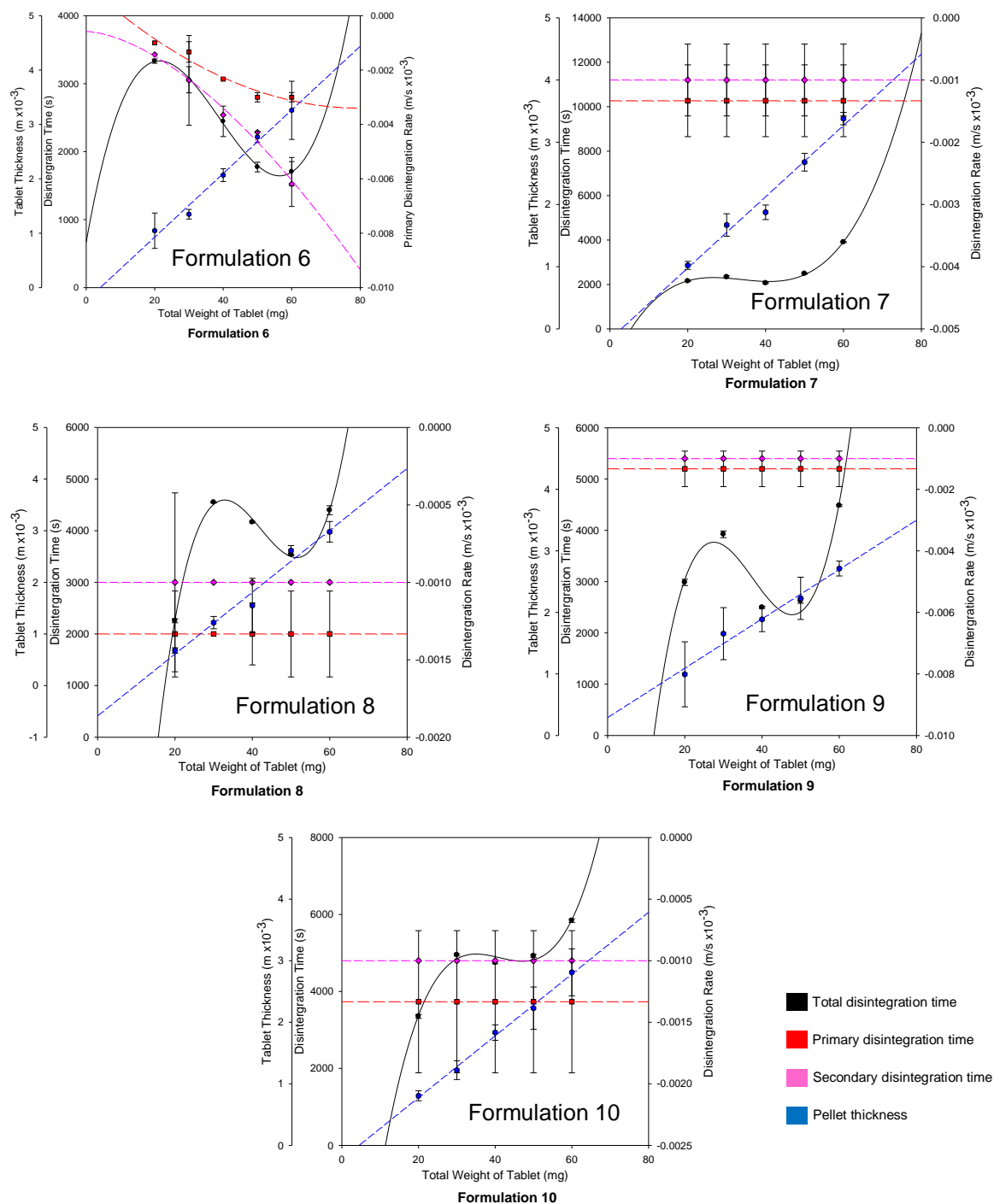


Figure 3.8: Total disintegration time, primary disintegration rate, secondary disintegration rate and mini-pellet thickness regression plots for formulation 6 – 10.

The primary disintegration rate (mm/s) is the breakdown of the *in situ* hot melt dispersion mini-pellet into granules per minute. The primary disintegration rate was determined to be the fastest in Formulation 5 pellets even though the bulk volume was the greatest whereas the primary disintegration rate was the slowest in Formulation 10. The presence of EDTA within mPEG induces faster primary disintegration because once the strong intermolecular bond is broken, the macrostructure of the *in situ* hot melt dispersion mini-pellet breaks down

to granules very rapidly. Whereas Avicel[®] reduces the primary rate of disintegration because the compound effectively eliminated void spaces that resulted in reduced surface area which solvent attack may occur at cold weld spots within the macrostructure of the *in situ* hot melt dispersion mini-pellet. In combination, these compounds could be used to customize the disintegration rate of *in situ* hot melt dispersion formulations in a predictable manner.

The secondary disintegration rate (mm/s) is the dissolution of *in situ* hot melt dispersion mini-pellet granules. The secondary disintegration rate was determined to be the fastest when EDTA weight concentrations within *in situ* hot melt dispersion mini-pellets were at the lowest respective concentrations. This may be a benefit to the *in situ* hot melt dispersion mini-pellet formulations. For example, EDTA in these *in situ* hot melt dispersion mini-pellet formulations would benefit from a slow secondary disintegration rate as this allows the granules of these formulations to penetrate deeper into the mucosal layer and chelate divalent cations deeper within the mucosal layer (Singhal and Curatolo, 2004). The primary disintegration is the rate limiting step of releasing drug during the disintegration process because the solvent can have access only to a relatively small surface area of the mini-pellet. The formation of granules during the secondary disintegration, increases the surface area that the solvent can access and increases the release rate of the drug with respect to the primary disintegration phase.

The successful industrial manufacture of a solid dosage form, such as the *in situ* hot melt dispersion mini-pellets, is dependent on the degree of compressibility a formulation may achieve (Singhal and Curatolo, 2004). The pellet thickness directly indicates the compressibility of the *in situ* hot melt dispersion mini-pellet formulations when compressed at the same force. For example, Formulation 10 had the greatest compressibility, but the entrapped EDTA weight concentration was not the highest of the tested formulations. Whereas Formulation 5 has the highest entrapped EDTA weight concentration but had a reduced degree of compressibility. An additional advantage of the higher compressibility of Formulation 10 is that the formulation weight could be adjusted to compensate for the reduced EDTA concentration with respect to Formulation 5 but maintain an almost equal volume. Therefore, Formulation 10 could achieve all the benefits of including Avicel[®] but maintains a relatively higher or similar EDTA payload to that of Formulation 5.

3.5.5. Surface Morphology Analysis of EDTA-mPEG *in situ* hot melt dispersion and Avicel[®]-EDTA-mPEG *in situ* hot melt dispersion mini-pellet formulations

The surface structure of the *in situ* mini-pellet formulations were viewed from the edge of the *in situ* hot melt dispersion mini-pellet and the center of the *in situ* hot melt mini-pellet using

SEM imaging, as seen in **Figure 3.9**. Formulation 1, which had the highest concentration of mPEG, had the most uniform surface structure whereas Formulation 5 that had the highest concentration of EDTA had a relatively heterogeneous surface structure. Formulations 6 and 10 which contained Avicel® had microcracks in the surface structure which was not similar to those of Formulations 1. The surface structure of the formulation indirectly indicated the physicochemical effect of including Avicel® and EDTA had on the macrostructure of the *in situ* hot melt dispersion mini-pellets. The SEM images of the melt dispersion formulations clearly indicated that the surface topography of EDTA-mPEG *in situ* hot melt dispersion mini-pellets is significantly more uniform than those formulations which contain Avicel®. The mPEG may have compressed at the surface level to fill large void spaces but the ability of the mPEG to fill the void space decreases within the core macrostructure of the mini-pellet.

3.5.6. The customization of EDTA-mPEG and Avicel®-EDTA-mPEG *in situ* hot melt dispersion mini-pellet formulations

The focus of this study was determining the physicochemical effect of Avicel® inclusion on EDTA-mPEG *in situ* hot melt dispersion mini-pellet formulations. Additionally, the predictability of physicochemical properties could be accurately determined from regression curve fitting. This allows for a customizable system to be developed where the physicochemical properties of the formulations is predictable. An example of this are shown in **Table 3.4**. The optimal hardness with respect to *in situ* hot melt dispersion mini-pellet weight was determined from the second derivative of the fitted regression curve equation. The *in situ* hot melt dispersion mini-pellet matrix hardness, total disintegration time, primary rate of disintegration, secondary rate of disintegration, mini-pellet thickness and amount of loaded EDTA can be predicted. The prediction of physicochemical properties of a formulation is not limited to optimal hardness but can be determined for any desired physicochemical property.

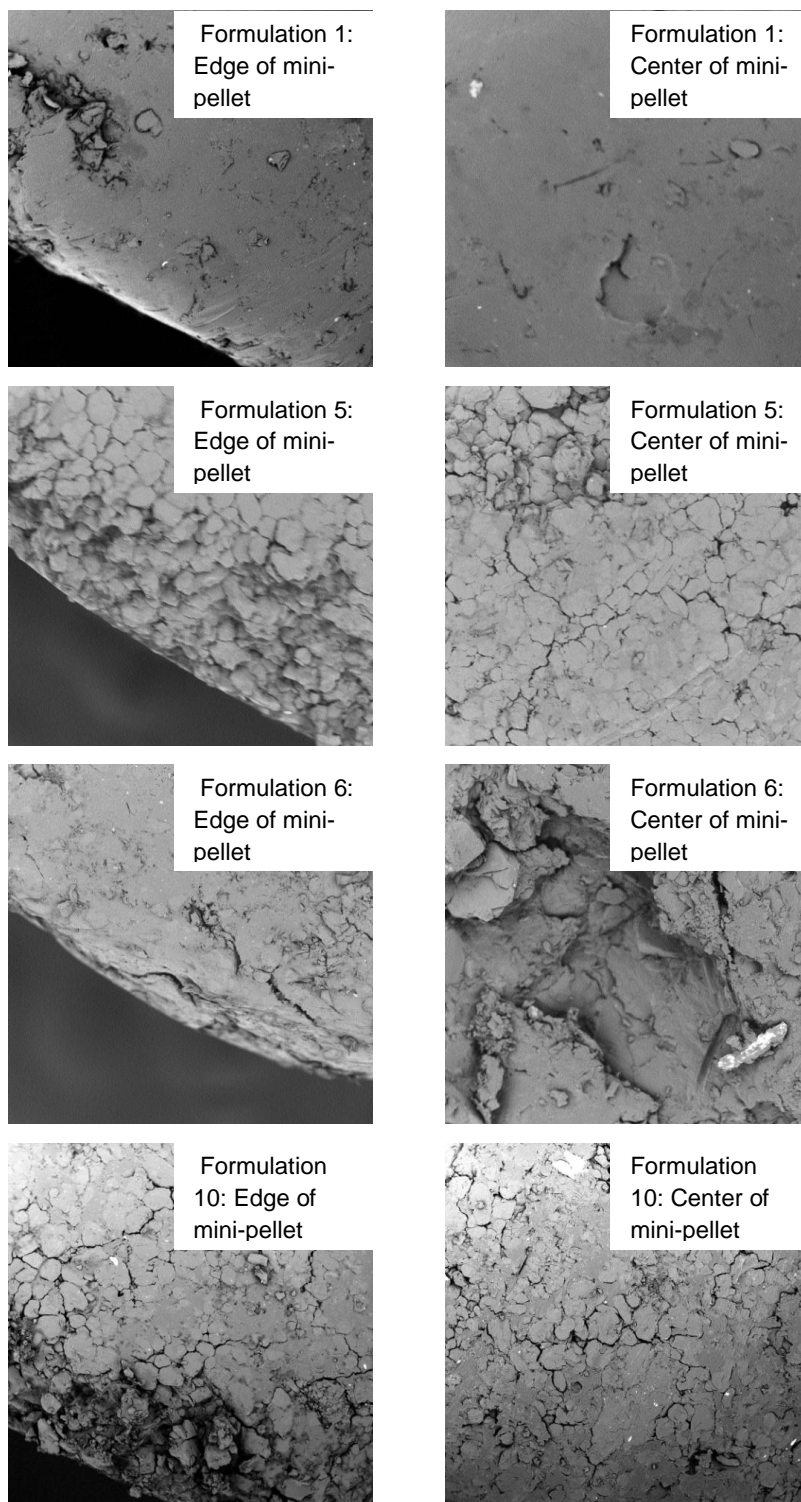


Figure 3.9: Scanning Electron images of the EDTA-mPEG and Avicel®-EDTA-mPEG *in situ* hot melt dispersion mini-pellet formulations.

Table 3.4. The optimal pellet properties determined from regression fitted curves for formulation 1, 5, 6 and 10

Parameter	Formulation 1 pellets	Formulation 5 pellets	Formulation 6 pellets	Formulation 10 pellets
Weight of optimal hardness (mg)	36.284	38.8175	45.0556	36.2778
Matrix hardness (N/mm)	67.28	72.29	75.32	75.53
Total disintegration time (s)	967.717	1587.518	2062.359	4965.965
Primary rate of disintegration (mm/s)	-0.00283	-0.00629	-0.00486	-0.0013
Secondary rate of disintegration (mm/s)	-0.00287	-0.00262	-0.00206	-0.001
Pellet thickness (mm)	2.051	3.079	2.396	1.592
EDTA weight (mg)	3.63	19.41	3.02	12.15

3.6. Concluding remarks

The incorporation of Avicel® RC/CL type R-591 enhanced the physicochemical properties of the *in situ* hot melt dispersion mini-pellet formulations of chelatory agent EDTA. In addition, the incorporation of Avicel® RC/CL type R-591 within the *in situ* hot melt dispersion formulation allowed for extended disintegration to occur. The physicochemical properties, such as matrix hardness or total disintegration time, of these formulations were described using mathematical regression curve fitting. Desired physicochemical properties, formulations were described using mathematical regression curve fitting. A desired physicochemical property degree, within a specific *in situ* hot melt dispersion formulation, can mathematically predicts the degree of other physicochemical properties to create a customizable formulation for a specific application. This would be extremely useful within the OGDD device where the properties of the drug-carrying entity or permeation-enhancing entity can be synergistically enhanced using a predictable customizable EDTA containing *in situ* hot melt dispersion mini-pellet formulation. The selection of the best *in situ* hot melt dispersion mini-pellet formulation could be simply selected from desired physicochemical properties using mathematically determined regression curves to meet the needs of the OGDD device.

CHAPTER 4

pH Responsive Hydrogel Formulations For The Oral Ghost Drug Delivery Device

4.1. Introduction

Targeted pH-responsive oral drug delivery, such as hydrogels, have been utilized to overcome the challenges in optimal drug absorption or reduction of side-effects (Calija et al., 2013; Islam et al., 2013; Lopes et al., 2013; Pandey et al., 2013). The ability of these pH responsive hydrogels to respond to the gastrointestinal pH gradient has been determined within USP dissolution buffers (simulated gastric and simulated intestinal pH). Recently, new biorelevant dissolution fluids have been developed to accurately predict the solubility of drugs or account for a change in drug dissolution profiles of an optimized drug delivery system (Witzleb et al., 2012; Gómez et al., 2013; Sangwai and Vavia, 2013; Takács-Novák et al., 2013). Biorelevant fluids have been suggested to simulate the physiological fluids within the GIT to a higher degree than USP dissolution fluids, especially for charged lipophilic compounds (Vertzoni et al., 2005; Fagerberg et al., 2010). Biorelevant dissolution fluids have been designed to obtain similar surface tension, pH buffer capacity, pH and osmolality that are present physiologically within the human GIT (Jantratid et al., 2009). In addition to human biorelevant dissolution fluids, canine biorelevant dissolution fluids have been designed to increase the *in vitro* and *in vivo* correlation of a drug entity profile during preclinical trial phases of drug development (Arndt et al., 2013). The beagle dog is often utilized during preclinical studies because this model animal is easy to utilize but an average male beagle dog can only achieve a body weight between 7 and 13Kg (Hu et al., 2011; Otabe et al., 2011; Liu et al., 2012). A porcine model is favoured by some researchers as these animals have been suggested to have a very similar anatomical, physiological GIT features to that of humans, can eat a similar diet to humans and can easily achieve the same weight of an adult human (Davis et al., 2001; O'Driscoll and Griffin, 2008).

This *in vitro-ex vitro* study was designed to evaluate a crosslinked acrylamide-methacrylic acid (AAM-MAA) pH responsive hydrogel within drug delivery device. The study was designed to firstly, evaluate the polymerization of crosslinked AAM-MAA hydrogel formulations and remove any of the formulations that underperformed during the synthesis reaction. The dried AAM-MAA hydrogel formulations were then subjected to spectroscopic and thermal analysis to determine the degree of crossed linking of the AAM-MAA at different reacted concentrations. Additionally, the AAM-MAA hydrogel formulations were then subjected to performance evaluation within biorelevant dissolution fluids and isolated porcine fluids. Finally, optimized hydrogel for the current application AAM-MAA hydrogel formulation

was observed through MRI studies within USP dissolution fluids. This study aims to demonstrate the impact that biorelevant dissolution fluids can have on the physicomachanical performance of a pH responsive hydrogel and compare this physicomachanical performance with the physicomachanical performance within isolated porcine fluids. Furthermore, this study also aimed to demonstrate that the altered physicomachanical performance of a pH responsive hydrogel within biorelevant dissolution fluids or isolated porcine gastrointestinal fluids may impact the dissolution profile of a variety of entrapped drugs for three formulations which were either relatively pH insensitive (expanded in acidic and neutral pH media), or contained an equal mass concentration of AAm-MAA or was very sensitive to pH (expanded only in neutral media).

4.2. Materials and Methods

4.3. Materials

Acrylamide ($\geq 98\%$ pure, M_w 71.08g/mol) was purchased from Fluka (Sigma-Aldrich, Buchs, Switzerland). Methacrylic acid (99% pure, 86.09g/mol) was purchased from Aldrich (Schnelldorf, Germany). Tetramethylethylenediamine (99% pure, 116.20g/mol), ammonium persulfate (98% pure, 228.20g/mol), Pluronic F-127, N,N'-methylenebis(acrylamide) (99% pure, 154.17g/mol), sodium hydroxide ($\geq 98\%$ pure), sodium chloride ($\geq 99\%$ pure), hydrochloric acid (37% $^{v/v}$), sodium deoxycholate ($\geq 98\%$ pure), maleic acid (99% pure), lysophosphatidylcholine ($\geq 99\%$ pure), sodium taurocholate ($\geq 90\%$ purity), sodium taurodeoxycholate ($\geq 97\%$ purity), sodium dihydrogen phosphate monohydrate ($\geq 99\%$ purity) were purchased from Sigma-Aldrich (St. Louis, MO, USA). dichloromethane ($\geq 99.9\%$ pure), sodium dihydrogen phosphate monohydrate ($\geq 99\%$ purity), acetic acid (99.99%) and orthophosphoric acid (85% $^{w/v}$, 99.99% pure) were purchased from Sigma-Aldrich (St. Louis, Missouri, USA). Egg phosphatidylcholine (97.5% pure) purchased from Lipoid GmbH (Ludwigshafen, Germany). Acetonitrile ($\geq 99.9\%$ pure) and sodium oleate ($\geq 99\%$ pure) was purchased from Sigma (St. Louis, MO, USA) at UPLC grade.

4.4. Methods

4.4.1. Synthesis of the pH responsive hydrogel to be implemented in the oral ghost drug delivery device

The synthesis of crosslinked acrylamide-methacrylic acid (AAm-MAA) hydrogel formulations was achieved through a modified free radical polymerization (Hames, 1990). Aqueous

solutions of acrylamide and methacrylic acid were prepared (**Table 4.1**). Additionally, solutions of *N,N'*-methylenebis(acrylamide) (BIS), Pluronic F-127 (F127), *N,N,N',N'*-tetramethylethylenediamine (TEMED) and ammonium persulfate (APS) were also prepared accordingly (**Table 4.1**). The monomer solutions were sequentially added to a glass polytop, followed by the crosslinker BIS, deionised water, and surfactant F127. Once the solution was homogenously mixed, free radical polymerization was induced with the addition of APS and TEMED at room temperature (Shibayama et al., 1999). Sodium hydrogen carbonate was immediately added to the polymerizing solution and allowed to generate carbon dioxide gas bubbles within the polymerizing solution for 60 seconds. The polymerizing solution was either poured into cylindrical moulds (0.4mm diameter) and allowed to cure overnight or poured between the cone and plate rheometer to measure the increase of viscosity with respect to time during the polymerization reaction. The hydrogel formulations nomenclature utilized throughout this study will correspond to the nomenclature utilized in **Table 4.1**. For instance, F1 (Formulation 1) will correspond to a hydrogel with a acrylamide concentration of 100%^{w/v} and methacrylic acid concentration of 0%^{w/v}.

Table 4.1. The composition of the crosslinked acrylamide-methacrylic acid hydrogel formulations

Formulation	[AAM] (% ^{w/v})	[MAA] (% ^{w/v})	[MBA] (% ^{w/v})	dH ₂ O	[F127] (% ^{w/v})	[APS] (% ^{w/v})	[TEMED] (% ^{w/v})	NaH CO ₃ (mg)
F1	100	0	2.5	-	10	20	20	100
F2	90	10	2.5	-	10	20	20	100
F3	80	20	2.5	-	10	20	20	100
F4	70	30	2.5	-	10	20	20	100
F5	60	40	2.5	-	10	20	20	100
F6	50	50	2.5	-	10	20	20	100
F7	40	60	2.5	-	10	20	20	100
F8	30	70	2.5	-	10	20	20	100
F9	20	80	2.5	-	10	20	20	100
F10	10	90	2.5	-	10	20	20	100
F11	0	100	2.5	-	10	20	20	100
Volume added to final <i>in situ</i> gelling solution (mL)	3	2	0.7	3	0.3	0.25	0.25	

*[AAM]: concentration of acrylamide

*[MAA]: concentration of methacrylic acid

*[MBA]: concentration of *N,N'*-methylenebis(acrylamide)

*dH₂O: deionised water

*[F127]: concentration of Pluronic F-127

*[APS]: concentration of ammonium persulfide

*[TEMED]: concentration of *N,N,N',N'*- tetramethylethylenediamine

4.4.2. Chemical structure analysis of the crosslinked AAm-MAA hydrogel formulations

Attenuated Total Reflectance-Fourier Transform Infrared (ATR-FTIR) analysis was performed on freshly prepared crosslinked AAm-MAA hydrogel formulations, dried crosslinked AAm-MAA hydrogel formulations, AAm, MAA, MBA, and pluronic F-127. A Perkin Elmer Spectrum 2000 FTIR spectrometer with a single reflectance MIRTGS detector, (PerkinElmer Spectrum 100, Llantrisant, Wales, UK) was utilized for analysis.

Dried samples were prepared by milling and sieved through an 800 μ m aperture sieve to generate fine dried powder particles which could be easily compacted against the diamond crystal. Freshly prepared samples (that were in the semi-solid state) were cut into small pieces which could easily compact against the diamond crystal under 130psi pressure. Samples were placed on a diamond crystal and processed by universal ATR polarization accessory for the FTIR spectrum series at a resolution of 4 cm^{-1} . Each sample was analysed after 100 scans (SNR:10) at 130psi between 650-4000 cm^{-1} range.

4.4.3. Thermal characterization of crosslinked AAm-MAA hydrogel formulations

Differential Scanning Calorimetry (DSC) analysis of crosslinked AAm-MAA hydrogel formulations ($n=3$) were conducted on a indium calibrated Differential Scanning Calorimeter (Mettler Toledo DSC1 STARe System, Switzerland) in a similar manner as reported previously (Prodduturi et al., 2005). Accurately weighed samples ($10\pm0.4\text{mg}$) were placed in a 40 μ L aluminium crucible pan. The thermal profile of each component which makes up the crosslinked AAm-MAA hydrogel and powdered samples of each AAm-MAA hydrogel formulation were analysed to determine any change in thermal properties. DSC protocols were run with a ramping temperature of 2, 5, and 10 $^{\circ}\text{C}/\text{min}$ (first run), respectively. Each sample was analyzed again at the same respective heating rate but the temperature range was extended from 25 - 270 $^{\circ}\text{C}$ (second run). The heat of fusion, onset of melting, melting peak temperatures and crystallization peak temperatures were determined for each crosslinked AAm-MAA formulation hydrogel.

4.4.4. Viscosity analysis of the polymerizing crosslinked AAm-MAA formulation hydrogels

The viscosity (η) of the polymerizing hydrogel formulations were determined at 10 $^{\circ}\text{C}$, 25 $^{\circ}\text{C}$ and 40 $^{\circ}\text{C}$ at shear rate 200 s^{-1} using a Modular Advanced Rheometer (ThermoHaake MARS

Modular Advanced Rheometer, Thermo Electron, Karlsruhe, Germany) equipped with a C35/1° Ti sensor. Measurements were performed employing the rheological parameters shown in **Table 4.2**.

Table 4.2. Rheological parameters utilized for the analysis of gelation initiation within the crosslinked acrylamide-methacrylic acid hydrogel formulations

Parameter	Value
Cone and plate gap	0.0051m
Driver version	0.29
Inertia	89051.00PA
A-factor	$1.721 \times 10^{-6} \text{Kg.m}^2$
M-factor	57.01rad/s
Temperature	10°C, 25°C, 40°C
Damping	30.00

The AAm-MAA monomer solution polymerization was induced with the addition of APS/TEMED, followed by the addition of sodium hydrogen carbonate for 60 seconds. After 60 seconds, the solution was immediately placed between the cone and base plate of the rheometer. The viscosity of the polymerizing hydrogel formulations was measured on 1mL samples for 10800 seconds. The viscosity of the polymerizing hydrogel solutions was measured with respect to time. A solvent trap was utilized to minimize evaporation.

4.4.5. Determination of the gel fraction of the crosslinked AAm-MAA hydrogel formulations

The gel fraction percent was determined as previously described (Hwang et al., 2010). Briefly, the freshly synthesized crosslinked AAm-MAA hydrogel formulations were dried at 50°C in an oven for 6 hours and weighed (W_0), under vacuum. The crosslinked AAm-MAA hydrogel formulations were then placed within Millipore® water for 24 hours and dried in an oven at 50°C, under vacuum. This process was repeated three times to remove any uncrosslinked monomers from the hydrogel matrix. Thereafter the hydrogels were dried at 50°C under vacuum, and placed once again in Millipore® water for 24 hours. The crosslinked AAm-MAA hydrogel formulations were dried and weighed once again (W_e). The gel fraction percent was determined according to **Equation 4.1** (Yoshii et al., 1999; Ajji et al., 2005):

$$\text{Gel fraction percent (\%)} = \frac{W_e}{W_0} \times 100 \quad (\text{Eqn. 4.1})$$

Where W_o and W_e are the weights of the hydrogel samples at the respective conditions.

4.4.6. Powdered X-ray Diffraction to determine the crystallinity of the hydrogel formulations

The powder XRD patterns were determined for the stimuli responsive hydrogel formulations utilizing a Miniflex diffractometer (Rigaku, Tokyo, Japan) with $\text{CuK}\alpha$ (1.5406Å) radiation. The powdered samples were analysed over a 0° to 90° 2-Theta range. The X-ray diffraction patterns were collated with Rigaku software (Version 2.0). The crystallinity degree was determined against XRD reflection that obtained a FWHM degree above 4.0 (reflection marked as amorphous).

4.4.7. Isolation of porcine small intestinal tissue and gastrointestinal fluids

The Large White pigs utilized in this study were obtained according to the *Guide for the Care and Use of Laboratory Animals* that was approved by the Animal Ethics Screening Committee of the University of Witwatersrand (Ethics Clearance number: 2011/33/03). The gastrointestinal fluids isolated from the pigs were collected during the fasted state which was induced by restricting food for 12 hours (water was provided *ad libitum*). The gastric and small intestinal fluids were collected after euthanization. The stomach and small intestine were isolated and a small incision was made to perforate the respective organ wall.

The pH and buffer capacity of the isolated gastric and small intestinal fluids (individual and pooled samples) were measured immediately (Arndt et al., 2013; Dressman et al., 1998). The pooled sample was maintained with an equal addition from each individual sample. To preserve the composition of the gastrointestinal fluid, the samples were immediately frozen in liquid nitrogen and maintained at -80°C (Arndt et al., 2013; Dressman et al., 1998). In order for distance-time studies and drug dissolution studies to be effectively preformed, removal of solid matter (food particles and ingested hay) from the samples was achieved by centrifugation at 5000rpm for 10 minutes at 10°C , followed by filtration of the supernatant through a $0.44\mu\text{m}$ Millipore Millex injection filter (Billerica, MA, USA).

4.4.8. USP 35 and biorelevant dissolution media utilized for the gravimetric swelling analysis and distance-time analysis

The USP 36 simulated gastric fluid pH 1.2 (USP pH 1.2) and USP simulated small intestinal

fluid pH 6.8 (USP pH 6.8) were prepared according to the USP 36. The fasted and fed state biorelevant media (FaSSGF, FaSSIF V2, FeSSIF V2) for the human model was prepared as previously described (Jantratid and Dressman, 2009; Fotaki and Vertzoni, 2010; Klein, 2010). The fasted and fed state biorelevant media (FaSSIFc, FaSSGFc pH 1.5, FaSSGFc pH 6.5) for the canine model was also prepared (Arndt et al., 2013).

4.4.9. Gravimetric swelling analysis of the crosslinked AAm-MAA hydrogel in USP simulated gastrointestinal and biorelevant fluids

Gravimetric swelling analysis of the crosslinked AAm-MAA hydrogel formulations was conducted as previously described, with a slight modification (Singh, 2007; Singh and Pal, 2012; Némethy et al., 2013). Briefly, dried crosslinked AAm-MAA hydrogel formulations (1cm length, 0.4cm diameter), were placed in the biorelevant fluids (FaSSGF pH 1.6, FaSSIF pH 6.5, FeSSIF pH 5.0, FaSSGFc pH 1.5, FaSSGFc pH 6.5, FaSSIFc pH 7.5), United States simulated gastrointestinal fluids (USP pH 1.2 and USP pH 6.8) and Millipore® water. The initial weight of each dried crosslinked AAm-MAA formulation hydrogel was determined at time zero. At predetermined time intervals (once every 30 minutes until 7 hours after initial weighing and once again after 24 hours), the crosslinked AAm-MAA formulation hydrogels were patted dry with absorbent tissue paper and weighed. Once all the weights of the samples were obtained over the time interval, the percent of swelling was determined according to the following **Equation 4.2**:

$$SP\% = \frac{W_{T_x} - W_{T_0}}{W_{T_0}} \times 100 \quad (\text{Eqn. 4.2})$$

Where $SP\%$ is the swelling percent, W_{T_x} is the weight at time X and W_{T_0} is the weight at time 0.

A scatter plot was generated from the swelling percent ($n=3$) at specific time points. A regression curve was fitted to the scatter plot and the rate of swelling percent was determined with respect to time was determined from the gradient of the regression curve. Additionally, the area under the curve (AUC) was calculated for each profile.

4.4.10. Distance-time studies of the crosslinked AAm-MAA formulation hydrogels

The distance-time studies of the crosslinked AAm-MAA formulation hydrogels were evaluated on a textural analyzer (TA.XT *plus*, Stable Microsystems) using a modified

methodology for the evaluation of disintegration (El-Arini and Clas, 2002). A textural probe was utilized to capture the swelling distance-time profile. Water soluble glue was used to attach the crosslinked AAm-MAA hydrogel formulations to a probe head which magnetically attached to the probe shaft. The reservoir contained 5mL of dissolution fluid (FaSSGF pH 1.6, FaSSIF pH 6.5, FeSSIF pH 5.0, FaSSGFc pH 1.5, FaSSGFc pH 6.5, FaSSIFc pH 7.5, USP pH 1.2, USP pH 6.8 or Millipore® water) or isolated porcine gastrointestinal fluids. The crosslinked AAm-MAA formulation hydrogel was lowered into the reservoir and as the crosslinked AAm-MAA hydrogel formulation comes in contact with the magnetic gridded base plate, the distance from the gridded base plate to the surface of the probe head is measured. The magnetic gridded plate is approximately 5cm in diameter with an etched grid pattern to facilitate the free movement of solvent under a placed dosage form. In addition, the magnetic gridded plate contains holes within intersections of the gridded pattern to enhance the free movement of solvent around the placed dosage form. The crosslinked AAm-MAA hydrogel formulation swells within the dissolution media or isolated porcine gastrointestinal fluid against a constant downward force of 0.01N exerted by the probe. The probe is moved upwards once the swelling force exerted by the hydrogel can overcome the constant downward force and this distance with respect to time is measured. The procedure was repeated in triplicate and the parameters utilized for this procedure is shown in **Table 4.3**.

Table 4.3. Parameters utilized to obtain the swelling distance-time profiles for crosslinked acrylamide-methacrylic acid hydrogel formulations

Mode	Measure Force in distance-time
Option	Hold until reset
Pre-test speed	2.0mm/s
Test speed	3.0mm/s
Post-test speed	10.0mm/s
Force	10g
Trigger type	Auto-3g
Load cell	5Kg
Tare mode	Auto

Specific time points (once every 600 seconds for 10800 seconds) were selected and the corresponding distance moved by the probe was determined. These measurements ($n=3$) were placed within a scatter plot, and a regression curve was fitted to the scatter plot (data not shown). The distance-time was determined for each time point and plotted within a three

dimensional bar graph. The distance-time point at each time point was determined according to **Equation 4.3**:

$$DT = \frac{D_x - D_0}{T_x - T_0} \quad (\text{Eqn. 4.3})$$

Where DT is the distance-time, D_x and D_0 is the distance moved at point x and at time point 0, respectively. T_x and T_0 is the corresponding time at point x and at time point 0, respectively.

4.4.11. The porosimetric characteristics of crosslinked AAm-MAA hydrogel formulation 6

The surface area and porosity analysis was performed on the F6 with respect to time points 120 minutes, 240 minutes and 1440 minutes within USP pH 1.2, USP pH 6.8 and Millipore® water utilizing a Porosimetric Analyzer (Micromeritics ASAP 2020, Norcross, GA, USA). The porosity analysis was conducted for F6 only because this formulation was utilized for the finalized OGDD device and the time points were selected to demonstrate how the hydrogel initial swelling influences porosity and the porosity achieved after equilibration. This formulation demonstrated sensitivity to the pH environment and could withstand a compressive force. The F6 hydrogels were initially swelled within the aforementioned dissolution fluids, at the respective time points a sample hydrogel was removed and then flash frozen with liquid nitrogen at the respective time. The F6 samples were then lyophilized in order to remove the respective solvent but maintain the architecture of the hydrogel sample. The respective parameter settings utilized for the porosimetric analysis are shown in **Table 4.4**.

Table 4.4. Parameters utilized for the porositometric analysis of crosslinked acrylamide-methacrylic acid hydrogel formulations

Parameter	Rate/target
Temperature ramp rate	10°C/min
Target temperature	40°C
Evacuation rate	50.0mmHg/s
Unrestricted evacuation from	30mmHg/s
Vacuum set point	500µmHg
Evacuation time	60min
Temperature ramp rate	10°C/min
Hold temperature	30°C
Hold time	900min

Subsequent to complete degassing, the sample tube was transferred to the analysis port where the surface area, pore volume, and pore size was obtained in accordance with Barrett-Joyner-Halenda (BJH) and Brunauer–Emmett–Teller (BET) theories. The BET gas absorption theory is conducted in a two-stage process (Sing et al., 1985). The BET equation was used in the linear form to determine the monolayer capacity based on **Equation 4.4**.

$$\frac{p}{n^a (p-p_0)} = \frac{1}{n_m^a \times C} + \frac{(C-1)p}{n_m^a C p_0} \quad (\text{Eqn. 4.4})$$

Where, n^a refers to the quantity of N_2 absorbed at the relative pressure $\frac{p}{p_0}$, n_m^a was the monolayer capacity and C was exponentially related to the enthalpy of absorption in the first absorption layer.

The total and specific surface area was determined from the monolayer capacity using **Equation 4.5** and **Equation 4.6**.

$$A_s(BET) = n_m^a \times L \times a_m \quad (\text{Eqn. 4.5})$$

$$a_s(BET) = \frac{A_s(BET)}{m} \quad (\text{Eqn. 4.6})$$

Where $A_s(BET)$ and $a_s(BET)$ are the total and specific surface areas, respectively, of the adsorbent (of mass m) and L is the Avogadro constant. The surface area, pore volume and pore diameter is determined in triplicate and the results were plotted in bar graphs.

4.4.12. UPLC analysis of the drug compounds utilized in this within the pH responsive hydrogel

The UPLC method utilized in this study was previously described (Serra et al., 2011). A Acuity High Strength Silica (HSS) T3 column (100mm x 2.1mm, 1.8 μ m) was utilized to isolate and separate theophylline, ciprofloxacin, indomethacin, metronidazole, sulfamethazole, sulpiride, zidovudine, 4-aminosalicylic acid and naproxen. The λ was set at 271nm and the column was maintained at 25°C. Mobile phase A (0.2% acetic acid) and mobile phase B (acetonitrile) was utilized as a gradient method: 0-10min, 5-35% B; 10-10.10min, 35-80% B; 10.10-11min, 80% B; 11-11.10min, 80-5% B and 11.10-12.50min, 5% B at a flow rate of 0.4mL/min. The area under curve (AUC) for each drug peak, over a wide range of concentrations (25mg/L, 20mg/L, 15mg/L, 10mg/L, 5mg/L, 2.5mg/L, 1.25mg/L and 0.75mg/L) was determined in order to generate a standard curve for each drug. An internal standard of caffeine (20mg/L) was utilized throughout the study to validate the accurate retention time and AUC for each procedure. Each sample was dried within an ANSI HPLC 2mL vial at 40°C for 12 hours and resuspended in 1mL of diluent (50% ν 0.2% acetic acid in acetonitrile). Replicate samples (n=3) containing the aforementioned model drugs at 3 different concentrations (5mg/L, 10mg/L, 20mg/L) was analysed on three separate days to evaluate the accuracy and the within-day and between-day imprecision (C.V.) An injection volume of 2 μ L was utilized throughout the study.

4.4.13. Loading drug within crosslinked AAm-MAA hydrogel F6

F6 was used as the platform to release the drugs (theophylline, metronidazole, zidovudine, indomethacin, sulfamethoxazole, ciprofloxacin, sulpiride, naproxen) that was loaded by equilibrium partitioning in a slightly modified manner as previously described (Schoener et al., 2012). These drugs have different Biopharmaceutical Classification System classes, thus not only does the pH responsiveness of the hydrogel affect release, but also the innate solubility of the drug compounds. The drugs were dissolved within nine solutions of 2% ν DMSO/Millipore[®] water solutions (25°C, 100rpm) which contained a final concentrations of theophylline (0.003M), ciprofloxacin (0.17M), indomethacin (0.18M), metronidazole (0.007M), sulfamethazole (0.003M), 4-aminosalicylic acid (0.0014M), zidovudine (0.001M) sulpiride (0.003M) and naproxen (0.003M), respectively. F6, which had non-reacted monomers removed, were placed within the drug solutions and allowed to swell over a period of 24 hours. The hydrogels were dried within a vacuum oven for 24 hours at 40°C.

4.4.14. Determination of drug entrapment efficiency

The estimated percentage of drug entrapment efficiency was determined before dissolution studies were undertaken. A hydrogel, which had been precisely cut into 1cm long cylinders, crushed into powder form (placed through a sieve of aperture 800µm) and weighed. The powder was then suspended in 100mL Millipore® water for 24 hours. A 5mL sample was withdrawn and filtered through a 0.44µm Millipore Millex injection filter (Billerica, MA, USA). The filtered sample was placed within an ANSI HPLC 2mL vial and the drug concentration calculated utilizing the previously described UPLC method. This procedure was conducted in triplicate and the entrapment efficiency was determined according to **Equation 4.7**:

$$\text{Drug entrapment efficiency (\%)} = \left(\frac{\text{Actual drug content}}{\text{theoretical drug content}} \right) \times 100 \quad (\text{Eqn. 4.7})$$

4.4.15. Dissolution studies from crosslinked AAm-MAA hydrogel formulation 6 within dissolution fluids and isolated porcine gastrointestinal fluids

The *in vitro* and *ex vivo* dissolution studies were conducted in a previously described manner (Dünnhaupt et al., 2012). Each drug loaded hydrogel sample (hydrogel sample that contained theophylline, ciprofloxacin, indomethacin, metronidazole, sulfamethazole, 4-aminosalicylic acid, zidovudine, sulpiride or naproxen) was placed within a 20mL glass polytop containing 10mL biorelevant dissolution fluid, USP dissolution fluid or isolated porcine gastrointestinal fluid for a time period of 24 hours. A limited volume of dissolution fluid utilized within this study because was due to a limited amount of isolated porcine gastrointestinal fluid that was available and the volume must stay constant for comparative purposes. The polytops were placed within an Orbit Shaker Incubator (LM-530-2, MRC Laboratory Instruments Ltd, Hahistadrut, Holon, Israel) at 37±0.5°C at 50rpm. Sink conditions were maintained throughout the study. At predetermined time points, a 1mL sample was withdrawn and replaced with a temperature equilibrated aliquot of the respective fluid. The samples were filtered through a 0.22µm Millipore Millex injection filter (Billerica, MA, USA) and subject to UPLC analysis. The cumulative percentage of drug dissolution and the concentration of drug dissolution were plotted against time. Each drug dissolution study was repeated in triplicate.

4.4.16. Drug release mechanism

The drug release mechanism from the AAm-MAA hydrogel formulation 6 for each drug within each dissolution fluid was determined utilizing DDSolver add-in for Microsoft Excel 2007 (Zhang et al., 2010). The release of drug from the AAm-MAA hydrogel formulation 6 was highly dependent on drug characteristics (log P values, pKa, molecular weight), environmental conditions (pH, ionic strength and temperature) and innate physicochemical characteristics of the hydrogel (effective crosslinker density, polymeric chain relaxation, and charged interactions between the drug molecule and the hydrogel macrostructure). The mean dissolution time at time point 90 minutes (MDT₉₀) and 1440 minutes (MDT₁₄₄₀) were determined utilizing **Equation 4.8**:

$$MDT = \sum_{i=1}^n \tau_i \frac{M_t}{M_{\infty}} \quad (\text{Eqn. 4.8})$$

Where M is the fraction of drug dose release in time $\tau_i = (t_i - t_{i-1})/2$ and M_{∞} corresponds to the loading dose. The area under curve for each drug dissolution profile was determined according to the trapezoidal rule. The calculations (MDT₉₀, MDT₁₄₄₀ and AUC) allow for efficient comparison between dissolution fluid types. The dissolution profile for each drug within each respective fluid was recorded within scatter plots and a regression fitting of each known drug dissolution model was applied to each profile. The five regression fittings which achieved a R^2 adjusted value greater than 98% were considered viable dissolution models. The dissolution modeling allows for comparison between the mechanisms in which drug dissolution is achieved within a specific dissolution fluid type. All drug dissolution studies were conducted in triplicate.

4.4.17. Morphological analysis images of crosslinked AAm-MAA formulation hydrogel 6

Scanning Electron Microscopy (SEM) imaging of F6 was conducted on a FEI ESEM Quanta 400F (FEI™, Hillsboro, OR, USA) electron microscope. Samples of F6 were placed within USP pH 1.2 dissolution fluid, USP pH 6.8 dissolution fluid and Millipore® water. At predetermined time points (0, 60, 90, 120, 150 and 180 minutes), a hydrogel sample for each dissolution fluid was withdrawn and flash frozen with liquid nitrogen (Yan et al., 2011). The samples were then maintained at -80°C for 48 hours and subsequently lyophilized with a two hour condensation phase at -60°C, followed by a 24 hour sublimation phase at 25mm Torr utilizing a Freezone 12 freeze drier (Lanconco, Kansas City, USA). Images of each

hydrogel sample were captured with an accelerated voltage of 30.00kV at 100 times magnification for comparative purposes.

4.4.18. Magnetic Resonance Imaging of crosslinked AAm-MAA formulation hydrogel 6

A dry F6 was placed within the flow through cell of a benchtop Magnetic Resonance Imaging (MRI) machine (Maran-i, Oxford Instruments, Oxordshire, UK) which was equipped with a 0.5 tesla permanent magnet system and had been stabilized at 37°C (Kulinowski et al., 2008; Tajiri et al., 2010). The hydrogel sample was held in place with a rubber retaining band in a plastic holder. Images were collected over the course of 24 hours at predetermined time intervals to visualise the real time swelling of hydrogel sample within a continuous flow system. The real time swelling of the F6 was assessed within USP pH 1.2 dissolution fluids, USP pH 6.8 dissolution fluids and Millipore® water. Additionally, a hydrogel sample was allowed to swell in USP pH 6.8 dissolution fluid for a period of 24 hours, within the MRI machine, and subsequently the USP pH 6.8 dissolution fluid was exchanged with USP pH 1.2 fluid. The ability of the crosslinked AAm-MAA hydrogel formulation to deswell in response to a decrease in pH was captured in real time. T1-weighted images were captured using a spin echo method and the single intensity of the MRI images was defined according to **Equation 4.9** (Tajiri et al., 2010):

$$S = M_0 \times \exp \frac{-TE}{T_2} \times \left(1 - \exp \frac{-TR}{T_1} \right) \quad (\text{Eqn. 4.9})$$

Where M_0 is magnetization, T_1 and T_2 are the relaxation times. TR and TE are repetition time and echo time, respectively.

4.5. Results and Discussion

4.5.1. Synthesis of hydrogel

The crosslinked AAm-MAA hydrogel formulations were synthesized according to the concentrations within **Table 4.1**. The polymerizing solutions of F2-F11 could easily be poured into the cylindrical moulds but the ploymerizing solution of F1 would polymerize too quickly to be poured into the cylindrical moulds. The hydrogels generally were clear to white in colour of defined cylindrical shape. The dried hydrogels were very hard and brittle once placed under a significant mechanical force. Intial studies such as Attenuated Total Reflectance-Fourier Tansform Infareds analysis, thermal characeterization, viscosity

analysis of polymerizing hydrogel solutions, gel fraction determination, powdered x-ray diffraction and swelling studies were performed for all hydrogel formulations. These studies were used to determine which hydrogel was sufficiently pH responsive and structurally suitable to be utilized within the OGDD device as the push mechanism for the mini-pellets within the device. Studies using biorelevant dissolution fluids for distance-time studies and swelling studies were utilized for the desirable formulation (F6), a formulation that had low sensitivity towards pH (F2) and a formulation with high sensitivity to pH but maintained reasonable structure under compression (F8). These studies were performed for comparative purposes. Lastly, porosity studies, MRI studies, drug (of different biopharmaceutical classification classes) dissolution studies that was performed in USP and biorelevant dissolution fluids and morphological studies were conducted on the most desirable formulation (F6) for the intended purpose for additional understanding of the how physomechanical properties of the hydrogel respond in different environments.

4.5.2. Viscosity analysis of the polymerizing crosslinked AAm-MAA formulation hydrogels

The viscosity of the crosslinking hydrogel formulations (**Figure 4.1** and **Figure 4.2**) were assessed to determine the time point at which significant crosslinking occurred and the relative time period allowed for the transfer of the polymerizing solution into a mould. This was observed by a deviation from Newtonian flow behaviour by an increase in viscosity. A cylindrical mould was utilized throughout the study to ensure that the available surface area and size of the hydrogel samples remained constant. Ideally, the blowing agent should be completely reacted before placing the polymerizing solution within a mould so that are maintained within the solution and bulk carbon dioxide gas has escaped the solution, preventing the formation of large heterogeneous voids within the gelled sample. Additionally, the polymerization reaction should occur at a rate that is economically viable for upscale applications.

The result of this analysis indicated that an increase in viscosity was higher in F8 than F6. Additionally, the point where crosslinking took place in F8 occurred at ~2000 seconds whereas the initiation of crosslinking took place around ~1800 seconds for formulation 6 when temperature conditions remained at 25°C.

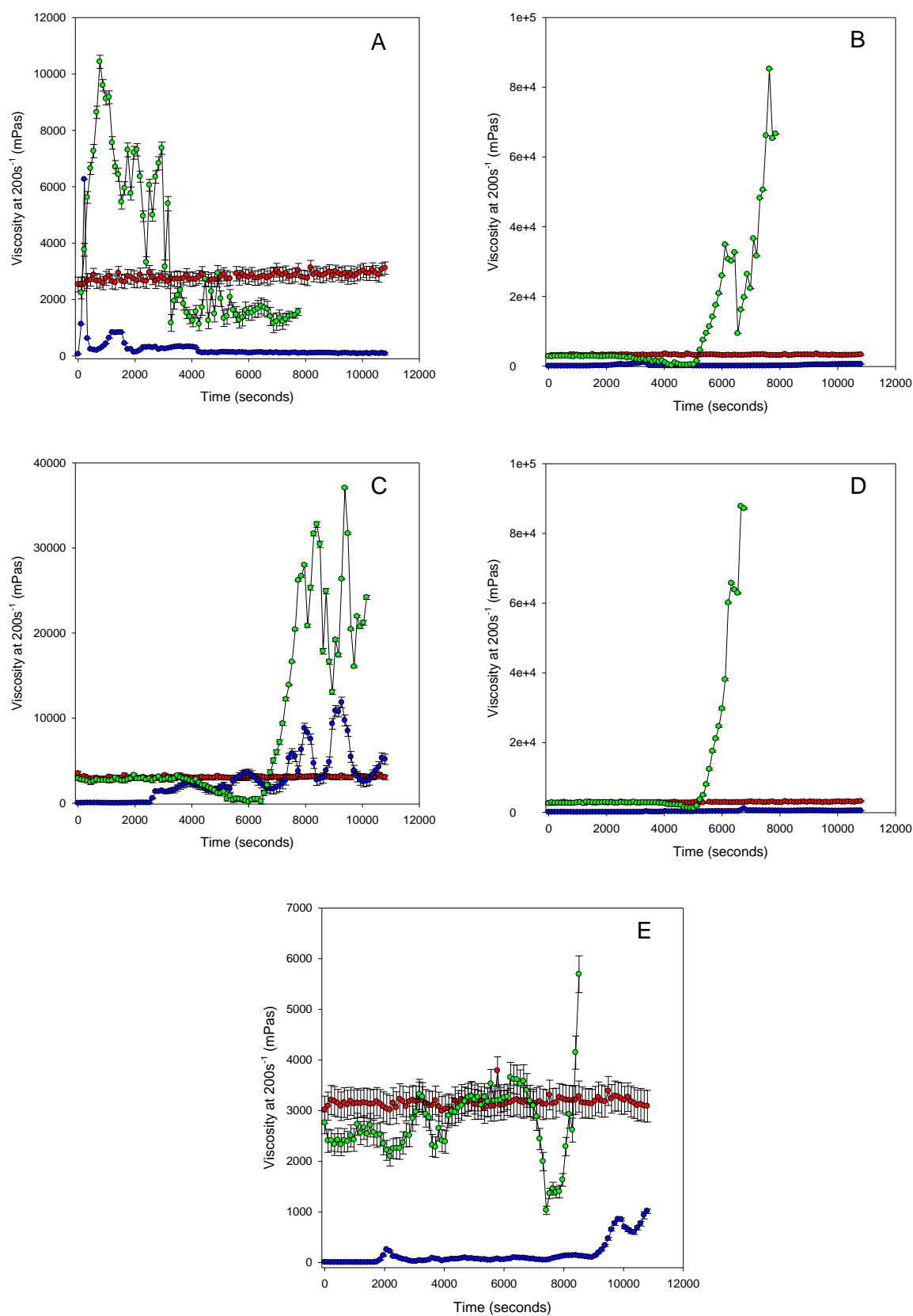


Figure 4.1: The viscosity analysis of AAm-MAA hydrogel formulation (F2-F6) under thermal conditions of 10°C (red profile), 25°C (blue profile) and 40°C (green profile). The profiles represented are for hydrogel formulations: F2 (A), F3 (B), F4 (C), F5 (D) and F6 (E).

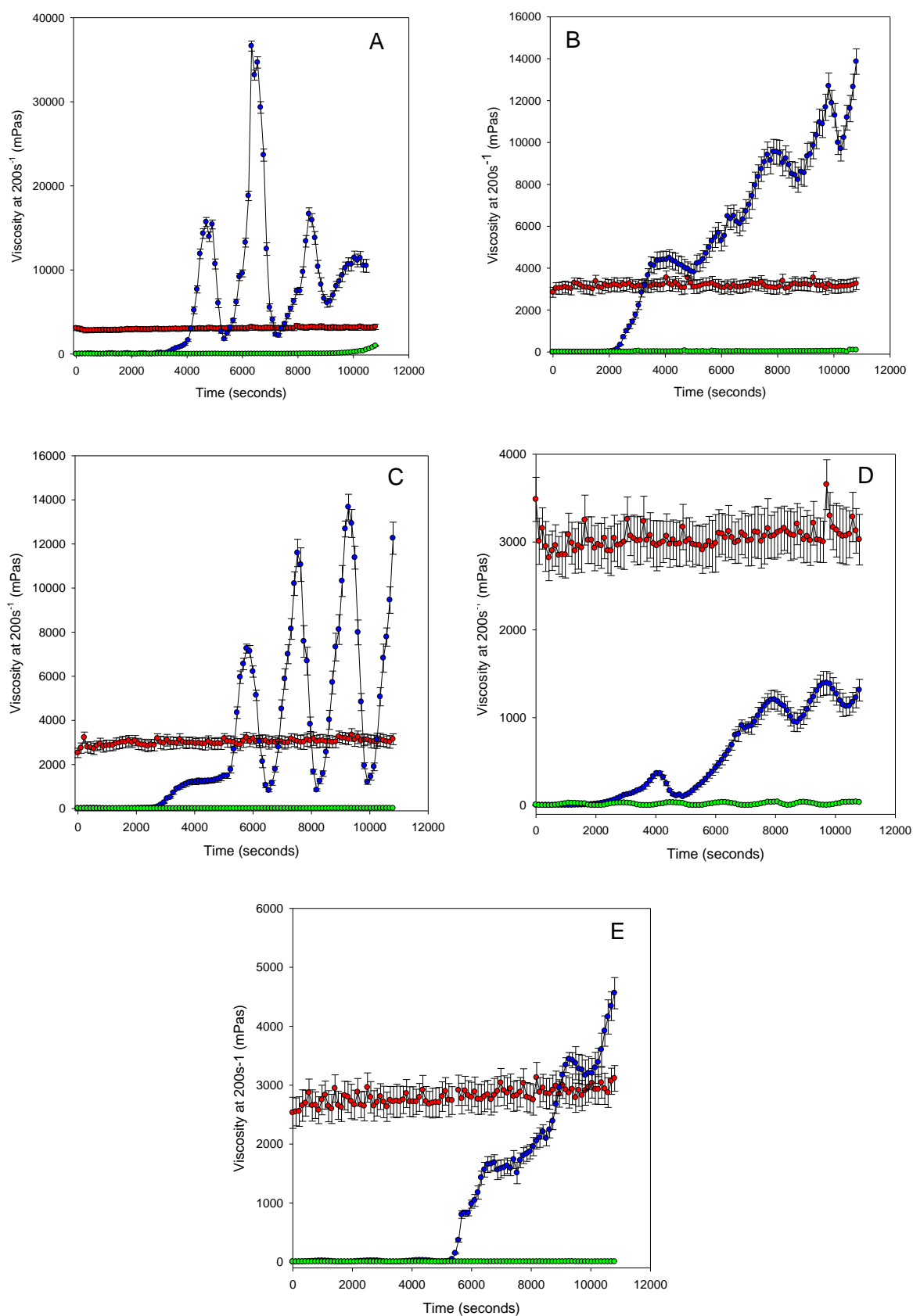


Figure 4.2: The viscosity analysis of AAm-MAA hydrogel formulation (F7-F11) under thermal conditions of 10°C (red profile), 25°C (blue profile) and 40°C (green profile). The profiles represented are for hydrogel formulations: F7 (A), F8 (B), F9 (C), F10 (D) and F11 (E).

There was no measurable increase in viscosity due to crosslinking under temperature conditions of 40°C. At 40°C, the evaporation of water from the polymerizing system occurs at a rapid rate, even with the utilization of a solvent trap. The removal of water from the polymerizing system inhibits the accurate determination of viscosity at this temperature. The viscosity measurement at 10°C results in a system that polymerizes too slowly for a notable change in viscosity to be determined. F2 underwent polymerization so rapidly that it was extremely difficult to obtain any accurate viscosity data before the solution had entered the gel state. It was noted that with increase concentrations of methacrylic acid, the polymerization reaction occurred at a slower rate.

As indicated in the viscosity results, a low temperature impacts the polymerization to the point where no polymerization may occur. Whereas a high temperature accelerates the evaporation of water from the system so rapidly that obtaining a flowable monomer solution that can be placed within a mould would be a challenge.

Fortunately, the utilization of room temperature (25°C) allowed for the monomer solution to be flowable, polymerize within a timely manner and presents the most economically beneficial conditions. A trend was noted in the gel percent determination; the inclusion of higher concentrations of methacrylic acid in the polymerizing solution reduced the ability of the APS/TEMED free radical polymerization system to be highly efficient. This was noted as well during the viscosity analysis of each polymerizing solution when the solutions generally required a longer time period to deviate from Newtonian flow. Some formulations with increase methacrylic acid did polymerize slightly faster than those with lower methacrylic acid but this may be due to a slightly more thermodynamically favoured reaction. For instance the polymerization was determined to occur in less than ~300 seconds for F2 (it was very difficult to obtain a precise time at which significant crosslinking initiation occurred) whereas F8 had an precise significant crosslinking time of 2000-2200 seconds. The initiation of significant crosslinking time between formulations is also important for upscale purposes. For instance, F1 formulation studies were suspended after the viscosity analysis because this formulation crosslinked too rapidly for a mould to be produced (even at low temperatures).

4.5.3. Determination of the gel fraction percent of the crosslinked AAm-MAA hydrogel formulations

The free monomers that were not incorporated within the hydrogel macrostructure during the free radical polymerization were removed from the hydrogel macrostructure during the gel

fraction percent analysis. The free monomers are removed by hydrating the solution within Millipore® water. An effective balance between the polymerization of polymeric monomers and incorporation of pH sensitivity has to be achieved.

The gel fraction percent was determined to be above 85% for all of the synthesized hydrogel formulations. The gel fraction percentage was higher within formulations that contained a higher concentration of acrylamide than methacrylic acid. Hydrogel F1 which contains only acrylamide had a gel fraction percent of 98% which is almost completely crosslinked. The gel fraction decreased to 85% for hydrogel F11 which contains only methylacrylic acid, indicating that methacrylic acid was not as effectively crosslinked by the free radical system (APS/TEMED). The bar graph representing the specific degrees of gel fraction percent for each formulation can be reviewed within the **Figure 4.3**. If the gel fraction percent becomes too low, the desirability of the formulation is significantly lowered. An example of this is in F11 which only contained monomers of methacrylic acid but had very low mechanical strength and maintenance of water within the macrostructure of the hydrogel was low. F1 was the behaved in an opposing manner whereby the mechanical strength of the hydrogel was high, the loss of percentage of unreacted monomers was minimal but the hydrogel formulation had an extremely low degree of pH sensitivity. These properties are emphasized in characterization studies performed within this study.

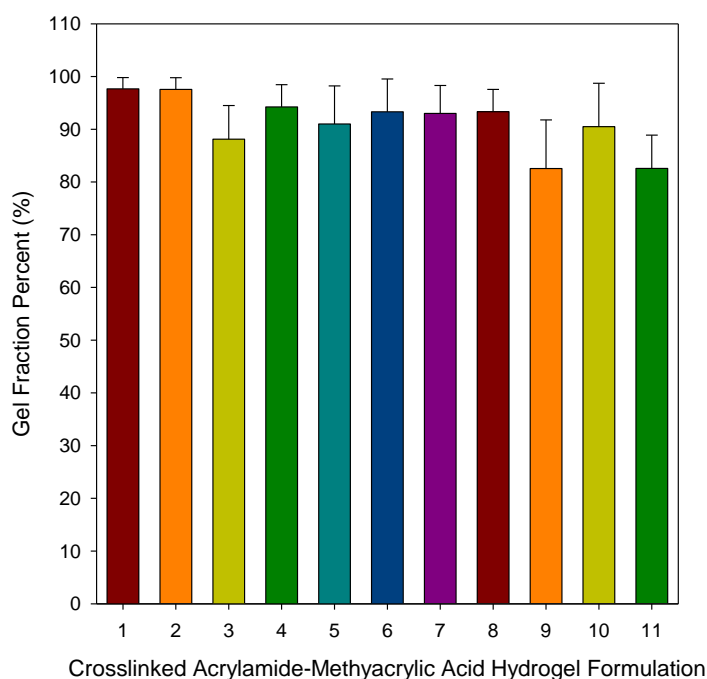


Figure 4.3: Bar graph representing the gel fraction percent for each of the AAm-MAA hydrogel formulations.

4.5.4. Attenuated Total-Reflectance-Fourier Transform Infrared analysis of crosslinked AAm-MAA formulation hydrogels

The ATR-FTIR analysis determined that the free radical polymerization of acrylamide and methacrylic acid was successful by incorporation of MBA within the hydrogel structure. Additionally, the absorbance intensity of characteristic functional groups within the hydrogel formulations may be reduced because these functional groups are participating in the crosslinking network structure. The ATR-FTIR spectrum of each AAm-MAA hydrogel formulation is shown in **Figure 4.4**. A peak occurred at 1648cm^{-1} . The freshly synthesised AAm-MAA hydrogel had peaks at 1655cm^{-1} and 1453cm^{-1} which was similar to the dried AAm-MAA hydrogel that had peaks at 1648cm^{-1} and 1444cm^{-1} (data not shown). The peak located at 1648cm^{-1} was determined to occur due to an amide-I band of the amide group of acrylamide (Nakason et al., 2010). Wavenumber peaks present in MBA (2769cm^{-1} and 1072cm^{-1}) were present in the AAm-MAA hydrogel formulation 6 at 2763cm^{-1} and 1071cm^{-1} . The characteristic wavenumber peak of methylacrylic acid at 1425cm^{-1} was lost within the polymerized hydrogel and a new peak occurred at 1425cm^{-1} .



Figure 4.4: The ATR-FTIR spectra in (A) represent crosslinked AAm-MAA hydrogel formulation 1 (pink profile), 2 (dark green profile), 3 (dark orange profile), 4 (purple profile) and 5 (dark blue profile). The ATR-FTIR spectra in (B) represent crosslinked AAm-MAA hydrogel formulation 6 (light orange profile), 7 (light blue profile), 8 (pink profile), 9 (light green profile), 10 (dark orange profile) and 11 (purple profile) were determined from dry samples (after gel fraction percent determination) at 130psi between $650\text{--}4000\text{cm}^{-1}$ against absorbance.

Wavenumber peaks that were common between the polymerized hydrogel and acrylamide were located at 1049cm^{-1} . This peak indicates that the AAm-MAA hydrogel may have C-O-C stretching vibrations (Dadsetan et al., 2010). The intensity of the wavenumber peaks was highest within formulation 1 and 11 that contained the highest concentration of acrylamide and methacrylic acid respectively. The reducing mass concentration ratio, with respect to each monomer, generally reduced the intensity of the characteristic wavenumber peaks.

4.5.5. The powder X-ray diffraction of the hydrogel formulations and the percentage of crystallinity

The PXRD indicates that the hydrogel formulations are highly crystalline in nature and have a similar crystal structure. A large variation in crystal structure was not expected because the formulations are composed of identical monomer and crosslinker components. The PXRD diffraction of the hydrogel formulations is shown in **Figure 4.5** and the degree of crystallinity is also shown in **Figure 4.5**. The major reflections for these hydrogel formulations occurred at 2θ -values of 36.2° , 42.8° , 63.1° , 77.3° and 80.9° . The degree of crystallinity was determined to be the highest for formulation 4 and 9 whereas the degree of crystallinity was determined to be lowest for formulation 11. The PXRD of the remaining hydrogel formulations can be reviewed in **Appendix 3**.

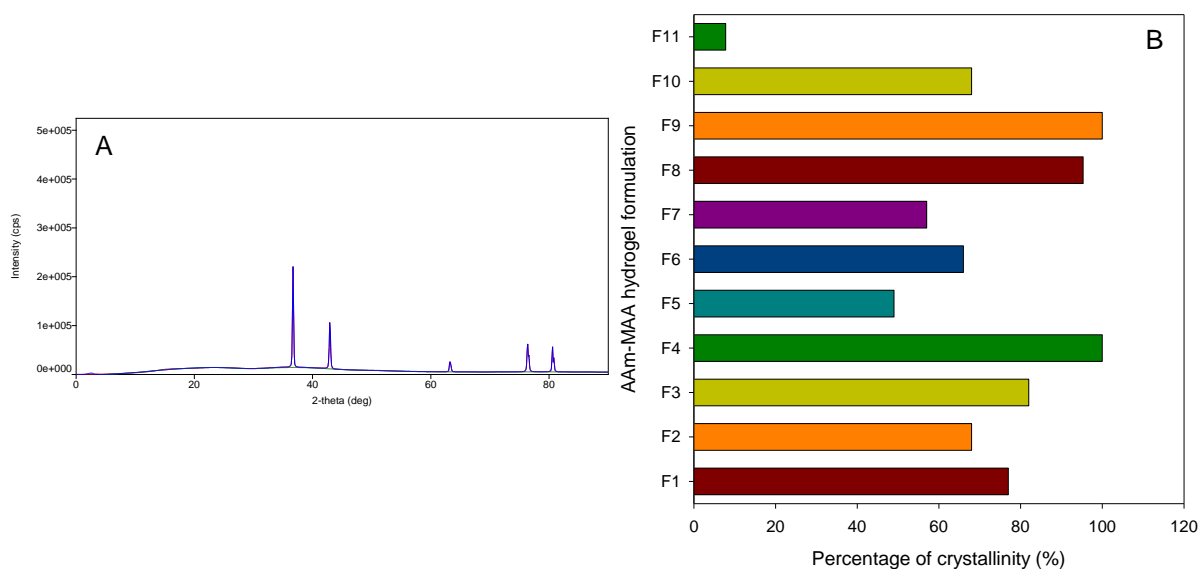


Figure 4.5: The PXRD profile of formulation 6 (A) and a bar graph of the percentage of crystallinity for each hydrogel formulation (B).

4.5.6. Thermal analysis of crosslinked AAm-MAA hydrogel formulation

The DSC thermograph traces for each stimuli responsive hydrogel can be reviewed within the **Figure 4.6**. The DSC of each hydrogel formulation has characteristic melting and crystalline events which are common throughout all the synthesized formulations. The DSC analysis of each hydrogel formulation at each heating rate generated unique degrees of melting and crystallization. For instance, F7 had a melting peak that occurred at 239.72°C (heating rate: 10°C/min; heat of fusion: -121.26J/g), 230.32°C (heating rate: 5°C/min; heat of fusion: -144.84J/g) and 218.38°C (heating rate: 2°C/min; heat of fusion: -167.04J/g). The main melting event of F10 occurred at 231.9°C (heating rate:10°C/min; heat of fusion: -38.85J/g), 224.17°C (heating rate:5°C/min; heat of fusion: -268.21J/g) and 228.2°C (heating rate: 2°C/min; heat of fusion: -394.4J/g). The thermal events within DSC thermogram traces of the hydrogel formulations generally occurred at lower temperatures with slower heating rates. The DSC analysis of each hydrogel formulation was conducted in triplicate at each heating rate.

4.5.7. Gravimetric swelling analysis of the crosslinked AAm-MAA hydrogel formulation 2, 6 and 8

The ability of the hydrogel to swell within a solution has been attributed to the effective crosslinking that exists between the polymerized monomers within a hydrogel matrix (Hwang et al., 2010). The concentration of pH sensitive monomers in the presence of constant crosslinking agent (i.e. BIS) concentration will also have an important influence on the ability of a hydrogel to swell within a solvent. This was evident in the gel fraction percent determination whereby, even though a high concentration of methylacrylic acid was present, the ability of the crosslinker to induce polymerization was limited in comparison to acrylamide. Millipore® water was utilized to assess the swelling potential of a particular hydrogel formulation and compare this ability to that within a dissolution fluid. Millipore® water allows the hydrogel formulations to swell unimpeded by a significant reduction in metal ion concentration and relatively neutral pH characteristics.

Gravimetric swelling analysis of F2, F6 and F8 were conducted in USP simulated dissolution fluids, biorelevant dissolution fluids and Millipore® water as shown in **Figure 4.7**. The swelling ability of the hydrogel formulation 2 could easily achieve over 2000% within neutral environments but also swelled up to 700% within acidic environments within a 24 hour period.

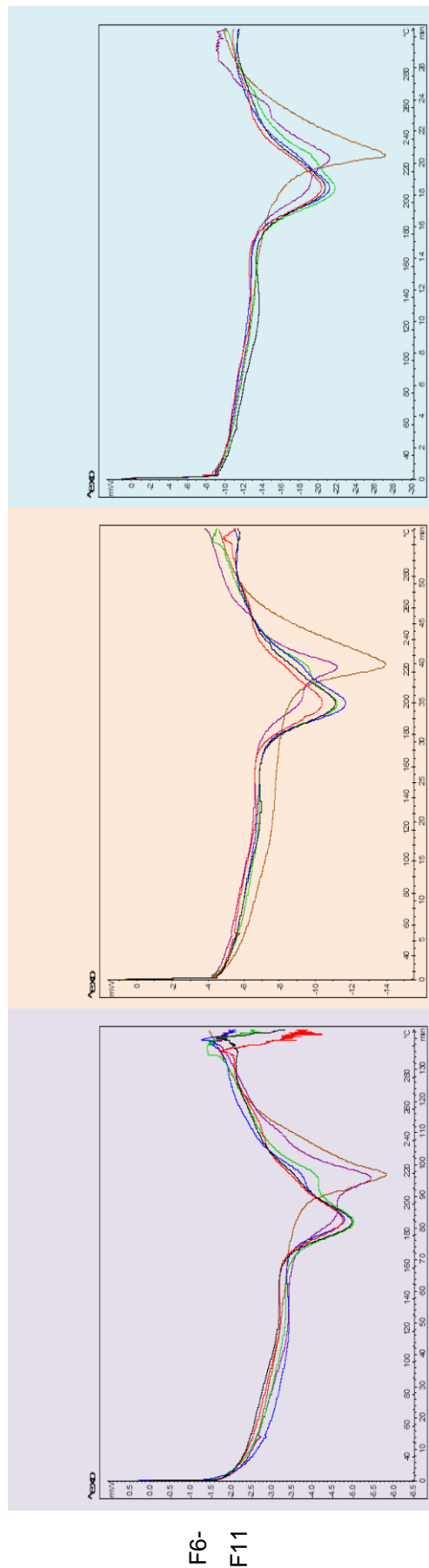
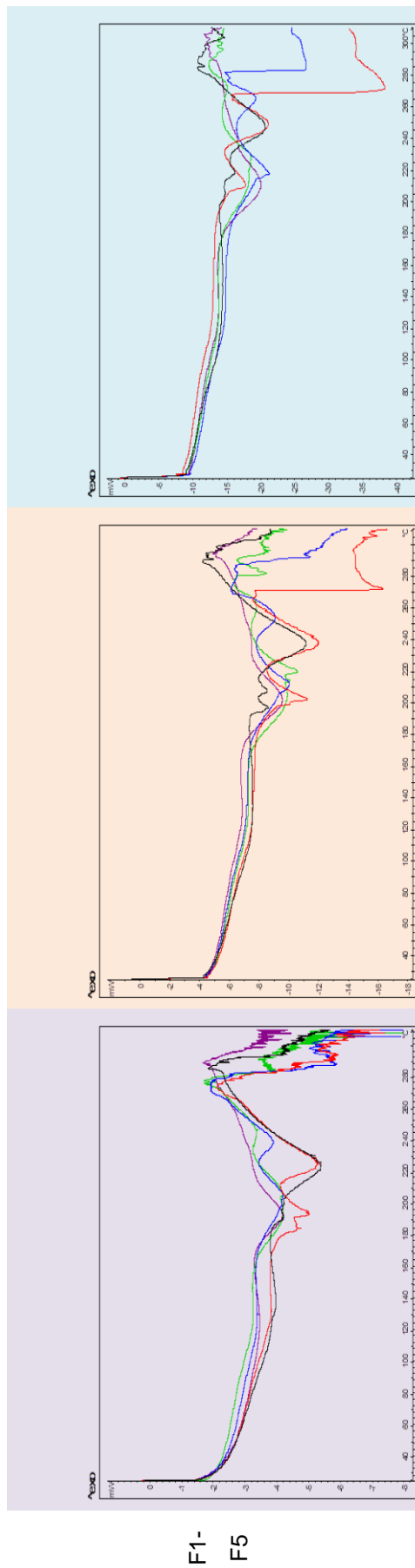


Figure 4.6: Differential Scanning Calorimetry of crosslinked AAm-MAA hydrogel formulations at 10°C/min (light blue boxes), 5°C/min (light red boxes) and 2°C/min (light purple boxes).

This had low sensitivity to pH when compared to formulation 6 which swells over 1200% within neutral environments but only swelled up to 130% within acidic environments. Formulation 6 is 3.6 times more sensitive to pH conditions than formulation 2. Formulation 8 achieved an impressive swelling ability of more than 1400% within neutral environments and a swelling ability of less than 95% within acidic environments which is ~5 times more sensitive to pH than formulation 2. This would indicate that formulation 8 would be a desirable hydrogel for drug delivery applications due to its increased sensitivity towards pH. The swelling ability of the hydrogel to swell within different biorelevant dissolution fluids was also investigated. The swelling percent against time profile

was determined using a regression fitting for the exponential to rise maximum (3 parameter model) as shown in **Figure 4.7 (A)**. The swelling percent-time scatter plot point for each hydrogel, within each dissolution fluid, existed within the 95% confidence interval (blue line) and 95% predicted confidence interval (red line). The scatter plot and the fitted regression model for F2, F6 and F8 in gravimetric swelling within dissolution fluids can be reviewed within the provided **Appendix 4**.

The area under the curve was determined using DDSolver add-in for Microsoft Excel 2007 for each swelling percent-time profile. The area under curve allows for direct comparison between the swelling profiles of the hydrogel formulation 2, 6 and 8. UPS pH 6.8 generated some of the greatest swelling ability between 42% to 97% with respect to Millipore® water. Whereas swelling ability within USP pH 1.2 was comparable to biorelevant media within F6 and F8. The swelling potential of F2 within USP pH 1.2 was 100% greater than comparative gastric simulating fluids. The swelling ability of hydrogel formulation 2 was much greater than hydrogel formulation 6 and 8. The degree or ability of the hydrogel formulation 6 and 8 to swell was similar but hydrogel formulation 8 did have a higher degree of pH sensitivity. The canine biorelevant media generally achieved a higher degree of swelling potential in comparison to human biorelevant media. The biggest difference was noted in F2 and F8 with FaSSGFc pH 6.5. This is likely due to the relatively low concentration of metal ions and bile salts, in addition to the high pH. These factors allow for the hydrogel formulations to retain a higher volume of water within a shorter time frame.

The gravimetric swelling ability of F2 was the greatest because this formulation contained the lowest concentration of methacrylic acid. As the methacrylic acid concentration within the hydrogel formulations was increased, the ability of the hydrogel formulation to be pH responsive was increased but the swelling potential was diminished. This is particularly important for targeted drug delivery applications whereby the drug is entrapped within the

hydrogel or the hydrogel is utilized within a device to facilitate targeted release. For the application purpose within a drug delivery device or targeted drug delivery, controlling the concentration of the pH responsive component will enable the device to respond to the gastrointestinal pH profile in a tuneable manner. This is evident in the pH sensitivity between F6 and F8 which increased ~100%. Additionally, the swelling ability of these hydrogel formulations was highly predictable. A pH responsive hydrogel that is highly predictable and easily tuneable is highly attractive for drug delivery applications.

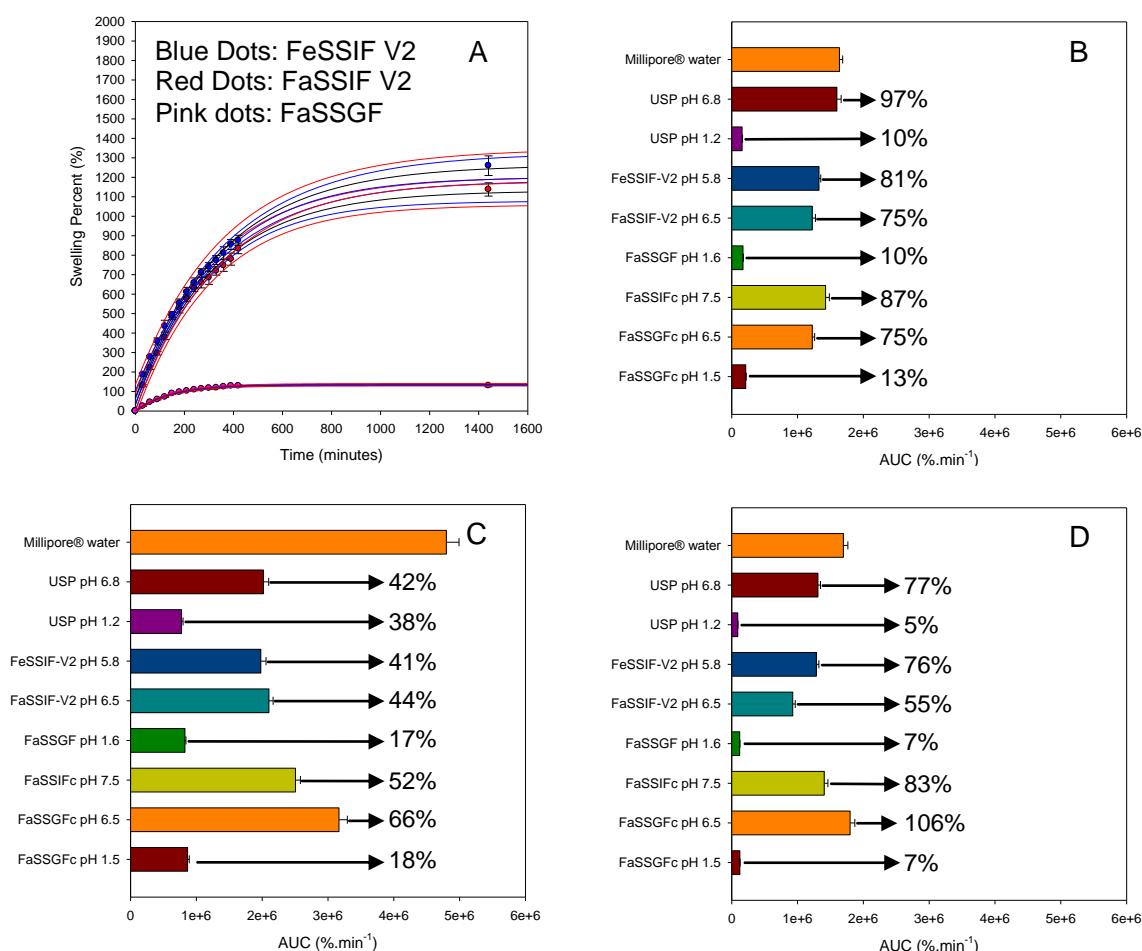


Figure 4.7: The gravimetric swelling profile of AAm-MAA hydrogel formulation 6 (A) and the area under curve for the gravimetric swelling profiles for AAm-MAA hydrogel formulation 6 (B), AAm-MAA hydrogel formulation 2 (C) and AAm-MAA hydrogel formulation 8 (D) within biorelevant fluid and USP simulated fluid.

4.5.8. Distance-time studies of the crosslinked AAm-MAA formulation hydrogels

The compression under constant force at which a hydrogel formulation can swell against is an indication of the physicommechanical strength of the hydrogel macrostructure under constant strain. This assessment was conducted on F2, F6 and F8 to determine the predicable physicommechanical properties of the hydrogel formulation within a multitude of

dissolution fluids but also within isolated porcine gastrointestinal fluids. The distance-time profile of F2, F6 and F8 is shown in **Figure 4.8**. The distance-time profile for each hydrogel formulation was plotted within a scatter plot and a regression curve was fitted to each scatter plot (data not shown). F6 deformed in FaSSGFc pH 1.5 and USP pH 1.2, whereas F8 deformed in FaSSGFc pH 1.5, USP pH 1.2 and FaSSGF pH 1.6. F2 did not deform in any of the dissolution fluids and achieved the highest distance per mm rates. As a hydrogel absorbs solvent from the environment, the hydrogel expands, even against a compressive force and this is measured as the distance (mm) per second increased from the the initial measured distance from the zeroed point. When the hydrogel undergoes deformation, the distance per second measurement is negative with respect to the initial zeroed point. The solvent environment has hydrated the hydrogel which allows the dried hydrogel to move from the solid state to the semi solid state, but the solvent environment has not provided the hydrogel macrostructure in the semi solid state with the chemical bond integrity to withstand a compressive force, thus allowing the compressive force to progressively displace the hydrogel away from the direction of the applied force. The fastest distance-time rates were achieved within Millipore[®] water by F2. The distance-time profiles each hydrogel formulation within USP pH 1.2, USP pH 6.8 and Millipore[®] water can be reviewed in **Appendix 5**.

The hydrogel formulations did not undergo deformation in any of the isolated porcine gastrointestinal fluids and the highest distance-time rates were achieved by F2. F2 performed in the isolated intestinal porcine fluids to the same degree as that in FaSSGF pH 1.6 and performed slightly worse in the isolated gastric fluids than in FaSSGFc pH 1.5. F6 and F8 exerted a positive distance per time displacement but F6 was slightly greater than F8. Interestingly, F2 demonstrated a burst swelling profile within both the dissolution fluids and within the isolated gastrointestinal fluids of the porcine model.

The performance of these hydrogel formulations within the dissolution fluids achieved similar initial compression resistance potential whereby F2 achieved the greatest compression resistance, followed by F6 and F8, respectively. But the compression resistance that was achieved within the isolated porcine gastrointestinal fluids did not correlate well with the velocities achieved within the dissolution fluids. The dissolution fluids are ideally utilized for preselection of the desirable hydrogel performance with respect to other hydrogel formulations, but the *in vivo* performance may be significantly reduced. This is particularly important for physicomechanical drug delivery applications and direct drug loading applications.

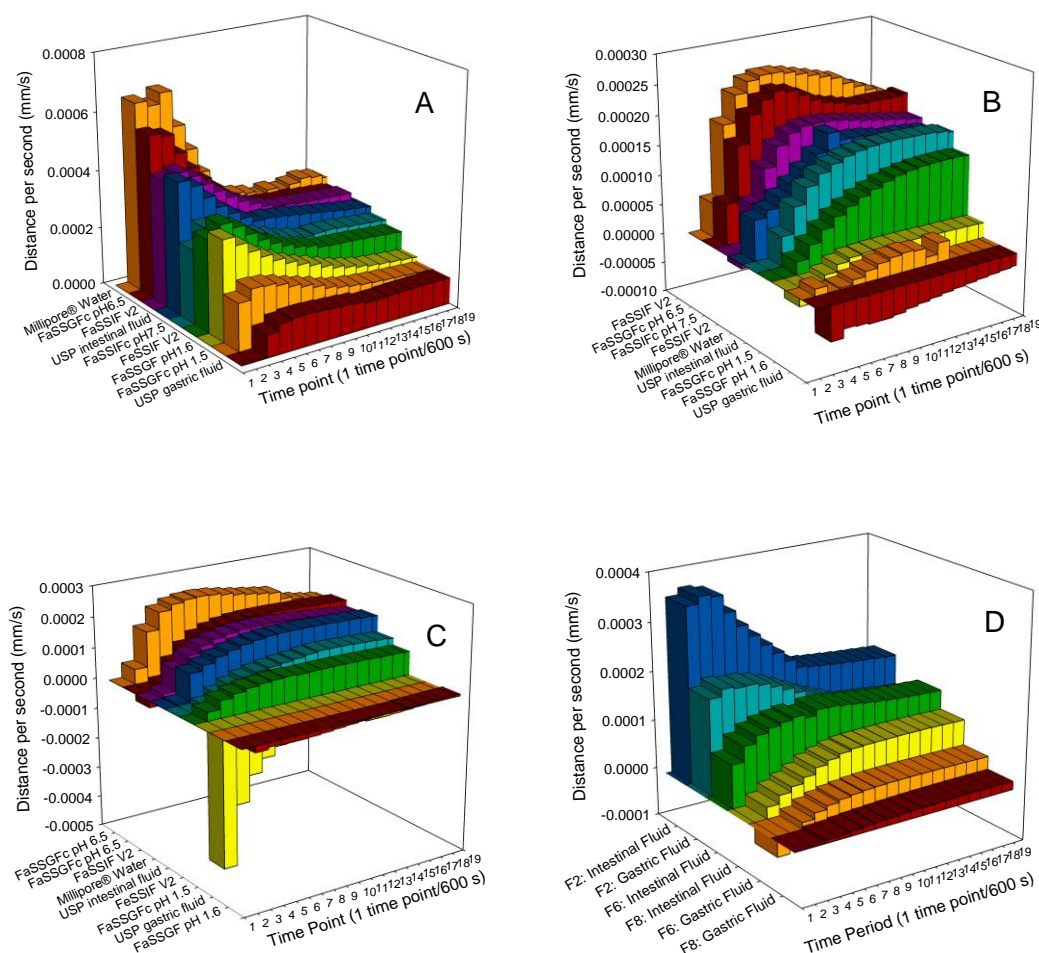


Figure 4.8: The distance-time profile of AAm-MAA hydrogel F2, F6 and F8 within biorelevant media and USP simulated fluids (A, B, C) and within isolated porcine fluids (D) with respect to sequential time points.

The understanding of swelling ability for each hydrogel formulation demonstrates that even though F8 achieved greater retention of dissolution fluids during the gravitational swelling analysis, the resistance to compression with respect to time property of F8 with respect to F6 was reduced. A drug delivery application which relies upon the ability of the hydrogel to swell in response to pH and resist a compressive force with respect to time would favour F6 over F8. Comparatively, a drug delivery application with a preference to pH responsiveness over physicomachanical robustness, would favour F8 over F6. Interestingly, F2 demonstrated a burst distance-time profile whereby the compression resistance of was initially very high and then reduced with time. This may have important implications for drug delivery applications whereby a burst compression resistance indicates that the macrostructure of the hydrogel was reinforced by the rapid accumulation of water. This occurs until the accumulation is slowed by the equalization of swelling capacity of the hydrogel formulation within the solvent environment and the applied downward force. F6 and

F8 accumulated higher velocities with respect to time that would be ideal for drug delivery applications whereby a steady increase dissolution of drug is preferred.

4.5.9. The porositometric characteristics of crosslinked AAm-MAA formulation hydrogel 6

The porositometric characterisation of F6 was conducted to determine the Brunauer–Emmett–Teller (BET) adsorption and desorption profiles (Yushin et al., 2006). The porosity analysis is shown in **Figure 4.9** (surface area), **Figure 4.10** (volume of pores and pore diameter). The porositometric analysis of F6 was conducted in USP dissolution fluids to assess the increase in the surface area, pore diameter and pore size with respect to time. Additionally, the porositometric analysis was conducted in Millipore® water for comparative purposes. The isotherms obtained from each sample were noted as a type IV isotherm whereby a small hysteresis is present (Sutar et al., 2008; He et al., 2010).

The surface area measurements demonstrated, as expected, that the F6 samples exposed to Millipore® water had the largest surface area. Additionally, the surface area determination of the hydrogel within USP pH 1.2 was significantly reduced in comparison to the other solvent environments utilized within this study. The surface area increases as the hydrogel is exposed to solvent because of the formation of progressively deeper channels that penetrates into the core of the hydrogel structure through the development of an intra-connected network that extend from the opening of the pore. With time, these channels become larger with respect to diameter and length that results in an increased surface area measurement. The surface area at each time point, irrespective of the solvent type, increased with respect to time. F6 hydrogel samples surface area increased 12.4 times in single point surface area measurement in the USP pH 1.2 dissolution fluid environment whereas a 1.62 time increase in single point surface area measurement was achieved in the USP pH 6.8 dissolution fluid. A similar trend was noted in the BET surface area, BJH absorption and BJH desorption measurements whereby the surface area increased many time greater within USP pH 1.2 dissolution fluid than USP pH 6.8 dissolution fluid. The utilization of liquid nitrogen to flash freeze samples of hydrogel at the respective times (to preserve architecture) and then lypholization of the hydrogels allowed these measurements to be obtained. The lypholized samples were handled with great care throughout the study so that a dry sample that contained the correct structure was measureable.

F6 had a mesoporous structure that can be deduced by the presence of H1-hysteresis loops within generally similar type IV isotherms (Chang et al., 2009; Sarawade et al., 2013). The

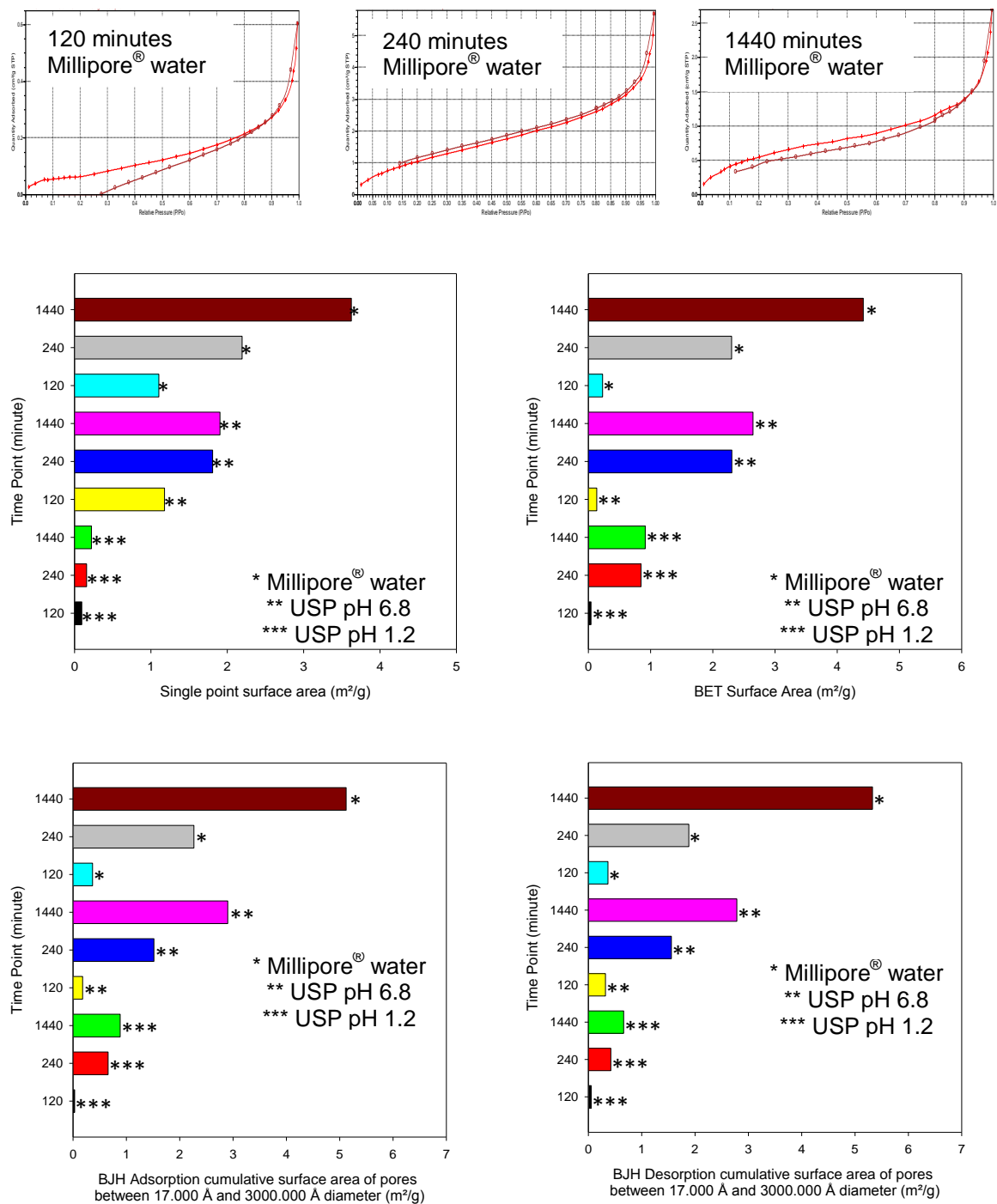


Figure 4.9: The porositometric surface area analysis with respect to time of AAm-MAA hydrogel F6 within USP simulated gastric fluid (USP pH 1.2), USP simulated intestinal fluid (USP pH 6.8) and Millipore® water.

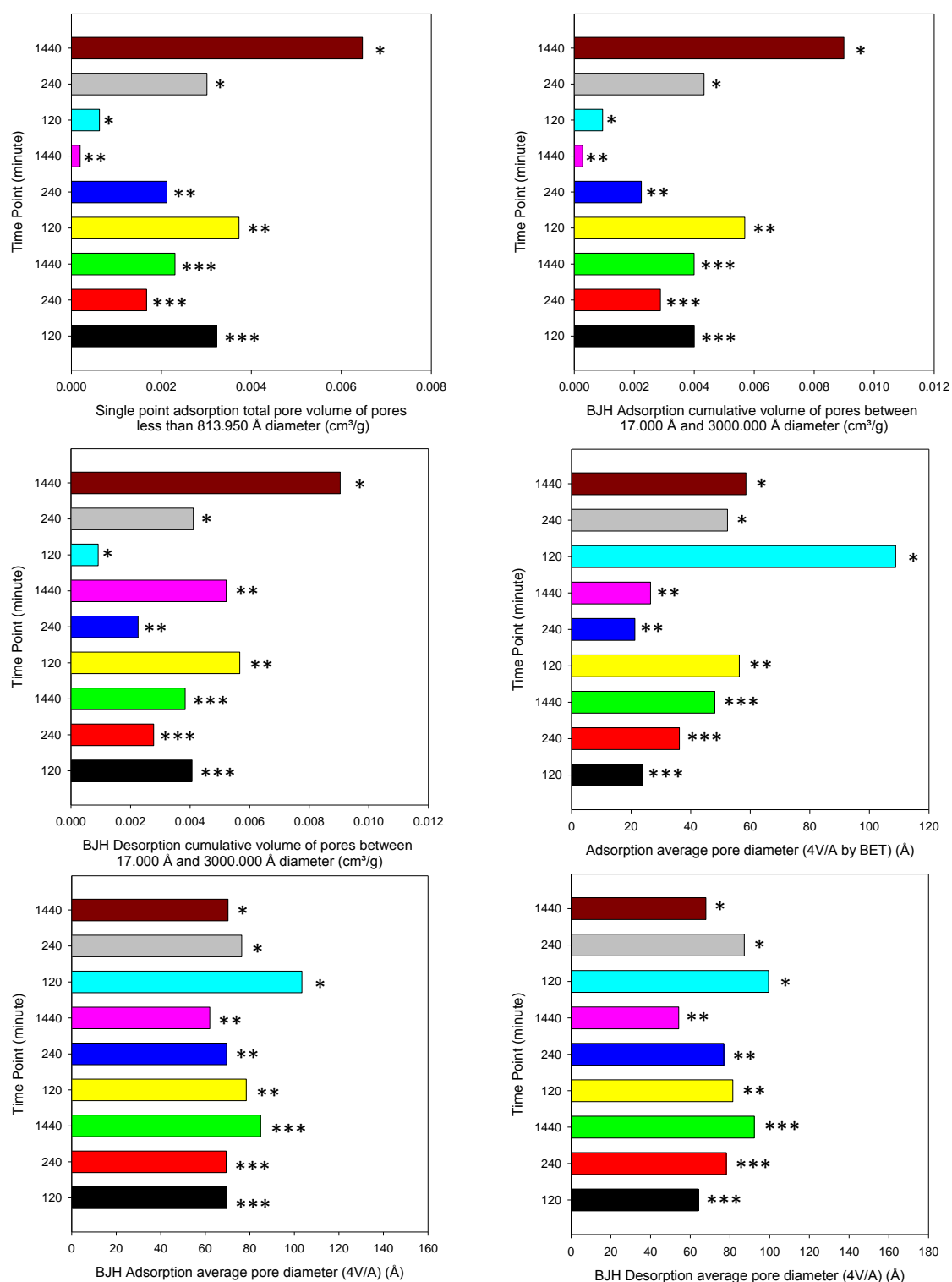
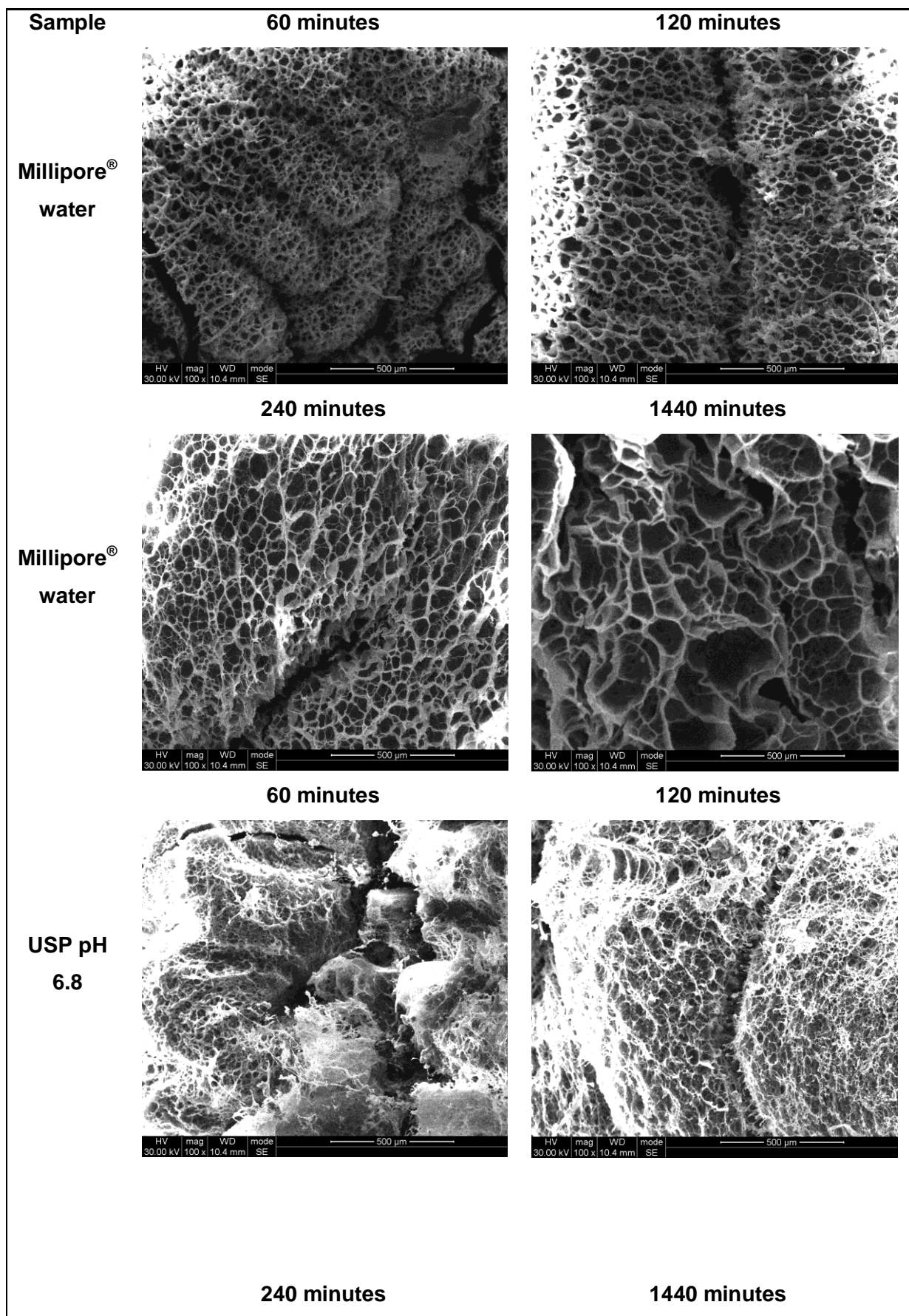


Figure 4.10: The porositometric pore volume and pore diameter analysis with respect to time of AAm-MAA hydrogel F6 within USP simulated gastric fluid (USP pH 1.2), USP simulated intestinal fluid (USP pH 6.8) and Millipore® water.

porositometric analysis indicated that within Millipore® water, these parameters increased several fold with respect to USP pH 1.2, illustrating that the increases observed during the

gravimetric swelling analysis and distance-time analysis is due to the expansion of pore dimensions that facilitated the capture of water within the macrostructure of the hydrogel (Shi et al., 2011; Guo et al., 2013). The lyophilisation process of the hydrogel samples removed aqueous solvent within the hydrogel macrostructure but maintained the architecture of the macrostructure that was achieved within each environment.

The pore morphology was observed utilizing SEM imaging of F6 samples that had been exposed to USP dissolution fluids or Millipore[®] water at predetermined time points. The presence of methacrylic acid is responsible for the observable differences of pore morphology within the dissolution fluid whereby in an acidic environment, the methacrylic acid is in the non-ionized state ($\text{CH}_3\text{C}(\text{CH}_3)\text{COOH}$) (Wang et al., 2010; Adnadjevic et al., 2011). The non-ionized state maintains a tight network structure due to extensive hydrogen bonding. This results in limited pores developing within the macrostructure of the hydrogel. The methacrylic acid undergoes ionization ($\text{CH}_3\text{C}(\text{CH}_3)\text{COO}^-$) within intestinal pH environments and results in repulsive electrostatic interactions which forces polymerized chains apart and facilitates the bulk movement of water into the hydrogel structure (Torres-Lugo et al., 2002; Kumar et al., 2006; Wang et al., 2010). As water moves into the macrostructure of hydrogel, water cages are formed around the negatively charged oxygen in the carboxyl group (Meng et al., 2013).



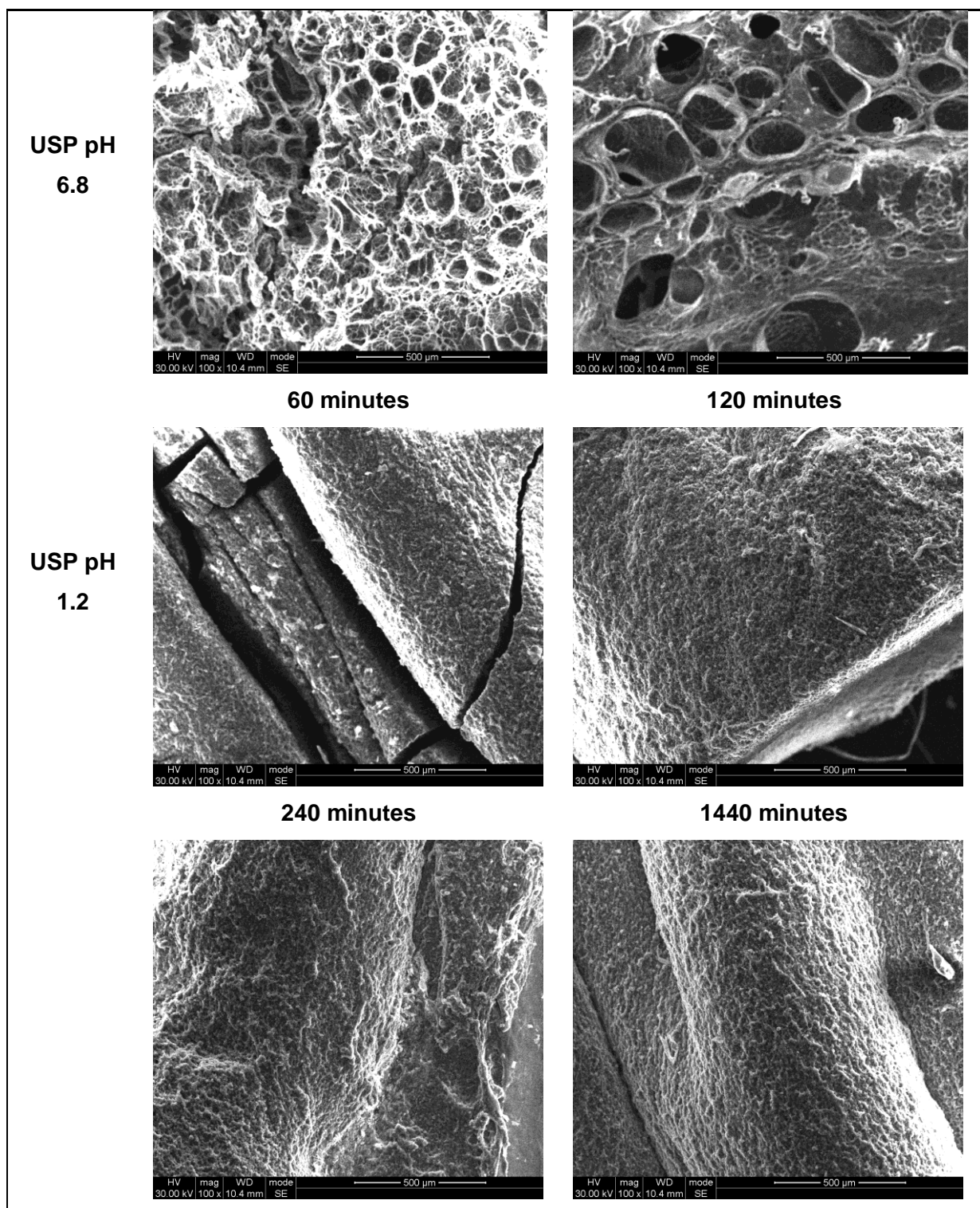


Figure 4.11: Scanning Electron Microscopy images of the crosslinked AAm-MAA hydrogel F6 within Millipore® water, USP simulated intestinal fluid (USP pH 6.8) and USP simulated gastric fluid (USP pH 1.2) at predetermined time points over a period of 1440 minutes.

These water cages stabilized the charged sites and allow the monomers within the hydrogel structure to relax during the expansion of pores. The utilization of a porogen, such as sodium hydrogen carbonate, was utilized to force the monomers to polymerize around the entrapped

carbon dioxide gas microbubbles (Kabiri et al., 2003). This physically reduced the density of crosslinker sites and allows for the accelerated dispersal of aqueous fluids through the hydrogel macrostructure by rapidly filling the voids created during the polymerization reaction. These pores are observable within the SEM images when the solvent has been sublimated out of the liquid nitrogen frozen hydrogel (Yan et al., 2011). The presence of metal ions within the USP dissolution fluids disrupts the formation of water cages around the negatively charge oxygen in the carboxyl group, and reduces the relaxation of the methacrylic acid monomers within the hydrogel. The effect of this disruption can be observed within the SEM images of F6 hydrogel samples within USP pH 6.8 dissolution fluid in comparison to Millipore® water. The inclusion of sodium bicarbonate as the porogen within hydrogel formulations was previously being recognized to create large pores that facilitate high rates of swelling (Kabiri et al., 2003).

4.5.10. UPLC detection of drug compounds

Theophylline (a BCS class I drug) was the first drug isolated and separated within the study to generate a standard curve (against internal reference caffeine). The retention time (RT) of theophylline and caffeine was determined to be 3.6 minutes and 4.7 minutes, respectively. The UPLC method was then utilized to generate a standard curve for ciprofloxacin (RT: 5.5min), indomethacin (RT: 11.7min), metronidazole (RT: 5.1min), sulfamethoxazole (RT: 7.3min) and sulpiride (RT: 11.3min), zidovudine (RT: 5.5min), 4-aminosalicylic acid (RT: 7.6min) and naproxen (RT: 8.7 min). The UPLC chromatograph for these drugs can be reviewed in the **Figure 4.11**.

The ability of the UPLC method to successfully separate the utilized drug compounds was determined in three different diluent solutions which clearly did not have overlapping retention times were assessed. The first diluent contained theophylline, caffeine, ciprofloxacin and indomethacin. The second diluent contained metronidazole, sulfamethoxazole and sulpiride whereas the third diluent contained zidovudine, 4-aminosalicylic acid and naproxen.

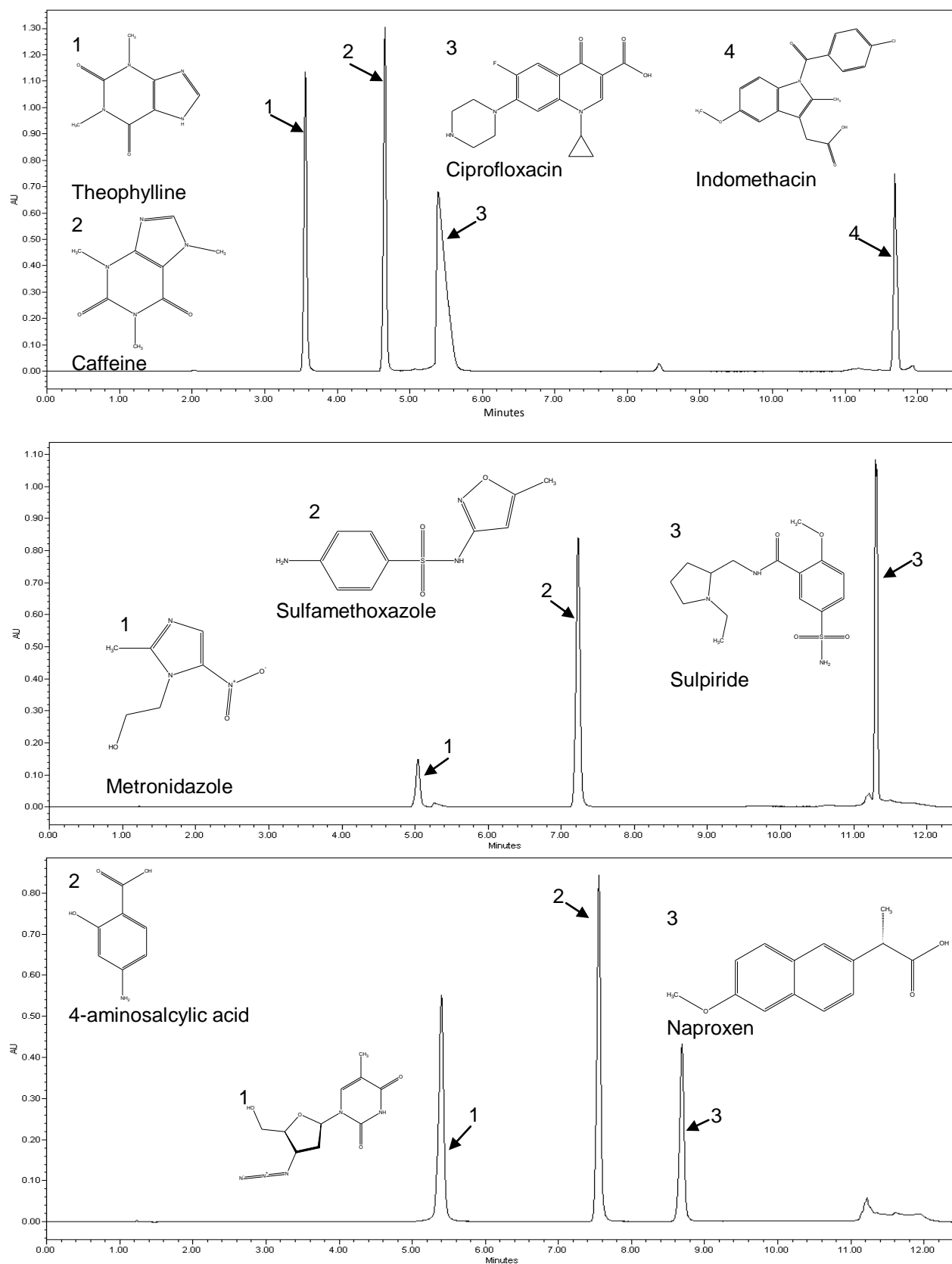


Figure 4.12: Ultra Performance Liquid Chromatography chromatograms of the retention time (RT) of theophylline (3.6min), caffeine (4.7min), ciprofloxacin (RT: 5.5min), indomethacin (RT: 11.7min), metronidazole (RT: 5.1min), sulfamethoxazole (RT: 7.3min) and sulpiride (RT: 11.3min), zidovudine (RT: 5.5min), 4-aminosalicylic acid (RT: 7.6min) and naproxen (RT: 8.7min).

4.5.11. Determination of drug entrapment efficiency within pH responsive hydrogel F6

The drug entrapment efficiency for hydrogel F6 for theophylline (0.003M), ciprofloxacin (0.17M), indomethacin (0.18M), metronidazole (0.007M), sulfamethazole (0.003M), 4-aminosalicylic acid (0.0014M) and zidovudine (0.001M) was determined to be 98.2%, 66.3%, 98.5%, 98.6%, 47.8%, 96.1% and 98.7%, respectively. The entrapment efficiency (0.03M) of sulpiride (0.003M) and naproxen was determined to be 31.4% and 24.8%, respectively. Sulpiride and naproxen had extremely low entrapment efficiency due to their very low water solubility, thus demonstrating that entrapment of a drug compound within the pH responsive hydrogel in this manner requires that the innate solubility of the API within water is high.

4.5.12. Dissolution analysis of crosslinked AAm-MAA hydrogel F6

The drug dissolution studies conducted in USP dissolution fluids, biorelevant dissolution fluids and isolated porcine GIT fluids indicate that the drug dissolution was, as expected, highly dependent on the physicochemical properties of the drug compound. Drug dissolution studies were conducted only on F6 because this formulation was the most desirable formulations from the tested formulations and there was a highly restrictive volume amount of isolated porcine GIT fluids available. The *in vitro* drug dissolution studies are shown in **Figures 4.12 4.13**. The *in vitro* dissolution of ciprofloxacin, indomethacin, metronidazole, sulfamethazole, 4-aminosalicylic acid and zidovudine is presented in **Appendix 6** and five fitted dissolution modelling with an R^2_{adjusted} above 0.98 is shown in **Appendix 7**. The *ex vivo* dissolution (conducted in isolated gastrointestinal fluids of the porcine model during the fasted state) of theophylline and ciprofloxacin is shown within **Figure 4.14**. The fractional dissolution of theophylline and ciprofloxacin against time was assessed with DDSolver add-in for Microsoft Excel 2007 and the five dissolution models that achieved an R^2_{adjusted} value greater of 0.998 was utilized. F6 was able to control the dissolution of some drugs. The presence of bile acids accelerated the dissolution of theophylline within biorelevant dissolution fluids and had a greater impact on the dissolution of theophylline than the pH of the dissolution fluid.

Theophylline

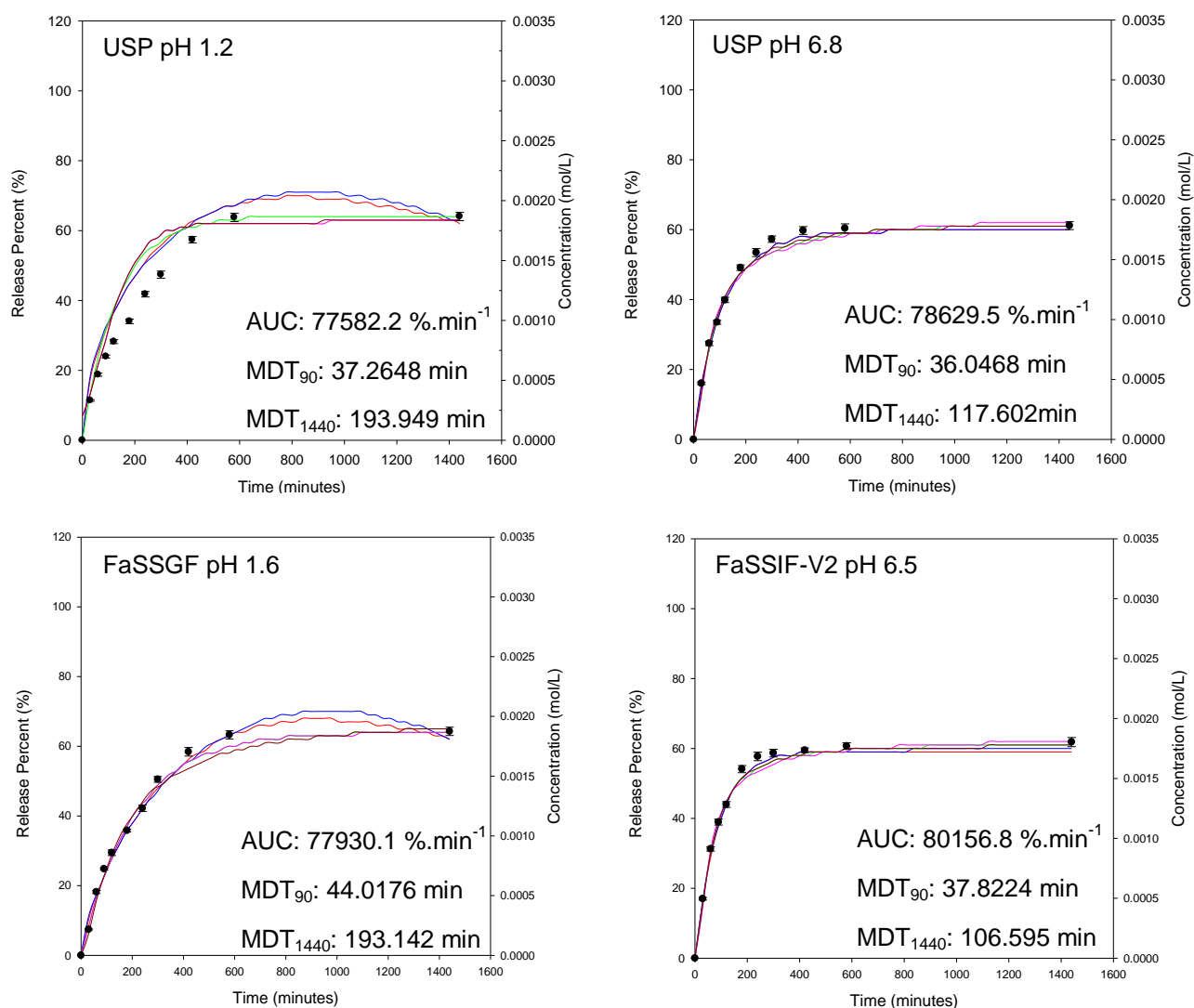


Figure 4.13: The *in vitro* dissolution of theophylline within USP simulated gastric fluid (USP pH 1.2), USP simulated intestinal fluid (USP pH 6.8), Fasted State Simulated Gastric Fluid pH 1.6 (FaSSGF pH 1.6) and Fasted State Simulated Intestinal Fluid Version 2 pH 6.5 (FaSSIF-V2 pH 6.5). The Area Under Curve (AUC), Mean Dissolution Time at 90 minutes (MDT₉₀) and Mean Dissolution Time at 1440 minutes (MDT₁₄₄₀) was determined for each dissolution profile. Five fitted dissolution modelling (red line, blue line, pink line, black line and green line) was shown for each dissolution profile.

Theophylline

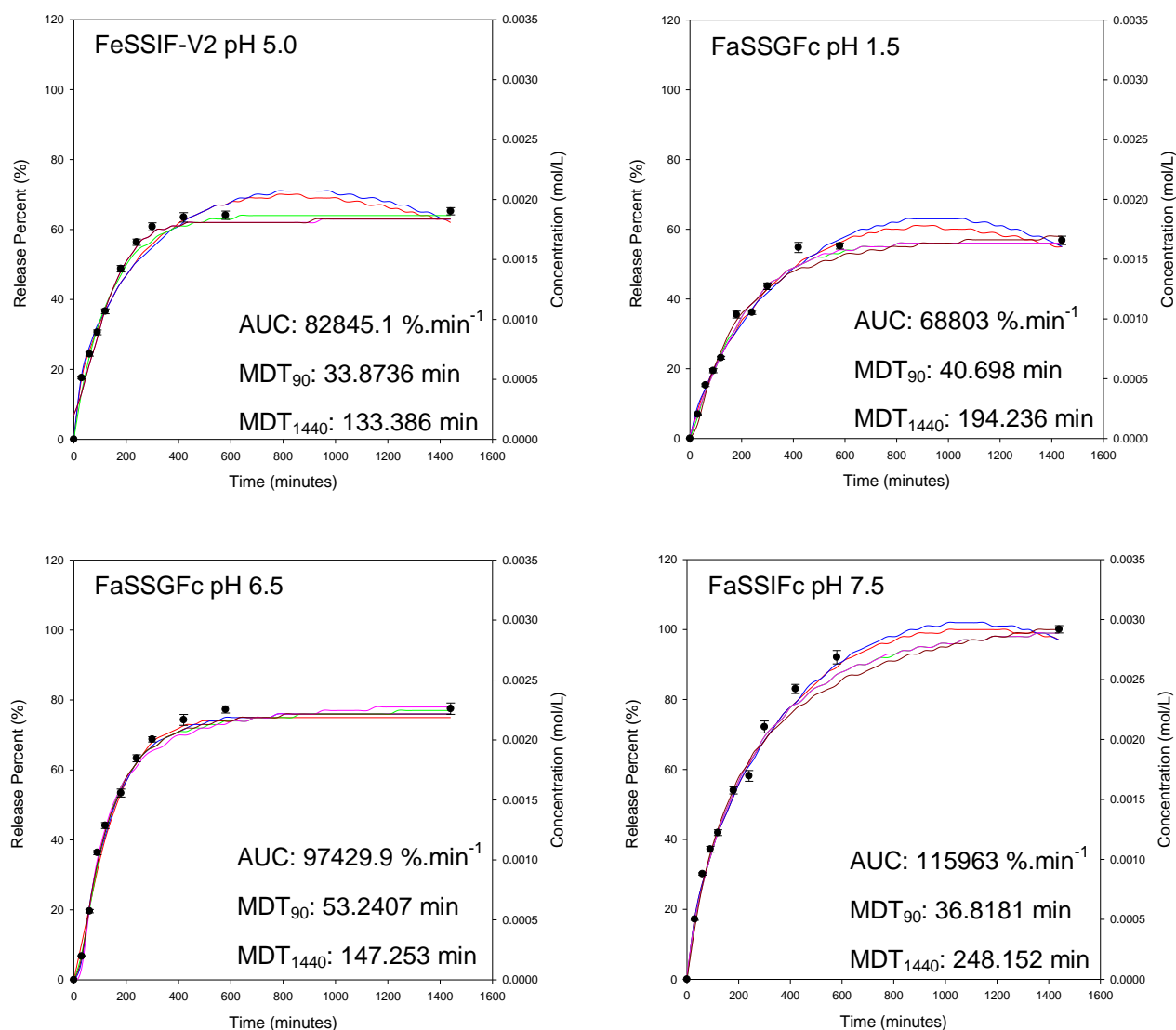


Figure 4.14: Fed State Simulated Intestinal Fluid pH 5.0 (FeSSIF pH 5.0) and Fasted State Simulated Gastric Fluid canine pH 1.5 (FaSSGFc pH 1.5), Fasted State Simulated Gastric Fluid canine pH 6.5 (FaSSGFc pH 6.5) and Fasted Stated Simulated Intestinal Fluid canine pH 7.5 (FaSSIFc pH 7.5). The Area Under Curve (AUC), Mean Dissolution Time at 90 minutes (MDT_{90}) and Mean Dissolution Time at 1440 minutes (MDT_{1440}) was determined for each dissolution profile. Five fitted dissolution modelling (red line, blue line, pink line, black line and green line) was shown for each dissolution profile.

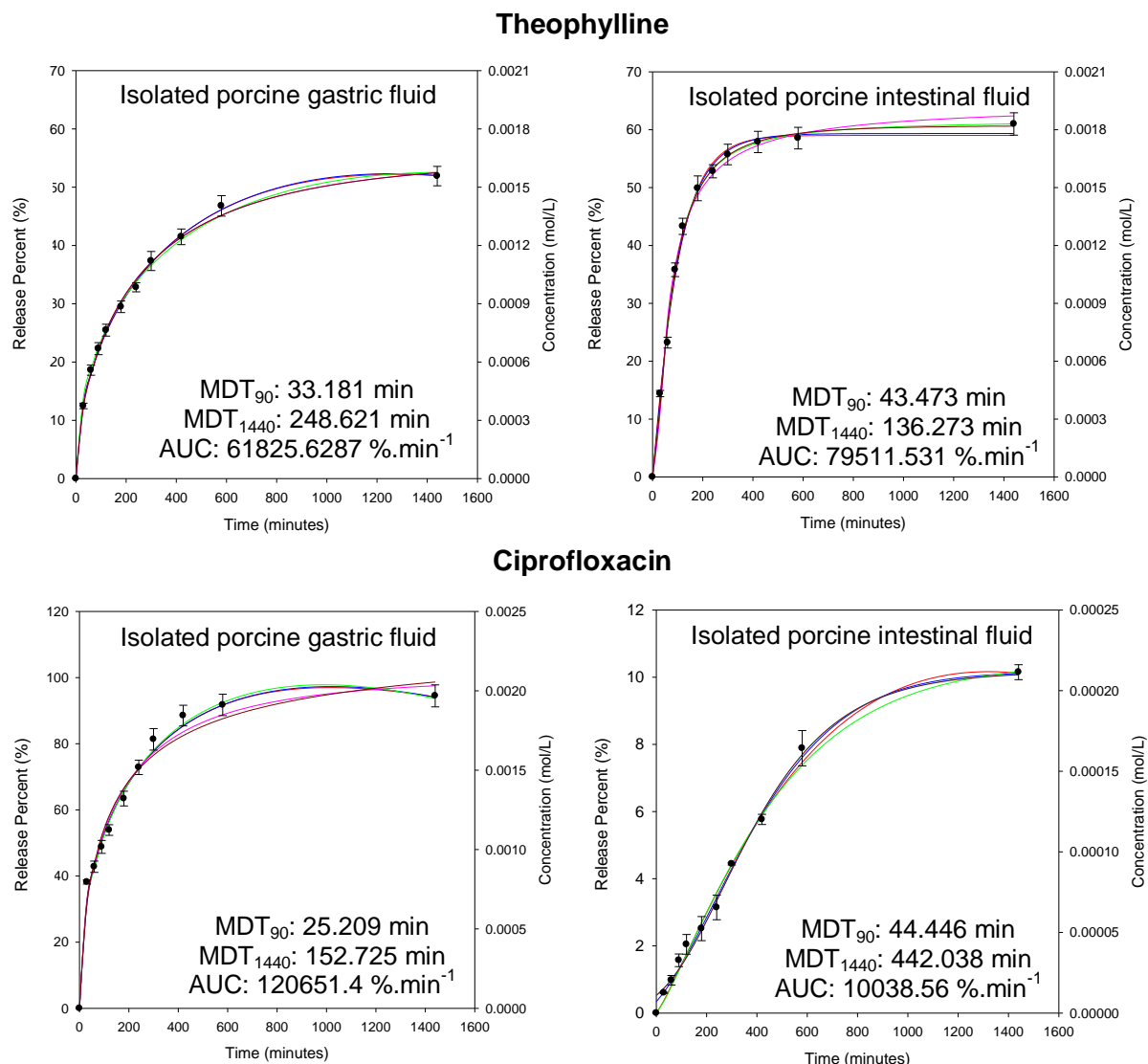


Figure 4.15: The *ex vivo* dissolution of theophylline and ciprofloxacin within isolated fasted gastric fluids and isolated fasted intestinal fluids of the porcine model. Dissolution modelling profile (R_{adjusted} value greater than 0.998) was determined utilizing DDSolver add-in for Microsoft Excel 2007 and is represented over the drug concentration-time scatter plot profiles. Mean dissolution time at 90 minutes (MDT_{90}), mean dissolution time at 1440 (MDT_{1440}) and area under curve (AUC) was determined for each profile.

The *ex vivo* analysis of drug dissolution was assessed with theophylline because of the high solubility capacity of the compound. Ciprofloxacin which is highly soluble within a gastric environment and has limited solubility within the intestinal environment was selected for dissolution studies within isolated porcine fluids. The n-octanol/pH 7.0 buffered solution partition coefficient ($\log P$) of ciprofloxacin and the lipophilicity of ciprofloxacin has been calculated utilizing fragmentation methods of atomic contributions to be -1.15 for C $\log P$ and 1.32 for $\log P$ (Vázquez et al., 2001; Kasim et al., 2004).

The mean dissolution time at 90 minutes (MDT_{90}) established that the drug dissolution of ciprofloxacin was the least restrictive within isolated gastric fluids but the most restrictive within isolated intestinal fluids. The restrictiveness of ciprofloxacin from the hydrogel matrix cannot be explained by the pH responsiveness of the hydrogel and is attributed to the innate physicochemical properties of ciprofloxacin. The MDT_{90} for theophylline increased only by 10 units between isolated porcine gastric fluid and isolated intestinal fluid.

The mean dissolution time at 1440 minutes (MDT_{1440}) increased for ciprofloxacin by 289% from isolated porcine gastric fluids to isolated porcine intestinal fluids. The MDT_{1440} of theophylline decreased 45% in isolated porcine intestinal fluid with respect to isolated porcine gastric fluid. The AUC is an indication of the extent at which the drug is successfully released, from the hydrogel sample within a solution, over the entire dissolution time period. The dissolution extent of theophylline increased 22% but the dissolution extent of ciprofloxacin decreased by 43%, within isolated porcine intestinal fluid with respect to isolated porcine gastric fluid.

Ciprofloxacin has been characterized as a zwitterionic molecule that has pK_{a1} and pK_{a2} values at 6.2 and 8.59, respectively, at 37°C (Escribano et al., 1997). The low solubility of ciprofloxacin within isolated porcine intestinal fluids (pH 8.4 ± 0.3), USP pH 6.8 and near neutral biorelevant dissolution fluids is due to the convergence of the isoelectric point of the compound and the pH of the dissolution environment. The ciprofloxacin dissolution within FaSSGF achieved the most similar extent of drug dissolution in comparison to isolated porcine gastric fluids, even though the extent was slightly underrepresented within FaSSGF.

The BCS classification of ciprofloxacin is a point of contention whereby some researchers have indicated that the drug belongs in BCS IV compounds (Wu et al., 2005; Brenda et al., 2009; Olivera et al., 2011) and other researchers (Custodia et al., 2008; Varma et al., 2012) has placed ciprofloxacin within BSC III. The BSC III classification of ciprofloxacin was incorrect, according to Olivera and co-workers (2001), due to the original determination within non-buffered aqueous solution at 25°C. Additionally, ciprofloxacin has been assigned a BDDCS IV (Benet et al., 2011). Whereas theophylline has been classified as a BCS I compound (Custodia et al., 2008; Varma et al., 2012) and a BDDCS I compound (Benet et al., 2011). Theophylline has been indicated to have a log P of 0.05 and a pK_a of 8.6, respectively (Hrabálek et al., 2006). The extent of theophylline dissolution within the isolated porcine gastric fluids was slightly lower than that in USP pH 6.8. FaSSGF and FaSSGFc pH 1.5. Whereas the extent of theophylline dissolution was very similar to that achieved within USP pH 6.8, FaSSIF-V2 and FeSSIF-V2. The purpose of this study was to demonstrate that

a dissolution profile within an *in vivo* gastrointestinal luminal environment can be highly dependent on the innate physicochemical properties of the drug compound in tandem with the physicomechanical properties of the drug delivery platform.

The F2 hydrogel has demonstrated altered physicomechanical properties within the biorelevant media and isolated porcine gastrointestinal fluids. The altered physicomechanical properties within these dissolution fluids had a significant impact in the drug dissolution profiling. The dissolution of metronidazole, sulfamethoxazole, 4-aminosalicylic acid, indomethacin, zidovudine and theophylline in near neutral pH biorelevant dissolution fluids was far more extensive than within an acidic pH biorelevant dissolution fluid. Comparatively, the dissolution of ciprofloxacin was far more extensive within acidic dissolution fluid than within near neutral dissolution fluid.

The physicomechanical properties of a hydrogel drug delivery platform can be underestimated or overestimated within dissolution fluids, which can have a knock on effect on the accurate prediction of drug release. Understanding of the innate physicochemical properties of the drug compound and the physicomechanical properties of a hydrogel within a specific dissolution environment should not be underestimated. For instance, the hydrogel formulations achieved a far greater ability to gravimetrically swell within USP dissolution fluids but the compression resistance of the hydrogel swelling under a constant force favoured near neutral biorelevant dissolution fluids. The dissolution of a drug compound may occur in an extremely extensive manner within FaSSGFc pH 6.5 in comparison to FaSSIFc pH 7.5 or vice versa. The pH difference between the two solutions is relatively small, but the concentration of bile salt and lipid compounds is vastly higher in FaSSIFc pH 7.5. The bile salt and lipid component within biorelevant dissolution fluids may reduce swelling, which limits the physical dissolution of the drug compound or the bile salt and lipid component may accelerate drug solubility which increases the extent of drug release. The collective understanding of a drug dissolution profile from the perspective of the innate physicochemical and physicomechanical properties of the drug compound and the hydrogel drug delivery platform will facilitate more successful applications of these technologies in the oral gastrointestinal tract.

4.5.14. Magnetic Resonance Imaging of crosslinked AAm-MAA formulation hydrogel 6

The real time Magnetic Resonance Imaging (MRI) analysis of F6 was determined in USP dissolution fluids and Millipore® water. Additionally, the dynamic swelling capability of F6 was assessed in response to the substitution of USP pH 6.8 to USP pH 1.2. The MRI of AAm-

MAA hydrogel F6 is shown in **Figure 4.16**.

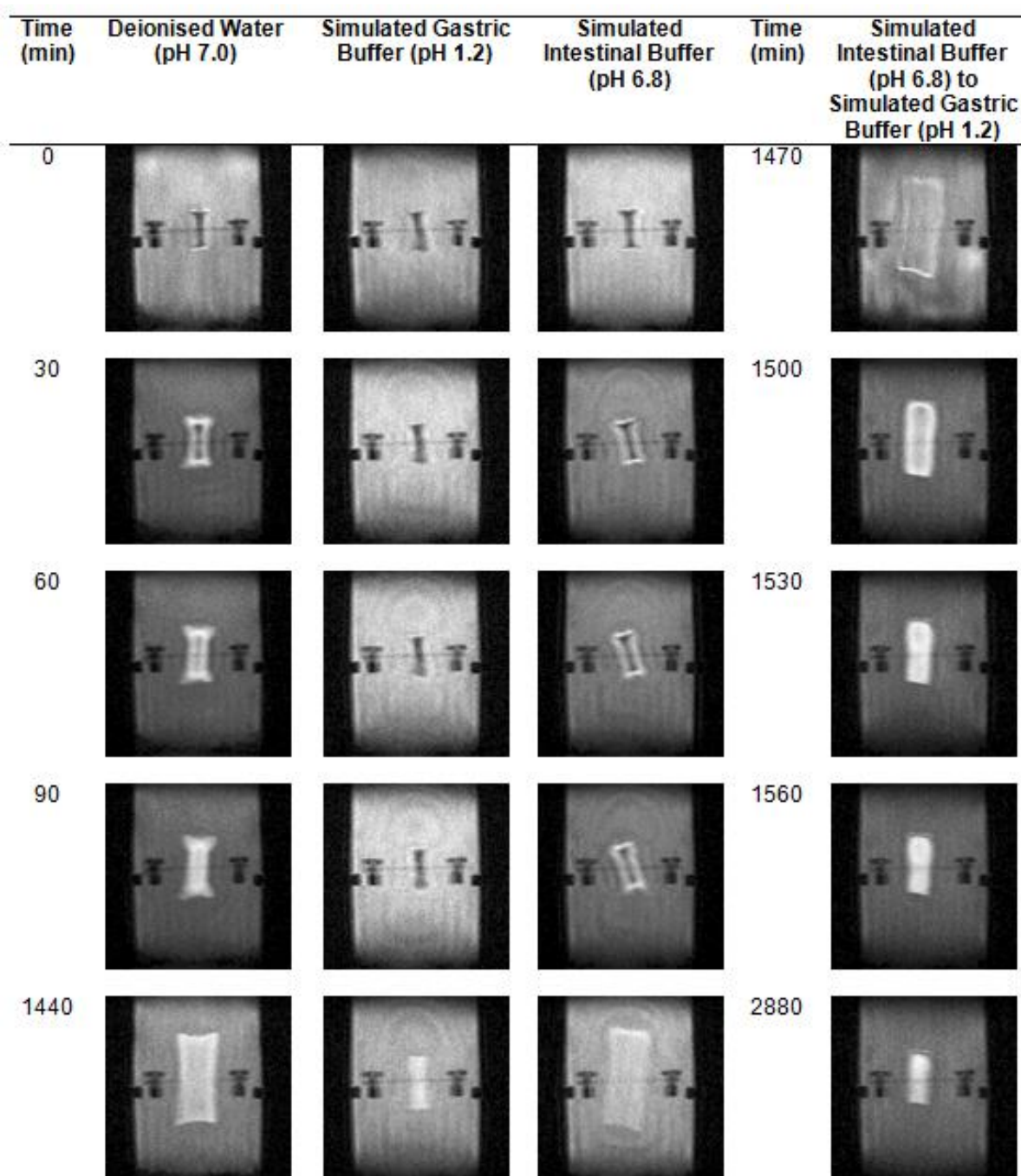


Figure 4.16: Magnetic Resonance Imaging of AAm-MAA hydrogel formulation 6 within deionised water, simulated gastric buffer (pH 1.2), simulated intestinal buffer (pH 6.8) and the dynamic equilibrating hydrogel that was first exposed to simulated intestinal buffer and then placed within simulated gastric buffer.

The real time swelling of the hydrogel formulation within Millipore® water demonstrated that swelled extensively whereas the hydrogel formulation swelled in a very limited capacity within USP pH 1.2 dissolution fluid. The real time measurement of the ability of the hydrogel

to respond to pH affirms the covalent crosslinking bonds between the monomers that make up this hydrogel and the truly pH responsive nature of the crosslinked AAm-MAA hydrogel formulation.

The ability of the F6 to shrink in response to a lower pH illustrates the true ability of the hydrogel to respond to pH and to maintain its structure during this process. This is extremely important for drug delivery applications. If the hydrogel had fractured upon reversal of pH (occurs with hydrogel systems composed of alginates), the surface area from which the loaded drug could be liberated from would be increased (Hamidi et al., 2008; Dadsetan et al., 2010; Matricaridi et al., 2013). The increased drug dissolution could cause the plasma concentration of a drug to reach toxic concentrations. Additionally, if the hydrogel formulation was utilized within a drug delivery device from a physicochemical perspective, the ability of the hydrogel to retain structure and respond to the gastrointestinal environment in a predictable manner would be highly preferable. The human gastrointestinal tract is a dynamic environment that is in constant flux due to population genetics, diet, and disease state (Guerra et al., 2012; Roeselers et al., 2012). A drug delivery application should attempt to account for this variability so that if the gastrointestinal pH profile of the individual patient is not representative of the population, the targeted dissolution of a drug can still be achieved. Even, if the dissolution of the drug compound is predictably faster or slower than what has been characterized under “ideal” circumstances. These studies indicated that F6 was very sensitive to the *ex vivo* gastrointestinal luminal environment and the MRI analysis indicates F6 would be able to predictively respond to the dynamic gastrointestinal *in vivo* environment.

4.6. Concluding remarks

The physicochemical and physicochemical properties of oral drug delivery hydrogel formulations should be assessed within biorelevant dissolution fluids. As demonstrated in this study, the gravimetric swelling and distance-time studies of a hydrogel formulation can be significantly altered by the presence of physiologically relevant entities such as bile acids and lipid components, even at similar pH. This can be an indication that *in vivo* drug dissolution may be altered by the cumulative effect of the physicochemical properties of the drug and the *in vivo* environment. The utilization of pH-sensitive hydrogel drug delivery formulations within an animal model should be reduced with the utilization of biorelevant dissolution fluids, as these dissolution fluids generally provide a more accurate determination of physicochemical characteristics than simple USP dissolution buffers.

CHAPTER 5

Optimized Eudragit® Coated Insulin Loaded Trimethyl Chitosan mPEG-EDTA Mini-Pellet Using a Box-Behnken Design

5.1. Introduction

The oral administration of peptide therapeutics is one of the most challenging aspects of current pharmaceutical research due to the innate susceptibility of these compounds to the GIT. Intensive research efforts into the oral administration of peptide therapeutics have been driven by promoting patient compliance, advances in mass peptide synthesis and exponential increases in peptide therapeutics availability (Jintapattanakit et al., 2009; Karsdal et al., 2011). There have been many approaches to achieve enhanced oral therapeutic peptide absorption within the GIT such as direct modification of the peptide molecule or modification of the localized environment (Fetih et al., 2009; Cui et al., 2009; Cheng and Lim, 2008, 2010; Huang et al., 2011). The *in vitro* development of a drug formulation which can alter the localized environment for the administration of a peptide therapeutic is a long and complicated process.

The principle focus of this chapter is the physicochemical perspective whereby the trimethyl chitosan (TMC) will be characterized and a Box-Behnken design will be utilized to generate an optimized oral dosage form. Insulin was utilized in this optimization study because this peptide is relatively inexpensive, widely available (in pure form) and has been utilized with trimethyl chitosan for oral delivery applications (du Plessis et al., 2010). In Chapter 6, insulin is substituted with salmon calcitonin because of ethical constraints in inducing diabetes within large mammal animals (e.g. the Large White Pig species) and salmon calcitonin has also been administered with TMC (Huang et al., 2011). TMC is a chitosan derivative which contains three methyl groups covalently attached to amino functional groups located within the chitosan backbone (Bravo-Osuna et al., 2007; Amidi et al., 2010). Interest in TMC:CI as a safe polysaccharide polymer that can be co-administered with peptide or protein therapeutics has increased significantly over the years (Bravo-Osuna et al., 2007; du Plessis et al., 2010). The five main properties of TMC:CI which has been the motivating force behind the interest in this particular chitosan derivative are: permeation enhancing abilities within the small intestine; bacteriostatic properties; non-toxic properties; mucoadhesive properties; and the *in vivo* degradation properties. The ability of this polymer to perform all these roles has been demonstrated in recent research and has even been used as a standard for comparing systemic absorption of a peptide therapeutic against newly developed permeation

enhancers (du Plessis et al., 2010). The main negative offset of TMC:Cl is the limited compressibility of the excipient.

In addition, auxiliary excipients ethylenediaminetetraacetic acid (EDTA), methoxypolyethylene glycol (mPEG), Ac-Di-Sol[®] and bile salt sodium, dicholate will be utilized within the mini-pellet formulations. Ac-Di-Sol[®] is a superdisintegrate excipient that enhances physical properties of a formulation when the formulation is not suspended in a solution and enhances rapid disintegration of the formulation when suspended in a solution. Bile salts such as sodium dicholate were utilized in the statistical formulation design to lower the surface tension and act as an additional permeation enhancer element (Fathi-Azarbayjani et al., 2009; Guan et al., 2011; Chun et al., 2012). The reduction of surface tension within a localized intestinal environment allows for increased solubilization rates, thereby liberating the peptide therapeutic within the desired location rapidly.

5.2. Materials and Methods

5.3. Materials

Chitosan (medium molecular weight) with a degree of deacetylation of 77.0% was purchased from Aldrich (Schnelldorf, Germany). Trimethyl chitosan chloride (TMC:Cl) was prepared by reductive methylation. Methoxypolyethylene glycol 2000 (mPEG), ethylenediaminetetraacetic acid (EDTA, 99.995% pure), sodium iodide (≥99.5% pure), methyl iodide (99.5% pure), sodium hydroxide (≥98% pure), sodium chloride (≥99% pure), hydrochloric acid (37%^{v/v}), sodium deoxycholate (≥98% pure), sodium sulphate (≥99% pure), maleic acid (99% pure), lysophosphatidylcholine (≥99% pure), sodium taurocholate (≥90% purity), sodium taurodeoxycholate (≥97% purity), dichloromethane (≥99.9% pure), sodium dihydrogen phosphate monohydrate (≥99% purity) and orthophosphoric acid (85%^{w/v}, 99.99% pure) were purchased from Sigma-Aldrich (St. Louis, Missouri, USA) at reagent grade and were utilised without further purification. Acetonitrile (≥99.9% pure) and sodium oleate (≥99% pure) was purchased from Sigma (St. Louis, Missouri, USA) at UPLC grade. Diethyl ether (≥98% purity), ethanol (≥99.8% pure), *N*-methyl-2-pyrrolidone (≥99.5% pure) was purchased from Merck (Halfway House, Gauteng, South Africa) at reagent grade and were utilised without further purification. Actrapid[®] HM (insulin) was purchased from a local pharmacy (Novo Nordisk Ltd., West Sussex, UK). Ac-Di-Sol[®] was purchased from FMC BioPolymer (Postterminalen, Haugesund, Norway). Egg phosphatidylcholine (97.5% pure) purchased from Lipoid GmbH (Ludwigshafen, Germany).

5.4. Methods

5.4.1. Synthesis of mini-pellet components

5.4.1.1. Preparation and characterization of trimethyl chitosan chloride

TMC:Cl was synthesized with slight modification as previously described (Polnok et al., 2004). Briefly, TMC:Cl was synthesized by a two reaction step and an ion-exchange step process. Two grams of chitosan (medium molecular weight, 77% deacetylated), 10mL of 20%^{w/v} sodium hydroxide solution and 4.8 grams of sodium iodide was dissolved in 80mL of pre-warmed *N*-methyl pyrrolidone ($60\pm0.2^{\circ}\text{C}$). The reaction was carried out over a 30 minute period in a heated water bath ($60\pm0.2^{\circ}\text{C}$). The homogenous solution was then removed from the heated water bath and 12mL of methyl iodide was immediately incorporated within the solution. The reaction was allowed to complete under reflux, by utilization of a Liebig condenser, under constant magnetic stirring (300rpm) for 90 minutes ($60\pm0.2^{\circ}\text{C}$). The homogenous polymer solution is then removed and the trimethyl chitosan iodine precipitated out of solution with 250mL diethyl ether and 250mL ethanol. Trimethyl chitosan iodine was collected and dried *in vacuo* ($60\pm0.5^{\circ}\text{C}$ for 48 hours). The dry trimethyl chitosan iodine was ground into a fine powder and utilized within the second reaction step. The second reaction step utilized the same procedure as that preformed in the first step but chitosan was substituted with trimethyl chitosan iodine. Once the polymer product from the second reaction had been dried and ground into a fine powder, the ion-exchange step was conducted. The second reaction step trimethyl chitosan iodine powder was dissolved in 80mL of 5%^{w/v} sodium chloride solution for 30 minutes under constant magnetic stirring (300rpm). Diethyl ether (250mL) and ethanol (250mL) was utilized to precipitate trimethyl chitosan chloride. The precipitated TMC:Cl was isolated by filtration and dried *in vacuo* ($60\pm0.5^{\circ}\text{C}$ for 24 hours). The reaction process can be reviewed in **Figure 5.1**.

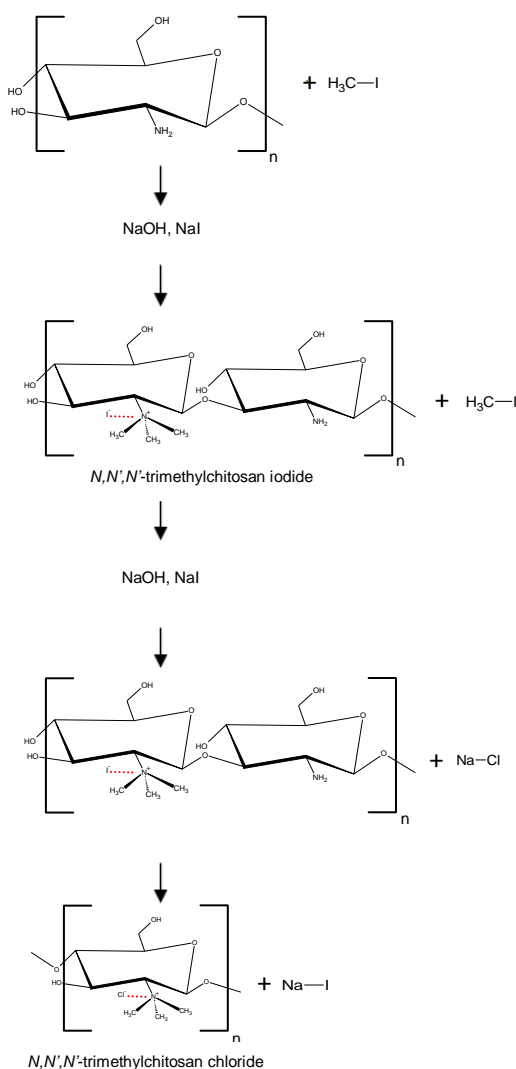
5.4.1.2. Preparation of EDTA-mPEG *in situ* hot melt dispersion powder (a component of the trimethyl chitosan mini-pellet formulation)

An *in situ* hot melt dispersion of 50%^{w/w} EDTA-mPEG was prepared. Briefly, the solid phase mPEG was heated to a liquid phase by melting at a temperature of 60°C . EDTA was added to the molten mPEG and homogenously mixed until a uniform distribution was achieved. The EDTA-mPEG *in situ* hot melt dispersion was allowed to cool under constant stirring until a solid phase was achieved. The solid mass was placed through a metal sieve with an aperture of $850\mu\text{m}$ to form a fine powder.

5.4.2. Characterisation of trimethyl chitosan and chitosan

5.4.2.1. Attenuated Total Reflectance-Fourier Transform Infrared analysis

Attenuated Total Reflectance-Fourier Transform (ATR-FTIR) spectroscopy was carried out on chitosan and TMC:Cl as a means of validating the successful inclusion of trimethyl groups at amino group sites along the chitosan backbone. A Perkin Elmer Spectrum 2000 FTIR spectrometer with a single reflectance MIRTGS detector, (PerkinElmer Spectrum 100, Llantrisant, Wales, UK) was utilized. Samples of chitosan and TMC:Cl were prepared and placed on a diamond crystal which was then processed by a universal ATR polarization accessory for the ATR-FTIR spectrum series, at a resolution of 4cm^{-1} . Each sample was analyzed after 100 scans (SNR:10) at 130psi between $650\text{-}4000\text{cm}^{-1}$ range against 100 0background scans.



N-methyl-2-pyrrolidone (80mL) is heated to 60°C utilizing a round bottom flask and a calibrated water bath. Chitosan (2g) and sodium iodide (4.8g) is added to the pre-warmed N-methyl-2-pyrrolidone. The solution is maintained at 60°C for 30 minutes. Methyl iodide (12mL) is added to the solution after 30 minutes. The round bottom flask which contains the reacting solution is placed on a pre-warmed (60°C) magnetic stirrer and allowed to react under constant reflux utilizing a Liebig condenser. The reacting solution is maintained for 90 minutes under constant reflux, after which diether ether (250mL) and ethanol (250mL) is utilized to precipitate trimethyl chitosan iodide. The precipitate is filtered and placed within a vacuum oven to dry for 48 hours.

The reaction is repeated where the chitosan is substituted with the dried trimethyl chitosan iodide. The second reaction step is carried out to increase the quarterisation of the final trimethyl chitosan chloride product.

The dried trimethyl chitosan iodide product from the second reaction is dissolved within a solution of 5% sodium chloride (40mL) to complete the ion exchange step of the reaction. The trimethyl chitosan chloride product is precipitate out of solution with ethanol (500mL) and diether ether (500mL) and dried in a vacuum oven (60°C) until dry.

Figure 5.1: Schematic representation of the synthesis of trimethyl chitosan chloride.

5.4.2.2. Thermal Gravimetric Analysis of trimethyl chitosan and chitosan for the temperature at which maximal degradation occurs

Thermal gravimetric analysis (TGA) of chitosan and TMC:Cl was carried out with the utilization of a Thermogravimetric Analysis-4000 (Perkin Elmer, Waltham, MA, USA) under constant inert nitrogen atmosphere. Accurately weighed samples ($10\pm0.5\text{mg}$) were placed within the textile crucible. The weight percentage of water, the maximum temperature of degradation (first derivative), the rate of degradation, onset of degradation and the endset of degradation was determined. The TGA protocol was performed with a ramping temperature of $10^\circ\text{C}/\text{min}$ between the temperature range of 30°C to 700°C .

5.4.2.3. Differential Scanning Calorimetry analysis to determine the unique heat capacities of trimethyl chitosan and chitosan

Dry samples of chitosan and TMC:Cl were subjected to Differential Scanning Calorimetry (DSC) analysis utilizing a Differential Scanning Calorimeter (Mettler Toledo, Columbus, OH, USA). Accurately weighted samples ($10\pm0.4\text{mg}$) were placed in $40\mu\text{L}$ aluminium crucible pans. An open crucible system was induced by a 0.2mm hole in the lid of the aluminium crucible pan, which was then hermetically sealed. An inert nitrogen atmosphere ($50\text{ mL}/\text{min}$) was maintained throughout the DSC protocols. The thermogram traces were compared to determine changes in the onset of melting, melting peak temperature and heat of fusion for each sample. DSC protocols were run with a ramping temperature of $2^\circ\text{C}/\text{min}$, $5^\circ\text{C}/\text{min}$ and $10^\circ\text{C}/\text{min}$ between the temperature range of $25\text{--}110^\circ\text{C}$ (first run) and, was repeated for the same sample between the temperature range of $25\text{--}500^\circ\text{C}$ (second run).

5.4.2.4. Powdered X-ray Diffraction for the determination of crystallinity in trimethyl chitosan and amorphism in chitosan

The powder XRD patterns were determined for chitosan and trimethyl chitosan chloride samples utilizing a 600 Watt Miniflex diffractometer (Rigaku, Tokyo, Japan) with $\text{CuK}\alpha$ (1.5406\AA) radiation. The powdered samples were analysed over a $0\text{--}90^\circ$ 2-Theta range. The crystallinity degree was determined to correlate the observed chitosan and trimethyl chitosan morphology.

5.4.2.5. Morphological analysis of trimethyl chitosan and chitosan

Scanning Electron Microscopy (SEM) imaging was conducted in order to determine the

surface structure and morphology of chitosan and TMC:Cl. Each sample was mounted on a stub with silicon tape and sputtered coated with gold for 210 seconds. Each sample was then placed in a FEI Phenom™ Desktop Scanning Electron Microscopy (Eindhoven, The Netherlands) so that SEM images could be acquired.

5.4.3. Isolation of porcine small intestinal tissue and gastrointestinal fluids

The Large White pigs utilized in this study were obtained according to the *Guide for the Care and Use of Laboratory Animals* that was approved by the Animal Ethics Screening Committee of the University of Witwatersrand (Ethics number:2011/33/03). The gastric and small intestinal fluids were collected after euthanization. The gastrointestinal fluids isolated from the pigs were collected during the fasted state. The fasted state was induced within the pigs by restricting food for 12 hours but the pigs were provided water *ad libitum*. This is a standard procedure for dosing pigs with an oral drug delivery system. The pigs were euthanized to achieve two objectives, retrieval of the small intestinal tissue and ensuring that the isolated gastrointestinal fluids was withdrawn from the appropriate organ by dissection. The stomach and small intestine was isolated and a small incision was made to perforate the respective organ wall. Blood was removed from the incision points with highly absorbent tissue paper and injection plungers were inserted into the incision points for the removal of the luminal fluid from the respective organ.

The pH and buffer capacity of the isolated gastric and small intestinal fluids (individual and pooled samples) were measured immediately. The pooled sample was maintained with an equal addition from each individual sample. To preserve the composition of the gastrointestinal fluid, the samples were immediately frozen in liquid nitrogen and maintained at -80°C. In order for drug dissolution and disintegration studies to be effectively performed, removal of solid matter (food particles and ingested hay) from the samples was achieved by centrifugation at 5000rpm for 10 minutes at 10°C, followed by filtration of the supernatant through a 0.44µm injection filter.

5.4.4. USP 35 and biorelevant dissolution fluid utilized for rheological, dissolution and disintegration experimentation

The USP 35 dissolution media for the simulated gastric (pH 1.2) and simulated small intestinal (pH 6.8) conditions were prepared according to the USP 35. The fasted and fed state biorelevant media (FaSSGF, FaSSIF V2, FeSSIF V2) for the human model was prepared as previously described (Jantratid and Dressman, 2009; Fotaki and Vertzoni, 2010;

Klein, 2010). The fasted and fed state biorelevant media (FaSSIFc, FaSSGFc pH 1.5, FaSSGFc pH 6.5) for the canine model was also prepared according to a previously described methodology (Arndt et al., 2013).

5.4.5. Viscosity analysis of the trimethyl chitosan chloride within dissolution media and isolated gastrointestinal fluids of the porcine model

The viscosity properties of dissolution fluids (USP and Biorelevant), isolated porcine gastrointestinal fluids (fasted state) and 0.1%^{w/v} TMC weight concentrations within each solvent were determined. The viscosity (η) was determined using a Modular Advanced Rheometer (ThermoHaake MARS Modular Advanced Rheometer, Thermo Electron, Karlsruhe, Germany) equipped with a C35/1° Ti sensor. Measurements were performed employing the rheological parameters shown in **Table 5.1**. All rheological procedures were run at 37°C.

Table 5.1. Rheological parameters utilized for the analysis of trimethyl chitosan chloride within dissolution media and isolated gastrointestinal fluids of the porcine model

Parameter	Value
Cone and plate gap	0.0051m
Driver version	0.29
Inertia	89051.00PA
A-factor	$1.721 \times 10^{-6} \text{Kg.m}^2$
M-factor	57.01rad/s
Temperature	37°C
Damping	30.00

The solutions were prepared and immediately placed between the cone and base plate of the rheometer. The samples (1mL) for 180s at a yield stress of 5s^{-1} and 200s^{-1} . The results were recorded ($n=3$) and subjected to a box and whisker statistical analysis.

5.4.6. Box-Behnken Design of insulin loaded trimethyl chitosan chloride mini-pellet formulations

A 3-factor Box-Behnken statistical experimental design was generated using Minitab® V15 software (Minitab Inc., PA, USA) in order to obtain 15 statistically relevant formulations. The Box-Behnken statistical design is utilized to establish a relationship between independent formulations variables with physicochemical and physicommechanical responses obtained from the insulin loaded trimethyl chitosan mini-pellet (insulin-TMC:Cl MiPe) formulations. Ac-Di-Sol® (10-30mg), sodium deoxycholate (0-5mg) and EDTA-mPEG *in situ* hot melt

dispersion (10-20mg) were selected as independent formulation variables. Insulin-TMC:CI (90mg) was included within each formulation and TMC:CI was added to each formulation so that the total weight of each formulation was 145mg. The responses deemed most important for these formulations were the matrix hardness, the mean dissolution time after 2.5 hours and the fractional dissolution after 8 hours. The polynomial equation for this design is shown as **Equation 5.1**. The independent factors and the dependent variables used in the design are listed in **Table 5.2**.

$$y = b_0 + b_1(mPEG) + b_2(ADS) + b_3(BS) + b_4(mPEG)^2 + b_5(ADS)^2 + b_6(BS)^2 + b_7(mPEG)(ADS) + b_8(mPEG)(BS) + b_9(ADS)(BS) \quad (\text{Eqn. 5.1})$$

Where y is the measured response associated with each factor combination of 50%^{w/w} mPEG-EDTA *in situ* hot melt dispersion, Ac-Di-Sol[®] (ADS) and sodium deoxycholate (BS). The regression co-efficients are represented by b₀ to b₉. The design required a total of 105 experimental runs (each formulation was measured in triplicate) and was analyzed using Minitab[®] V15 software.

Table 5.2. The 3-factor, 3-level Box-Behnken Design variables utilizing MINITAB V15 software

Independent Variables	Levels		
	Low	Medium	High
mPEG-EDTA (% ^{w/w}) ^a	10	15	20
Ac-Di-Sol [®] (% ^{w/w}) ^b	10	20	30
BS (% ^{w/w}) ^c	0	2.5	5
Dependent Variables	Low	High	Objective
Matrix Hardness	60	110	Maximum
MDT within 2.5 hours ^d	0.9	1.55	Maximum
Maximal fractional dissolution after 8 hours	0.4	1.0	Maximum

^amPEG-EDTA indicate 50%^{w/w} methoxypolyethylene glycol 2000-ethylenediaminetetraacetic acid

^bAc-Di-Sol[®] indicates croscarmellose sodium

^cBS indicates sodium deoxycholate

^dMDT indicates mean dissolution time

5.4.7. Preparation of insulin loaded trimethyl chitosan chloride mini-pellet formulations

5.4.7.1. High Performance Liquid Chromatography of insulin

The concentration of insulin within dissolution solvents was determined utilizing a High Performance Liquid Chromatography (HPLC) machine with a Waters 1525 Binary Pump,

2489 UV/visible detector and an auto-sampler attachment (Waters, Milford, MA, USA). A C₁₈ silica based reverse phase Symmetry 300 column (Waters, Milford, MA, USA) with a particle size of 5µm was utilized for isolation and accurate determination of insulin concentration. The absorbance was monitored at 214nm and the column temperature was maintained at 40°C. Solvent A (100% acetonitrile) and Solvent B (28.4g of sodium sulphate dissolved in 1000mL Millipore water, and 2.7mL orthophosphoric acid to adjust pH to 2.3 [the pH of the solution was adjusted with ethanolamine]) was utilized in an isocratic gradient of Solvent A and Solvent B at a ratio of 26:74 (Yomota et al., 1996).

5.4.7.2. Insulin incorporation and entrapment studies of insulin within trimethyl chitosan chloride powder

The homogenous incorporation of insulin within TMC:Cl powder was achieved by accurately weighing 2500mg TMC:Cl powder which was dissolved in Millipore® water to a final concentration of 5%^{w/v}. The TMC:Cl solution was stirred at 30rpm for 30 minutes, at which point a viscous yellow solution was obtained. The insulin solution (Actrapid® HM 100) was added and homogeneously incorporated within the TMC:Cl solution at room temperature for 30 minutes, in order to obtain a final concentration of 1IU insulin per 3.2mg of TMC:Cl powder. The dispersion was frozen at -80°C for 48 hours. The frozen insulin-TMC:Cl solution was lyophilized with a 2 hour condensation phase at -60°C and a 24 hour sublimation phase at 25 mmTorr utilizing Freezone 12 freeze drier (Lanconco, Kansas City, USA). After freeze-drying, the sample was placed within sealed glass polytops and maintained at -20°C (Pringels et al., 2004; Silva et al., 2006). The water content of the lyophilized insulin samples was determined with a Karl Fischer volumetric titrator (Mettler Toledo, Columbus, USA) with a DN143-SC sensor attachment. The Karl Fischer volumetric titrator was maintained at 25°C with a start potential of 596.5mV and a titrant concentration of 5.33724mg/mL. The homogenous entrapment efficiency of insulin within TMC:Cl powder was determined by weighing a defined amount of lyophilized TMC:Cl powder (*n*=3). The TMC:Cl powder/insulin lyophilized product was dissolved within 20mL of USP 35 simulated intestinal buffer (pH 6.8, 37°C). A 1mL sample was withdrawn from each solution after 3 hours and placed within an ANSI HPLC vial. The concentration of the samples was measured using HPLC. The homogenous entrapment efficiency was calculated according to **Equation 5.2**.

$$HEE = \frac{C_{t3 \text{ (measured)}}}{C_{\text{loaded dose}}} \times 100 \quad \text{(Eqn. 5.2)}$$

Where HEE is homogenous entrapment efficiency, $C_{t3 (measured)}$ is the concentration of insulin measured at 3 hours; $C_{loaded\ dose}$ is the amount of insulin originally loaded into the trimethyl-chitosan suspension.

5.4.7.3. Direct compression of mini-pellets

Insulin-TMC:Cl powder, mPEG-EDTA *in situ* hot melt dispersion powder, Ac-Di-Sol[®] microcrystalline cellulose and dry TMC:Cl powder was accurately weighed according to the Box-Behnken design and utilized to produce mini-pellet formulations through dry granulation. The homogenous excipient mixtures were compressed at 3.4MPa within a modified punch and die set to produce 4mm diameter mini-pellets. The mini-pellets were immediately stored at -20°C.

5.4.8. Textural profile analysis of insulin loaded trimethyl chitosan chloride mini-pellet formulations

5.4.8.1. Physicomechanical analysis

The physicochemical properties of the mini-pellet formulations were evaluated with respect to matrix hardness (MH), and deformation energy (DE). A calibrated Textural Analyzer (TA.XTplus, Stable Microsystems, Surrey, UK) fitted with a flat tip steel probe (2mm diameter; for MH and DE) was utilized. The parameters utilized for the analysis is outlined in **Table 5.3**. All studies ($n=3$) were conducted at standard operating procedures (25°C, 1atm. pressure). MH (N/mm²) and DE(J) were both determined based on force-distance profiles, in particular, MH was elucidated from the gradient between the initial force and the maximum force attained, and the DE from the Area Under Curve (AUC).

Table 5.3. Textural profiling parameters settings employed for physicochemical, mucoadhesive and disintegration characterisation of the mini-pellet formulations

Parameters	MH ^a (N/mm ²)	DE ^b (J)	Mucoadhesive test	Disintegration test
Option		Return to start		Hold until reset
Pre-test speed (mm/s)	1	1	0.5	2.0
Test speed (mm/s)	0.5	0.5	0.5	3.0
Post-test speed (mm/s)	10	10	10	10.0
Applied force (N)	0.1	0.1	5	0.01
Trigger type	Auto	Auto	Auto	Auto
Trigger force (N)	0.05	0.05	0.05	0.05
Load cell (Kg)	5	5	5	5
Target mode	Distance	Distance	Distance	Distance
Tare mode	Auto	Auto	Auto	Auto

^aMatrix Hardness

^bDeformation energy

5.4.8.2. *Ex vivo* mucoadhesive analysis

The *ex vivo* mucoadhesive analysis was performed ($n=3$) for each mini-pellet formulation generated within the Box-Behnken design and a blank chitosan mini-pellet formulation. Fresh porcine small intestine epithelium tissue was dissected longitudinally and then dissected horizontally into 5cm x 5cm square pieces (Hagesaether et al., 2009). The small intestinal epithelium tissue pieces were then washed with sterile saline solution (0.9%^{w/v} NaCl) to remove the mucus layer which was tainted with imbedded partly digested matter. A solution which contained mucin (3%^{w/v}) and phosphate buffer (pH 6.8) was prepared to simulate the mucous layer (Hagesaether et al., 2009). The small intestine epithelium tissue samples were attached to a 2cm cylindrical probe with nylon string and then attached to the TA.TX *plus* Texture Analyzer (Stable Micro Systems, Surrey, UK). The mini-pellet was attached to the stage of the Texture Analyzer using double sided adhesive tape (Hagesaether et al., 2009). Mucin solution (60 μ L) was applied to the mini-pellet formulation and the Textural analyzer probe was immediately lowered to come in contact with the mini-pellet. This process facilitated mucoadhesion between the insulin-TMC:CI MiPe formulation and the porcine small intestinal tissue sample. The probe was then raised slowly to measure the Work of Adhesion (WA) which is determined from the AUC in the force distance profile. The maximum detachment force (MDF) was determined from the maximum inflection point of the force distance profile. The procedure was repeated with fresh small intestine epithelium tissue samples for each insulin-TMC:CI MiPe formulation without the application of mucin solution for comparative purposes. The parameters utilized within this analysis are presented in **Table 5.3**.

5.4.9. Dissolution studies and dissolution fitting analysis of mini-pellet formulations

In vitro dissolution of insulin from the Eudragit[®] coated insulin-TMC:CI MiPe formulations was determined by a method described previously (Dünnhaupt et al., 2012). Insulin-TMC:CI mini-pellets were spray coated with Eudragit[®] (4%^{w/w} solution of Eudragit[®] L100 and 4%^{w/w} solution of Eudragit[®] S100 within an organic solvent composed of 33%^{v/v} ethanol and 67%^{v/v} acetone. Triethyl citrate was added to the solution at a concentration of 35%^{w/w} of the Eudragit[®] component of the spray coating solution). The Eudragit[®] coated insulin-TMC:CI MiPe formulations were dried at room temperature for 3 hours (coating layer was 0.5mm/surface as determined by comparative measurements between pre-coated and coated mini-pellet formulations). Eudragit[®] coated insulin-TMC:CI MiPe formulations were placed in 20mL glass polytops containing 10mL USP 35 simulated gastric fluid (pH 1.2) for 2 hours and in 10mL USP 35 simulated intestinal fluid (pH 6.8) for 8 hours. Polytops were placed within an Orbit Shaker Incubator (LM-530-2, MRC Laboratory Instruments Ltd, Hahistadrut, Holon, Israel) at 37±0.5°C and 50rpm, sink conditions were maintained throughout the study.

For each mini-pellet formulation, nine replicates were tested, all from the same production batch. Samples were withdrawn at 0, 15, 45, 90, 150, 270, 390 and 450 minutes and replaced with an equal volume of USP 35 simulated gastric or intestinal fluid which had been equilibrated at 37±0.5°C to maintain sink conditions. The samples were filtered through a 0.22µm Millipore Millex filter (Billerica, MA, USA) and placed within ANSI 48 HPLC vials. The samples were maintained at 4°C and analyzed using HPLC within 12 hours of acquisition. Concentrations were calculated by interpolation from a standard curve. Cumulative corrections were made for previously removed samples in determining the total amount released. The concentration of insulin (IU/mL) against time (hour) profile for each Eudragit[®] coated insulin-TMC:CI MiPe formulation was generated utilizing DDSolver add-in for Microsoft Excel 2007. The mean dissolution time (MDT) over the first 2.5 hours was determined according to the **Equation 5.3**. The fractional dissolution of insulin after 8 hours for each formulation was determined according to **Equation 5.4**.

$$MDT = \sum_{i=1}^n \tau_i \frac{M_t}{M_{\infty}} \quad (\text{Eqn. 5.3})$$

Where M is the fraction of dose released in time $\tau_i = (t_i - t_{i-1})/2$ and M_{∞} corresponds to the loading dose.

$$FD_{t8} = \frac{C_{t8}}{C_{TD}} \quad (\text{Eqn. 5.4})$$

Where FR_{t8} is fractional dissolution after 8 hours, C_{t8} is the concentration of insulin at 8 hours, C_{TD} is the total dose of insulin within the formulation.

5.4.10. *In vitro* and *ex vivo* characterization of the optimized Eudragit® insulin loaded mini-pellet formulation within biorelevant dissolution fluid and isolated porcine gastrointestinal fluids

5.4.10.1 Physicomechanical characterization of the optimized insulin loaded trimethyl mini-pellet formulation

The physicomechanical characterization and *ex vivo* mucoadhesive analysis of the optimized insulin-TMC:CI MiPe formulation was conducted in the same manner as described during the Box-Behnken studies.

5.4.10.2. Disintegration analysis

The disintegration studies of the optimized Eudragit® insulin-TMC:CI MiPe formulation was evaluated on a Textural analyzer (TA.XT plus, Stable Microsystems, UK). A specialty probe was attached to the Textural analyzer that facilitates the capture of a disintegration profile. Water soluble glue was used to attach the optimized Eudragit® insulin-TMC:CI MiPe to a probe head which magnetically attaches to the probe shaft. A reservoir of USP 35 simulated fluids, biorelevant dissolution fluids for the canine and human model was utilized as reservoir fluids. In addition, isolated porcine gastric and small intestinal fluids (fasted state) were also utilized as reservoir fluids. The optimized Eudragit® coated insulin-TMC:CI MiPe formulation was lowered into the reservoir, the mini-pellet comes in contact with a magnetic gridded base plate and the distance from the magnetic gridded base plate to the surface of the probe head is captured. As the insulin-TMC:CI MiPe formulation disintegrates within the respective dissolution solvent or isolated gastrointestinal fluid, the probe is lowered and the distance moved over time is captured as a disintegration profile. The disintegration profile for each fluid was compiled and the disintegration rate at each respective time period was determined ($n=3$). The obtained data points (including standard deviations) were placed within a scatter plot and a regression curve was fitted to these scatter points. The parameters utilized for Textural disintegration analysis is outlined in **Table 5.3**.

5.4.10.3. Dissolution of optimized Eudragit[®] coated insulin loaded trimethyl chitosan mini-pellet formulation

The optimized Eudragit[®] coated insulin-TMC:CI MiPe formulation was prepared in the same manner as that of the Eudragit[®] coated Insulin-TMC:CI MiPe formulations from the Box-Behnken design. The major addition to these dissolution studies is the inclusion of biorelevant media. Additionally, isolated gastrointestinal porcine fluids (fasted state) were utilized for *ex vivo* dissolution studies.

The concentration of insulin (IU/mL) against time (hour) profile for each dissolution fluid or isolated gastrointestinal fluid was generated utilizing DDSolver add-in for Microsoft Excel 2007. The mean dissolution time (MDT) over the first 2.5 hours was determined according to the **Equation 5.3**. The fractional dissolution of insulin after 8 hours for each formulation was determined according to **Equation 5.4**.

5.4.11. Statistical regression analysis of obtained data measurements

The statistical deviation of each obtained data measurement ($n=3$) was determined using Microsoft[®] Office Excel[®] 2007 (Build 12.0.4518.1014, Microsoft Corporation, USA). The obtained data measurements and the standard deviations were plotted within scatter plots using SigmaPlot V11.0 (Build 11.0.0.77, Systat Software Inc., Germany). Regression curves were fitted to the scatter plots and R^2 values for each regression curve were determined using SigmaPlot V11.0. A Shapiro-Wilk test was utilized during the calculation of each regression curve to determine if obtained data measurements were normally distributed populations at an alpha level of 0.05 using SigmaPlot V11.0. In addition, a constant variance test ($P=0.05$) for each regression curve was determined to indicate if the dependent variable remains constant despite a dynamically changing value of the independent variable using SigmaPlot V11.0. The 95% confidence interval and 95% predicted confidence interval was determined for the each regression curves.

5.5. Results and Discussion

This Chapter attempts to fully illustrate the *in vitro* development process of an oral peptide drug delivery dosage form from characterization of polymer excipients to development of an optimal formulation through a statistical design. The TMC bulk excipient characterization is very important because the grade of the parent material chitosan and method of synthesizing TMC:CI can vary significantly and thus alter the properties of the final derived

polymer product. Finally, the porcine model fluid was utilized in this study as this model animal has been indicated to have very similar anatomical and physiological gastrointestinal tract features to that of the human species. In addition, the physical mass of the porcine model can easily achieve equivalent mass to that of an average adult human which allows for a drug molecule to distribute within a similar volume of biological fluid volume.

5.5.1. Characterization of trimethyl chitosan chloride and chitosan

5.5.1.1. Attenuated Total Reflectance-Fourier Transform infrared analysis

TMC:Cl is a synthesized derivative of chitosan that is a pale yellow, free flowing powder excipient that readily dissolves within neutral solvents to form a light yellow solution. Chitosan was not utilized in this study because chitosan does not dissolve within neutral conditions and this is a formulation issue when the biological perspective is considered. Therefore, TMC:Cl was synthesized in order to retain the positive innate properties of chitosan and allow for these highly desirable properties to be extended into the neutral environment by increasing the solubility of the parent compound. During the synthesis of TMC:Cl the number of positive charges on the polymer chain is increased causing the polymeric molecule to expand in solution due to repelling electrostatic forces between the functional groups (Martins et al., 2011). TMC:Cl is able to increase transport of large compounds, such as peptide therapeutics, because the charge density and structural features along the backbone structure of this chitosan derivative enables augmented absorption across mucosal epithelia by opening tight junctions (Martins et al., 2011).

The ATR-FTIR analysis of TMC:Cl and chitosan are utilized for comparative purposes. The ATR-FTIR spectra of TMC:Cl (A), insulin-TMC:Cl powder (B) and chitosan (C) are shown in **Figure 5.2**. The chemical structures of TMC:Cl and chitosan can also be reviewed at the respective ATR-FTIR profile. The maximum peaks obtained from the ATR-FTIR analysis of TMC:Cl, insulin loaded chitosan and chitosan is shown in **Table 5.4**. The ATR-FTIR indicate that TMC:Cl was successfully synthesized as indicated by the presence peak 1475cm^{-1} and 1559cm^{-1} , whereas peak 1577cm^{-1} is specific to chitosan (Mourya and Inamdar, 2009). The peak located at 1475cm^{-1} is attributed to the asymmetrical angular deformation of the C-H bonds of methyl groups. The peak at 1577cm^{-1} for chitosan and 1555cm^{-1} for TMC:Cl is due to angular deformation of N-H bond of amino groups but the intensity of peak 1555cm^{-1} is reduced in comparison to peak 1577cm^{-1} due to *N*-methylation (Martins et al., 2011). The peak at 1555cm^{-1} within the TMC:Cl spectra indicates the presence of N-H bending but the *N*-methylation reaction was partial, as the presence of mono and disubstituted amino groups

are possible. The peak range $1415\text{--}1430\text{cm}^{-1}$ is assigned to the characteristic absorption of N-CH_3 . The alterations of peak 1150cm^{-1} within chitosan indicate that the introduction of alkyl groups occurred at C-3 and C-6 within TMC:Cl (Mourya and Inamadar, 2009).

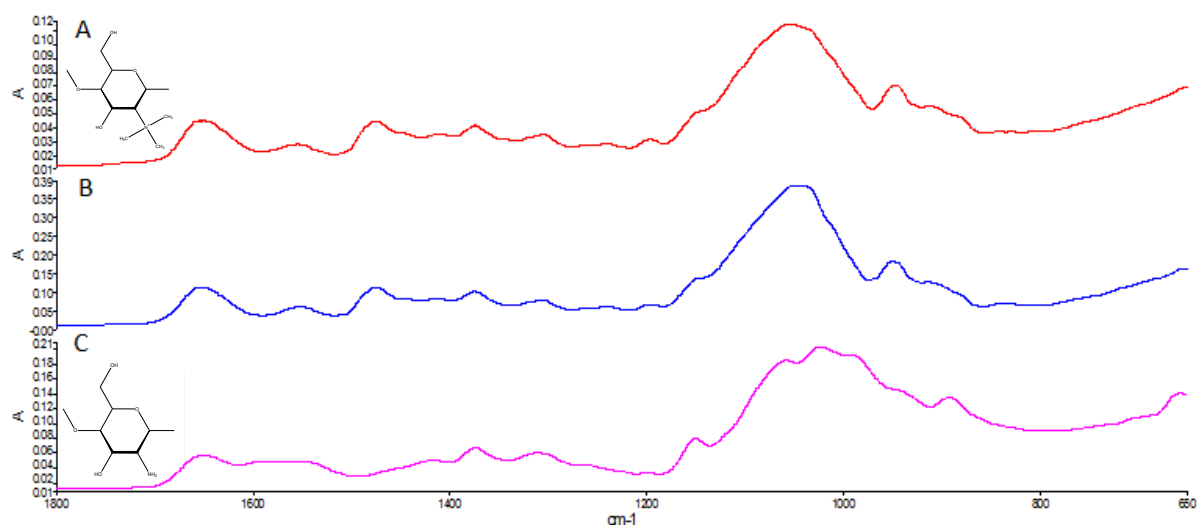


Figure 5.2: ATR-FTIR spectra of trimethyl chitosan chloride (A), insulin-loaded trimethyl chitosan chloride powder (B), and medium molecular weight chitosan (C) between the spectra range of 1800cm^{-1} and 650cm^{-1} at 130psi. The chemical structures of trimethyl chitosan chloride and chitosan is represented above the respective ATR-FTIR profiles.

Table 5.4. ATR-FTIR of trimethyl chitosan chloride, insulin-loaded trimethyl chitosan chloride powder and medium molecular weight chitosan

ATR-FTIR Peaks (cm^{-1})		
Chit ^a	TMC:Cl ^b	Insulin -TMC:Cl ^c
1579	1557	1555
1312	1474	1475
1150	1415	1415
1023	1306	1375
892	1241	1307
	1198	1240
	1055	1198
	948	1039
		951

^a: Chitosan

^b: Trimethyl chitosan chloride

^c: Insulin-loaded trimethyl chitosan chloride powder

The characteristic ATR-FTIR wavenumber peaks for the methyl group was observed within the synthesized TMC:Cl but absent within the parent compound chitosan. This indicates that TMC:Cl was successfully synthesized. The presence of insulin within the insulin-TMC:Cl powder was not detectable with ATR-FTIR analysis because the physical mass of the peptide therapeutic was so low.

5.5.1.2. Thermal gravimetric analysis of trimethyl chitosan chloride and chitosan

The thermal gravimetric analysis (TGA) of TMC:Cl and chitosan determined that there were two stages during which weight of polymer was lost. The two stages were observed within the first derivative of the TGA profile for each respective polymer. TGA of TMC:Cl and chitosan is shown in **Figure 5.3**. The TGA profile for TMC:Cl is represented by the solid blue line (A) and chitosan by the solid red line (B). The first derivative profile of TMC:Cl is represented by the broken blue line (C) and the first derivative profile of chitosan is represented by the broken red line (D). The maximum degradation temperature, water loss at maximum temperature, percentage of water loss, weight percentage loss of polymer at maximum degradation temperature and the weight percentage of the polymer remaining at 500°C values are presented in **Table 5.5** for TMC:Cl and chitosan.

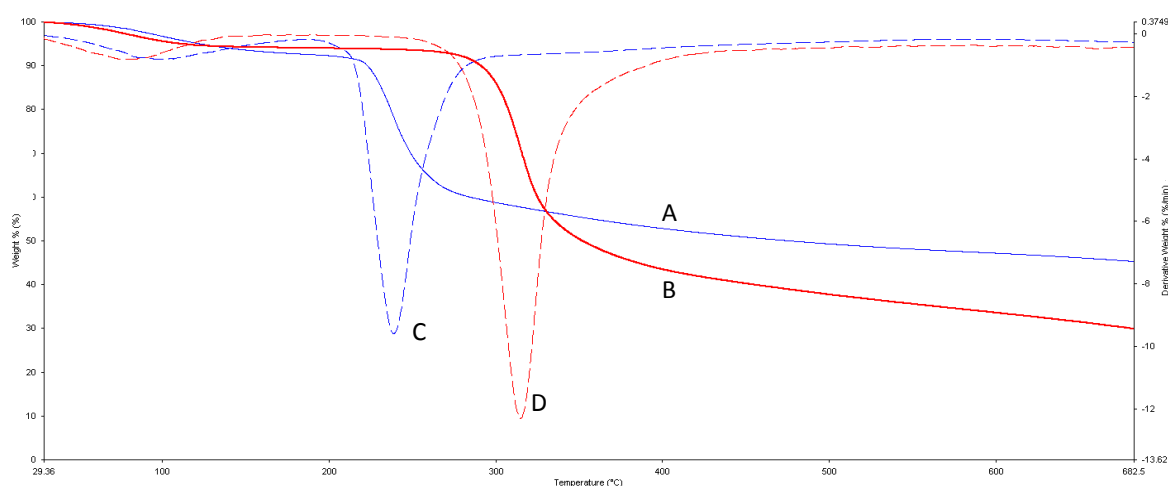


Figure 5.3: Thermogravimetric Analysis (TGA) profiles of trimethyl chitosan chloride (A), TGA profile of chitosan (B), first derivative TGA profile of trimethyl chitosan chloride (C) and first derivative TGA profile of chitosan (D).

The first stage of polymer weight loss occurred with the liberation of microscopic water from the respective polymers and was represented as a broad peak in the first derivative profile. This broad peak indicates the thermal range at which water was lost (onset and endset) and the highest point of this peak indicates the maximal percentage of water loss. Additionally,

the highest point of the first stage peak (in the first derivative profile) also indicates the temperature at which the maximal amount of water is liberated from the sample and is referred to as one of the maximal degradation temperatures.

The percentage of weight of macroscopic water present was minimally different between TMC:Cl and chitosan (~1.7%). Chitosan had a slightly lower amount of water content compared to TMC:Cl but the temperature at which maximal weight percentage of water is removed is 4.15°C higher in TMC:Cl. In addition, the percentage of weight loss, at 500°C, was ~11.6% less for TMC:Cl in comparison to chitosan. It should be noted that the extent of degradation within TMC:Cl was significantly less than that of chitosan, as seen in **Figure 5.4**.

Table 5.5. Thermogravimational analysis of trimethyl chitosan chloride and chitosan

Parameter	Chitosan	Trimethyl Chitosan Chloride
Maximum degradation temperature (°C)	314.8	238.91
Water loss at maximum temperature (°C)	77.63	81.78
Percentage of water loss at maximal degradation temperature (%)	5.789	7.486
Percentage of weight loss at maximal degradation temperature (%)	60.471	45.25
Weight remaining at 500°C (%)	37.705	49.298

It was noted that chitosan had a higher amount of microscopic water content but liberated the water content at a lower temperature. The presence of a greater density of hydroxyl and amino groups within chitosan, in comparison to TMC:Cl, may provide a greater number of dipole-dipole interactions with water molecules and enhance the volumetric entrapment of water within the polymeric network (Domard et al., 1986; Martins et al., 2011).

The primary degradation of TMC:Cl and chitosan occurs within the second stage that can be observed as the second large peak within the first derivative profile for each respective polymer. The temperature at which maximum degradation occurs within chitosan is higher than within TMC:Cl, suggesting that chitosan is more thermally stable than TMC:Cl (Britto and Campana-Filho, 2004). The percentage of degradation within the second stage of degradation was lower in TMC:Cl than the parent compound chitosan. Therefore, even though TMC:Cl started to degrade at a lower temperature, the physical amount of degradation was lower with respect to chitosan. And this becomes more apparent when the

TGA profiles of TMC:CI and chitosan intersect at $\sim 325^{\circ}\text{C}$, after which the percent of degradation for TMC:CI is less than chitosan. This suggests that chitosan acts as a more efficient thermal sink initially, whereby heat energy is absorbed and prevents degradation of the chitosan network until a critical temperature is achieved. Whereas TMC:CI had less of this heat sink capacity initially, possibly due to the quaternization process, and therefore degradation began more rapidly but never achieves the level of degradation that occurred within chitosan. This information is important with respect to formulation and indicates the degree water affinity of TMC with chitosan and the stability of these excipients.

5.5.1.3. Dynamic Scanning Calorimetry analysis

The DSC first run (data not shown) was utilized to remove macroscopic water from the sample without destroying the sample (Kittur et al., 2002). The second run DSC profiles for TMC:CI and chitosan at each respective heating rate is shown in **Figure 5.4**. A melting-crystallization-melting-crystallization pattern is always observed for DSC thermogram profiles of TMC whereas a single crystallization peak (excluding initial melting peak) is always observed within DSC thermograms of chitosan. The DSC thermogram indicates that TMC:CI, at heating rate of $10^{\circ}\text{C}/\text{min}$, presents a melting and crystalline peak located at 217°C and 270°C , respectively. Whereas during the second DSC run (at heating rate $10^{\circ}\text{C}/\text{min}$) of chitosan presented one major crystalline peak at 306°C . The calculated heat of fusion and peak temperatures for TMC:CI and chitosan at each heating rate is shown in **Table 5.6**.

The DSC profiles of TMC:CI and chitosan, at each heating rate, appeared visually similar in **Figure 5.4**, but analysis of the peak temperatures and heat of fusions differ significantly between the samples. The exothermic events in the thermogram are crystallization peaks whereby an increased amount of heat energy, with respect to the reference sample, is required to increase the temperature of the sample. Whereas, endothermic events are melting peaks (the amount of heat energy, with respect to the reference sample, required to increase the temperature of the sample is reduced). The major exothermic peak for chitosan has been suggested to be indicative of the amine decomposition within 2-amino-2-deoxy- β -D-glucopyranose monomers (Guinesi and Cavaleiro, 2006). The exothermic events occurred within TMC:CI at lower temperatures than that of chitosan, indicating that the heat capacity of TMC:CI was altered during the quaternization process.

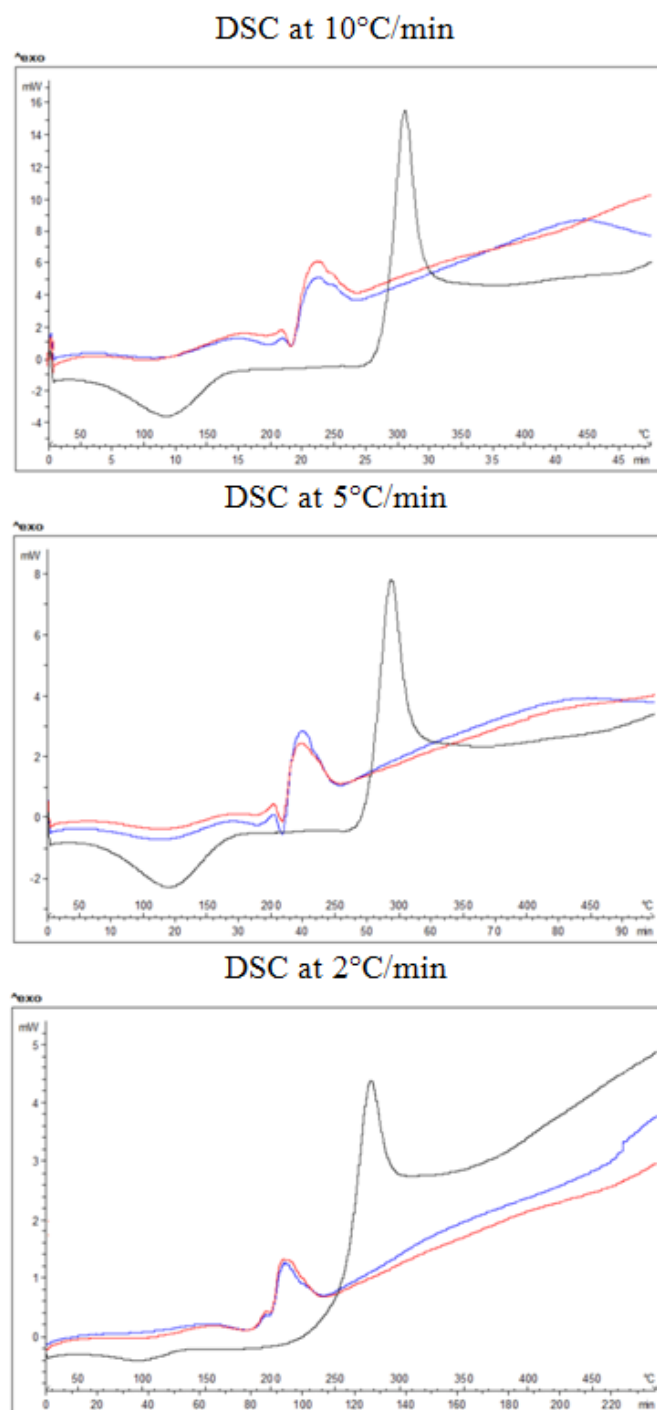


Figure 5.4: Dynamic Scanning Calorimetry (DSC) of trimethyl chitosan chloride and chitosan at increasing heating rates of 10°C/min, 5°C/min and 2°C/min between the temperature range of 30°C to 500°C. Each DSC thermogram represents chitosan (black line), TMC:Cl (blue line) and insulin loaded trimethyl chitosan chloride powder (red line).

The broad exothermic peak indicates that TMC:Cl underwent a slowed thermal event because the heat capacity over this temperature range increased. The heat capacity of chitosan over the same thermal range remained constant with respect to the reference sample. The thermal profile comparison between chitosan and TMC:Cl indicates that the parent compound has been modified due to the quaternization process.

Table 5.6. Dynamic Scanning Calorimetry (DSC) analysis of trimethyl chitosan chloride and chitosan at heating rate 10°C/min, 5°C/min and 2°C/min

Trimethyl Chitosan				
Heating rate 10°C/min				
	Peak 1	Peak 2	Peak 3	Peak 4
Heat of Fusion (ΔH)	-4.55 (±0.39)	4.06 (±0.31)	68.68 (±1.14)	-137.28 (±2.42)
Peak (°C)	198.08 (±0.17)	210.27 (±0.61)	217.51 (±0.03)	239.19 (±0.75)
Heating rate 5°C/min				
Heat of Fusion (ΔH)	-13.75 (±2.1)	5.13 (±0.35)	-5.1 (±0.72)	65.37 (±3.45)
Peak (°C)	208.31 (±1.53)	201.91 (±0.19)	190.95 (±0.63)	222.06 (±0.76)
Heating rate 2°C/min				
Heat of Fusion (ΔH)	-148.38 (±1.68)	4.96 (±1.67)	39.25 (±1.53)	-236.39 (±3.67)
Peak (°C)	196.86 (±1.42)	198.26 (±1.14)	202.47 (±0.72)	202.53 (±1.27)
Insulin loaded Trimethyl Chitosan				
Heating rate 10°C/min				
Heat of Fusion (ΔH)	-7.55 (±0.11)	2.89 (±0.43)	74.39 (±0.71)	-111.62 (±0.48)
Peak (°C)	199.42 (±0.85)	206.27 (±0.28)	211.39 (±0.73)	243.31 (±0.14)
Heating rate 5°C/min				
Heat of Fusion (ΔH)	-9.61 (±4.8)	7.63 (±2.15)	-9.76 (±0.28)	54.16 (±1.55)
Peak (°C)	211.83 (±0.64)	197.26 (±3.23)	189.51 (±3.71)	215.88 (±2.84)
Heating rate 2°C/min				
Heat of Fusion (ΔH)	-146.82 (±3.93)	4.27 (±4.7)	32.47 (±5.92)	-228.38 (±5.33)
Peak (°C)	193.47 (±0.29)	197.69 (±2.85)	202.53 (±1.27)	216.57 (±0.92)
Chitosan				
Heating rate 10°C/min				
Heat of Fusion (ΔH)	-90.6 (±2.5)	164.86 (±3.99)	NA	NA
Peak (°C)	119.63 (±0.95)	306.38 (±0.08)	NA	NA
Heating rate 5°C/min				
Heat of Fusion (ΔH)	-53.86 (±0.98)	146.51 (±1.59)	NA	NA
Peak (°C)	109.21 (±0.48)	293.54 (±0.45)	NA	NA
Heating rate 2°C/min				
Heat of Fusion (ΔH)	-46.32 (±4.67)	152.41 (±1.83)	NA	NA
Peak (°C)	99.08 (±2.35)	277.13 (±0.23)	NA	NA

5.5.1.4. Scanning Electron Microscopy images of trimethyl chitosan and chitosan

The Scanning Electron Microscopy images obtained of trimethyl chitosan chloride and chitosan can be reviewed in **Figure 5.5**. The trimethyl chitosan chloride sample (A) has uniformly flat surfaces and reduced charging. Chitosan sample (B) demonstrated a higher degree of charging and contained more amorphous surfaces. A significant difference in the morphology between chitosan and TMC:Cl can be observed within the acquired SEM images. TMC:Cl has flat angular surfaces whereas chitosan has an amorphous surface structure. Additionally, regions of charging within chitosan is more apparent than trimethyl chitosan which indicates that the electrons are not as effectively distributed across the surface of chitosan due to the amorphous structure of chitosan. This prompted the utilization powdered XRD to determine the precise change in the physical crystalline properties that occurred within chitosan after the quaternization process.

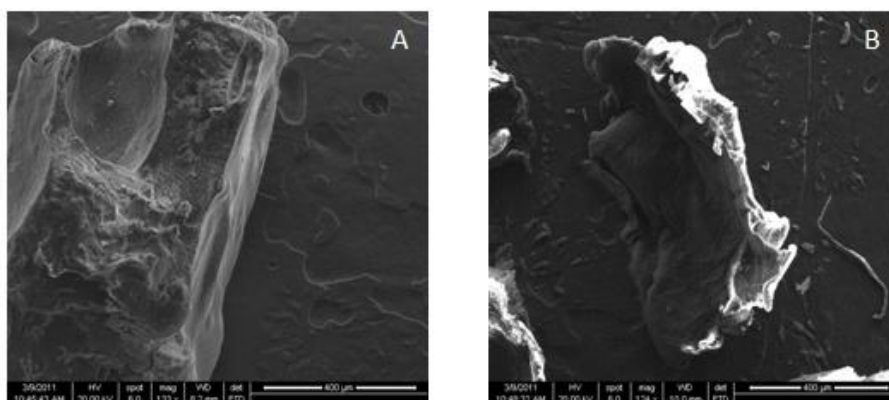


Figure 5.5: Scanning Electron Microscopy (SEM) images of trimethyl chitosan chloride (A) and chitosan (B).

5.5.1.5. Powdered X-ray Diffraction analysis of trimethyl chitosan chloride and chitosan

The powder XRD profiles of TMC:Cl (blue profile) and chitosan (red profile) is shown in **Figure 5.6** for comparative analysis. The major XRD reflections for medium molecular weight chitosan occurred at 2θ -values of 20.0° (58590), 36.7° (79700 cps), 42.9° (46670 cps), 63.3° (17888 cps), 76.4° (37853 cps) and 80.6° (31535 cps). Whereas the major XRD reflections for TMC:Cl occurred at 2θ -values of 20.0° (11495 cps), 31.5° (31771 cps), 45.2° (17010 cps), 56.3° (7723 cps), 66° (5033 cps), 75.1° (5548 cps) and 83.8° (4918 cps). The degree of crystallinity was determined to be 31.8% for chitosan and 86% for TMC:Cl.

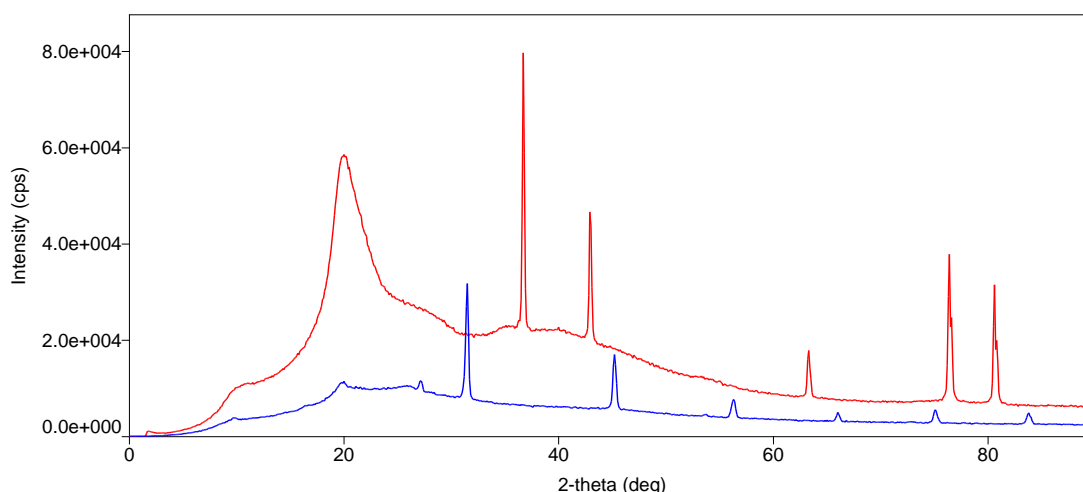


Figure 5.6: Powdered X-ray Diffraction profiles of trimethyl chitosan chloride (blue profile) and 77% deacetylated medium molecular weight chitosan (red profile).

The major XRD reflection that occurred at 20.0° within chitosan became essentially lost within the trimethyl chitosan. Interestingly the major reflection peaks did not overlap between the parent compound and the derivative product. The major change in the powdered XRD pattern between chitosan and TMC:Cl indicates that the physical crystal structure of the derivative changed significantly during the quaternization process. The increase of the crystallinity can also be attributed to the quaternization process. Additionally, the intensity of the XRD reflections within TMC:Cl was reduced in comparison to chitosan. The higher degree of crystallinity within the TMC:Cl is one of the major factors that impacts the compaction of this excipient into a solid dosage form. Auxiliary excipients, EDTA-mPEG hot melt dispersion powder and Ac-Di-Sol[®], were utilized to reduce the impact of the crystalline nature of TMC:Cl.

The low compressibility of this highly soluble crystalline derivative presents a formulation challenge during the tableting process. This challenge was overcome by incorporating mPEG-EDTA *in situ* hot melt dispersion powder into the formulations so that during the tableting process, the heat energy output from the mechanical compaction of the excipients can be mitigated by the EDTA-mPEG *in situ* hot melt dispersion powder during the thermal-physical deformation process and induce the process of “void filling”. Void filling allows for the TMC to be compacted more efficiently and generate a more desirable macrostructure. TMC:Cl was synthesized according to a previously described methodology, with slight modification, that generated the most favourable outcomes. These outcomes include the optimal degree of quaternization that facilitates paracellular transport of peptide therapeutics and limits the loss of mucoadhesivity (Kotzé et al., 1999; van der Merwe et al., 2004; Atyabi et al., 2007; Sayin et al., 2008; Markov et al., 2010).

5.5.2. Viscosity analysis of fluids and mini-pellet components

The viscosity analysis of the biorelevant media, isolated gastrointestinal fluids and the respective fluids which contained 0.1%^{w/v} trimethyl chitosan was determined at a two different shear rates and was characterised as having Newtonian flow. A box and whisker plot was utilized to determine the average and mean viscosity of each fluid under a different shear rate. The results for the shear rate 5s⁻¹ and 200s⁻¹ is shown in **Figure 5.7**. The average viscosity of the biorelevant fluids was ~10 000mPas less than that of the isolated gastrointestinal fluids (even though the gastrointestinal fluids had been filtered). Additionally the mean viscosity of Millipore[®] water was slightly less than that of biorelevant media. The most unexpected result was that the presence of low concentrations of TMC:CI resulted in a general decrease in viscosity.

The Newtonian flow characteristic observed in the isolated gastrointestinal fluids of the porcine model is mainly due to the removal of the mucus through the utilization of filtration. Even with the removal of the vast majority of the mucus content within the gastrointestinal fluids, the viscosity of the isolated fluids was still higher than that biorelevant media. The reduction of the viscosity due to the presence of low concentrations of TMC:CI could be due to the development of a slippage zone around the polymer chains through the presence of bile acids and micronized mucus particles. The molecular weight of TMC:CI has been suggested to decrease with increased exposure to hydroxide ions by facilitating the cleavage of glycosidic bonds (Hamman and Kotzé, 2001; Snyman et al., 2002; Verheul et al., 2008; Martins et al., 2013). The reduced viscosity of the TMC:CI solution is directly affected by the number of quaternization steps employed to synthesis the TMC:CI (Hamman and Kotzé, 2001).

The viscosity of a fluid is extremely important for the application of drug delivery. The reduction of viscosity due to low concentrations of trimethyl chitosan, which would occur *in vivo* due to progressive disintegration and the hydrodynamic nature of the gastrointestinal tract, could result in the accelerated dispersion of the peptide therapeutic within the localized environment. Additionally, this could have an impact the glycocalix portion of the mucosal layer within the small intestine significantly. With a reduced viscosity, the top layer of the mucosal structure breaks down more rapidly and provides accelerated access to the glycocalix. Additionally, the mucoadhesiveness of TMC:CI can facilitate a closer proximity between the peptide therapeutic and the tight junctions located within the intestinal epithelium.

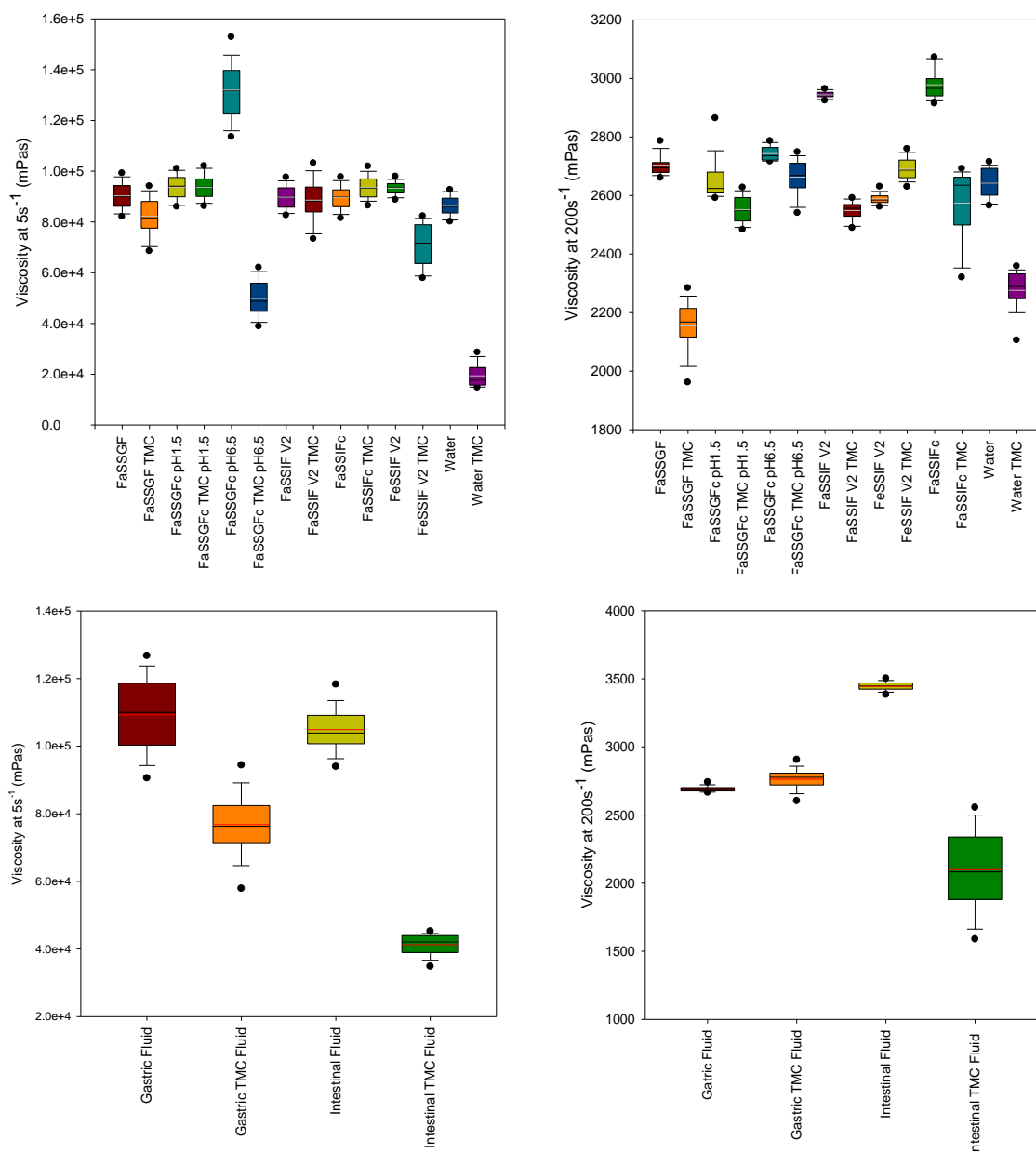


Figure 5.7: The viscosity analysis of biorelevant media and isolated gastrointestinal fluids of the porcine model (fasted state). Trimethyl chitosan (0.1% w/v) was dissolved in the respective solvents.

5.5.3. Box-Behnken Design of insulin loaded trimethyl chitosan chloride mini-pellet formulations

The inclusion of the excipient types within these formulations was designed to optimize the properties of a physical oral dosage form but also to enhance the bioavailability/release of a peptide therapeutic. The use of EDTA-mPEG *in situ* hot melt dispersion was thought to enhance the disintegration potential of the mini-pellet formulations. In addition, EDTA-mPEG *in situ* hot melt dispersion also efficiently filled void spaces that occurred due to the presence of crystalline TMC:Cl. It was found that with the inclusion of this melt dispersion, that the

matrix hardness was reduced. The reduced matrix hardness was then offset with the inclusion of Ac-Di-Sol[®], because Ac-Di-Sol[®] is a known disintegrant and increased the matrix hardness (Mehat et al., 2012; Aduja et al., 2013). This combination complemented each other to produce a synergist effect, where the highly soluble EDTA-mPEG hot melt dispersion would rapidly increase the surface area upon exposure with a solvent and Ac-Si-Sol[®] would swell upon exposure with a solvent. This sets up a dynamic whereby as voids are created in the macrostructure of the mini-pellet (due to EDTA-mPEG *in situ* hot melt dispersion), the macrostructure of the mini-pellet decomposed into granules (due to Ac-Di-Sol[®]), thus promoting a highly efficient disintegration mechanism. The combination of these excipients was utilized to generate formulations by a Box-Behnken design, as shown in **Table 5.7**. Each formulation was prepared in triplicate and subjected to drug dissolution studies, physicochemical analysis to determine matrix hardness and mucoadhesion.

The ability of the excipients to reduce or accelerate free drug dissolution was measured as the mean dissolution time (MDT). A rapid peptide therapeutic dissolution was assessed by determining the MDT after 2.5 hours. The mPEG-EDTA *in situ* hot melt dispersion had minimal effect on MDT whereas Ac-Di-Sol[®] significantly affected MDT on the mini-pellet formulations. Low concentrations of Ac-Di-Sol[®] resulted in an increase of MDT, as expected, since Ac-Di-Sol[®] is utilized as a superdisintegrant for solid dosage forms (Güres and Kleinbudde, 2011; Iwao et al., 2013). The mini-pellet formulations which could achieve a high degree of MH and effectively limit the instantaneous dissolution of the peptide therapeutic is extremely important when considering the bulk excipient TMC:CI. TMC:CI is an exceptional chitosan derivative which allows for enhanced paracellular transport of peptide therapeutics and contains a significant mucoadhesive element (van der Merwe et al., 2004; Sandri et al., 2005; Jintapattanakit et al., 2008). The mucoadhesive property of trimethyl chitosan would be circumvented, with respect to drug delivery, if the peptide therapeutic is released too rapidly. The peptide therapeutic would dissociate from the dosage form into the intraluminal environment and not in close proximity to the intestinal wall where the mucoadhesive properties and the paracellular promoting transport of TMC:CI would be effective for absorption. If the MH of the formulation is poor, the solid dosage form would be very difficult to transport and manufacture (Tang et al., 2008; Moore et al., 2010). The mini-pellet formulation must also achieve a high degree of fractional dissolution as this is the ability of the entire dosage form to dissolve the entire loaded insulin peptide therapeutic.

The fractional dissolution is a measure of the amount of drug that was liberated at a certain time point. The fractional dissolution was assessed after 8 hours because most, if not all, the effective loaded peptide therapeutic should be liberated from the dosage form. The

formulations that achieved the highest fractional dissolution were highly desirable. The fractional dissolution analysis indicated that a high concentration of sodium deoxycholate is beneficial to the formulation. It should be noted that the positive effects of Ac-Di-Sol® can be mitigated by a low concentration ratio of mPEG-EDTA *in situ* hot melt dispersion powder or sodium deoxycholate. This may be due to the high water soluble property of mPEG-EDTA *in situ* hot melt dispersion powder or sodium deoxycholate which at lower quantities can limit the formation of erosion cracks and reduce the rate at which the surface area of the internal mini-pellet macrostructure is available for solvent attack.

Table 5.7. The formulation of the mini-pellets according to a Box-Behnken design

Formulation	StdOrder	RunOrder	PtType	Blocks	mPEG-EDTA* (mg)	Ac-Di-Sol® (mg)	Bile Salt (mg)
1	12	1	2	1	15	30	5
2	3	2	2	1	10	30	2.5
3	1	3	2	1	10	10	2.5
4	8	4	2	1	20	20	5
5	7	5	2	1	10	20	5
6	11	6	2	1	15	10	5
7	4	7	2	1	20	30	2.5
8	14	8	0	1	15	20	2.5
9	10	9	2	1	15	30	0
10	5	10	2	1	10	20	0
11	9	11	2	1	15	10	0
12	6	12	2	1	20	20	0
13	13	13	0	1	15	20	2.5
14	15	14	0	1	15	20	2.5
15	2	15	2	1	20	10	2.5

*50%w/w mPEG-EDTA hot melt dispersion

The residual plots for the generated formulations are shown in **Figure 5.8**. The normal probability plot of residuals for the responses indicates that the matrix hardness had the best representation within the generated formulations whereas the Mean Dissolution Time (MDT) at 2.5 hours had the weakest representation.

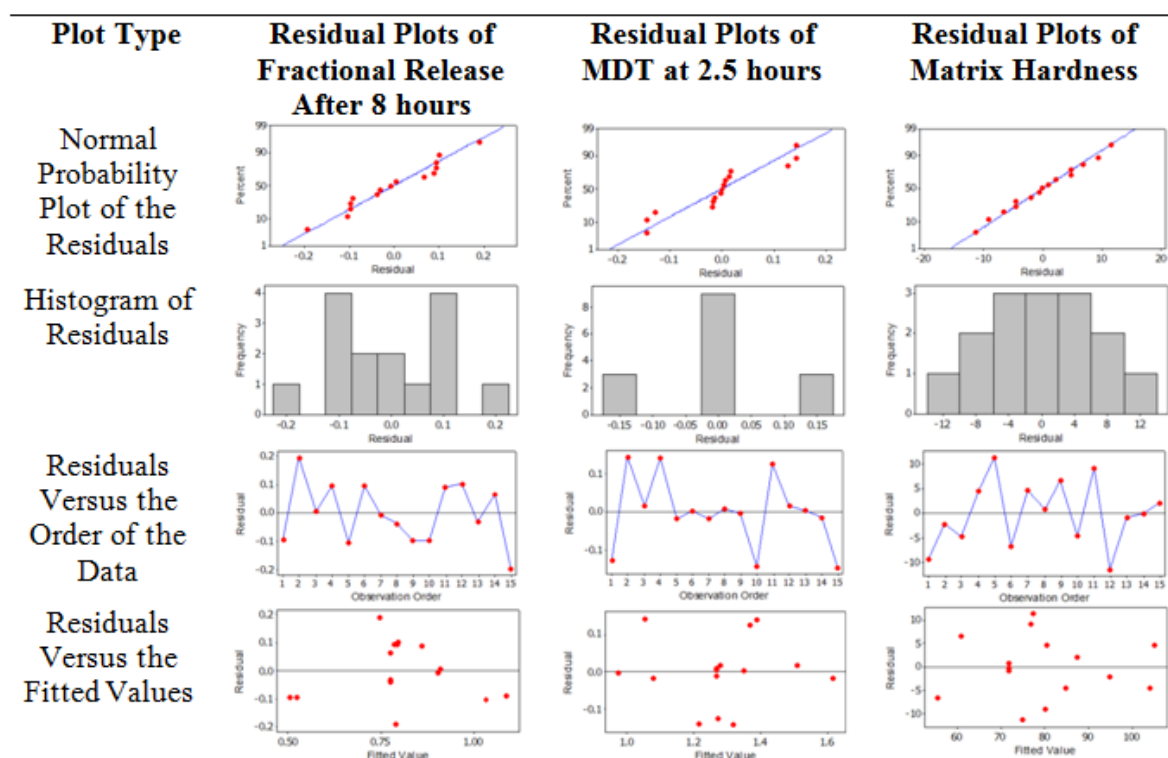


Figure 5.8: Residual Plots of Fractional Dissolution after 8 hours, Mean Dissolution Time (MDT) after 2.5 hours and Matrix Hardness determined from the Box-Behnken design of insulin-TMC:CI mini-pellets.

5.5.4. Physicomechanical and *ex vivo* mucoadhesive analysis of insulin loaded trimethyl chitosan chloride mini-pellet formulations

The optimized insulin-TMC:CI MiPe formulation was determined using the Box-Behnken design. The *in silico* predicted responses of the optimized formulation were very similar to the obtained experimental results. The MDT, fractional dissolution after 8 hours and the matrix hardness were considered important parameters because a rapid dissolution of insulin is desirable to maintain an *in vivo* concentration gradient (Maroni et al., 2012; Ling and Chen, 2013).

The physicomechanical analysis of the fifteen mini-pellet formulations and a chitosan mini-pellet formulation is shown in **Figure 5.9**. Additionally, the *ex vivo* mucoadhesion analysis of the fifteen mini-pellet formulations and a chitosan mini-pellet formulation is also shown in **Figure 5.9**. The formulations that are isolated within the blue area represent formulations which are desirable whereas formulations that are within the red areas are considered to have performed poorly within the current set of parameters and conditions. The formulations which are located within the green area are considered neutral as these formulations have not performed exceptionally well or exceptionally poorly.

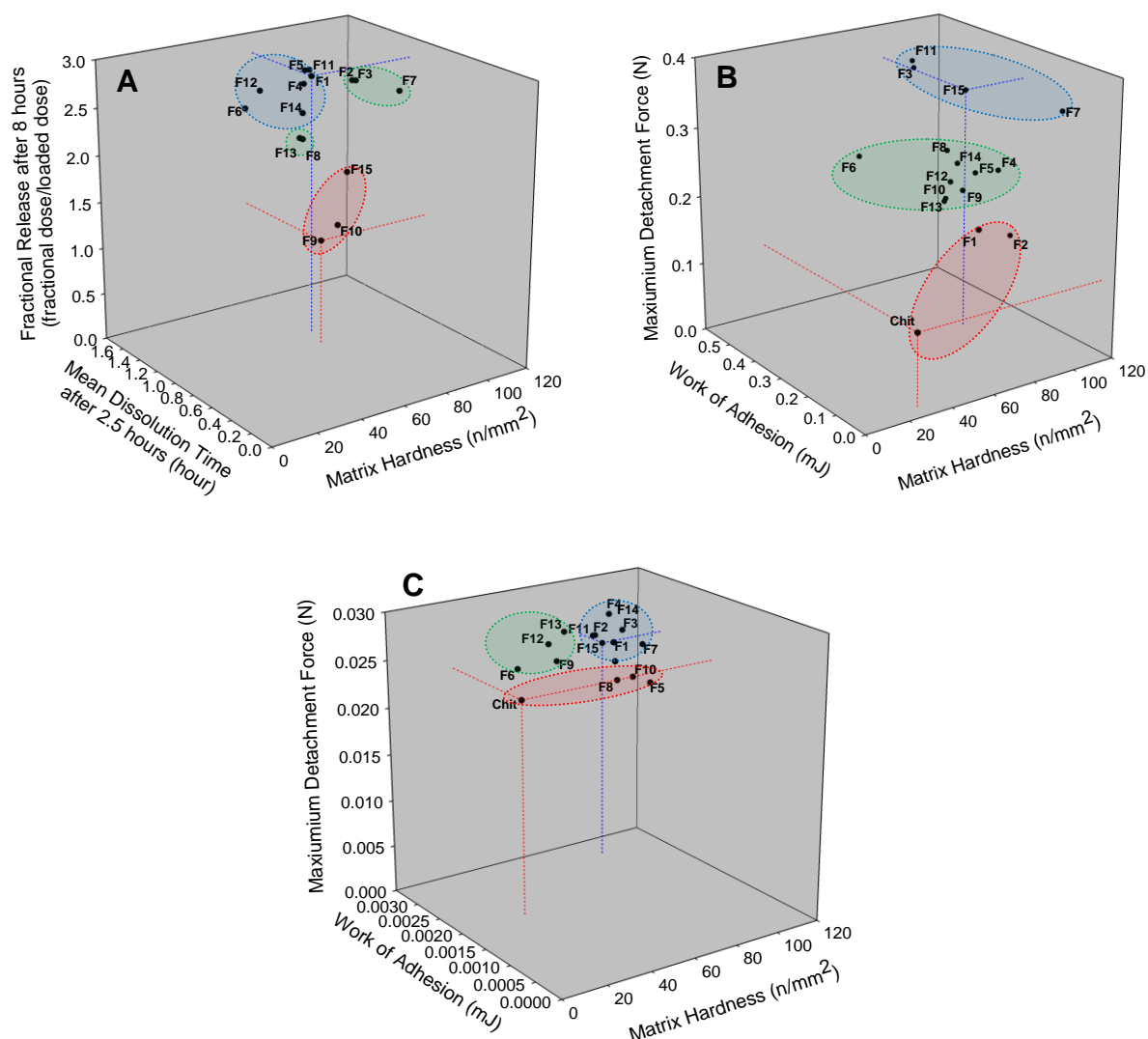


Figure 5.9: Three dimensional scatter plots of the matrix hardness against dissolution analysis (A) and mucoadhesive analysis, respectively, for the Box-Behnken mini-pellet formulations (F1-F15) and chitosan mini-pellet formulation (Chit). Mucin-coated porcine intestinal epithelium samples (B) and non-mucin-coated porcine intestinal epithelium samples (C) were utilized to determine mucoadhesive properties of the mini-pellet formulations.

The insulin loaded TMC:CI MiPe formulation 9 and 10 achieved the worst MDT and fractional dissolution after 8 hours performance with respect to matrix hardness. Whereas formulation 1, 4, 5, and 11 achieved the best MDT and fractional dissolution after 8 hours performance with respect to matrix hardness. The mucoadhesive performance of the formulations was evaluated with respect to matrix hardness as well. Interestingly, poor formulation (F1 and F2) performance in the presence of mucin solution was not indicative of poor performance in the absence of mucin solution. Comparatively, formulation (F3, F7, F11 and F15) performance in the presence of mucin solution was indicative of excellent

performance in comparison the the physicommechanical performance of these formulations in the absence of mucin solution. The work of adhesion of the fifteen formulations increases as the TMC:CI weight concentration increases. The WA of the mini-pellet formulations remained relatively constant (± 1 N difference) when a 0.3%^{w/v} mucin solution was not utilized during the mucoadhesive analysis.

The maximum detachment force (MDF), measured as adhesion, was determined for the fifteen Box-Behnken design mini-pellet formulations and the chitosan mini-pellet formulation. MDF was determined to be greater for formulations which contained TMC:CI, with respect to the chitosan containing formulation, when a mucin solution was applied. The MDF of the mini-pellets remained relatively constant, similar to the WA measurements, when no mucin solution was utilized. The maximum detachment force was reduced ~10 fold and the work of adhesion was reduced ~100 fold when the 0.3% mucin solution was not present.

The mucoadhesive properties of TMC:CI has been compared with many other mucoadhesive polymers, such as pectinate, and has often demonstrated significant mucoadhesive properties but sometimes failing to be equivalent with known mucoadhesive polymers (Hagesaether et al., 2009). This has been attributed to overhydration of the TMC:CI which causes a significant reduction in the mucoadhesive properties of the polymer (Atyabi et al., 2007). The Eudragit[®] spray coating that was utilized in this study was incorporated to reduce the overhydration of TMC:CI and to target the mini-pellet formulation for the jejunum-ileum environment of the small intestine. The jejunum-ileum environment of the small intestine is the best site for TMC:CI mediated peptide therapeutic absorption due to the reduced integrity of tight junctions and the presence of a mucus layer (Kotzé et al., 1999; Markov et al., 2010). The chitosan mini-pellet formulation demonstrated the lowest degree of mucoadhesive ability in comparison the mini-pellet formulations which contained trimethyl chitosan. The increased positive charge that exists within trimethyl chitosan, with respect to chitosan, may assist in enhanced dipole-dipole interactions between these molecules. The mucoadhesive ability was effectively terminated in the absence of the 0.3%^{w/v} mucin solution and was comparable with that of chitosan. This indicates that the ability of TMC:CI to facilitate drug delivery applications, since if no mucin is present within the site of delivery, the ability of TMC:CI to interact with tight junctions would be limited and maintaining a close proximal association with the intestinal wall would be negatively impacted.

5.5.5. Insulin entrapment studies, dissolution studies and dissolution fitting analysis of optimized Eudragit® coated insulin loaded trimethyl chitosan chloride mini-pellet formulation

High Performance Liquid Chromatography (HPLC) was utilized to determine the concentration of insulin entrapped within the lyophilized insulin-TMC:CI to be 95(±0.4)% of the original loaded dose. HPLC analysis was conducted on all dissolution samples to determine the concentration of insulin at each time point. Insulin was detected at retention time (RT) at 10 (±0.1) minutes and the HPLC chromatogram can be reviewed in **Figure 5.10**. The concentrations of insulin at each dissolution time point were determined by utilizing a standard curve of insulin concentration against absorbance (data not shown). The Eudragit® coated insulin-TMC:CI MiPe formulations generally had a high correlation with Makoid-Banakar that had a time lag parameter, which can also be reviewed in **Figure 5.10**.

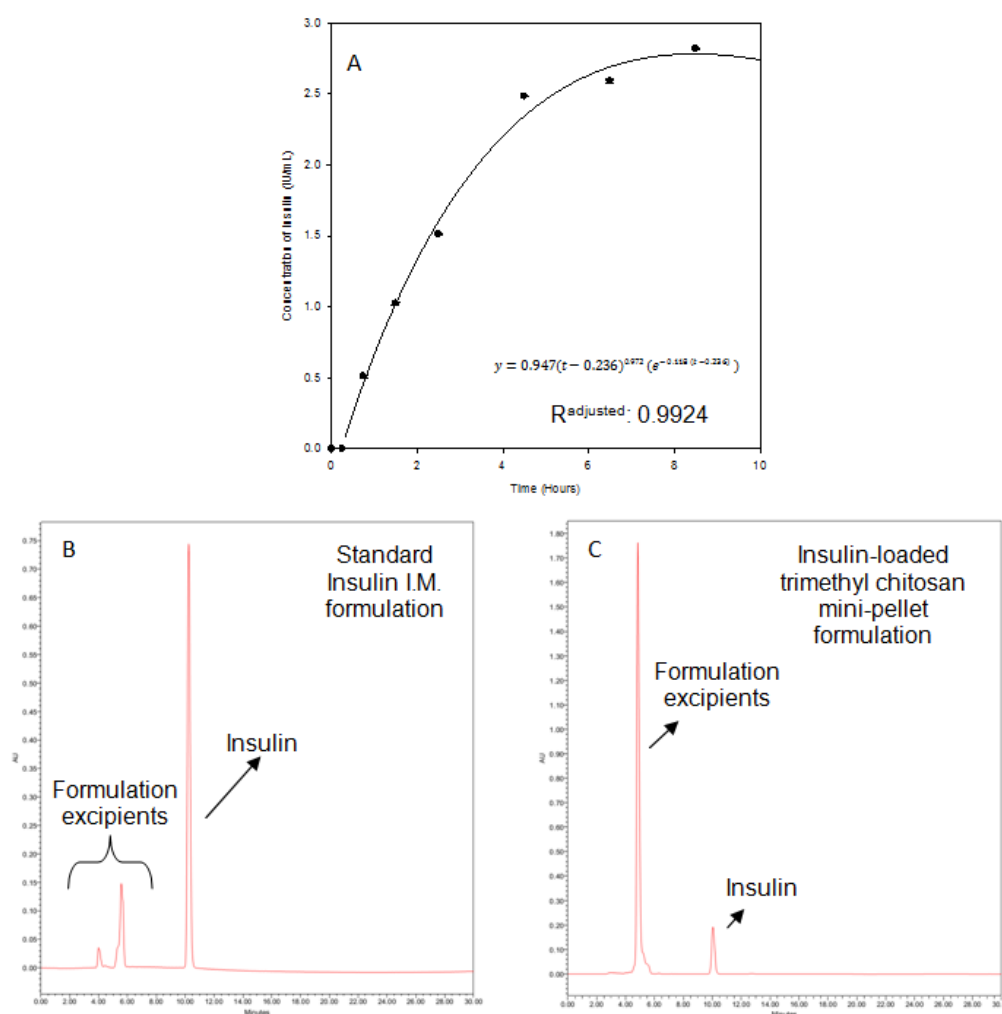


Figure 5.10: Dissolution profile of insulin for Formulation 1 of insulin-loaded trimethyl chitosan chloride mini-pellet which conforms to a Makoid-Banakar with Tlag regression fitted scatter plot (A). The High Performance Liquid Chromatography analysis of the market available Intramuscular (I.M.) insulin formulation (B) and insulin released from trimethyl chitosan formulation 1 (C).

5.5.6. The statistical analysis of the experimental results obtained from the Box-Behnken design formulations

The experimental results obtained from the Box-Behnken design formulations were analysed using Minitab. The responses (fractional dissolution after 8 hours; MDT and MH) were compared against the major excipient components as surface plots (which can be reviewed in **Figure 5.11**). These results were then utilized to generate a desired optimized formulation which had the highest possible degree of responses. The generated optimized formulation had a desirability of 94.16% and the calculated *in silico* responses and can be reviewed in **Figure 5.12**.

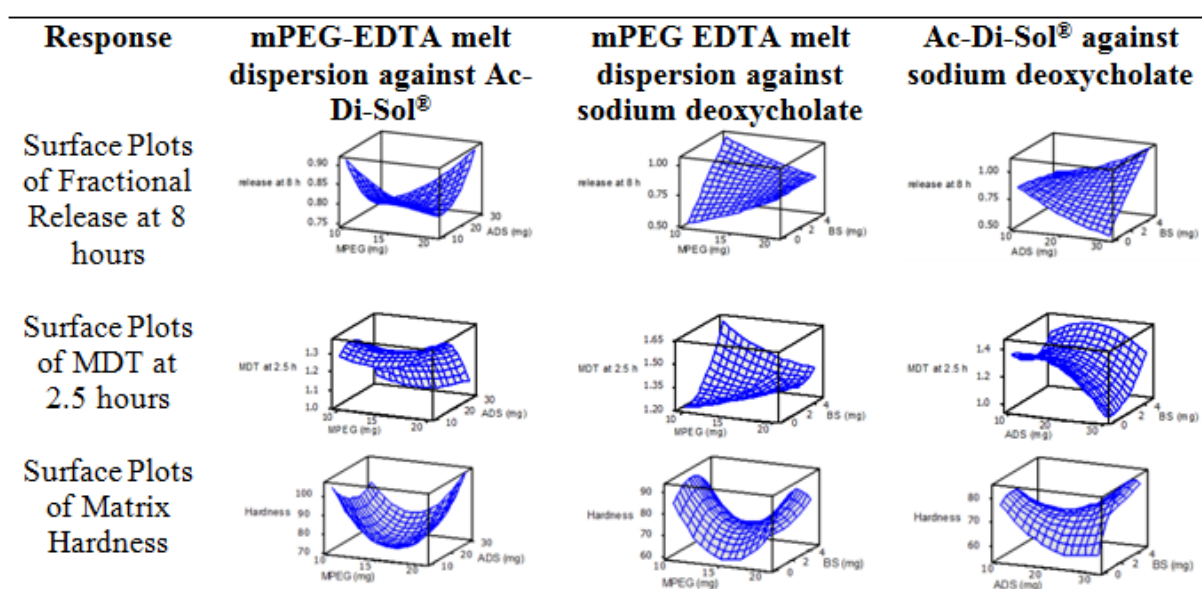


Figure 5.11: Three dimensional surface plots of the insulin-loaded trimethyl chitosan chloride mini-pellet components with respect to the responses (Fractional Dissolution after 8 hours, Mean Dissolution Time (MDT) after 2.5 hours and Matrix Hardness).

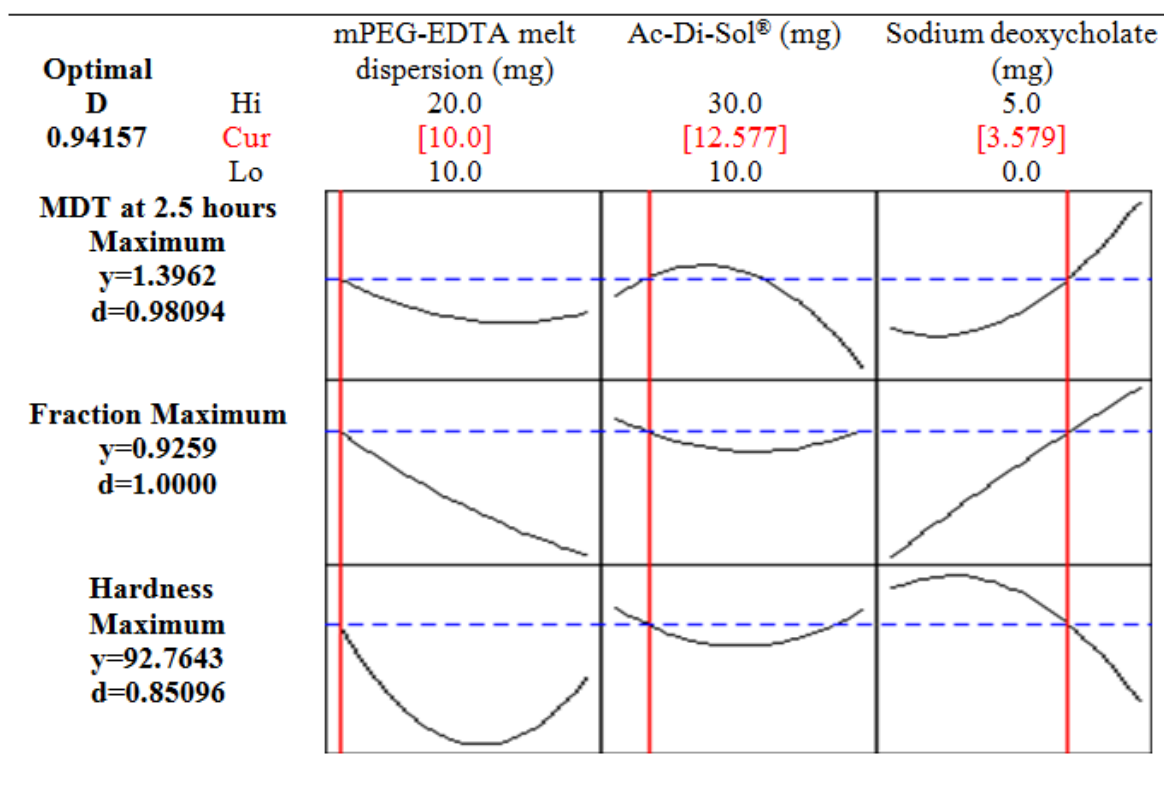


Figure 5.12: Optimized insulin-loaded trimethyl chitosan chloride mini-pellet formulation output from Box-Behnken Design.

5.5.7. *In vitro* and *ex vivo* characterisation of the optimized Eudragit® insulin loaded mini-pellet formulation within biorelevant dissolution fluid and isolated porcine gastrointestinal fluids

5.5.7.1. Physicomechanical characterisation of the optimized insulin loaded trimethyl chitosan chloride mini-pellet formulation

The optimized formulation of insulin-TMC:CI MiPe formulation from the Box-Behnken design and responses (MDT after 2.5 hours and the fractional dissolution after 8 hours) which can be reviewed in **Figure 5.13**. The optimized formulation was experimentally determined to have a MDT time of 1.3959 hours whereas the MDT value generated *in silico* was 1.3962 hours. The experimentally determined fractional dissolution after 8 hours was determined to be 94.06% whereas the *in silico* predicted fractional dissolution was 92.59%.

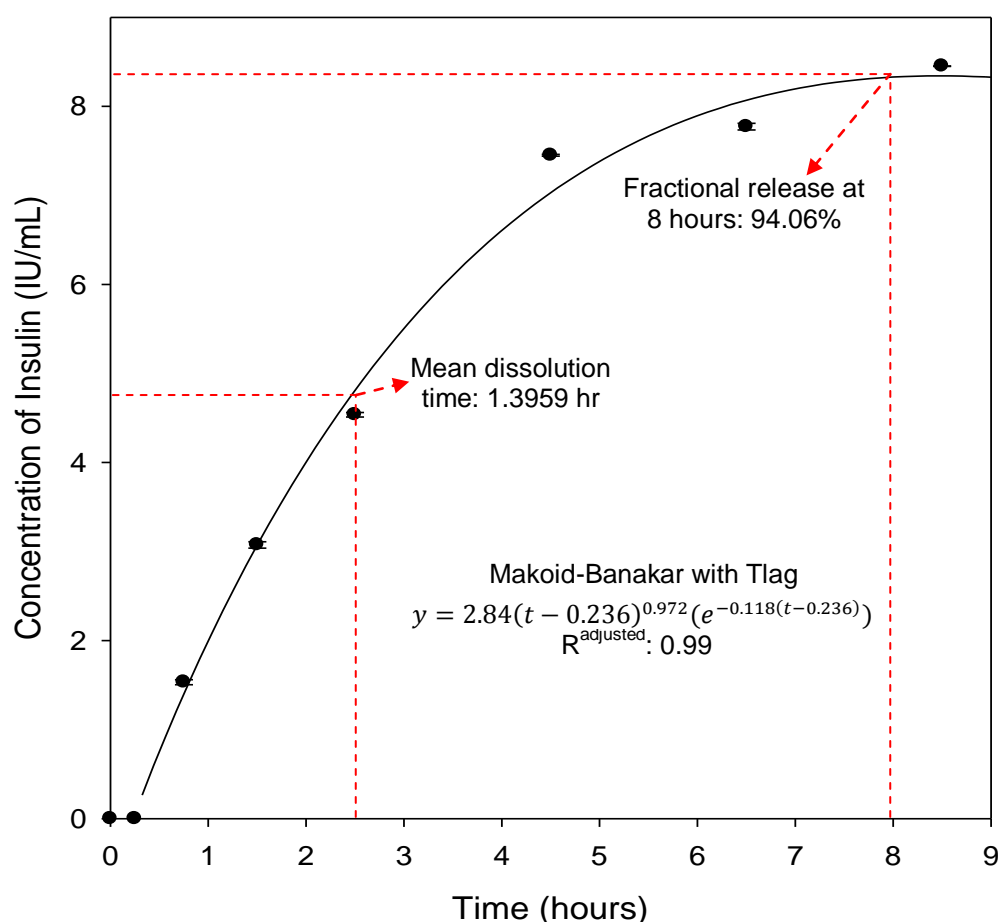


Figure 5.13: A graphical representation of the three responses (mean dissolution time after 2.5 hours [1.3959 hours] and fractional dissolution after 8 hours [94.06%]) for the optimized insulin-loaded trimethyl chitosan chloride mini-pellet formulation. A Makoid-Banakar with Tlag regression kinetic model was fitted to the concentration of insulin versus time scatter plot with an R^2 value of 0.99.

The *ex vivo* mucoadhesive Textural analysis force distance profile of 3%^{w/v} mucin coated porcine small intestine epithelium tissue, non mucin coated porcine small intestine epithelium tissue and matrix hardness of the optimized insulin loaded Box-Behnken mini-pellet formulation is shown in **Figure 5.14**. The WA of the optimized insulin-TMC:Cl MiPe formulation was determined to be 0.457mJ and 0.003mJ for mucin coated and non mucin coated intestinal epithelium tissue, respectively. The maximum MDF determined as adhesion is 0.405N and 0.031N for mucin coated and none mucin coated intestinal epithelium tissue, respectively. The matrix hardness was determined experimentally to be 94.22N/mm whereas the *in silico* predicted matrix hardness was 92.76N/mm. The *in silico* predicted matrix hardness under estimated the experimental matrix hardness by ~2N/mm which is minimal and accurate within experimental error conditions.

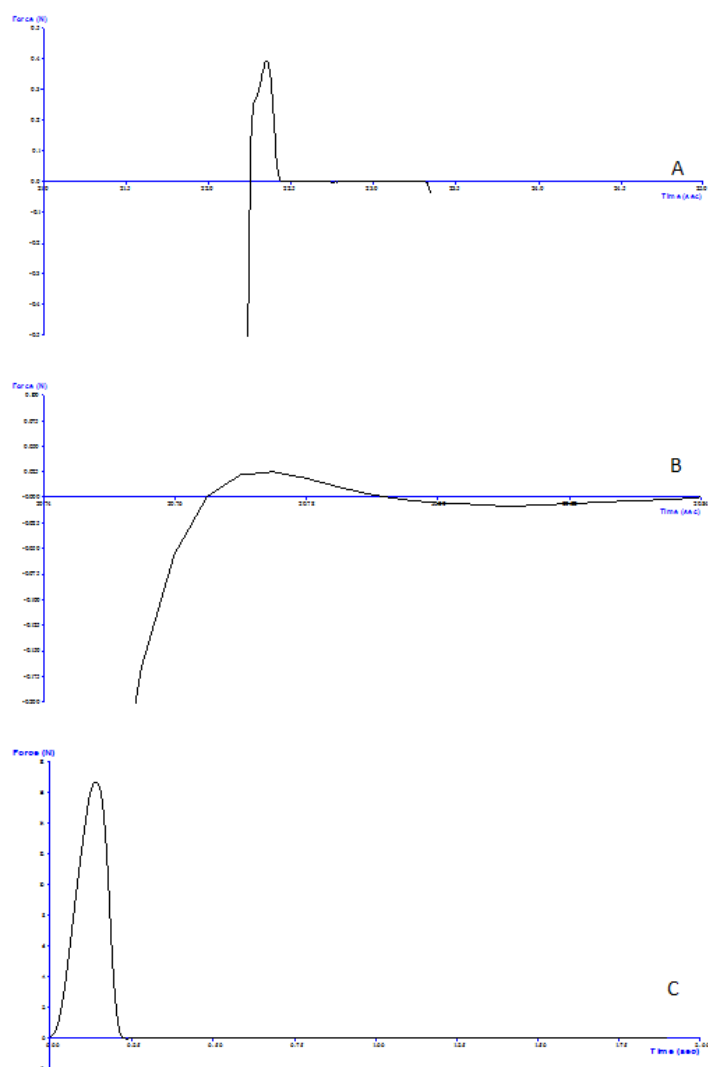


Figure 5.14: The Textural analysis force distance profile of 3%^{w/v} mucin coated porcine small intestine epithelium tissue (A), none mucin coated porcine small intestine epithelium tissue (B) and matrix hardness (C) of the optimized insulin loaded Box-Behnken mini-pellet formulation.

5.5.7.2. Disintegration analysis of the optimized Eudragit[®] coated insulin loaded trimethyl chitosan mini-pellet formulation

The disintegration behaviour within biorelevant media and isolated gastrointestinal fluids of the porcine model was assessed on the optimized Eudragit[®] coated insulin-TMC MiPe formulation. The disintegration rate of the optimized Eudragit[®] coated TMC:CI MiPe formulation at predetermined time points within each biorelevant media is shown in **Figure 5.15**. The canine media that was near neutral pH achieved the highest rates of disintegration initially. The initial disintegration rate of trimethyl chitosan within FaSSIF and FeSSIF was almost identical but the rates were significantly reduced in comparison to the canine neutral pH media. The disintegration within acidic media was significantly reduced by the presence of Eudragit[®] coating. This indicated that the macrostructure of the mini-pellet is significantly

affected by the dissolution media. The isolated intestinal fluids of the porcine model had the third highest initial rate of disintegration.

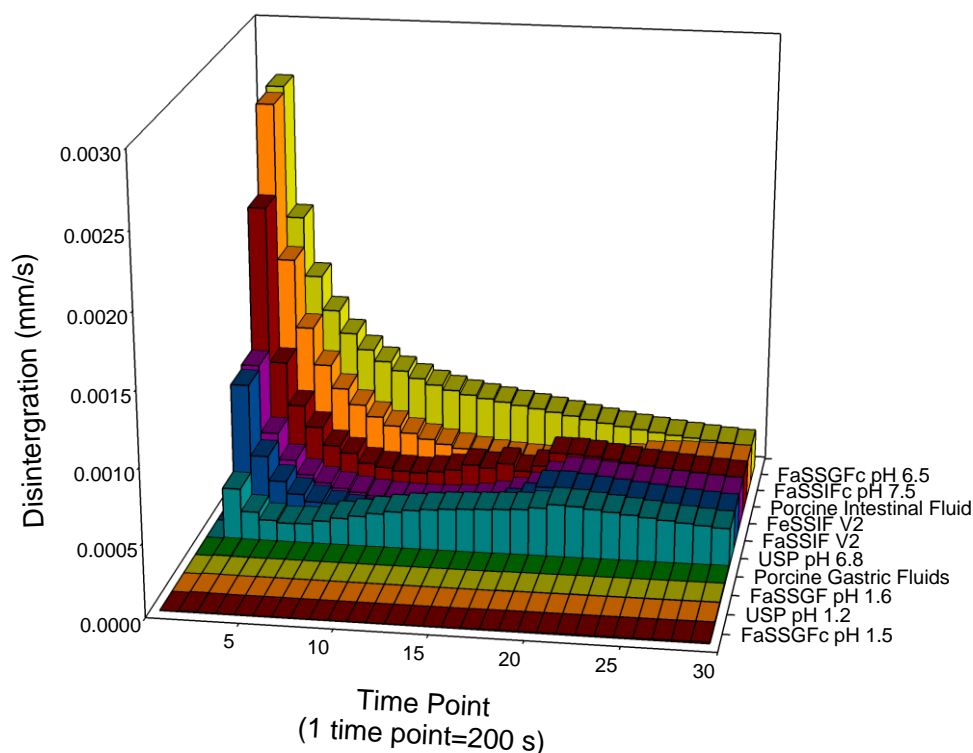


Figure 5.15: Three dimensional bar graph of the disintegration profile of the optimized Eudragit[®] coated insulin loaded trimethyl chitosan mini-pellet within biorelevant media and USP dissolution fluids ($n=3$; SD within 10% of the measured value).

The ability of a solid dosage form to directly impact the drug plasma concentration has been demonstrated with the development of controlled release formulations. The utilization of biorelevant media to characterize the solubility profiling of new chemical entities (NCE) or dissolution profiling is considered a major advancement to obtaining closer *in vitro-in vivo* correlations. Currently, the direct profiling of disintegration behaviours of a solid dosage form in biorelevant media has not been investigated. As observed within **Figure 5.15**, the biorelevant media type has a significant impact on the disintegration behaviour of the formulation. Additionally, the disintegration behaviour within the intestinal fluids of the porcine model more closely resembles that of the biorelevant canine media than the biorelevant human media. The USP simulated intestinal media was a poor representation of the disintegration behaviour of the solid dosage form. FaSSIF V2 and FeSSIF V2 almost preformed identically, which suggested that the presence of bile salts did not play a significant role in the disintegration profile. Incidentally, the disintegration profile of the FaSSIF V2 and FeSSIF V2 was similar to that of FaSSIFc where there is an initial high rate of disintegration followed by a much slower rate of disintegration. This indicates that the

presence of bile salts or lipophilic components within the biorelevant media had a significant effect on the disintegration behaviour of the optimized mini-pellet formulation. As indicated during the acquisition of viscosity profiling of the biorelevant media, a “slippage layer” may be formed during solubilisation which could assist in disrupting the macrostructure of the mini-pellet and accelerating the rate of disintegration within these media.

5.5.7.3. Dissolution of the optimized Eudragit® coated insulin loaded trimethyl chitosan chloride mini-pellet formulation

The dissolution of the optimized Eudragit® coated insulin loaded TMC:CI MiPe was determined in a step up procedure whereby the dosage form was first exposed to the gastric environment and then transferred to the small intestinal environment. The dissolution profile of the optimized Eudragit® coated insulin loaded TMC:CI MiPe formulation within biorelevant media and isolated gastrointestinal fluids of the porcine model is shown in **Figure 5.16**. In addition, the respective MDT at 2.5 hours and 10.5 hours is represented within each profile. This dissolution profiles have been fitted to the Makoid-Banakar (with Tlag) dissolution model to a R^2 adjusted value between 0.96 to 0.99. The dissolution of the model peptide therapeutic insulin during these experiments was significantly reduced by the presence of the Eudragit® coating. Interestingly, the dissolution profile obtained from isolated gastrointestinal tract fluids of the porcine model is most closely represented to that obtained from canine biorelevant media (with respect to MDT and AUC). The optimized Eudragit® coated insulin loaded MiPe formulation retained its structure after being placed within the acidic environment for 1.5 hours and then rapidly released insulin within intestinal environment.

The resulting dissolution profile indicates that the fundamental elements (pH, buffer capacity, surface tension and osmolality) are more similar to the canine model than that of the human model. The results from the disintegration analysis indicated that rate of disintegration for the mini-pellet formulation initially occurred faster within the canine biorelevant media than that of the human biorelevant media. The faster disintegration within the canine biorelevant media facilitated the faster liberation of insulin. The trimethyl chitosan chloride component of the mini-pellet formulations within FaSSIFc could have undergone faster solubilisation because of a higher pH (e.g. with respect FaSSIF-V2) or bile salt concentration (e.g. with respect FaSSIF-V2). Insulin could have then been permitted into the solubilised state due to the accelerated breakdown of the macrostructure within the canine media and isolated porcine small intestinal fluids. The Makoid-Banakar with Tlag dissolution model was fitted to the dissolution profile within each respective fluid because there was a lag period where no

drug was being released. This is due to the Eudragit[®] coating and the delayed onset of disintegration.

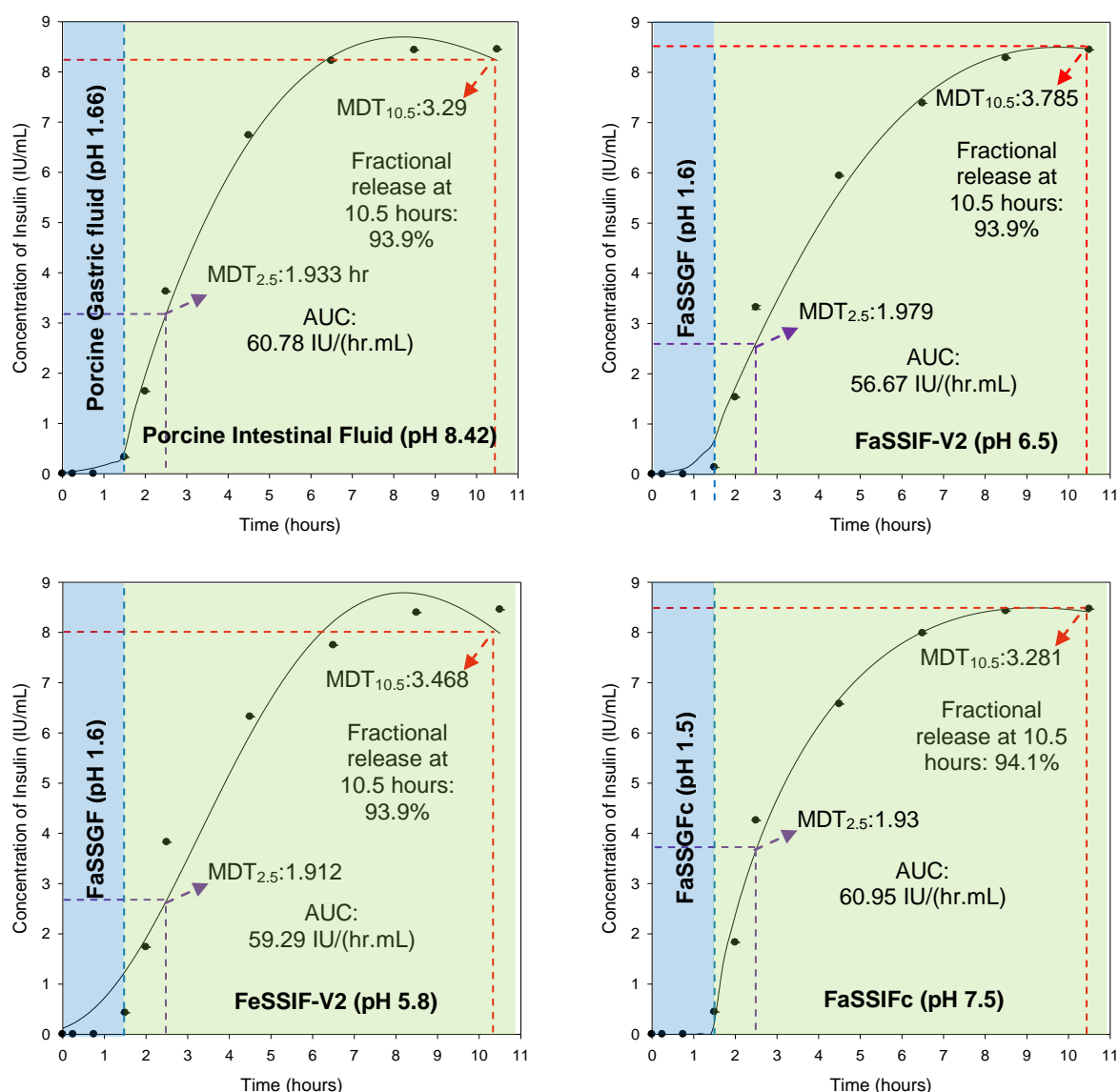


Figure 5.16: The dissolution profiles of Eudragit[®] coated insulin loaded trimethyl chitosan mini-pellets within biorelevant media (human and canine) and isolated gastrointestinal fluids of the porcine model (fasted state). The blue areas within the dissolution profiles is the time period in which the dosage form was placed within the corresponding gastric environment and the green areas within the dissolution profiles is the time period which the same dosage form was placed within the corresponding intestinal environment.

5.6. Concluding remarks

Peptide drugs are highly potent but are highly sensitive to the hostile environment within the gastrointestinal tract (Frokjaer and Otzen, 2005). The full characterization of TMC:CI was utilized to overcome the negative attributes of this polymer, such as the high crystallinity of this polymer. The weight percentage of peptide therapeutic which is included within an oral

formulation is so small that the physical presence of the peptide therapeutic will have little effect on the overall dissolution or physicochemical properties of the solid dosage form. An optimized mini-pellet formulation which contained 10mg of EDTA-mPEG hot melt dispersion (50:50), 12.57mg of Ac-Di-Sol®, 3.58mg sodium deoxycholate, and the mass of trimethyl chitosan was adjustable to achieve a final pellet weight of 145mg. This formulation achieved the predicted *in silico* responses generated by the Box-Behnken design precisely. The dissolution of insulin from the optimized formulation was altered within the biorelevant dissolution fluid with respect to the USP dissolution fluid. This was attributed to the unique physicochemical properties of this formulation being affected by the innate physicochemical properties of the biorelevant fluid such as the presence of bile acids and lipophilic entities within the dissolution fluid. Additionally, the disintegration profiling of this formulation within biorelevant dissolution fluid was also affected significantly by the innate physicochemical properties of these fluid with respect to the USP dissolution fluid. An optimized formulation should be evaluated within biorelevant dissolution fluid, even though this process is time consuming and relatively expensive, because these dissolution fluids have a superior representation of the *in vivo* luminal fluid that the USP dissolution fluid.

CHAPTER 6

***In Vitro-In Vivo* Correlation of the Optimised Oral Ghost Drug Delivery Device in the Porcine Model**

6.1. Introduction

The protocol for the *in vivo* analysis of the Oral Ghost Drug Delivery device was reviewed by the Animal Ethics Screening Committee (AESC) of the University of Witwatersrand and was assigned the clearance certificate number 2011/33/03 (**Appendix 1**). The development of the non-degradable non-responsive shell component and the assembly of the Oral Delivery Device was considered the final challenge. Insulin is a hormone utilized for the treatment of type I diabetes and in extreme instances can be administered as second line treatment for type II diabetes (Katzung, 2007). Insulin was utilized in this study as a model peptide for the optimization of the peptide loaded trimethyl chitosan mini-pellet formulations. Insulin was not utilized within *in vivo* studies because of the ethical and moral implications of inducing a diabetic condition within large animals such as porcine. Salmon calcitonin was utilized within *in vivo* studies as this hormone is a xenobiotic peptide within the porcine model, has a low toxicity profile, can be accurately measured with ELISA techniques and salmon calcitonin could be placed within an adult sized dosage form. Insulin and salmon calcitonin have been successfully administered with trimethyl chitosan for oral applications (Yin et al., 2009; du Plessis et al., 2010; Chaudhury and Das., 2011; Huang et al., 2011; Marais et al., 2013). Calcitonin is a hormone used to prevent bone reabsorption in osteoporosis patients, treatment of Paget's disease and hypercalcaemia. Calcitonin is administered as an intravenous (I.V) infusion, subcutaneous injection or intramuscular injection between three times weekly to a daily basis (Katzung, 2007). Parenteral administered salmon calcitonin is often administered as a dose between 50 to 100IU (Hartman, 2007).

The Oral Ghost Drug Delivery device was evaluated within the porcine model due to the ability of the porcine model to achieve a body mass ($\geq 50\text{Kg}$) similar to an adult human, tolerance to frequent blood sampling and similar physiological with respect to humans (Thörn et al., 2011). Additionally, the porcine model has been implemented for a multitude of multisampling studies that investigated drug transport and metabolism due to the close similarities of these processes with respect to humans (Petri et al., 2006; Persson et al., 2008; Sjodin et al., 2008; Bergman et al., 2009; Thörn et al., 2009). The gastrointestinal tract of the pig model is very similar to that of the human with respect to a remarkable gastrointestinal pH profile, dietary similarities and transition times within the gastrointestinal tract (Lennernäs, 2007). A further similarity can be found in the coronary artery distribution of

the porcine model which very similar to that of the human model (Brunet et al., 2006). Small animal models such as rats and mice cannot survive frequent withdrawals of blood sampling and cannot ingest large dosage forms that are intended for adult humans (Cryan et al., 2007). The frequency in which blood samples can be withdrawn from the animal allows for accurate determination of the pharmacokinetic data and allows for effective implementation of *in vitro-in vivo* correlations.

The *in vivo* studies were conducted to achieve two unique objectives. The first objective was the determination of the pharmacokinetic characteristics of salmon calcitonin that had been administered with the Oral Ghost Drug Delivery device. The pharmacokinetic parameters were determined with noncompartmental modelling and compartmental modelling. The noncompartmental model (based on algebraic functions) does not take into account recirculation and exchange of a drug from the accessible to the non-accessible sampling locations (e.g. from muscle tissue to plasma) or vice versa. Whereas, compartmental models (based on linear or nonlinear differential equations) take into account of recirculation and exchange of a drug from accessible to non-accessible sampling locations. The second objective was developing an *in vitro-in vivo* correlation between the dissolution profiling and the measured plasma concentrations of salmon calcitonin. The *in vitro* dissolution profiling was conducted within USP dissolution fluid and biorelevant dissolution fluid. Additionally, dissolution of salmon calcitonin from the Oral Ghost Drug Delivery device was evaluated within isolated gastrointestinal fluid of the porcine model. This allowed for the determination of which dissolution fluid achieved the most accurate profile with respect to the *in vivo* pharmacokinetic parameters. The *in vitro-in vivo* correlation between the *in vitro* dissolution profiling and the *in vivo* plasma drug concentrations has seven processes: measuring the *in vitro* dissolution; fitting the *in vitro* dissolution to a known dissolution model; measuring the plasma drug concentration with respect to time; generating a Unit Impulse Response (UIR); deconvolution of the UIR, correlation building and correlation validation. The correlation validation was utilized to determine which pharmacokinetic parameter was most accurately represented by an *in vitro* dissolution fluid.

6.2. Materials and Methods

6.3. Materials

A total of 5 healthy female white pigs were used in this study with an average weight of 35kg were purchased from a local farmer. Fresh blank plasma was routinely drawn and supplied from the catheterised pigs. Chitosan (medium molecular weight) with a degree of

deacetylation of 77.0% was purchased from Aldrich (Schnelldorf, Germany). GMP grade salmon calcitonin was purchased from Bachem (Bachem AG, Bubendorf, Switzerland). A salmon calcitonin immunoassay kit (S-1166) was purchased from Bachem (Bachem AG, Bubendorf, Switzerland). Trimethyl chitosan was prepared through reductive methylation. Acrylamide ($\geq 98\%$ pure, MW 71.08g/mol) was purchased from Fluka (Sigma-Aldrich, Buchs, Switzerland). Methacrylic acid (99% pure, 86.09g/mol) was purchased from Aldrich (Schnelldorf, Germany). Methoxypolyethylene glycol 2000 ($\geq 99\%$ pure), sodium iodide (99.999% pure), methyl iodide ($\geq 99.0\%$), sodium hydroxide ($\geq 98\%$ pure), sodium chloride ($\geq 98\%$ pure), sodium dihydrogen phosphate monohydrate ($\geq 99\%$ pure), sodium bicarbonate ($\geq 99.5\%$ pure), hydrochloric acid (37%^{v/v}), sodium deoxycholate ($\geq 98\%$ pure), sodium taurocholate ($\geq 90\%$ pure), sodium taurodeoxycholate ($\geq 97\%$ pure), orthophosphoric acid (85%^{w/v}, 99.99% pure), tetramethylethylenediamine (99% pure, 116.20g/mol), ammonium persulfate ($\geq 98\%$ pure, 228.20g/mol), Pluronic F-127, *N,N'*-methylenebis(acrylamide) (99% pure, 154.17g/mol), maleic acid (99% pure), ethylenediaminetetraacetic acid ($\geq 99.995\%$ pure) were purchased from Sigma-Aldrich (St. Louis, Missouri, USA) at reagent grade and where utilised without further purification. Dichloromethane ($\geq 99.9\%$ pure), diethyl ether ($\geq 99.0\%$ pure), acetic acid (99.99% pure), ethanol ($\geq 99.8\%$ pure) and *N*-methyl-2-pyrrolidone ($\geq 99.5\%$ pure) were purchased from Merck at reagent grade and were utilised without further purification. Ac-Di-Sol[®] and Avicel[®] RC/CL type RC-591 (co-dried blend of microcrystalline cellulose and sodium carboxymethylcellulose) was purchased from FMC BioPolymer (Philadelphia, PA, USA). Egg phosphatidylcholine (97.5% pure) purchased from Lipoid GmbH (Ludwigshafen, Germany). Acetonitrile ($\geq 99.9\%$ pure) and sodium oleate ($\geq 99\%$ pure) was purchased from Sigma (St. Louis, Missouri, USA) at UPLC grade.

6.4. Methods

6.4.1. Preparation of the optimised Oral Ghost Delivery Device

6.4.2. Manufacture of non-responsive non-degradable shell component

The non-responsive non-degradable shell component was manufactured utilising a USA Food and Drug Administration approved plastic for food grade materials. The plastic composes of Ultra High Molecular Weight Polyethylene (UHMW-PE) under the trade name Polystone[®] M. Rods of UHMW-PE were purchased and lathed to an accurate diameter of 6 mm. The lathed rods of UHMW-PE were cut into lengths of 10mm segments. A 750 CNC Bed milling machine (Ajax Machine Tools, Hampshire, UK) was utilised to hollow out the rod segments to a depth of 9mm and a diameter of 5.5mm. A rod segment was then placed in a

table top vice grip and eight 1mm diameter orifices were drilled along the base (part of the rod segment which was not hollowed out) and an additional four 1mm orifices were drilled into the base of the UHMW-PE segment. This formed the non-responsive non-degradable shell component. The schematic representation of the non-responsive non-degradable shell component is illustrated in **Figure 6.2**.

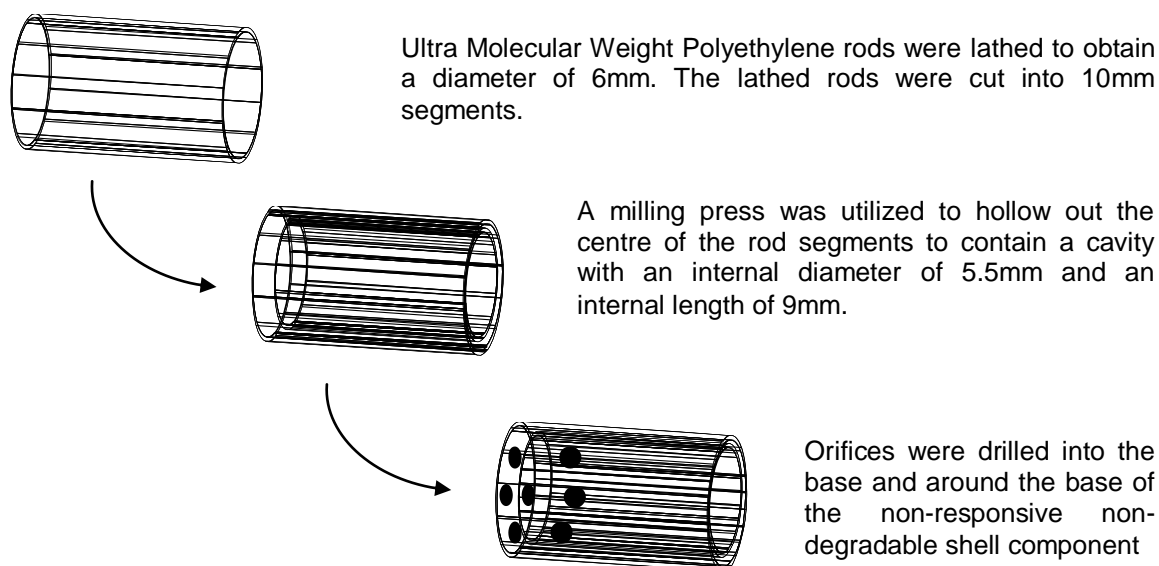


Figure 6.1: Schematic representation of the non-responsive non-degradable shell component of the Oral Ghost Drug Delivery device manufacture process.

6.4.3. Synthesis of the stimuli responsive hydrogel as the trigger mechanism of the Oral Ghost Delivery Device

The stimuli responsive hydrogel was synthesised in the same manner as **Section 4.4.1**. Briefly, the stimuli responsive hydrogel was synthesized using acrylamide (AAm) monomers and methacrylic acid (MAA). *N-N*-Methylenebisacrylamide (BIS) is a crosslinking agent that was utilised to crosslink AAm to MAA. Pluronic F-127 was used to enhance the solubilisation of AAm, MAA and MBA in deionised water. Ammonium persulfate, a radical initiator, and tetramethylethylenediamine (TEMED), a catalyst, were used in the crosslinking reaction between AAm and MAA. The concentrations and sequential addition of chemical components that make up the AAm-MAA stimuli responsive hydrogel can be reviewed in **Table 6.1**.

Once all the respective solutions were prepared and added to a glass beaker under constant magnetic stirring, 100mg of sodium bicarbonate was immediately added. The sodium bicarbonate generated carbon dioxide gas within the polymerising solution, thus

inducing the formation of a porous gel. Moulds were produced that would allow the *in situ* curing process to take place within a cylindrical shape (inner diameter of cylindrical moulds was 4.77mm). The moulds were placed in a glass beaker and incubated in a water bath at $37\pm0.5^{\circ}\text{C}$ for 12 hours. Once the curing process was completed, the *in situ* cured rods were then removed from the cylindrical moulds and cut, transversely, into 0.5mm pieces and then longitudinally into 0.3mm pieces.

Table 6.1. The concentrations of sequentially added chemical components whilst constantly stirring, in order to form the AAm-MAA stimuli responsive hydrogel

Solution component	Concentration (% ^w / _v)	Volume added to final <i>in situ</i> gelling solution (mL)
Acrylamide	50	3
Methacrylic acid	50	2
N,N'-Methylenebis(acrylamide)	2.5	0.7
Deionised water	-	3
Pluronic F-127	10	0.3
Ammonium persulfate	20	0.25
Tetramethylethylenediamine	20	0.25

6.4.4. Manufacture of the erodible methyl cellulose disc

Erodible methyl cellulose discs were manufactured in a similar manner to that of the Avicel[®]-EDTA-mPEG *in situ* hot melt dispersion mini-pellets. Methyl cellulose was accurately weighted out (20mg) and placed within the punch and die set to produce mini-pellets with a diameter of 4mm and a length of 1mm. A methyl cellulose disc was placed between the stimuli responsive hydrogel and the drug carriers to restrict contact with water within the drug delivery system. In addition, the methyl cellulose disc, which eroded very slowly within a hydrophilic environment, acted as a surface that the stimuli responsive hydrogel could physically act against. The ability of the stimuli responsive hydrogel to act as the Trigger Mechanism within the drug delivery system was enhanced by the presence of the methyl cellulose disc.

6.4.5. Manufacture of the Avicel[®]-EDTA-mPEG *in situ* hot melt dispersion mini-pellet

The Avicel[®]-EDTA-mPEG *in situ* hot melt dispersion mini-pellet was manufactured in the same manner as that in **Section 3.4.1**. Melt dispersions of EDTA-mPEG were synthesised at the respective ratio of 33.5%^w/_w mPEG, 33.5%^w/_w EDTA and 33%^w/_w Avicel[®] RC/CL type R-591. The mPEG was first melted to 60°C on a watch glass heated by a calibrated hot plate magnetic stirrer. Once the solid mass of mPEG was melted to a liquid phase, EDTA was added to the molten mPEG. The EDTA was homogeneously distributed within the molten

mPEG with a wooden spatula. Once a uniform distribution was obtained, the EDTA-mPEG hot melt dispersion was removed from the hot plate magnetic stirrer and allowed to cool under constant stirring. Once the EDTA-mPEG hot melt dispersion had become a cool solid, the solid mass was placed through a metal sieve with an aperture of 850 μ m to form a fine powder. Avicel[®] RC/CL type R-591 was accurately weighted out and mixed (at 250rpm) with the fine EDTA-mPEG powder until a homogenous mixture was obtained. The homogenous mixture was then accurately weighted out into 30mg aliquots and placed within the punch and die set. Mini-pellets were produced under a pressure of 3.5MPa with a diameter of 4mm and a length of 3.27mm.

6.4.6. Synthesis of trimethyl chitosan

TMC:CI was synthesized in the same manner as in **Section 5.4.1**. Briefly, TMC:CI was synthesized by a two reaction step and an ion-exchange step process. Two grams of chitosan (medium molecular weight, 77% deacetylated), 10mL of 20%^{w/v} sodium hydroxide solution and 4.8g of sodium iodide was dissolved in 80mL of pre-warmed *N*-methyl pyrrolidone (60 \pm 0.2 $^{\circ}$ C). The reaction was carried out over a 30 minute period in a heated water bath (60 \pm 0.2 $^{\circ}$ C). The homogenous solution was then removed from the heated water bath and 12mL of methyl iodide was immediately incorporated within the solution. The reaction was allowed to complete under reflux, by utilization of a Liebig condenser, under constant magnetic stirring (300rpm) for 90 minutes (60 \pm 0.2 $^{\circ}$ C). The homogenous polymer solution is then removed and the trimethyl chitosan iodine precipitated out of solution with 250mL diethyl ether and 250mL ethanol. Trimethyl chitosan iodine was collected and dried *in vacuo* (60 \pm 0.5 $^{\circ}$ C for 48 hours). The dry trimethyl chitosan iodine was ground into a fine powder and utilized within the second reaction step.

The second reaction step utilized the same procedure as that performed in the first step but chitosan was substituted with trimethyl chitosan iodine. Once the polymer product from the second reaction had been dried and ground into a fine powder, the ion-exchange step was conducted.

The second reaction step trimethyl chitosan iodine powder was dissolved in 80mL of 5%^{w/v} sodium chloride solution for 30 minutes under constant magnetic stirring (300rpm). Diethyl ether (250mL) and ethanol (250mL) was utilized to precipitate trimethyl chitosan chloride. The precipitated TMC:CI was isolated by filtration and dried *in vacuo* (60 \pm 0.5 $^{\circ}$ C for 24 hours).

6.4.7. Manufacture of salmon calcitonin loaded trimethyl chitosan mini-pellet

The dried trimethyl chitosan (TMC) was dried and ground into a fine powder which was placed through a 400 μ m aperture sieve to ensure uniform powder. An accurate weight of 2500mg trimethyl chitosan powder was dissolved in 40mL of Millipore water (pH 7.0) by magnetic stirring at 300rpm for 30 minutes, at which point a viscous yellow solution was obtained. The salmon calcitonin was added in order to obtain a final concentration of 600IU salmon calcitonin per 3.2mg of powder. The dispersion was frozen at 193K for 48 hours. The powder sample was lyophilised with a 2 hour condensation phase at -60°C and a 24 hour sublimation phase at 25mm Torr in a Freezone 12 freeze drier (Lanconco, Kansas City, USA). After freeze-drying, the sample was placed in sealed glass polytops and frozen at -20°C (Silva et al., 2006; Pringels et al., 2008).

Dry granulation was utilised, which involved: salmon calcitonin loaded-lyophilised trimethyl chitosan, mPEG, Ac-Di-Sol[®] microcrystalline cellulose and dry trimethyl chitosan powder which were accurately weighted according to the optimised insulin-loaded trimethyl chitosan mini-pellet optimised Box Behnken design formulation. Once the powdered components were accurately weighted, the samples were mixed until a homogenous mixture was obtained. The homogenous mixture was compressed within a modified punch and die set to produce 4mm pellets under a compression of 3.4MPa. The pellets were immediately placed in glass polytops and frozen at -20°C.

6.4.8. Assembly of the Oral Ghost Drug Delivery device and spray coating Eudragit[®]

The Oral Ghost Drug Delivery device was assembled by placing the swellable trigger system (accurately weighted 10mg) within the internal bottom of the non-responsive non-degradable shell component. A methyl cellulose disc was placed onto the swellable trigger system, followed by a salmon calcitonin-loaded trimethyl chitosan mini-pellet and finally an Avicel[®]-EDTA-mPEG *in situ* hot melt dispersion mini-pellet. The top system was then spray coated in an enteric coating solution. The enteric coating solution contained a 4%^{w/w} solution of Eudragit[®] L100 and a 4%^{w/w} solution of Eudragit[®] S100 within an organic solvent composed of 33%^{v/v} ethanol and 67%^{v/v} acetone. Triethyl citrate was added to the solution at a concentration of 35%^{w/w} of the Eudragit[®] component of the coating solution. The top coated Oral Ghost Drug Delivery device was placed within glass polytops and stored at -20°C until use. A schematic representation of the Oral Ghost Delivery Device assembly is illustrated in **Figure 6.2**.

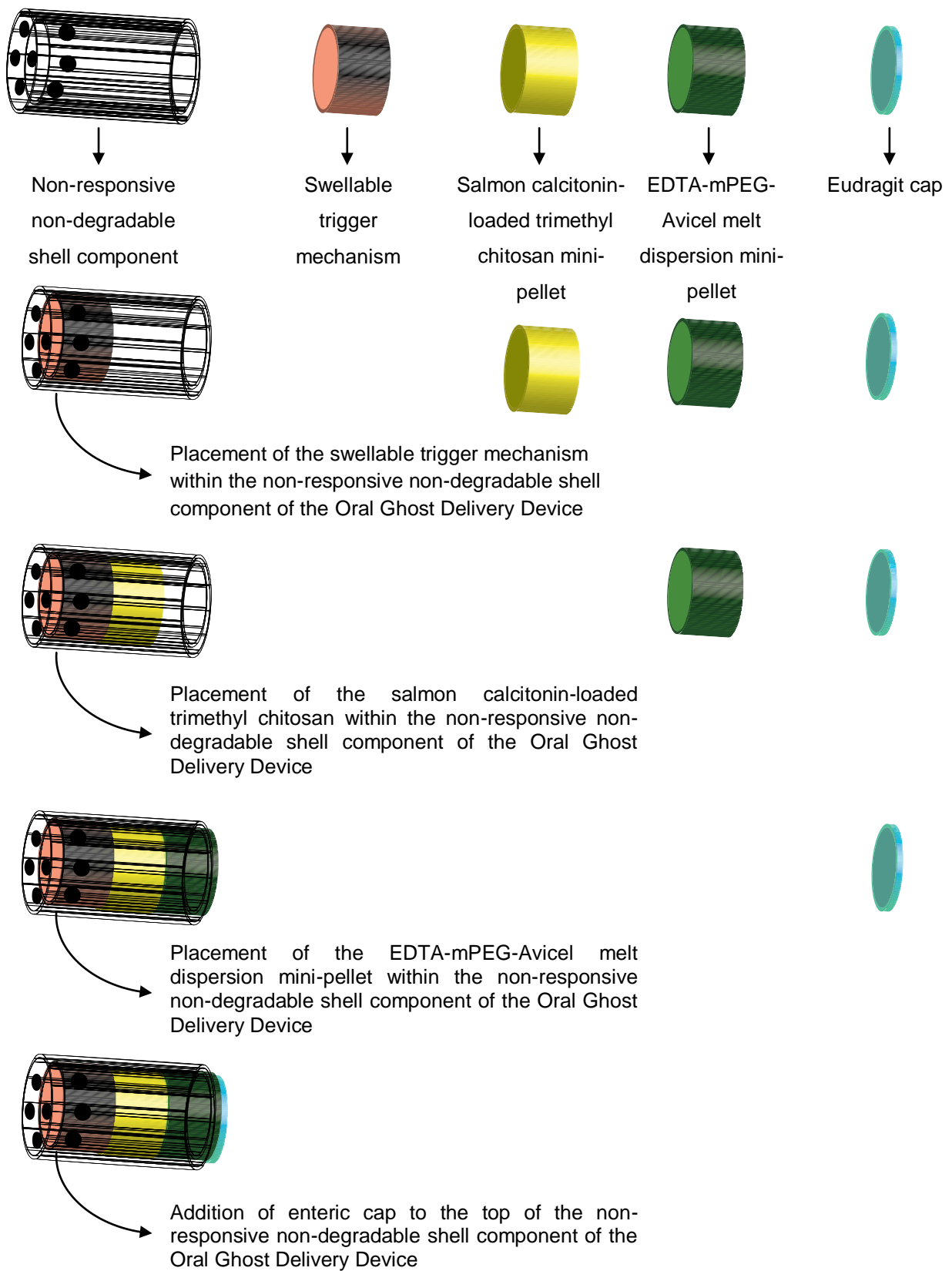


Figure 6.2: A schematic representation of the Oral Ghost Drug Delivery device assembly.

6.4.9. Isolation of porcine gastrointestinal fluids

The Large White pigs utilized in this study were obtained according to the *Guide for the Care and Use of Laboratory Animals* that was approved by the Animal Ethics Screening Committee of the University of Witwatersrand (Ethics number:2011/33/03). The isolation of gastrointestinal fluid was conducted in the same manner as indicated in **Section 4.4.7**. Briefly, the gastrointestinal fluids isolated from the pigs were collected during the fasted state which was induced by restricting food for 12 hours (water was provided *ad libitum*). This is the standard operating procedure for dosing pigs with an oral drug delivery system. The gastric and small intestinal fluids were collected after euthanization. The stomach and small intestine were isolated and a small incision was made to perforate the respective organ wall.

The pH and buffer capacity of the isolated gastric and small intestinal fluids (individual and pooled samples) were measured immediately. The pooled sample was maintained with an equal addition from each individual sample. To preserve the composition of the gastrointestinal fluid, the samples were immediately frozen in liquid nitrogen and maintained at -80°C. In order the drug dissolution studies to be effectively preformed, removal of solid matter (food particles and ingested hay) from the samples was achieved by centrifugation at 5000rpm for 10min at 10°C, followed by filtration of the supernatant through a 0.44µm Millipore Millex injection filter (Billerica, MA, USA).

6.4.10. Dissolution of salmon calcitonin from the Oral Ghost Drug Delivery device

The dissolution of salmon calcitonin from the Oral Ghost Drug Delivery device was conducted in a similar manner as described in **Section 5.4.9**. Briefly, the Oral Ghost Drug Delivery device was placed within a dissolution fluid set (USP pH 1.2-USP pH 6.8; FaSSGF-FaSSIF V2; FaSSGF-FeSSIF V2, FaSSGFc pH 1.5-FaSSIFc pH 7.5, isolated porcine gastric fluid-isolated porcine small intestinal fluid) that had been previously described (Dünhaupt et al., 2012). A 10mL volume of dissolution fluid was placed into a polytop and was equilibrated at 37±0.5°C and 50rpm within an Orbit Shaker Incubator (LM-530-2, MRC Laboratory Instruments Ltd, Hahistadrut, Holon, Israel). A 0.01mL sample was withdrawn at each predetermined time point, and diluted in 4.99mL Millipore water to achieve a dilution factor of 500. A volume of 50µL was placed within the salmon calcitonin ELISA kit and was further diluted to achieve a dilution factor of 1000. The extremely high dilution factor was utilized to reduce the impact of the bile acid components on the UV spectroscopic absorption readings and to for the *ex vivo* dissolution procedures to be conducted in triplicate (a limited volume of

isolated gastrointestinal fluid was available after filtration procedures).The ELISA kit procedure will be discussed in **Section 6.4.13**.

6.4.11. Standard market product for absolute bioavailability comparison

Miacalcin® (Novartis Pharma AG, Basel, Switzerland) was purchased and administered intramuscularly at the standard dosage (100IU) to the pig model as recommended for the treatment of post menopausal osteoporosis. In reality an IM injection is not the absolute reference for pharmacokinetic parameters, but in this current administration application is appropriate as there is no IV injectable forms utilized for the treatment of osteoporosis.

6.4.12. *In vivo* studies in the pig model utilising the optimised Oral Ghost Drug Delivery device

6.4.12.1. Animal studies design for the *in vivo* assessment of the salmon calcitonin bioavailability from the Oral Ghost Delivery Device in comparison to the marketed product Miacalcin®

The animal study included three groups: Group 1 (Test) which included administration of the Oral Ghost Delivery Device (salmon calcitonin-loaded) to 5 pigs; Group 2 (Control) which included administration of the Oral Ghost Delivery Device (no salmon calcitonin) to 5 pigs; Group 3 (Comparison) which included administration of an intramuscular injection of Miacalcin® (contains salmon calcitonin) to 5 pigs. Blood samples from each group will be collected from the respective groups at predetermined time points. The concentration and amount of salmon calcitonin from each blood sample will be determined so that the pharmacokinetic data can be compared for each group within the study. A flow chart of the animal study design may be reviewed within **Figure 6.3**. The 5 pigs utilized for this study was utilized for each arm of this study with a 2 day washout period (>9 half lives of salmon calcitonin).

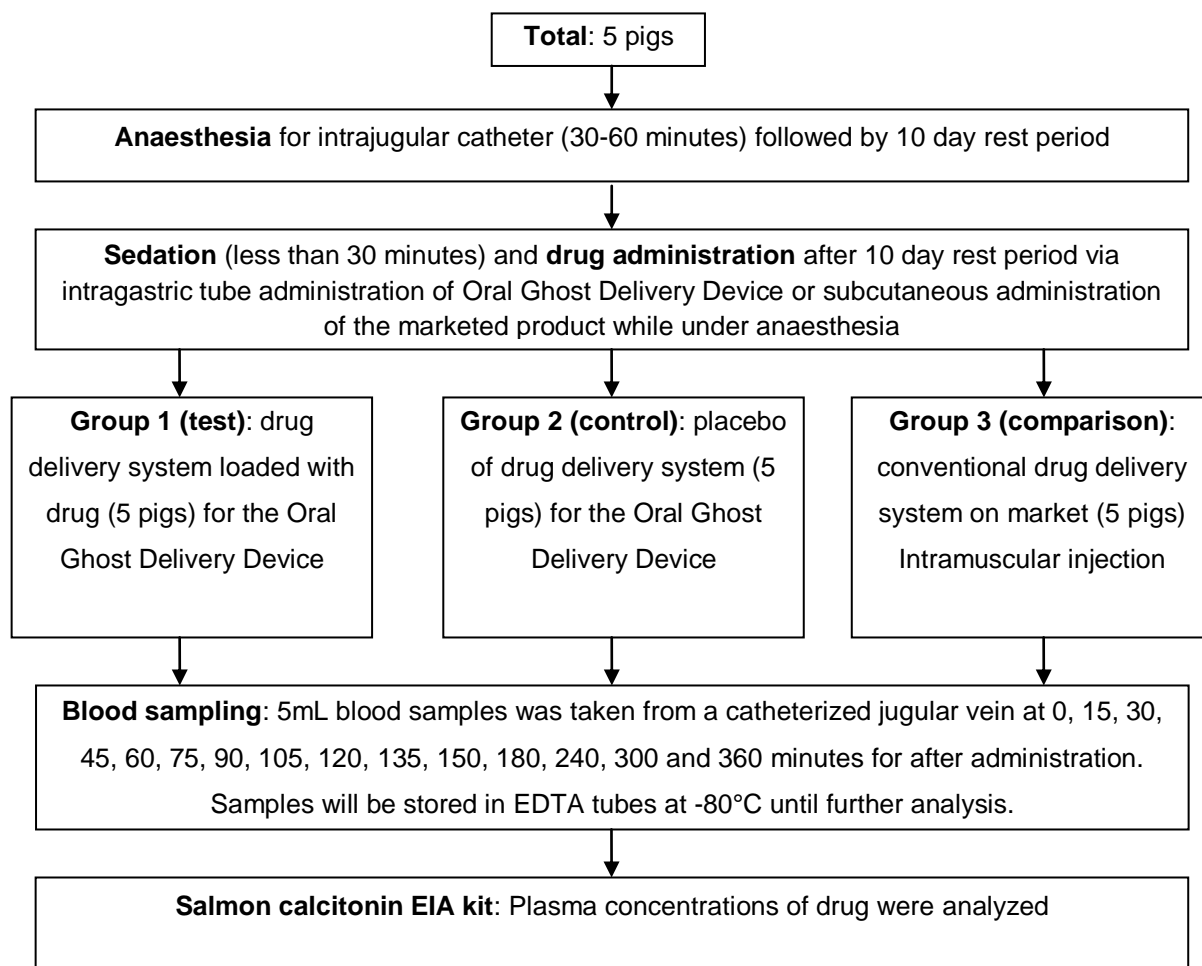


Figure 6.3: Animal study design which contains three groups: Group 1 (Test) consists of animal administered salmon calcitonin containing Oral Ghost Delivery Device; Group 2 (Control) consist of the Oral Ghost Delivery Device within loaded salmon calcitonin and Group 3 (Comparison) consist of the marketed intramuscular drug delivery system containing salmon calcitonin.

6.4.12.2. Development of a blood sampling protocol through the insertion of a resident catheter for the accurate analysis of plasma samples

The implantation of a permanent catheter within the pig model was preformed to reduce suffering to the animal due to the frequency of blood sampling and to increase the accuracy of blood sampling from the animals. Six Large White pigs which weighed between 35-37Kg was anaesthetised with ketamine (11mg/Kg intramuscularly) and midazolam (0.3mg/Kg intramuscularly). To reduce analgesia and inflammation Buprenorphine (0.5mg/Kg intramuscularly) and Carprofen (4mg/Kg intramuscularly) were administered. The pigs were intubated and anaesthesia was maintained with a gas mixture of 2%_{v/v} isoflurane and 100%_{v/v} oxygen.

The pigs were then transferred to the operation theatre where aseptic conditions could be maintained. A 7 French gauge double lumen 35cm (CS-28702) (Arrow Deutschland GmdH, Erding, Germany) was surgically implanted into the left jugular vein of the pig. The left jugular vein was first exposed by blunt dissection along the dorsal side of the jugular groove located on the left lateral aspect of the neck. The catheter was inserted into the lumen of the jugular vein to a length of 10cm. The lumen of the catheter was sutured into place within the vein utilising a purse suture technique. A trocar was utilised to tunnel subcutaneously to an exit point cranial to the dorsal aspect of the scapula so that the remaining length of the catheter (25cm) could exit the animals neck. The external injection ports of the catheter were sutured to the skin to limit bending and the incidence of the catheter being pulled out of place by the pig after surgery. The catheter was immediately flushed with heparinised saline (5000IU/L of 0.9%^{w/v} NaCl saline). The pigs were allowed to heal after surgery for a period of 10 days and undergo further habituation through the removal of small volumes of blood from the ports of the implanted jugular catheter. The catheter was maintained by regular (twice daily) flushing with 5000IU/L 0.9%^{w/v} NaCl heparinised saline.

6.4.12.3. Dosing procedure for the Oral Ghost Drug Delivery device and intramuscular administration of salmon calcitonin

The pigs were anaesthetised with ketamine (11mg/Kg) and midazolam (0.3mg/Kg) directly into the jugular vein catheter. Once anaesthetised, the pig was maintained in the anaesthetised state with the utilisation of a 2%^{v/v} isoflurane and 100%^{v/v} oxygen gas mixture. An intragastric tube (1.8cm outer diameter and 1.3cm inner diameter) was inserted into the stomach of the pig and the OGDD device was placed within the intragastric tube. Water was used to flush the OGDD device into the stomach of the pig. The anaesthetised state allowed for maintenance of the catheter (e.g. signs of infection and removal of dirt located at the site at which the catheter exited the pig's neck) and removal of stitches along the dorsal jugular groove of the neck. The pigs were returned to their respective pens to recover under observation.

6.4.12.4. Blood withdrawal protocol

Blood (5mL) was withdrawn from the conscious pig at 0, 15, 30, 45, 60, 75, 90, 105, 120, 135, 150, 180, 240, 300 and 360min. Blood samples were stored in EDTA blood tubes and then centrifuged at 5000rpm for 15 minutes at 4°C. The separated plasma was removed and stored in a -80°C freezer until further analysis. The catheter was disinfected during each withdrawal point to prevent local and systemic infection. The catheter was first flushed with

heparinised saline to remove any clots that may have formed within the catheter or at the end of the catheter which was inserted into the jugular vein.

6.4.13. Procedure of utilizing the enzyme linked immunoassay kit for the determination of salmon calcitonin concentration

The concentration of salmon calcitonin within blood samples was determined utilising an EIA according to the kits standard operating procedure. A standard curve was generated by preparing standards at 25ng/mL, 5ng/mL, 1ng/mL, 0.2ng/mL, 0.04ng/mL, 0.008ng/mL and 0ng/mL. These standards were added to the plate in duplicate and generated an OD value between 0 and 3.4 at final wavelength measurement at 450nm. Two buffer solutions, Buffer A and Buffer B, were included with the purchase of the kit. An equal volume ratio of Buffer A and blood plasma was placed within an eppendorf. The sample was centrifuged at 5000rpm for 20 minutes at 4°C. The supernatant was removed from the sample and placed within an eppendorf tube. A SEP-COLUMN was washed with 1mL Buffer B. The SEP-COLUMN was washed three times with Buffer to generate an equilibrated SEP-COLUMN. The supernatant of the sample was then placed onto the SEP-COLUMN and a volume of 6mL Buffer A was utilised to wash the column. A 3mL volume of Buffer B was then utilised and the salmon calcitonin containing wash was collected within an eppendorf tube. The eppendorf was placed within a dry ice bath and UPLC grade methanol was utilised to evaporate the water phase from the sample. Finally, the residue remaining within the eppendorf tube was dissolved within EIA buffer (provided with purchase), a 50µL volume of sample containing EIA buffer was removed and pipetted into a well of the 96 well plate. A volume of 25µL antiserum within EIA buffer was added to each well that contained a sample (a standard curve utilised known concentrations of salmon calcitonin instead of samples derived from pig plasma). The EIA 96 well plate was incubated at room temperature for 1 hour. Each well which contained blank, sample and standard had 25µL Bt-tracer (provided with purchase) added to it and was incubated for an additional 2 hours. The plate was washed with EIA buffer and 100µL of streptavidin-HRP was added to each well and incubated for another hour. Each well was washed once again and 100µL TMB solution (provided with purchase) was added to each well. The EIA 96 well plate was incubated for another hour and the reaction was terminated with the addition of 100µL 2 N HCl per well. The entire well plate was read simultaneously at 450nm within 5 minutes of HCl addition.

6.4.14. Pharmacokinetic analysis of *in vivo* drug concentration profiles

The concentrations of salmon calcitonin were determined from the blood plasma utilizing the ELISA kit and these plasma drug concentrations were plotted against time in a scatter plot. The Area Under Curve from time 0 to infinity ($AUC_{0-\infty}$) was determined from the plasma drug concentration-time profile at each time point and plotted against time. Additionally, the Area Under Moment Curve from time 0 to infinity ($AUMC_{0-\infty}$) was also determined from the plasma drug concentration-time profile and also plotted against time. The $AUMC_{0-\infty}$ was determined by dividing the last concentration of drug observed in plasma by respective K_{el} (Qurrat-ul-Ain et al., 2003; Gavini et al., 2006). The AUMC from the last value to infinity was calculated as **Equation 6.1**:

$$AUMC_{last-infinity} = c_{last} \times \frac{t_{last}}{K_{el}} + \frac{t_{last}}{K_{el}} \quad (\text{Eqn. 6.1})$$

The plasma drug concentration-time profiles were utilized to determine the pharmacokinetic parameters in both compartmental and noncompartmental analysis for the orally administered Oral Ghost Drug Delivery device and the intramuscular administered marketed standard Miacalcin®. All pharmacokinetic analysis was conducted with Winnonlin (Pharsight, Version 5.1).

6.4.15. *In vitro-in vivo* correlation

The *in vitro-in vivo* correlation was conducted with the utilization of dissolution profiling of salmon calcitonin within biorelevant media, the orally administered OGDD device which had been loaded with salmon calcitonin and intramuscularly administered salmon calcitonin. The *in vitro-in vivo* correlation was generated utilizing Winnonlin (Pharsight, version 5.1). The *in vitro-in vivo* correlation was built up over a seven processes (*in vitro* dissolution, *in vitro* dissolution model fitting, *in vivo* plasma drug concentration-time profiling, generation of a Unit Impulse Response, deconvolution, correlation building and correlation validation). These processes are discussed in Emami and more recently in Lu et al. (Emami, 2006; Lu et al., 2011).

6.4.15.1. The *in vitro* dissolution of salmon calcitonin within USP and biorelevant dissolution fluids

The *in vitro* dissolution of the OGDD device was conducted in a two step process whereby the dosage form was initially placed within gastric representative dissolution fluid for 60 minutes and then placed within intestinal representative dissolution fluid for 8.5 hours. A total of four dissolution sets (USP pH 1.2 to USP pH 6.8; FaSSGF to FaSSIF-V2; FaSSGF-FaSSIF-V2; FaSSGFc pH 1.6 to FaSSIFc pH 7.5) were utilized to generate fractional release-time profiles. Additionally, a fractional release-time profile was determined within an *ex vivo* set (isolated porcine gastric fluid to isolated porcine intestinal fluid). The utilization of these dissolution sets allows for the determination of which dissolution fluid facilitates the closest *in vivo* plasma drug concentration-time profile.

6.4.15.2. *In vivo* administration of salmon calcitonin

The *in vivo* administration of salmon calcitonin was carried out in via the oral route with the utilization of the OGDD device and intramuscularly. The intramuscular administration of salmon calcitonin was required to achieve a 100% absorption profile so that an effective bioavailability of salmon calcitonin via the oral route can be calculated.

6.4.15.3. Deconvolution of the Unit Impulse Response

The Unit Impulse Response (UIR) is derived to describe *the in vivo* pharmacokinetic profile following an instantaneous dose (e.g. I.M. administration of salmon calcitonin) to obtain the rate at which one unit of drug enters the central compartment. The process of deconvolution utilizes the UIR generated from the *in vivo* pharmacokinetics to determine the drug absorption rate required to achieve an observed plasma drug concentration-time profile from an orally administered formulation. In this study the deconvolution process was determined to calculate the absorption rate of salmon calcitonin from the small intestine into the systemic circulation and was applied to generate the *in vitro-in vivo* correlation. The underpinning principles that facilitate the exploitation of deconvolution will be discussed briefly. The first underpinning principle is that of linear assumptions defined by the linear superposition principle. The linear superposition principle, in a pharmacokinetic perspective, establishes that under linear conditions the total concentration of drug in the body is the sum of the remaining concentrations from each administered dose at that point in time when a measurement was observed. This is achieved by considering drug transportation kinetics as non-parametric (having no characteristic structure or defining structure) and that drug

transport is stochastic (a system that is determined probabilistically). It can then be asserted that drug transport (point A) and subsequent absorption-distribution can be measured (point B).

A drug molecule at time point 0 can be measured in a volume (V) within a system by entering the system at location A (the transportation point). With respect to time, the drug molecule will move within a defined volume through the process of absorption-distribution at point B. The probability that a drug molecule will be at point B with respect to point A at time 0 can be represented as function $g(t)$. A dosage form usually consists of an astronomical number of drug molecules (N) and is administered simultaneously. It is also assumed, usually, that no interaction between drug molecules exists at the transportation point A and therefore no transportation kinetic alteration occurs due to presence of high amounts of drug molecules at transport point A. The probability of a drug molecule of being at point B at time t is random and independent for each drug molecule of the administered dosage and the $g(t)$ for each drug molecule is identical. The identical function $g(t)$ for each drug molecule facilitates the implementation of the linear superposition principle and that the concentration of drug molecules at point B at time t is proportional to dose (A large dose N has a large number of drug molecules will probably be greater at measurement point B than a smaller dose with less drug molecules) but $g(t)$ is also independent because transport of each drug molecule is independent other drug molecules.

A system usually has a constant transport process (i.e. diffusion) that has a constant transport rate for each drug molecule from point A to point B, with respect to time. The probability of a drug molecule being present at point B at time t is dependent on the time since being transported at point A and is independent of the eclipsed time span at point A. It can then be asserted that the probability of a molecule being at point B is $g(t-t_A)$ where t_A is the time since being transported from point A to point B. This is referred to as time-invariance. If N drug molecules leave point A simultaneously, the probability of a drug molecule being located at point B at time t is equal. The exact time for a drug molecule to start leaving point A is always unknown within a system and t_A can be replaced with a probability density function $h(t)$, as shown in **Equation 6.2**:

$$Pr(t_a \geq t) = \int_0^t h(u) du \quad (\text{Eqn. 6.2})$$

Where $h(u)$ is the probability function of an unknown time. The probability of the drug molecule at point B at time t is the average of $g(t-t_A)$ because if the same drug molecule

entered the same point A and was transported to point B at time t , a multitude to times, an average can be achieved. The possible values of t_A can be calculated according to **Equation 6.3**:

$$\bar{g}(t) = \int_0^t g(t - t_A) \times h(t_A) dt_A \quad (\text{Eqn. 6.3})$$

If N drug molecules enter point A, and each drug molecule leaves point A at random times as indicated by the probability density function $h(t)$, then the number of drug molecules at point B at time t is the product of N and the probability of being at B at time t , as shown by **Equation 6.4**:

$$N_B(t) = N\bar{g}(t) = N \int_0^t g(t - t_A) \times h(t_A) dt_A = \int_0^t g(t - t_A) \times N'_A(t_A) dt_A \quad (\text{Eqn. 6.4})$$

If the number of molecules present at point B at time t is converted to mass units, as shown by **Equation 6.5**:

$$M_B(t) = \int_0^t g(t - t_A) \times f(t_A) dt_A \quad (\text{Eqn. 6.5})$$

Where $M_B(t)$ is the mass of drug molecules at point B at time t and $f(t)$ is the rate of absorption (mass per unit time) into point A at time t . Additionally, the volume of the system (V_s) of point B can be included to determine the concentration of the drug molecule with respect to time ($c(t)$) at point B, and calculated by **Equation 6.6**:

$$c(t) = \int_0^t f(t - u) \times c_\delta(u) du \equiv f(t) \times c_\delta(t) \quad (\text{Eqn. 6.6})$$

Where c_δ is equal to $g(t)/V_s$ and is known as the Unit Impulse Response (UIR). The drug input rate is represented at $f(t)$ in the above equation. The process of determining the input function $f(t)$ is known as deconvolution because in order to obtain this parameter, the convolution integral needs to be deconvolved. Additionally, the UIR function (c_δ) is equal to the probability that a drug molecule that entered point A at time 0 will be present at point B at time t is divided by the volume of the system.

6.4.15.4. Correlation of fitted salmon calcitonin dissolution observations and fitted dissolution model profiles

A correlation between the fitted dissolution of salmon calcitonin from the Oral Ghost Drug Delivery device within the dissolution environment (e.g. FaSSGF-FaSSIF V2 dissolution set) and the absorption of salmon calcitonin in the *in vivo* environment is generated through the process of determining the input rate function $f(t)$, as described in **Section 6.4.14.3**.

6.4.15.5. Correlation validation

The *in vitro-in vivo* correlation is validated by determining the AUC and maximum concentration based on model predictions and compared to the AUC and maximum concentrations obtained within the *in vivo* environment. In order to achieve this validation, the fitted fractions absorbed and UIRs are convolved and a noncompartmental analysis is run to predict the pharmacokinetic data observed within the *in vivo* plasma drug concentration-time profile. The greater the number of noncompartmental parameters that achieve similar or identical observations that are similar to fitted pharmacokinetic parameters, the better the correlation. The ideal ratio of observed to fitted pharmacokinetic parameters should be a 1:1 ratio. The correlation was conducted for each salmon calcitonin dissolution profile within each dissolution fluid and isolated porcine gastrointestinal fluid to determine which dissolution fluid set achieved the greatest *in vitro-in vivo* correlation.

6.5. Results and Discussion

6.5.1. The insertion of a chronic catheter for chronic withdrawal of blood samples

The 6 pigs were prepared for surgery by the administration of an anaesthetic agent ketamine (11mg/Kg intramuscularly) and midazolam (0.3mg/Kg intramuscularly) directly into the neck. In all 6 pigs an endotracheal tube was inserted to maintain free passage of air to the lungs and for the administration of isoflurane/oxygen during surgical procedures. The oxygen levels and blood pressure was monitored for each pig throughout the anaesthetised procedures. In order for the insertion of the intrajugular catheter to occur without inducing infection at the site of the surgery, the neck was prepared by shaving the neck hair and cleaning the skin with veterinary disinfectant spray. The animal was then wheeled into the operating theatre to undergo insertion of the jugular catheter surgery. The preparation of the pig for surgery photographs may be reviewed in **Figure 6.4**.

The pig underwent surgery as described in **Section 6.2.4.2**. The insertion of the intrajugular catheter within each pig was successful and all the utilized pigs for this study recovered fully from the surgery. The health of the pigs utilized for this study was monitored by measuring body weight weekly and observation of any adverse event such as infection at the site of the surgery. The insertion of the intrajugular catheter photographs may be reviewed in **Figure 6.5**.

6.5.2. Isolation of the porcine gastrointestinal fluids in the fasted state

The isolation of the porcine gastrointestinal fluids in the fasted state was carried out for comparative dissolution. The pH of the fasted gastric intraluminal fluids and fasted small intestinal intraluminal fluids from the porcine model was determined to have a mean pH of 1.54 (SD±0.4) and 8.4 (SD±0.27), respectively. The buffer capacity of the fasted gastric intraluminal fluids and fasted small intestinal intraluminal fluids from the porcine model was determined to have a mean of 26.4mmol/L/pH and 38.2mmol/L/pH, respectively. The isolation and subsequent filtered isolated porcine gastrointestinal tract is photographed in **Figure 6.6**.

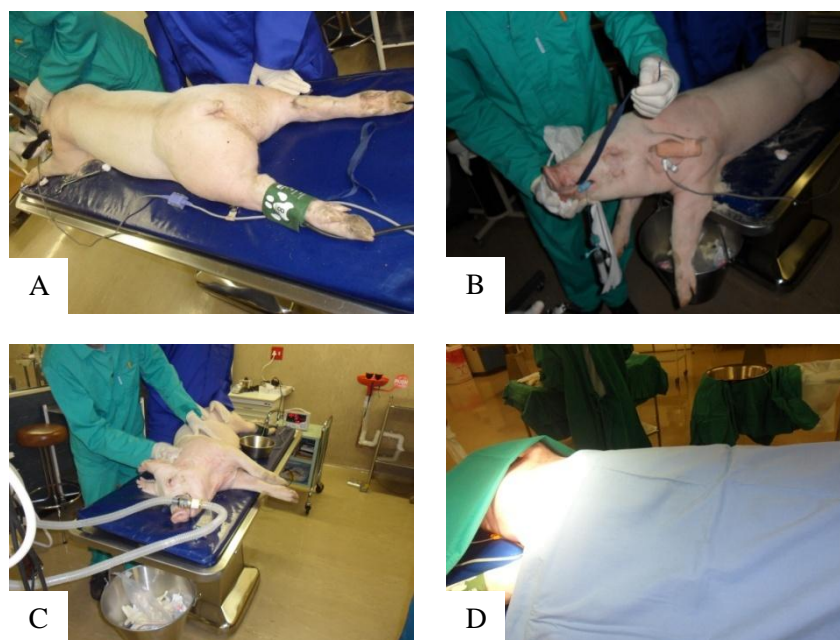


Figure 6.4: Photographic depiction of the surgical preparative measures utilised for the pigs in this study. The blood pressure was monitored (A), the endotracheal tube was inserted into the pig (B), a gas mixture of oxygen and isoflurane gas was utilized to maintain sedation (C) and the pig was then transferred into the sterile surgical room (D).

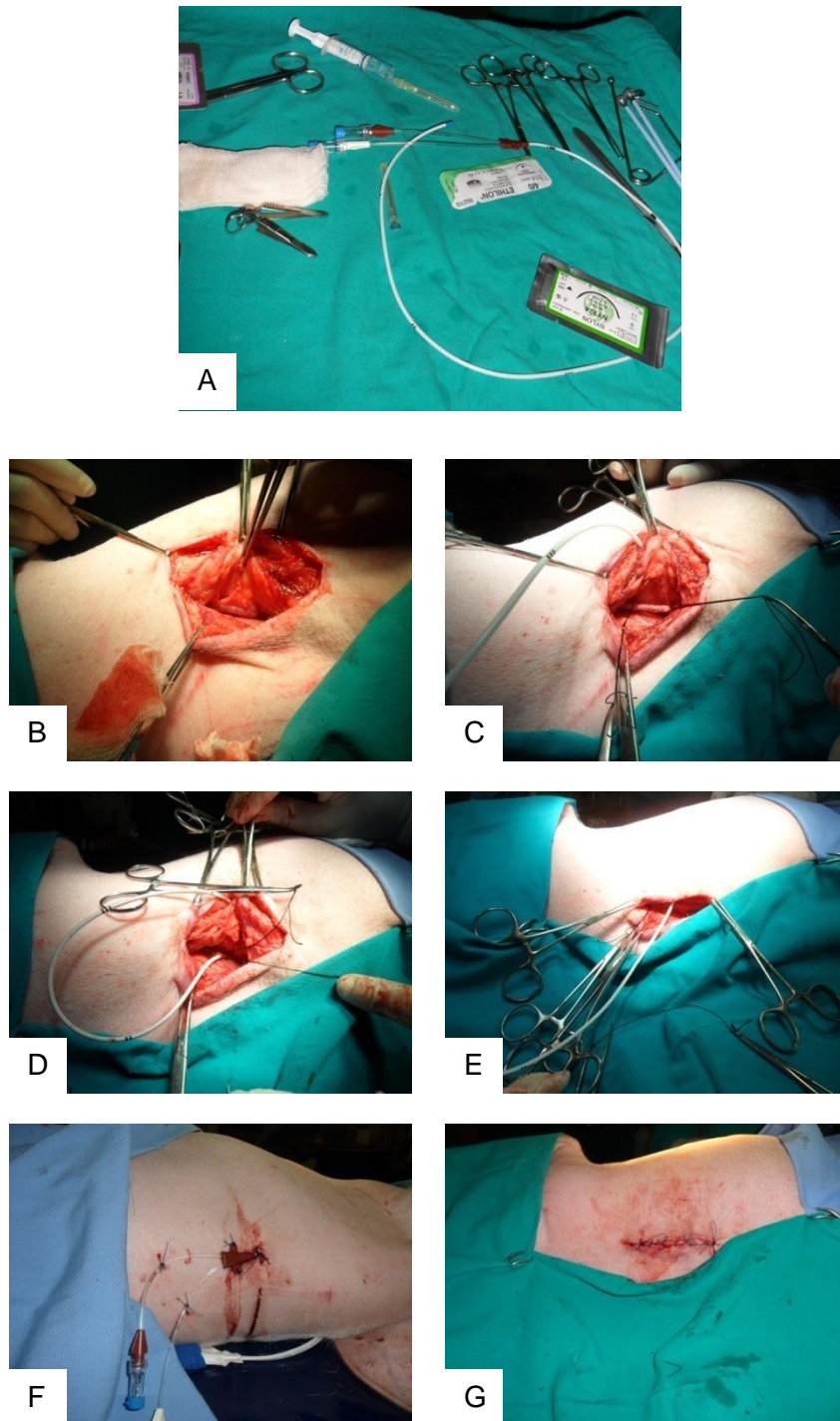


Figure 6.5: Photographic depiction of the insertion of the intrajugular catheter surgery utilised for the pigs in this study. The components and surgical tools utilized for the implantation of the intrajugular catheter is photographed in (A). The first stage of the intrajugular catheter implantation surgery is the blunt dissection along the neck and is photographed in (B). The isolation of the jugular vein in the neck is photographed in (C). The implantation of the intrajugular catheter within the jugular vein is photographed in (D). The intermuscular positioning of the remaining catheter tubing (so that the pig may grow without pulling out the catheter which has been placed within the jugular vein) is photographed in (E). The sutured external ports of the intrajugular catheter to the dorsal aspect of the neck are photographed in (F). The sutured incision along the ventral aspect of the neck is photographed in (G).

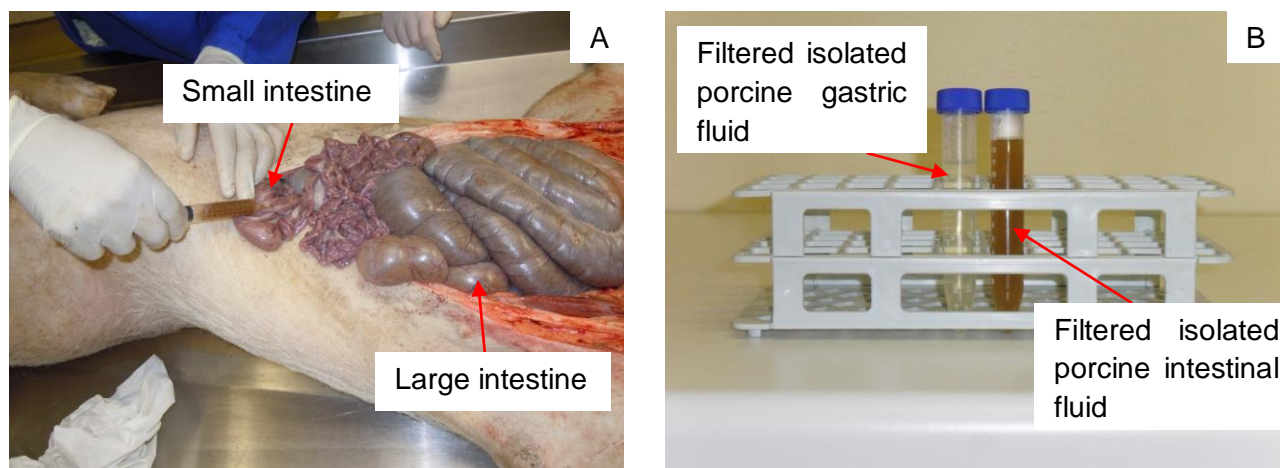


Figure 6.6: Isolation of the gastrointestinal fluid from the porcine model (A) and the filtered porcine gastrointestinal fluid (B).

6.5.3. Dissolution of the salmon calcitonin loaded Oral Ghost Drug Delivery device

The dissolution of salmon calcitonin from the Oral Ghost Drug Delivery device, in FaSSGF-FeSSIF V2 set and isolated porcine gastrointestinal fluid set, was fitted with Winnonlin (Pharsight, Version 5.1) and shown in **Figure 6.7**. The mean dissolution time (MDT) and the slope factor (β) for the Weibull dissolution fitting model at each time point of the dissolution profiling is shown in **Figure 6.7**. The dissolution fitting, MDT and β profiling for the USP pH 1.2-USP pH 6.8, FaSSGF-FaSSIF V2 and FaSSGFc pH 1.5-FaSSFGc pH 7.5 can be reviewed in **Appendix 8**. The Weibull model fitting achieved a high correlation for the FaSSGF-FeSSIF V2 set (0.9989) and isolated gastrointestinal fluid set (0.9964) was achieved. These fitted dissolution models are utilized in the *in vitro-in vivo* correlation for the principle aim of this study that is the determination of the dissolution fluid set that would generate the tightest *in vitro-in vivo* correlation. The utilization of biorelevant dissolution fluids typically does not occur during quality assurance because of the high costs associated with pure bile salt and egg phosphatidylcholine (Vertzoni et al., 2004).

The components of biorelevant dissolution fluid, as discussed previously, has been indicated to represent the intraluminal fluids that exist within the small intestine and the stomach (Dressman et al., 1998). The details that enables biorelevant dissolution fluid to be more representative than USP dissolution fluids will be discussed briefly. The inclusion of osmolality-adjusting agents such as potassium and sodium ions are often included within dissolution fluid to enable an effective electrolyte-water representation of the biological fluid under a specific condition. The electrolyte-water representation of USP simulated intestinal

fluids incorporates potassium ions but the concentrations implemented within this dissolution fluid are too high when compared with the biological fluid.

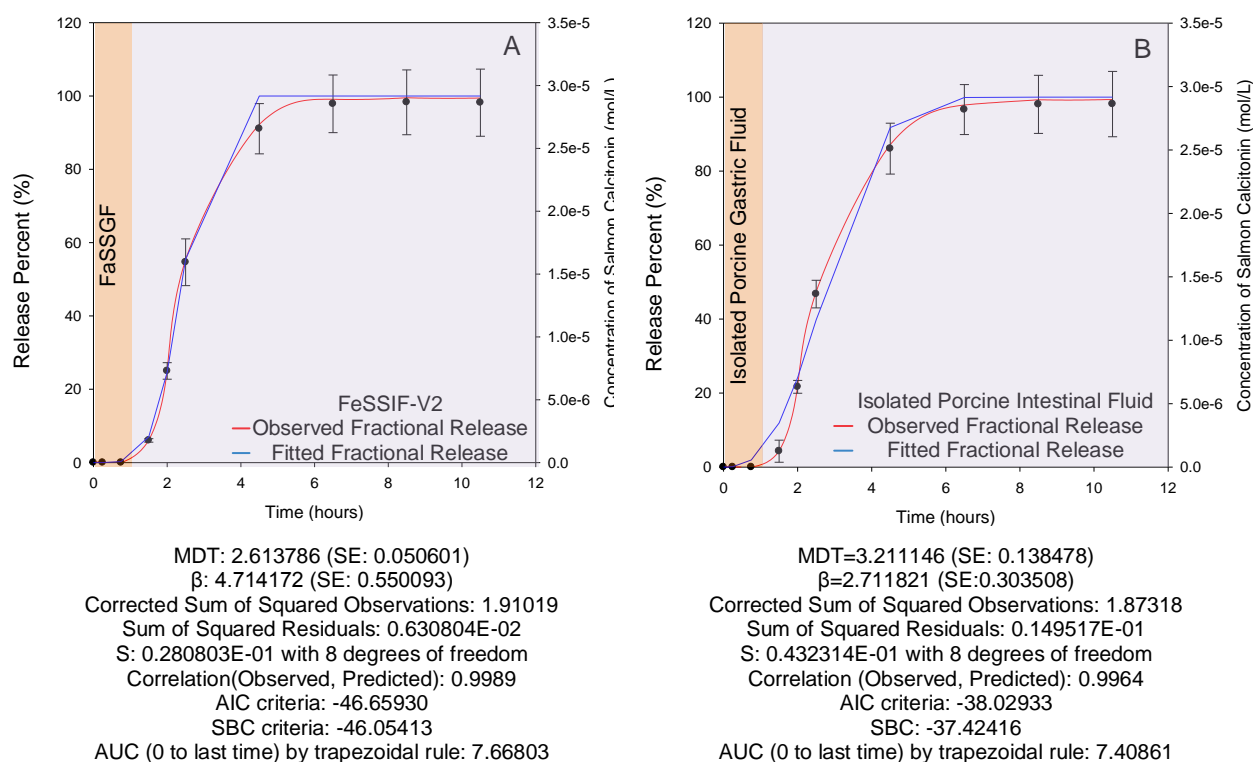


Figure 6.7: The *in vitro* dissolution modeling of salmon calcitonin from the Oral Ghost Drug Delivery device within biorelevant dissolution fluid FaSSGF-FeSSIF V2 set (A) and isolated porcine gastric-isolated intestinal set (B).

The fasted human intestinal fluid has potassium ionic concentration of ~5mM whereas the USP simulated intestinal fluid (pH 6.8) utilizes an ionic concentration of 50mM potassium ions, which is a 10 fold overrepresentation with respect to the biological fluid (Banwell et al., 1971; Lindahl et al., 1997; The USP, 2012; Vertzoni et al., 2004). Additionally, the sodium ionic concentration within the fasted human small intestine has been indicated within the range of 100-140mM whereas the sodium ionic concentration that is currently implemented within USP simulated intestinal fluids is 22mM, which is at least a 4.5 fold underrepresentation with respect to the biological fluid (Banwell et al., 1971; Davenport, 1982; Lindahl et al., 1997; The USP, 2012; Vertzoni et al., 2004).

During the development of the biorelevant human fasted state simulated intestinal fluid, the osmolality-adjusting agent was substituted from potassium to sodium to achieve a higher degree of representation with respect to the biological fluid (Vertzoni et al., 2004). For interests sake, the osmolality and buffer capacity of USP simulated intestinal fluid (pH 6.8) is 114mOsmol/Kg and 18.5mmol/L/pH, respectively (Verzoni et al., 2004). Bicarbonates are

the buffering species utilized within the fasted small intestinal luminal fluids to maintain pH and buffer capacity (Dressman et al., 1998). But the incorporation of biocarbonates as a buffering species within buffers intended for dissolution purposes proved impractical due to a host of introduced variabilities (variable pH, buffer capacity, ionic strength, and osmolality) if carbon dioxide was not continually introduced into the buffer system (Vertzoni et al., 2004). This eventually led to the utilization of maleic acid as the buffering system for biorelevant dissolution fluids, even though this buffer system is not physiologically relevant, it does accurately represent the physiological buffer system within the human fasted intestine and a step up from utilizing phosphate ions as the combined osmolality/buffer system mechanism (Vertzoni et al., 2004; Sandra Klein, 2010). Sodium taurocholate was utilized as the principle representative bile acid (sodium taurocholate is the salt derivative of taurocholic acid) species within the biorelevant dissolution fluids because human bile contains tri-hydroxy-taurine, relatively insensitive to pH/ionic/temperature changes that causes aggregation of taurocholate micelles and was considered highly desirable for extended storage periods or dissolution applications that may occur over a 24 hour period (Hofmann, 1993; Weidmann and Kamel, 2002; Vertzoni et al., 2004).

The last consideration for the development of biorelevant dissolution fluids was the phosphatidylcholine concentration and species type that was representative of the human biliary phospholipid excretion, of which 95% is phosphatidylcholine and 5% is phosphatidylethanolamine (Alvaro et al., 1986; Vertzoni et al., 2004). Egg phosphatidylcholine was selected and included within the biorelevant dissolution fluid formulation because egg phosphatidylcholine contains the phospholipid species that are representative, and at mass concentrations that were very similar, of the human fasted state intestinal fluid (Angelico et al., 1992; Hayes et al., 1992; Hatsushika et al., 1993; Hay et al., 1993; Vertzoni et al., 2004).

6.5.4. Pharmacokinetic analysis of *in vivo* drug concentration profiles

The *in vivo* salmon calcitonin concentration-time profile is shown in **Figure 6.8**. The data from five pigs were utilized only because one pig was removed from the study before dosing could take place. The pig that was removed from the study fell ill and it was deemed ethical to remove this pig from the study. The *in vivo* profile of intramuscular (I.M.) administered salmon calcitonin is the classical single dose profile of a parenteral administered formulation whereby the plasma salmon calcitonin concentration decreases exponentially with respect to time. The plasma salmon calcitonin concentration was undetectable within 60 minutes of administration. Whereas the plasma salmon calcitonin concentration-time profile achieved

from the oral administration of the salmon calcitonin within the Oral Ghost Drug Delivery device had an initial lag time. Thereafter a significant increase of plasma salmon calcitonin concentration increases rapidly but it should be noted that at time point 60 minutes, a significant standard deviation is noted. The large standard deviation at this time point could be due to the high intersubject variable or the slight deviation of the pH profile that exists within the gastrointestinal tract of the porcine model. The orally administered salmon calcitonin demonstrated the classical single dose profile of an orally administered formulation whereby initially there is absorption phase until a peak drug concentration is achieved followed by an exponential decrease in drug concentration.

The AUC and AUMC from time 0 to time infinity was calculated and is the profiles of these parameters against time is shown in **Figure 6.9**. The AUC-time and AUMC-time profiling of salmon calcitonin for the I.M. administration of salmon calcitonin generated, as expected for a 100% bioavailable single dose, an exponential rise to a maximum value. Whereas the AUC and AUMC for the orally administered salmon calcitonin profiles demonstrated a sigmoidal fit which is correlates with the lag time of absorption. The lag time of salmon calcitonin absorption from the Oral Ghost Drug Delivery device is due to the utilization of an enteric coating that is pH responsive to the jejunum-ileum environment and the presence of a pH responsive hydrogel utilized for the physicommechanical application of ejecting the mini-pellet formulations from the device.

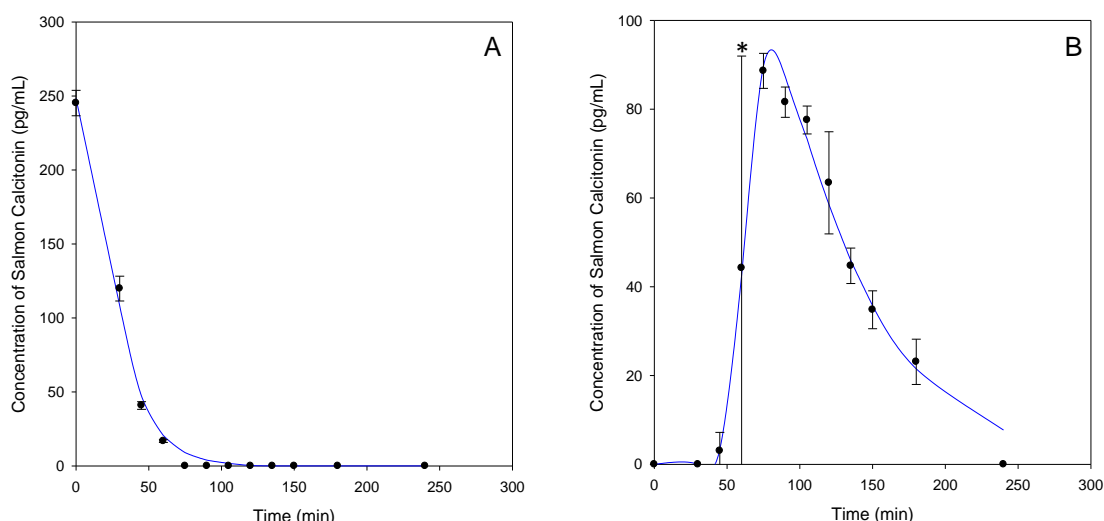


Figure 6.8: The *in vivo* plasma salmon calcitonin concentration-time profile for the intramuscular administration of salmon calcitonin (A) and the orally administered salmon calcitonin-time profile for the Oral Ghost Drug Delivery device (B) [*High variability due to the gastrointestinal transition time from the stomach to the small intestine induces high intersubject variability].

The AUC and AUMC were utilized within the noncompartmental analysis to determine the mean residence time. The AUC and AUMC are both calculated with the trapezoidal rule from time 0 to time infinity. The terminal elimination rate constant is calculated using **Equation 6.7**:

$$AUC_{t_0}^{t_\infty} = \frac{C_{p \text{ last}}}{\lambda} \quad \text{or} \quad AUMC_{t_0}^{t_\infty} = \left(\left(\frac{C_{p \text{ last.t last}}}{\lambda} \right) + \left(\frac{C_{p \text{ last}}}{\lambda^2} \right) \right) \quad (\text{Eqn. 6.7})$$

Where $AUC_{t_0}^{t_\infty}$ is the area under the curve from time 0 to time infinity, $C_{p \text{ last}}$ is the plasma drug concentration that was last measured, λ is the terminal elimination rate constant, $AUMC_{t_0}^{t_\infty}$ is the area under the moment curve from time 0 to time infinity, $C_{p \text{ last.t last}}$ is the plasma drug concentration measured against the last time point.

The AUC and AUMC are thereafter utilized to measure the MRT for an intravenously administered dose, accord to **Equation 6.8**:

$$MRT = \frac{AUMC}{AUC} \quad (\text{Eqn. 6.8})$$

Where MRT is the mean residence time, $AUMC$ is the area under the moment curve, AUC is the area under the curve.

For the extravascularly administrated drug the mean transit time (MTT) is calculated, according to **Equation 6.9**:

$$MTT = MRT + MAT \quad (\text{Eqn. 6.9})$$

Where MTT is the mean transit time, MRT is the mean residence time and MAT is the mean absorption time. The MTT can be calculated according to **Equation 6.10**:

$$MRT = \frac{AUMC}{AUC} \quad (\text{Eqn. 6.10})$$

Where MRT is the mean residence time, $AUMC$ is the area under the moment curve, and AUC is the area under the moment curve.

The MRT for an intravenous administration and the MTT for an extravascular administration is not equivalent because the difference between the MRT and MTT is the MAT for the

extravascular administration of a drug. The MTT and MRT for the intramuscular and oral administration for salmon calcitonin will be estimated in **Section 6.5.4.1**.

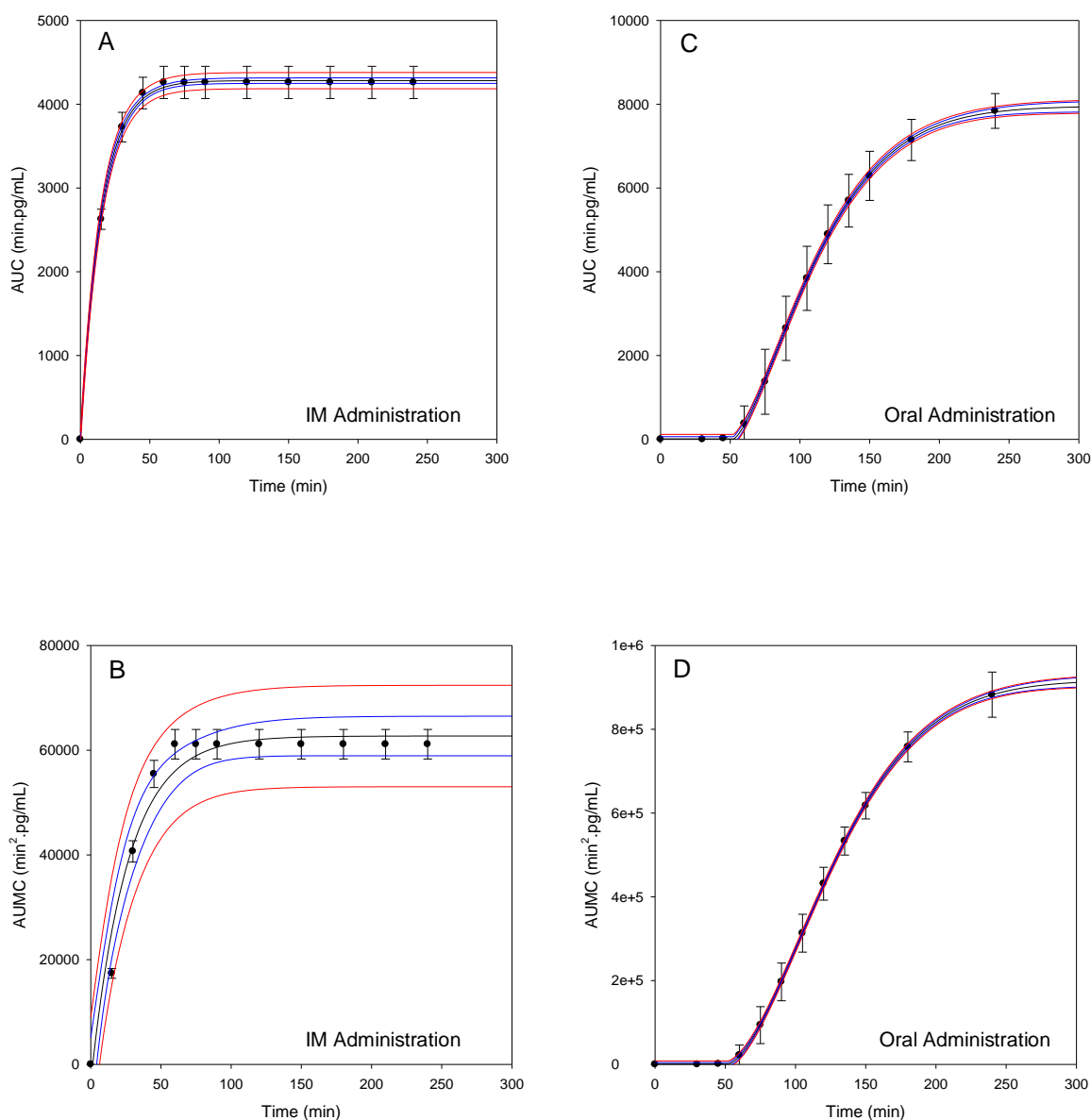


Figure 6.9. The AUC (A) and AUMC (B) derived from *in vivo* plasma salmon calcitonin concentration-time profile for the intramuscular administration of salmon calcitonin. The AUC (C) and AUMC (D) derived from orally administered salmon calcitonin concentration-time profile for the Oral Ghost Drug Delivery device.

6.5.4.1. Noncompartmental analysis

The noncompartmental analysis of the *in vivo* plasma salmon calcitonin concentration-time profiles was determine for the I.M. administered salmon calcitonin and orally administered

salmon calcitonin in the Oral Ghost Drug Delivery device is shown in **Table 6.2**. A high statistical R^2 adjusted for the I.M. administration (0.9819) and oral administration (0.9835), respectively. The maximum concentration (C_{max}) of salmon calcitonin was determined to be 2.6 times higher for the I.M. administered salmon calcitonin than the orally administered salmon calcitonin. The higher C_{max} may induce the noted side effects associated with the I.M. administration of salmon calcitonin (e.g. nausea, vomiting, eye pain) because of high concentrations may enter the toxic range of the therapeutic range whereas the oral formulation has a much lower C_{max}. This may reduce the side effects with the administration of oral salmon calcitonin but also slightly extend the exposure of the drug which may result in better or equivalent treatment therapeutic responses.

Clearly the mean residence time (MRT) will increase between the I.M. and orally administered salmon calcitonin formulation as the oral formulation releases salmon calcitonin within the small intestine. The MRT increased by ~7.9 fold between the oral and IM administration of salmon calcitonin. The MAT for the oral administration of salmon calcitonin was determined to ~116 minutes.

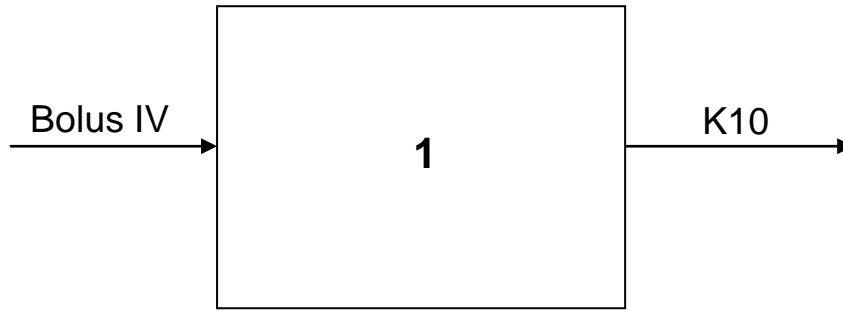
Table 6.2. The noncompartmental pharmacokinetic parameters determined from the intramuscular (I.M.) administration of salmon calcitonin and the oral administration of salmon calcitonin from the Oral Ghost Drug Delivery device.

Parameter	Units	I.M. Average (SD)	Oral Average (SD)
R^2		0.991	0.992
R^2 adjusted		0.982	0.984
Correlation XY		-0.998 (± 0.0016)	-0.998 (± 0.0029)
Number of points for Lamba Z		3	3
Lamba Z	1/min	0.065 (± 0.004)	0.015 (± 0.003)
Lamba Z (lower)	min	15 (± 0)	126 (± 13.416)
Lamba Z (upper)	min	45 (± 0)	180 (± 0)
HL Lamba Z	min	10.723 (± 0.615)	46.77 (± 8.967)
Tlag	min		39 (± 8.216)
Tmax	Min	0 (± 0)	69 (± 8.216)
Cmax	pg/mL	245.242 (± 8.587)	92.028 (± 5.456)
Cmax Dose	pg/mL/mg	7357.328 (257.622)	92.028 (± 5.456)
C0	pg/mL	245.242 (± 8.587)	
Tlast	min	45 (± 0)	180 (± 0)
Clast	pg/mL	16.816 (± 0.936)	23.09 (± 5.097)
AUClast	min.pg/mL	6883.609 (± 188.385)	7145.957 (± 492.204)
AUCall	min.pg/mL	7010.02 (± 192.03)	7838.652 (± 415.011)
AUCINF Observed	min.pg/mL	7149.039 (± 188.476)	8755.055 (± 533.135)
AUCINF Dose Observed	min.pg/mL/mg	214473.311 (5654.342)	8755.055 (± 533.135)
AUC % Extrapolated Observed	%	5.934 (± 0.583)	18.214 (± 6.454)
AUC % Back Extrapolated Observed	%	0 (± 0)	
Vz Observed	L	73.427 (± 10.391)	
CI Observed	mL/min	4662.585 (323.148)	
Vz F Observed	L		8683.581 (± 1224.886)
CI F Observed	mL/min		114551.6 (± 6819.484)
AUCINF predicted	min.pg/mL	7143.134 (± 185.758)	8735.278 (± 541.132)
AUCINF dose predicted	min.pg/mL/mg	214296.152 (5572.796)	8735.278 (± 541.132)
AUC % Extrapolated predicted	%	5.805 (0.685)	18.033 (6.339)
AUC % Back Extrapolated predicted	%	0 (± 0)	
Vz predicted	L	73.487 (± 10.277)	
CI predicted	mL/min	466.439 (318.863)	
Vz F predicted	L		7702.965 (± 1238.49)
Vz F predicted	mL/min		114823.5 (± 6973.627)
AUMClast	min ² .pg/mL	111597.503 (± 2592.511)	757968.9 (± 35626.86)
AUMCINF Observed	min ² .pg/mL	131703.316 (± 3148.244)	1162597 (± 194881.6)
AUMC % Extrapolated Observed	%	22.113 (± 1.922)	33.556 (± 9.767)
AUMCINF predicted	min ² .pg/mL	131256.005 (3156.683)	1157618 (± 193098.2)
AUMC % Extrapolated predicted	%	21.7047 (± 2.264)	33.3009 (± 9.612)
MRTlast	min	13.419 (0.144)	106.3517 (± 6.739)
MRTINF Observed	min	16.215 (± 0.4421)	132.364 (± 16.815)
MRTINF pred	min	16.155 (± 0.487)	132.109 (± 16.644)
Vss Observation	L	85.897 (7.085)	
Vss predicted	L	85.746 (7.282)	

6.5.4.2. Compartmental analysis

The compartmental analysis of salmon calcitonin was conducted to determine if recirculation and exchange of the drug between “grouped tissue types” had affected the derived pharmacokinetics of the noncompartmental analysis utilizing the Gauss-Newton method. The classical one compartment IV bolus, no lag time, 1st order elimination model was applied to the obtained *in vivo* plasma salmon calcitonin concentration-time profile after IM administration of salmon calcitonin, is shown in **Figure 6.10**, and obtained an extremely high correlation of 0.99, as indicated in **Table 6.3**. Additionally, the classical one compartment, 1st order elimination, initial time lag, 1st order elimination model was applied to the obtained *in vivo* plasma salmon calcitonin-time profile after oral administration of the salmon calcitonin loaded Oral Ghost Drug Delivery Device, is shown in **Figure 6.11**, and once again obtained an extremely high correlation of ≥ 0.98 , as indicated in **Table 6.3**.

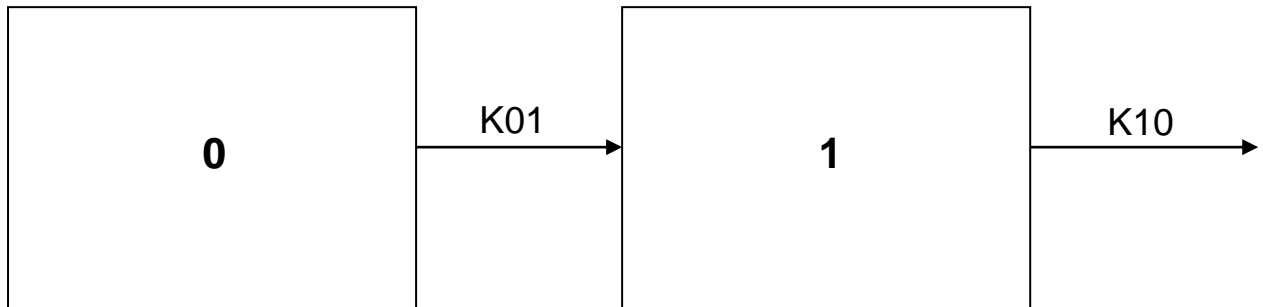
The one compartment model was utilized for both the intramuscular and oral administration of salmon calcitonin whereby the body is defined as a single central compartment. The distribution of salmon calcitonin throughout the central compartment is rapid and equally distributed throughout the tissues, within the limits of observable detection for the intramuscular administration. The one compartment model illustrates that the plasma drug concentration is only primarily influenced parameter by the drug elimination from the system. Thus, the model is simply characterised by the volume of the system, dosage of drug, and plasma drug concentration within the system for the intramuscular administration. The oral administration of salmon calcitonin is slightly different from that of the intramuscular administration. The main difference lies in the inclusion of absorption phase whereby salmon calcitonin was released within the small intestine and distributed in the intraluminal fluids, then underwent the process of absorption. The good correlation of the one compartmental model for the orally administered salmon calcitonin, indicates that once the absorption phase was completed, salmon calcitonin distributed throughout the body in a rapid and uniform manner.



$$C(t) = \left(\frac{D}{V}\right) \times e^{(-K_{10} \times t)}$$

Where: C (t) is concentration with respect to time, D is administered dose, K₁₀ is the rate of elimination, and V is the volume of distribution

Figure 6.10: The one compartment IV-bolus, no lag time, 1st order elimination of intramuscular administration of salmon calcitonin.



$$C(t) = \left(\frac{\left(\frac{D \times K_{01}}{V} \right)}{(K_{01} - K_{10})} \right) \times (e^{(-K_{10} \times t)} - e^{(-K_{01} \times t)})$$

Where: C(t) is concentration with respect to time, D is administered dose, K₀₁ is the rate of absorption, K₁₀ is the rate of elimination and V is the volume of distribution

Figure 6.11: The one compartment 1st order, initial lag time, 1st order elimination of oral administration of salmon calcitonin in the Oral Ghost Drug Delivery device.

Table 6.3. The statistical analysis of the compartmental pharmacokinetic parameters determined from the intramuscular administration of salmon calcitonin and the oral administration of salmon calcitonin from the Oral Ghost Drug Delivery device for each pig utilized.

	Pig 1		Pig 2		Pig 3		Pig 4		Pig 5	
	IV	Oral	IV	Oral	IV	Oral	IV	Oral	IV	Oral
CSS (Obs)	58206	15686	64373	16153	61635	12657	67856	14101	56275	13827
SSR	193.47	330.63	237.12	280.04	659.99	129.8	366.17	281.42	166.51	274.9
S (DF)	4.398 (10)	6.42 (8)	4.869 (10)	5.91 (8)	8.12 (10)	4.02 (8)	6.051 (10)	5.93 (8)	4.08 (10)	5.86 (8)
Corr (Obs, Pred)	0.99	0.98	0.99	0.99	0.99	0.99	0.99	0.99	0.99	0.99
AIC criteria	67.18	77.61	69.62	75.61	81.91	66.39	74.83	75.67	65.38	75.39
SBC criteria	68.15	79.55	70.59	77.55	82.87	68.33	75.80	77.61	66.35	77.33

CSS (Obs): Corrected sum of squared observations

SSR: Sum of squared residuals

S (DF): Standard error of weighted residuals and the Degrees of freedom (observations minus the number of zero weights)

Corr(Obs, Pred): Correlation of observed and predicted

AIC criteria: Akaike information criterion

SBC criteria: Schwarz Bayesian information criterion

*Pig 6 was removed from the study before administration procedures due to illness

The compartmental analysis of plasma salmon calcitonin concentration-time profile that had been I.M. administered generated AUC/AUC_{INF} and Cmax values that were almost identical to that obtained within the noncompartmental analysis, indicating that during the I.M. administration recirculation exchange mechanism did not induce a significant alteration of drug distribution. Whereas the compartmental analysis of salmon calcitonin concentration-time profile, that had been orally administered with the utilization of the Oral Ghost Drug Delivery device, also had a very similar Cmax and AUC/AUC_{INF}, which indicated that recirculation and exchange of salmon calcitonin had not affected the noncompartmental pharmacokinetic analysis of the salmon calcitonin. The noncompartmental pharmacokinetic analysis is based on alibragic analysis that does not take into account recirculation and exchange of a drug compound between tissue layers. Compartmental analysis is based on linear or nonlinear differential equations which takes into account the recirculation and exchange of drug compounds. If the calculated pharmacokinetic parameters form the same plasma concentrations-time points results in slightly different values, recirculation and exchange of the drug compound could account for these slight differing values. The compartmental analysis of salmon calcitonin from the I.M. and oral administration can be reviewed in **Table 6.4**.

Table 6.4. The compartmental pharmacokinetic parameters determined from the intramuscular administration of salmon calcitonin and the oral administration of salmon calcitonin from the Oral Ghost Drug Delivery device.

Parameter	Unit	I.M.	Oral
AUC	min.pg/mL	6853.234 (± 222.6873)	8796.044 (± 406.2473)
AUMC	min ² .pg/mL	191651.972 (± 371.129)	
K10	1/min	0.03576 (± 0.0032)	
K01 Half Life	Min		9.207 (± 0.9141)
K10 Half Life	Min	19.384 (± 1.732)	40.844 (± 1.474)
Clearance	pg/mL	4863.397 (± 412.8633)	
Clearance Fraction	mL/min		113687.477 (± 5619.986)
Tmax	Min		84.611 (± 7.5616)
MRT	Min	27.965 (± 5427.105)	
Vss	L	136.005 (± 4.7592)	
Cmax	pg/mL	245.063 (± 8.8633)	96.763 (± 4.22)

6.5.5. Unit Impulse Response

The generation of a unit impulse response is a pivotal process during the development of an *in vitro-in vivo* correlation because it measures the absorption-time scale between the orally administered formulation and the 100% bioavailable parenteral administration of the drug. The Unit Impulse Response (UIR) is independent of the dissolution of salmon calcitonin from the Oral Ghost Drug Delivery device and is therefore identical for all the *in vitro-in vivo* correlations. The generation for the UIR can be reviewed in **Figure 6.12** whereby the fitted plasma salmon calcitonin concentration-time profile for the oral administration has been overlaid with fitted plasma salmon calcitonin concentration-time points. These points are compared with the 100% bioavailable formulation plasma drug concentration-time profile to generate an input rate-time profile. Thereafter a cumulative input-time profile is generated that represents the “ideal” dissolution profile from the observed plasma salmon calcitonin concentration-time profile that was orally administered.

6.5.6. *In vitro-in vivo* correlation

The *in vitro-in vivo* correlation is generated through the process of deconvolution whereby the “ideal” dissolution profile is generated through the process of convolution and thereafter the *in vitro* dissolution is compared with this “ideal” profile. This correlation also utilized to generate an absorbance scale-time profile (AbsScale-time) and a time scale-time profile (Tscale-time). The fractional dissolution (F_{diss}) and factional absorption (F_{Abs}) is correlated by comparing the *in vitro* dissolution and the *in vivo* absorption with respect to each other at each fitted time point. These parameters are fitted to the *in vitro-in vivo* correlation model, as shown in **Equation 6.11**:

$$F_{abs} = AbsScale \times F_{diss}(Tscale \times T_{vivo}) \quad (\text{Eqn. 6.11})$$

Where F_{ab} is the fractional absorption in the *in vivo* environment, $AbsScale$ is the absorption scale generated through deconvolution, F_{diss} is the fractional dissolution in the *in vitro* environment, $Tscale$ is the time scale generated through deconvolution and T_{vivo} is the time in the *in vivo* environment.

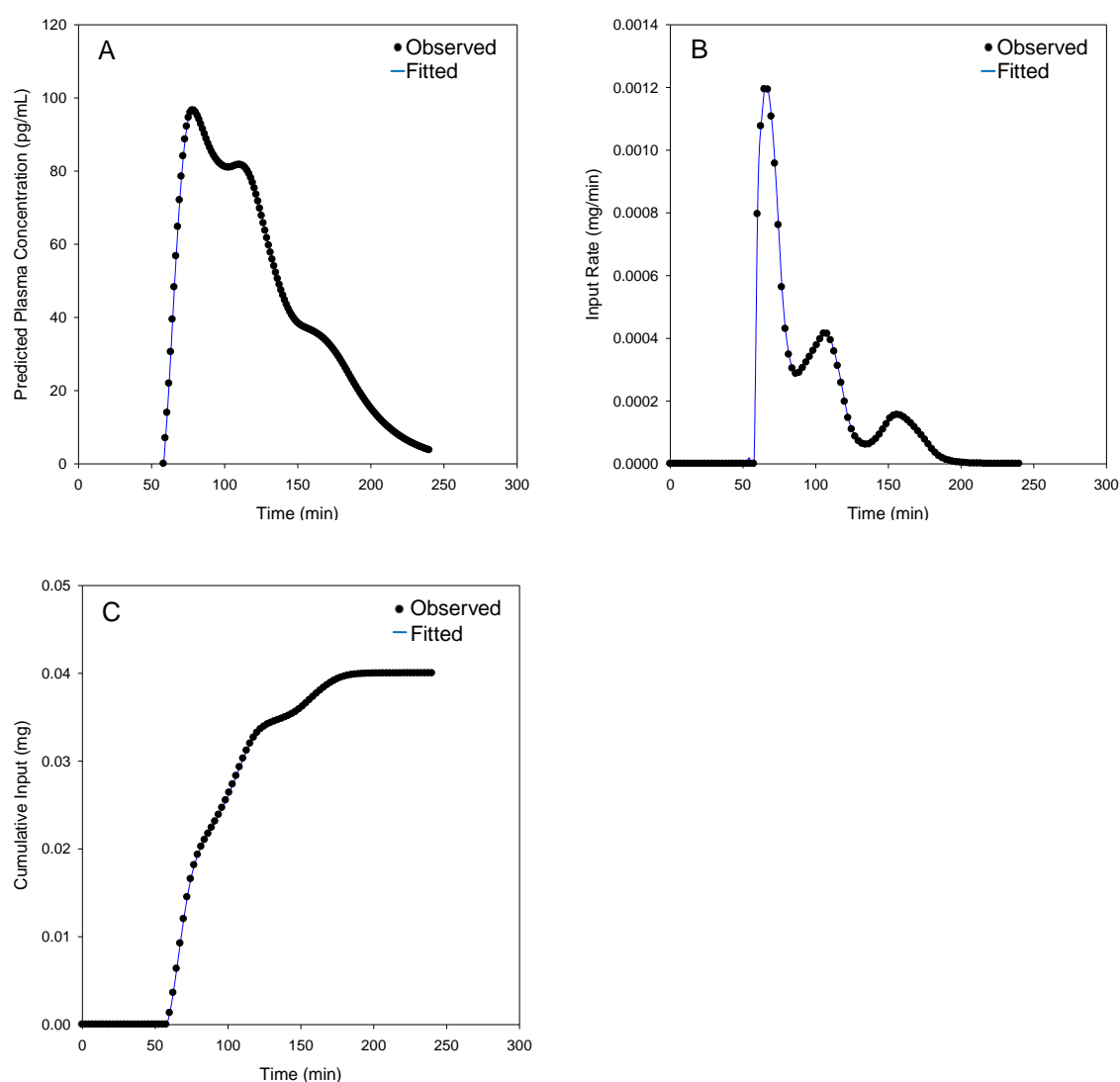
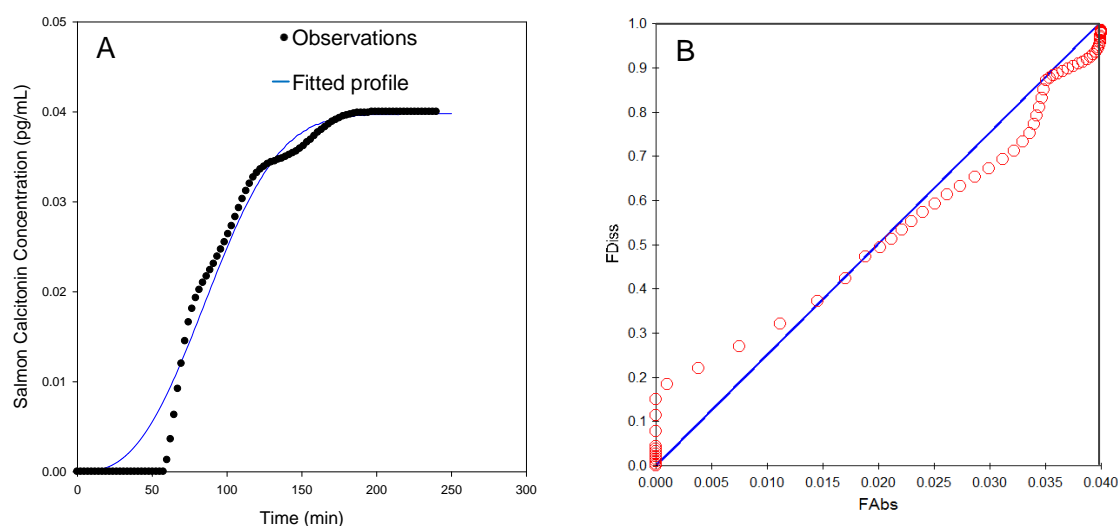


Figure 6.12: The generation of a Unit Impulse Response (UIR) where the fitted plasma salmon calcitonin concentration-time profile (A), the input rate-time profile (B) and the cumulative input-time profile (C) was generated from the 100% bioavailable intramuscular administration of salmon calcitonin and orally administered salmon calcitonin in the Oral Ghost Drug Delivery device utilizing Winnonlin (Pharsight, Version 5.1).

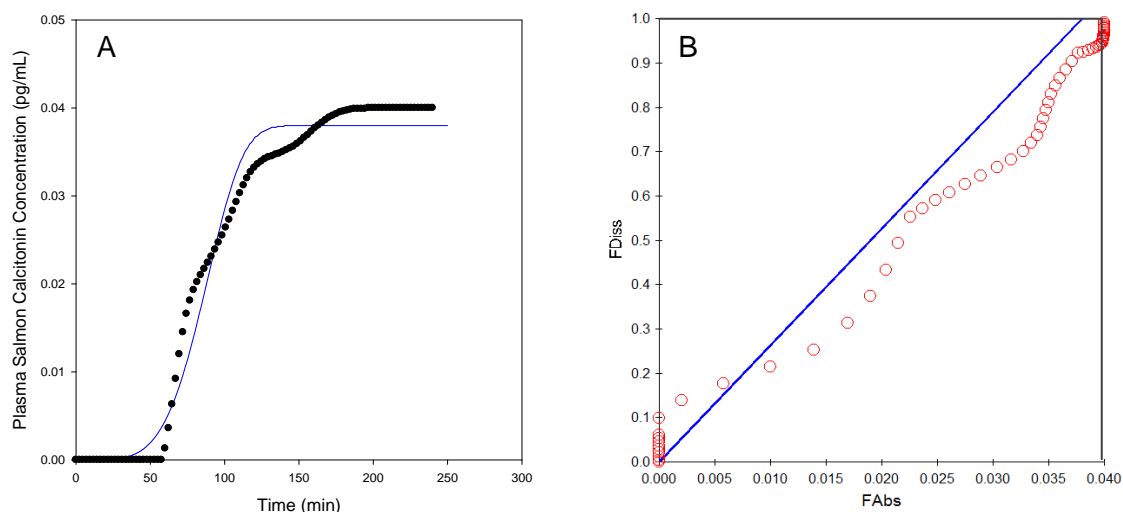
The *in vitro-in vivo* correlation parameters that were generated through the process of convolution and deconvolution that was derived from the isolated porcine gastrointestinal fluid and the FaSSGF-FaSSIF V2 dissolution fluid set is shown in **Figure 6.13** and **Figure 6.14**, respectively. The *in vitro-in vivo* correlation, unlike the generation of the UIR in this study, is dependent of the *in vitro* dissolution environment and will generate unique parameters for the *in vivo-in vitro* correlation model. Therefore an *in vitro-in vivo* correlation had to be conducted for each dissolution fluid set and the unique convolution-deconvolution parameters for USP pH 1.2-USP pH 6.8, FaSSGF-FaSSIF V2 and FaSSGFc pH 1.5-FaSSGFc pH 7.5 can be reviewed in **Appendix 9**.



Statistical Analysis of the Predicted Dissolution Profile

Corrected Sum of Squared Observations: 0.269844E-01
Sum of Squared Residuals: 0.496869E-03
S: 0.224028E-02 with 99 Degrees of freedom
Correlation (Observed, Predicted): 0.9923
AIC: -764.32565
SBC criteria: -759.09541
AUC (0 to last time) by trapezoidal rule: 5.87141

Figure 6.13: The *in vitro-in vivo* correlation generated from the dissolution of salmon calcitonin from the Oral Ghost Drug Delivery device within isolated porcine gastrointestinal fluids (fasted state). The fitted dissolution of salmon calcitonin concentration-time profile (A) and the Fractional Absorbed-Fractional Dissolved profile (B) were generated from the deconvolution of the observed plasma salmon calcitonin concentration-time profile that was obtained in the *in vivo* administration of the Oral Ghost Drug Delivery device. The blue line in (B) represents an ideal correlation and red circles in (B) represent the measured FDis:FAbs correlation.



Statistical Analysis of the Predicted Dissolution Profile

Corrected Sum of Squared Observations: 0.269844E-01
Sum of Squared Residuals: 0.550564E-03
S: 0.235823E-02 with 99 degrees of freedom
Correlation (Observed, Predicted): 0.9897
AIC criteria: -753.96131
SBC: -748.73107
AUC (0 to last time) by trapezoidal rule: 5.87141

Figure 6.14: The *in vitro-in vivo* correlation generated from the dissolution of salmon calcitonin from the Oral Ghost Drug Delivery device within FaSSGF-FaSSIF V2 dissolution set. The fitted dissolution of salmon calcitonin concentration-time profile (A) and the Fractional Absorbed-Fractional Dissolved profile (B) were generated from the deconvolution of the observed plasma salmon calcitonin concentration-time profile that was obtained in the *in vivo* administration of the Oral Ghost Drug Delivery device. The blue line in (B) represents an ideal correlation and red circles in (B) represent the measured FDis:Fabs correlation.

6.5.7. *In vitro-in vivo* correlation validation

The *in vitro-in vivo* correlation validation is the final step whereby the *in vitro-in vivo* correlation utilized to generate *in vivo* noncompartmental pharmacokinetic parameters from a dissolution profile. The *in vivo* noncompartmental pharmacokinetic parameters that were generated from the *in vitro* dissolution of salmon calcitonin from the Oral Ghost Drug Delivery device in isolated porcine gastrointestinal fluids and the FaSSGF-FaSSIF V2 dissolution set is shown in **Table 6.5**. The *in vitro-in vivo* correlation validation derived from the USP pH 1.2-USP pH 6.8, FaSSGF-FaSSIF V2 and FaSSGFc pH 1.5-FaSSIFc pH 6.8 can be reviewed in **Appendix 9**.

The FaSSGF-FaSSIF V2 dissolution set generated the tightest *in vitro-in vivo* correlation from the dissolution media. USP pH dissolution generated the poorest *in vitro-in vivo* correlation with respect to C_{max}, AUC_{last} and MDT_{last}. Interestingly, isolated

gastrointestinal fluids from the porcine model did not generate the tightest correlation but did perform better than the USP dissolution fluid set. There could be many explanations for this occurrence such as destabilization of the bile salt components, variance in pH and ionic concentration during the dissolution profiling. The control of the physicochemical and physicomechanical properties of within designed dissolution fluids are controlled to a far higher degree than can be achieved within a pooled sample of biological fluids. This may translate into a cumulative reduced performance of the isolated gastrointestinal fluids with respect to the biorelevant dissolution fluids.

The observed and fitted plasma salmon calcitonin concentration-time profile that was derived from the *in vitro* dissolution of salmon calcitonin from the Oral Ghost Drug Delivery device can be reviewed in **Figure 6.15**. The unique convolution and deconvolution parameters utilized to generate the fitted *in vivo* salmon calcitonin concentration-time profile can be reviewed in **Figure 6.15**. Additionally, the AUC and AUMC for the observed and fitted plasma salmon calcitonin concentration-time profile can also be reviewed in **Figure 6.15**. The AUC and AUMC profiles are utilized to determine the time periods at which the fitted plasma salmon calcitonin-time profile overestimates or underestimates the plasma concentration of salmon calcitonin with respect to the observed plasma salmon calcitonin-time profile. As indicated previously, the AUC and AUMC are utilized to determine the MRT for both the fitted and observed pharmacokinetic parameters. The *in vitro-in vivo* correlation validation profiles are presented for the dissolution within isolated porcine gastrointestinal fluids is also shown for the FaSSGF-FeSSIF V2 in **Figure 6.16**. Additionally, these profiles are presented for the USP pH 1.2-USP pH 6.8, FaSSGF-FaSSIF V2 and FaSSGFc pH 1.5-FaSSIFc pH 7.5 dissolution fluid sets in **Appendix 9**. According to the fitted error calculations the C_{max} was best correlated by the FaSSGF-FeSSIF V2 dissolution set (followed by isolated porcine gastrointestinal fluid set, FaSSGF-FaSSIF V2 set, USP pH 1.2-USP pH 6.8 set and lastly FaSSGFc pH 1.5-FaSSIFc pH 7.5). The AUC_{last} was best correlated by the FaSSGF-FaSSIF V2 dissolution set (followed by FaSSGF-FeSSIF V2 set, isolated gastrointestinal fluid set, FaSSGFc pH 1.5-FaSSIFc pH 7.5 and lastly USP pH 1.2-USP pH 6.8 set).

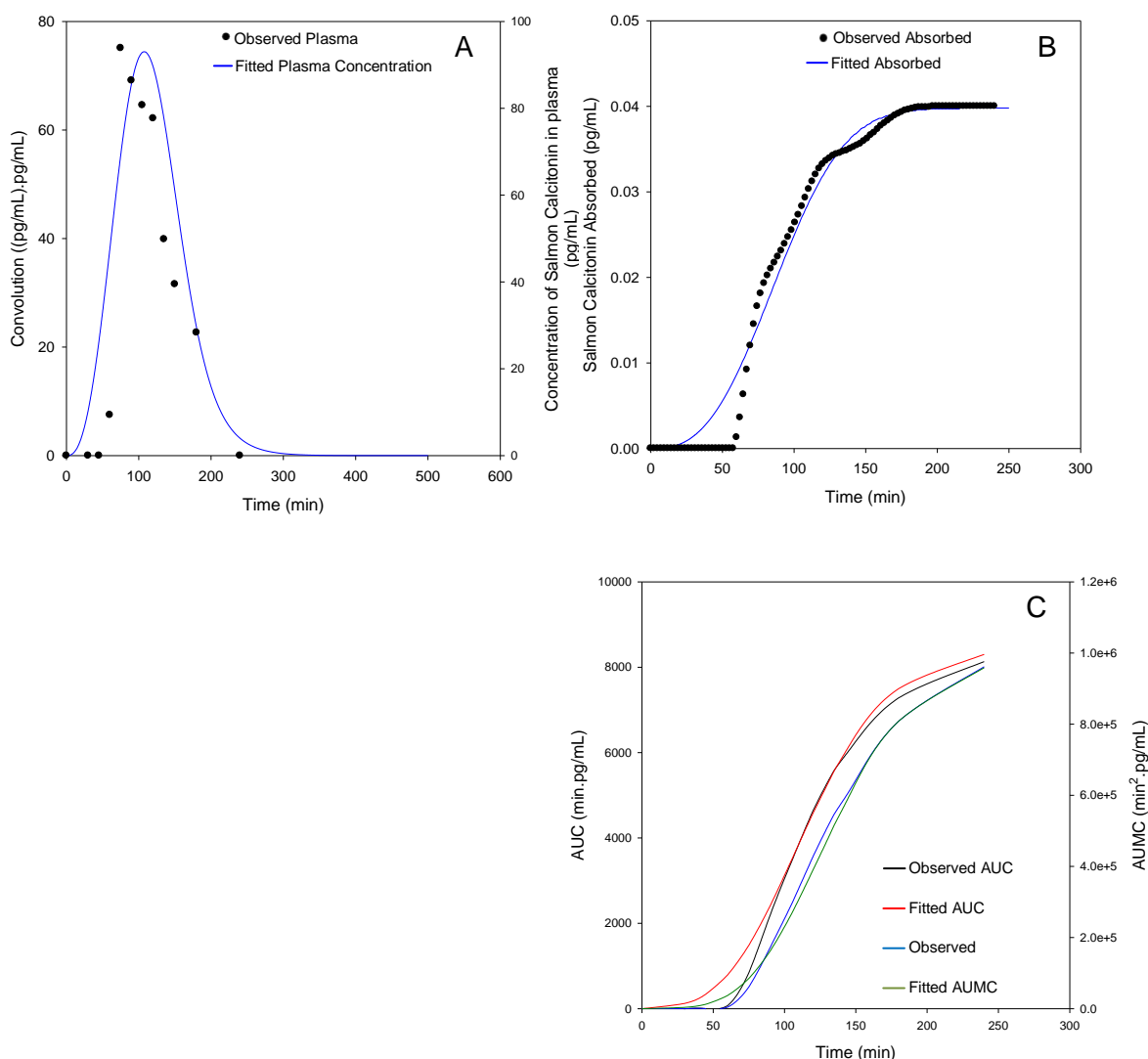


Figure 6.15: The *in vitro-in vivo* correlation validation generated from the dissolution of salmon calcitonin from the Oral Ghost Drug Delivery device within isolated porcine gastrointestinal fluids (fasted state). The fitted and observed *in vivo* plasma salmon calcitonin concentration-time profile (A) and the fitted and observed Fractional Absorbed-time profile (B). Additionally, the observed and fitted AUC-time and the observed and fitted AUMC-time profiles (C) were generated from *in vitro-in vivo* correlation process.

Finally, the MDTlast achieved the highest correlation for the FaSSGF-FaSSIF V2 (followed by FaSSGF-FaSSIF V2 set, isolated porcine gastrointestinal fluid set, FaSSGF pH 1.5-FaSSIFc pH 7.5 and lastly USP pH 1.2-USP pH 6.8). The utilization of biorelevant dissolution fluid should be, as indicated by Verzoni et al., (2004) should be utilized for the most optimized dosage form due to the expense and time required to conduct these dissolution procedures (Verzoni et al., 2004). But the significant benefit is the potential illustration of the physicochemical and physicochemical properties of the drug delivery

device or system that may not have occurred in USP dissolution fluid and to which degree these properties are altered.

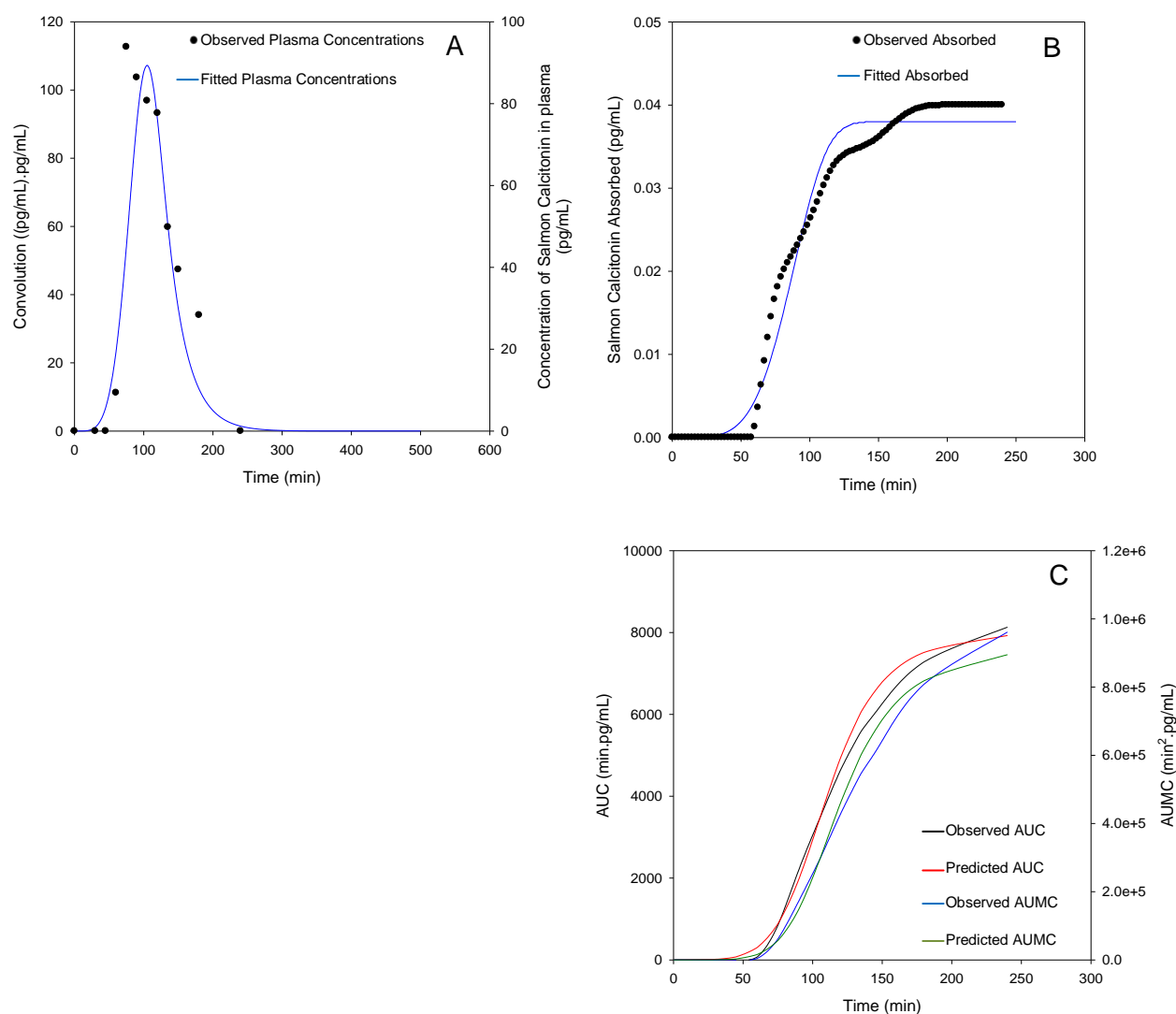


Figure 6.16: The *in vitro-in vivo* correlation validation generated from the dissolution of salmon calcitonin from the Oral Ghost Drug Delivery device within the FaSSGF-FeSSIF V2 set. The fitted and observed *in vivo* plasma salmon calcitonin concentration-time profile (A) and the fitted and observed Fractional Absorbed-time profile (B) were generated. Additionally, the observed and fitted AUC-time and the observed and fitted AUMC-time profiles (C) were generated from *in vitro-in vivo* correlation process.

Table 6.5. The noncompartmental pharmacokinetic parameters determined from the *in vitro-in vivo* correlation generated from the dissolution analysis of salmon calcitonin from the Oral Ghost Drug Delivery device in isolated porcine gastrointestinal fluids (fasted state) and the FaSSGF-FeSSIF V2 dissolution set.

Parameter	Units	<i>In Vivo</i>	Fitted from isolated gastrointestinal fluids (fasted state)	Fitted from FaSSGF-FeSSIF V2 dissolution set
R²		0.9919	0.9947	1
R² adjusted		0.9838	0.9895	1
Correlation (X,Y)		-0.9959	-0.9974	-1
Number points		3	3	4
lambda Z				
Lambda Z	1/min	0.0123	0.0307	0.0356
Lambda Z lower	min	135	150	135
Lambda Z upper	min	180	240	240
Half Life Lambda z	min	56.1973	22.6133	19.4602
Tlag	min	45	0	0
Tmax	min	75	105	105
Cmax	pg/mL	93.8674	74.3135	107.2579
Cmax D	pg/mL/mg	93.8674	74.3135	107.2579
Tlast	min	180	240	240
Clast	pg/mL	28.3373	3.2087	1.4398
AUClast	min*pg/mL	7281.047	8300.917	7926.316
AUCall	min*pg/mL	8131.166	8300.917	7926.316
AUCINF observed	min*pg/mL	9578.508	8405.597	7966.737
AUCINF D observed	min*pg/mL/mg	9578.508	8405.597	7966.737
AUC %Extrap observed	%	23.9856	1.2454	0.5074
Vz F observed	mL	8664317	3881231	3524039
CL F observed	mL/min	104400.4	118968.4	125521.9
AUCINF predicted	min*pg/mL	9556.405	8409.718	7966.856
AUCINF D predicted	min*pg/mL/mg	9556.405	8409.718	7966.856
AUC %Extrap predicted	%	23.8098	1.2938	0.5089
Vz F predicted	mL	8483894	3879329	3523986
CL F predicted	mL/min	104641.9	118910.1	125520
AUMClast	min*min*pg/mL	808258.7	958581	895149
AUMCINF observed	min*min*pg/mL	1408070	987119.4	905985
AUMC %Extrap observed	%	42.5981	2.8911	1.196
AUMCINF predicted	min*min*pg/mL	1402299	988242.9	906016.8
AUMC %Extrap predicted	%	42.3619	3.0015	1.1995
MRTlast	min	111.0086	115.4789	112.9338
MRTINF observed	min	147.003	117.436	113.721
MRTINF predicted	min	146.7392	117.512	113.7233

6.6. Concluding remarks

The *in vivo* oral administration of salmon calcitonin from the Oral Ghost Drug Delivery device in porcine model animal has demonstrated that the oral peptide therapeutic delivery can be achieved with this device. Additionally, the administration of this device was achieved without abdominal surgery within an animal model that has the closest non-primate gastrointestinal physiology with that of humans. The implementation of biorelevant dissolution fluids will become more pertinent as advances in oral drug delivery technology become more sensitive to innate physiological or biochemical properties of the gastrointestinal tract. For instance, the Oral Ghost Drug Delivery device relies on the presence of a steep pH profile within the gastrointestinal tract to achieve the desired targeted release. As demonstrated previously, the Trigger Mechanism that induces the displacement of the mini-pellet entities from the device is sensitive to the ionic concentration of the aqueous environment but may also be sensitive to the presence of bile acids. These physicochemical properties of the aqueous environment will clearly have an impact on the physicomachanical performance of the Trigger Mechanism within the device. These impacting principles can be extended to the optimized mini-pellet formulations. With the significant social pressure for reduced experimental studies conducted on animal models, the evaluation and refinement of *in vitro* procedures that can meet these goals should be aggressively pursued. This study successfully attempts to bridge the gap between *in vitro*-*ex vivo*-*in vivo* experimentation in a way that can be utilized to reduce animal experimentation in future work.

CHAPTER 7

Conclusions and Recommendations

7.1. Conclusions

The development of peptide therapeutics as highly potent, effective and selective treatment options for chronic conditions will continue to grow exponentially with each year. The pharmaceutical industry is investing billions in life science research that ranges from gene therapy and cancer biology to neurological and osteological biochemical profiling. Many of the potential therapeutic agents derived from these research areas are of a biopharmaceutical identity. The development of patient friendly means to administer these compounds should be aggressively pursued to fully maximize the benefits of these therapeutics.

The Oral Ghost Drug Delivery device attempts to overcome many of the issues pertaining to the oral administration of peptide therapeutics. The device attempts to be highly targeted within the gastrointestinal tract due to the extremely high cost of this peptide therapeutics. This is achieved with a combination of a Eudragit® cap and a pH responsive hydrogel. The second change is the localization of the solid dosage form within the small intestine to facilitate an effective drug concentration that promotes the absorption of the peptide therapeutic. This is achieved with a mini-pellet formulation that incorporated trimethyl chitosan, a known mucoadhesive, excipient. The absorption of the peptide therapeutic is an additional challenge that was overcome with a dual action approach. The inclusion of EDTA within the *in situ* hot melt dispersion mini-pellet and within the drug carrier mini-pellet was aimed at reducing the monovalent and divalent ionic concentration load within a localized environment. This has been suggested to induce the opening of tight junctions located within the epidermal layer of the small intestine. Additionally, the inclusion of EDTA has been indicated to reduce the effectiveness of intestinally located peptidase enzymes. A reduction in the peptidase enzyme activity increases the effective amount of active peptide therapeutic for absorption. Thus, the promotion of the peptide therapeutic transport via the paracellular transport mechanism and the reduction in peptidase enzyme activity increase the plasma drug concentration of the peptide therapeutic. Trimethyl chitosan has also been indicated to increase the paracellular transport of peptide therapeutics by opening the tight junctions which can augment the effect of EDTA within a localized environment. All of these mechanisms have been unified and incorporated within one device to ensure that a peptide therapeutic can achieve successful absorption within the gastrointestinal tract.

The administration frequency of the OGDD device will be highly dependent of the disease state of the patient, the peptide therapeutic that is being administered and the achievable pharmacokinetic parameters through customization of the OGDD device. The customization of the OGDD device can be achieved in two unique processes whereby the pH responsive hydrogel can be synthesized to swell faster or be more sensitive to a pH profile and the Avicel[®]-EDTA-mPEG *in situ* hot melt dispersion can be modified to administer greater amounts of chelatory compounds within the localized environment. Additionally, the length and width of the non-responsive shell component can be easily adjustable to the needs of a specific application.

The oral administration of salmon calcitonin from the Oral Ghost Drug Delivery device was successfully achieved with a C_{max} of ~94pg/mL, AUC_{last} of ~7280min.pg/mL and MTD_{last} of 111min. The *in vitro-in vivo* correlation of salmon calcitonin was achieved at the highest degree when the FaSSGF-FaSSIF V2 dissolution set. This was a significantly better improvement over the utilization of USP pH 1.2-USP pH 6.8 dissolution set.

7.2. Recommendations

The *in vivo* C_{max} is much lower than the parentally administered salmon calcitonin of ~245pg/mL which can be overcome by increasing the loaded salmon calcitonin dosage in the Oral Ghost Drug Delivery device. The utilization of biorelevant dissolution fluid to generate tighter *in vitro-in vivo* correlations when analysing novel or innovative drug delivery systems should be pursued to increase the predictability of the drug delivery system within the *in vivo* environment. Additionally, it should be noted that there is substantial differences within the gastrointestinal environment across animal species and these differences should be characterized as fully as possible, in order to reduce the usage of animals for *in vivo* analysis.

An *in situ* hot melt dispersion of a thermally stable drug within mPEG 2000 is a novel method for obtaining an easy to prepare homogeneously distributed dosage form. A metal chelatory compound was utilized in this work because a non-specific metal chelatory can enhance the paracellular transport of a peptide therapeutic and reduce the activity of intraluminal small intestine peptidases. A variety of metal chelators, that are thermostable and chelate specific ions could be utilized instead of EDTA to achieve a more specific inhibition of a peptidase subspecies. Or specific chelatory compound that has demonstrated significant potential to open tight junctions can also be included within the hot melt dispersion. A hot melt

dispersion is highly desirable within the industrial setting because a more homogenous distribution of a drug entity can be achieved and a reduction in solvents are employed. An extension of this novel approach could be the inclusion of a specific thermal stable compound, that is not chelatory in nature, which can reduce the presystemic metabolism of the peptide therapeutic, could offer significant benefit to this application. The advantage of including Avicel® with these formulations is the enhancement of the physicomachanical properties of the *in situ* hot melt dispersion as often a polymeric material that can undergo melting in a stable manner, does not produce a solid dosage form that can be resilience to handling or transportation. The physicomachanical influence of including alternative chelatory or peptidase inhibitory compounds should be investigated before applying the approaches because the alternative API could alter the physicomachanical properties significantly. Lastly, alternative polymeric materials that can undergo stable melting should be investigated that may enhance the dissolution of the chelatory compound within the small intestinal tract in some beneficial manner. This could either be a more localized dissolution of the chelatory compound or a more advantageous dissolution profile of the chelatory compound.

The inclusion of trimethyl chitosan within the OGDD device did convey significant advantages to the oral absorption of the peptide therapeutic. An extension of this approach could be the further modification of trimethyl chitosan to include a covalently bonded specific chelatory compound that has the potential to reduce the activity of a peptidase subspecies that is particularly active against the administered peptide therapeutic entity. This would increase the effective amount of active peptide therapeutic within a localized environment. If this approach is pursued, the formulation scientist should be very vigilant that the significant benefits of this polymeric material are not lost during the modification reaction. The peptide therapeutic could also be entrapped within nanosized particles and then suspended within a matrix of trimethyl chitosan. The nanonized particles could increase the absorption of the peptide therapeutic within the *in vivo* environment and enhance the half life of the peptide therapeutic within the systemic circulation, hence augmenting the pharmacological properties of the peptide therapeutic. The generation of an solid oral dosage form that utilizes nanonized particle may cause the nanonized particles to be disrupted and facilitate a limited advantage. Additionally, the greater the processing that a peptide therapeutic is subjected to, the greater probability that the peptide therapeutic will loss activity due to the highly sensitive nature of these compounds.

Lastly, the inclusion of an additional small molecular weight drug within the swellable trigger mechanism of the OGDD device could be utilized to enhance the treatment of a chronic

condition or enhance the treatment of comorbidity. The main issue of this approach is ensuring that the inclusion of a small molecular weight drug does not induce significant or unexpected physicochemical alterations to the swellable trigger mechanism. Altered physicochemical properties of the swellable trigger mechanism could cause the device to fail in its primary purpose of delivering a peptide therapeutic within a targeted location in the small intestine. Additionally, the small molecular weight drug should not cause a drug-drug interaction or negatively influence the abilities of the chelatory compound. Often, small molecular weight drugs are stabilized as a salt variant which could increase the availability of monovalent or divalent metal ions within the targeted drug location. This may cause a reduced chelatory potential and by causal effect allow the peptidase enzymes to retain full activity or reduce the paracellular transport rate of the peptide therapeutic within the systemic circulation. These issues could be overcome with the utilization of specific chelatory compounds or by exploiting a small molecular weight drug that has not been stabilized with a metal ion.

7.3. Future Outlook

The OGDD device is a significant step to administering peptide therapeutics to the oral route without utilizing intra-abdominal surgery during *in vivo* studies. With further refinement, the device could easily be translated into human subjects after careful examination of any potential toxicity and significant clinical trial data. The device offers the patient an alternative to parenteral administration that may benefit the therapeutic outcome of chronic conditions or acute conditions (e.g. administration of vaccines). The OGDD device has a high customizable potential that could be augmented to achieve the successful oral administration of many biopharmaceuticals within targeted locations in the gastrointestinal tract. This will become increasingly important as greater quantities and variants of biopharmaceuticals become clinically certified for treatment of human conditions.

REFERENCES

- Adnadjevic B, Tasic G, Jovanovic J. Kinetic of non-isothermal dehydration of equilibrium swollen poly(acrylic acid-co-methacrylic acid) hydrogel. *Thermochim Acta*. 2011, 512:157-162.
- Agyei D, Danquah MK. Industrial-scale manufacturing of pharmaceutical-grade bioactive peptides. *Biotechnol Adv*. 2001, 29:272-277.
- Ahuja M, Kumar A, Yadav P, Singh K. Mimosa pudica seed mucilage: Isolation; characterization and evaluation as table disintegrant and binder. *Int J Bio Macromol*. 2013, 57:105-110.
- Ajji Z, Othman I, Rosiak JM. Production of hydrogel wound dressing using gamma radiation. *Nucl Instrum Methods Phys Res: Sect B*. 2005, 229:375-380.
- Amasheh S, Meiri N, Gitter AH, Schöneberg T, Mankertz J, ASchulzke JH, Fromm M. Claudin-2 expression induces cation selective channels in tight junctions of epithelial cells. *J Cell Sci*. 2002, 115:4969-4976.
- Amidi M, Nastrobattista E, Jiskoot W, Hennink WE. Chitosan-based delivery systems for protein therapeutics and antigens. *Adv Drug Deliv Rev*. 2010, 62:59-82.
- Amidi M, Romeijn SG, Borchard G, Junginger HE, Hennink WE, Jiskoot W. Preparation and characterization of protein loaded N-trimethyl chitosan nanoparticles as nasal delivery system. *J Control Release*. 2006, 111:107-116.
- Ammar HO, Salama HA, El-Nahhas SA, Elmotasem H. Design and evaluation of chitosan films for transdermal delivery of glimepiride. *Curr Drug Deli*. 2008, 5:290-298.
- Andreeva AY, Krause E, Müller E-C, Blasig IE, Utepbergenov DI. Protein kinase C regulates the phosphorylation and cellular localization of occludin. *J Biol Chem*. 2001, 276:38480-38486.
- Andrews GP, Abidiak OA, Jones DS. Physicochemical characterization of hot melt extruded bicalutamide-polyvinyl pyrrolidone solid dispersion. *J Pharm Sci*. 2010, 99:1322-1335.
- Angelico M, Corrandini SG, Masella R, Alvaro D, Cantafora A, Capocaccia L. Molecular composition of biliary phosphatidylcholines, as related to cholesterol saturation, transport and nucleation in human gallbladder bile. *J Hepatol*. 1992, 15:59-66.
- Arndt M, Chokshi H, Tang K, Parrott NJ, Peppas C, Dressman JB. Dissolution media simulating the proximal canine gastrointestinal tract in the fasted state. *Euro J Pharm Biopharm*. 2013, 84: 633-641.
- Arnon SS, Schechter R, Inglesby TV, Henderson DA, Bartlett JG, Ascher MS, Eitzen E, Fine AD, Hauer J, Layton M, Lillibridge S, Osterholm MT, O'Toole T, Parker G, Perl TM, Russell PK, Swardlow DL, Tonat K. Botulinum toxin as a biological weapon: Medical and public health management. *JAMA*. 2001, 28:1059-1070.

- Atyabi F, Maizoob S, Dorkoosh F, Sayyah M, Ponchel G. The impact of trimethyl chitosan on *in vitro* mucoadhesive properties of pectinate beads along different sections of gastrointestinal tract. *Drug Dev Ind Pharm*. 2007, 33:291-300
- Aungst BJ. Intestinal permeation enhancers. *J Pharm Sci*. 2000, 89:429-442.
- Balda MS, Flores-Maldonado C, Cereijido M, Matter K. Multiple domains of occludin are involved in regulation of paracellular permeability. *J Cell Biochem*. 2000, 78:85-96.
- Balda MS, Whitney JA, Flores C, González S, Cereijido M, Matter K. Functional dissociation of paracellular permeability and transepithelial electrical resistance and disruption of the apical basolateral intramembrane diffusion barrier by expression of a mutant tight junction membrane protein. *J Cell Biol*. 1996, 134:1031-1049.
- Baldrick P. The safety of chitosan as a pharmaceutical excipient. *Regul Toxicol Pharmacol*. 2010, 56:290-299.
- Banwell JG, Gorbach SL, Pierce NF, Mitra R, Mondal A. Acute undifferentiated human diarrhea in the tropics. II. Alterations in intestinal fluid and electrolyte movements. *J Clin Invest*. 1971, 50:890-900.
- Benet LZ, Broccatelli F, Oprea TI. BDDCS applied to over 900 drugs. *AAPS J*. 2010, 13:519-547.
- Bennett RG, Heimann DG, Hamel FG. Degradation of relaxin family peptides by insulin-degrading enzyme. *Ann NY Acad Sci*. 2009, 1160:38-41.
- Bergman E, Lundahl A, Fidblom P, Hedeland M, Bondesson U, Knutson L, Lennernäs H. Enterohepatic disposition of rosuvastatin in pigs and the impact of concomitant dosing with cyclosporine and genfibrozil. *Drug Metab Dispos*. 2009, 37:2349-2358.
- Bernkop-Schnürch A, Krajicek ME. Mucoadhesive polymers as platforms for peroral peptide delivery and absorption: Synthesis and evaluation of different chitosan-EDTA conjugates. *J Control Release*. 1998, 50:215-223.
- Bernkop-Schnürch A, Paikl C, Valenta C. Novel bioadhesive chitosan-EDTA conjugate protects leucine enkephalin from degradation by aminopeptidase N. *Pharmaceut Res*. 1997, 14:917-922.
- Boonyo W, Junginger HE, Waranuch N, Polnok A, Pitaksuteepong T. Chitosan and trimethyl chitosan (TMC) as adjuvants for inducing immune response in mice following nasal administration. *J Control Release*. 2007, 121:168-175.
- Boot RG, Blommaert FC, Swart E, van der Ghauharali-Vlugt K, Bijl N, Moe C, Place A, Aerts JMFG. Identification of a novel acidic mammalian chitinase distinct from chitotriosidase. *J Biol Chem*. 2001, 276:6770-6778.
- Boothby LA, Doering PL, Kipersztok S. Bioidentical hormone therapy: a review. *Menopause*. 2004, 11:356-367.

- Brandner JM. Tight junctions and tight junction proteins in mammalian epidermis. *Eur J Pharm Biopharm.* 2009, 72:289-294.
- Bravo-Osuna I, Millotti G, Vauthier C, Ponchel G. *In vitro* evaluation of calcium binding capacity of chitosan and thiolated chitosan poly(isobutyl cyanoacrylate) core-shell nanoparticles. *Int J Pharm.* 2007, 338:284-290.
- Bray BL. Large-scale manufacture of peptide therapeutics by chemical synthesis. *Nat Rev Drug Discov.* 2003, 2:579-593.
- Breitenback J. Melt extrusion: from process to drug delivery technology. *Euro J Pharm Biopharm.* 2002, 54:107-117.
- Brenda SA, Jimenez K, Manzo RH, Olivera ME. Solubility behaviour and biopharmaceutical classification of novel high-solubility ciprofloxacin and norfloxacin pharmaceutical derivatives. *Int J Pharm.* 2009, 371:106-113.
- Brin MF, Lew MF, Adler CH, Comella CL, Factor SA, Jankovic J, O'Brien C, Murray JJ, Wallace JD, Willmer-Hulme A, Koller M. Safety and efficacy of NeuroBloc (botulinum toxin type B) in type A-resistant cervical dystonia. *Neurology.* 1999, 22:1431-1438.
- Britto D and Campana-Filho SP. A kinetic study on the thermal degradation of *N,N,N*-trimethylchitosan. *Polym Degrad Stabil.* 2004, 84:353-361.
- Brunet B, Doucet C, Venisse N, Hauet T, Hébrand W, Papet Y, Mauco G, Mura P. Validation of Large White Pig as an animal model for the study of cannabinoids metabolism: Application to the study of THC distribution in tissues. *Forensic Sci Int.* 2006, 161:169-174.
- Cafaggi S, Russo E, Stefani R, Parodi B, Caviglioli G, Sillo G, Bisio A, Aiello C, Viale M. Preparation, characterisation, and preliminary antitumor activity evaluation of a novel nanoparticulate system based on cisplatin-hyaluronate complex and *N*-trimethyl chitosan. *Invest New Drug.* 2011, 29:443-455.
- Calija B, Cekić N, Savić S, Daniels R, Marković B, Milić J. pH-sensitive microparticles for oral drug delivery based on alginate/oligochitosan/Eudragit® L100-55 "sandwich" polyelectrolyte complex. *Colloids Surf B.* 2013, 110:395-402.
- Campion JM, Maricic MJ. Osteoporosis in men. *Am Fam Physician.* 2003, 67:1521-1526.
- Cevher E, Sensoy D, Taha MAM, Abramam A. Effect of thiolated polymers to textural and mucoadhesive properties of vaginal gel formulations preparation with polycarbophil and chitosan. *AAPS PharmSciTech.* 2008, 9:953-965.
- Chang S-S, Clair B, Ruelle J, Beauchêne J, Di Renzo F, Quignard F, Zhao G-J, Yamamoto H, Gril J. Mesoporosity as a new parameter for understanding tension stress generation in trees. *J Exp Bot.* 2009, 60:3023-3030.

- Chaudhury A and Das S. Recent advancement of chitosan-based nanoparticles for oral controlled delivery of insulin and other therapeutic agents. *AAPS PharmSciTech*. 2011, 12:10-20.
- Chem F, Zhang ZR, Huang Y. Evaluation and modification of *N*-trimethyl chitosan chloride nanoparticles as protein carriers. *Int J Pharm*. 2007, 336:166-173.
- Chem Y-H, Lu Q, Goodenough DA, Jeanson B. Nonreceptor tyrosine kinase c-Yes interacts with occludin during tight junction formation in canine kidney epithelial cells. *Mol Biol Cell*. 2002, 13:1227-1237.
- Chen EYT, Yang N, Quinton PM. A new role for bicarbonate in mucus formation. *Am J Physiol Lung Cell Mol Physiol*. 2010, 299:L542-L549.
- Chen F, Zhang Z-R, Yuan F, Qin X, Wang M, Huang Y. *In vitro* and *in vivo* study of *N*-trimethyl chitosan nanoparticles for oral protein delivery. *Int J Pharm*. 2008, 249:226-233.
- Chen J, Liu M, Chen S. Synthesis and characterization of thermo- and pH-sensitive kappa-carrageenan-g-poly(methacrylic acid)/poly(*N,N*-diethylacrylamide) semi-IPN hydrogel. *Mater Chemis Phys* 2009, 115:339-346.
- Chen M-C, Mi F-L, Liao Z-X, Hsiao C-W, Sonaje K, Chung M-F, Hsu L-W, Sung H-W. Recent advances in chitosan-based nanoparticles for oral delivery of macromolecules. *Adv Drug Delivery Rev*. 2013, 65:865-879.
- Cheng W and Lim L-Y. Comparison of reversible and non reversible aqueous-soluble lipidized conjugates of Salmon calcitonin. *Mol Pharm*. 2008, 5:610-621.
- Cheng W and Lim L-Y. Design, synthesis, characterisation and *in vivo* activity of a novel salmon calcitonin conjugate containing a novel PEG-lipid moiety. *J Pharm Pharmacol*. 2010, 62:296-304.
- Chervenak J. Bioidentical hormones for maturing woman. *Maturitas*. 2009, 64:86-89.
- Chuang EY, Lin KJ, Su FY, Mi FL, Maiti B, Chen CT, Wev SP, Yen TC, Juang JH, Sung HW. Noninvasive imaging oral absorption of insulin delivered by nanoparticles and its stimulated glucose utilization in controlling postprandial hyperglycemia during OGTT in diabetic rats. *J Control Release*. 2013, DOI: 10.1016/j.conrel.2013.05.006.
- Chun IK, Lee KM, Lee KE, Gwak HS. Effects of bile salts on gastrointestinal absorption of pravastatin. *J Pharm Sci*. 2012, 101:2281-2287.
- Citi S. Protein kinase inhibitors prevent junction dissociation induced by low extracellular calcium in MDCK epithelial cells. *J Cell Biol*. 1992, 117:169-178.
- Cone RA. Barrier properties of mucus. *Adv Drug Deliv Rev*. 2009, 61:75-85.
- Copeman M, Matuz J, Leonard AJ, Pearson JP, Dettmar PW, Allen A. The gastroduodenal mucus barrier and its role in protection against luminal pepsin: The effect of 16,16 dimethyl prostaglandin E₂, carbopol-polyacrylate, sucralfate and bismuth subsalicylate. *J Gastroenterol Hepatol*. 1994, 9:S55-S59.

- Cordenonsi M, D'Atri F, Hammar E, Parry DA, Kendrick-Jones J, Shore D, Citi S. Cingulin contains globular and coiled-coil domains and interacts with ZO-1, ZO-2, ZO-3, and myosin. *J Cell Biol.* 1999, 147:1569-1582.
- Cryan S-A, Sivadas N, Garcia-Contreras L. *In vivo* animal models for drug delivery across the lung mucosal barrier. *Adv Drug Rev.* 2007, 59:1133-1151.
- Cui F, Qian F, Zhao X, Yin L, Tang C, Yin C. Preparation, characterization and oral delivery of insulin loaded carboxylated chitosan grafted poly(methyl methacrylate) nanoparticles. *Biomaterials.* 2009, 10:1253-1258.
- Custodia JM, Wu CY, Benet LZ. Predicating drug disposition, absorption/elimination/transporter interplay and the role of food on drug absorption. *Adv. Drug Delivery Rev.* 2008, 60:717-733.
- Dadsetan M, Liu Z, Pumberger M, Giraldo CV, Ruesink T. A stimuli-responsive hydrogel for doxorubicin delivery. *Biomaterials.* 2010, 31:8051-8062.
- Davenport HW. *Physiology of the digestive tract*, 5th edition. Year Book Medical Publishers Inc., London. 1982; p201.
- Davis SS, Illum L, Hinchcliffe M. Gastrointestinal transit of dosage forms in the pig. *J Pharm Pharmacol.* 2001, 53:33-39.
- de Britto D, Filho SPC, Assis OBG. Role of alkyl moiety and counter ions on the thermal stability of chitosan derivatives. *J Appl Polym Sci.* 2011, 121:815-822.
- de Sousa FB, Oliveria MF, Lula IS, Sansiviero MTC, Cotés ME, Sinisterra RD. Study of inclusion compound in solution involving tetracycline and β -cyclodextrin by FTIR-ATR. *Vib Spectrosc.* 2008, 46:57-62.
- Decaffmeyer M, Thomas A, Brasser R. Les médicaments peptidiques: mythe ou réalité? *Biotechnol Agron Soc Environ.* 2008, 12:255-263.
- Degim T and Celebi N. Controlled delivery of peptides and proteins. *Curr Pharm Des.* 2007, 13:99-177.
- Deli MA. Potential use of tight junction modulators to reversibly open membranous barriers and improve drug delivery. *Biochim Biophys Acta.* 2009, 1788:892-910.
- Di Colo G, Burgalassi S, Zambito Y, Monti D, Chetoni P. Effects of different N-trimethyl chitosan on *in vitro/in vivo* ofloxacin transcorneal permeation. *J Pharm Sci.* 2004, 93:2851-2862.
- Domard A, Rinaudo M, Terrassin C. New method for the quaternization of chitosan. *Int J Biol Macromol.* 1986, 8:105-107.
- Dressman JB, Amidon GL, Reppas C, Shah VP. Dissolution testing as a prognostic tool for oral drug absorption: Immediate release dosage forms. *Pharmaceutical Research.* 1998, 15:11-22.

- du Plessis LH, Kotzé AF, Junginger HE. Nasal and rectal of insulin with chitosan and N-trimethyl chitosan chloride. *Drug Deliv.* 2010, 17:399-407.
- du Plessis LH, Lubbe J, Strauss T, Kotzé AF. Enhancement of nasal and intestinal calcitonin delivery by the novel Pheroid™ fatty acid based delivery system, and by N-trimethyl chitosan chloride. *Int J Pharm.* 2010, 385:181-186.
- Dünnhaupt S, Barthelmes J, Iqbal J, Perera G, Thurner CC, Friedl H, Bernkop-Schnürch A. *In vivo* evaluation of an oral drug delivery system for peptides based on S-protected thiolated chitosan. *J Control Release.* 2012, 160:477-485.
- Eisenach JH, Atkinson JL, Faeley RD. Hyperhidrosis: Evolving therapies for a well-established phenomenon. *Mayo Clin Proc.* 2005, 80:657-666.
- El-Arini SK, Clas S-D. Evaluation of disintegration testing of different fast dissolving tablets using the texture analyzer. *Pharm Sev Technol.* 2002, 7:361-371.
- Ellison CD, Ennis BJ, Hamad ML, Lyon RC. Measuring the distribution of density and tableting force in pharmaceutical tablets by chemical imaging. *J Pharm Biomed Anal.* 2008, 48:1-7.
- Emami J. *In vitro-in vivo* correlation: from theory to applications. *J Pharm Pharm Sci.* 2006, 9:169-189.
- Escribano E, Calpena AC, Garrigues TM, Freixas J, Domenech J, Moreno J. Structure-absorption relationships of a series of 6-fluoroquinolones. *Antimicrob Agents Chemother.* 1997, 41:1996-2000.
- Fadda HM and Basit AW. Dissolution of pH responsive formulations in media resembling fluids: bicarbonate versus phosphate buffers. *J Drug Deliv Sci Technol.* 2005, 15:273-279.
- Fadda H and Basit AW. Drug solubility in human jejunal fluids and physiologically relevant media: relative importance of buffer composition and intestinal surfactants. *AAPS J.* 2007, 9:T2033.
- Fagerberg JH, Tsinman O, Sun N, Tsinamn K, Avdeef A, Bergström CA. Dissolution rate and apparent solubility of poorly soluble drugs in biorelevant dissolution media. *Mol Pharm.* 2010, 7:1419-1430.
- Fasano A. Physiological, pathological, and therapeutic implication of Zonulin-mediated intestinal barrier modulation: living on the edge of wall. *Am J Pathol.* 2008, 172:1243-1252.
- Fasano A, Baudry B, Pumpilin DW, Wasserman SS, Tall BD, Ketley JM, Kaper JB. *Vibrio cholera* produces a second enterotoxin, which affects intestinal tight junctions. *Proc Nat Acad Sci USA.* 1991, 88:5242-5246.

- Fasano A and Uzzau S. Modulation of intestinal tight junctions by Zonula occludens toxin permits enteral administration of insulin and other macromolecules in an animal model. *J Clin Invest.* 1997, 99:1158-1164.
- Fathi-Azarbayjani A, Jouyban A, Chan SY. Impact of surface tension in pharmaceutical sciences. *J Pharm Pharmaceutical Sci.* 2009, 12:218-228.
- Felber ES. Botulinum toxin in primary care medicine. *J Am Osteopath Assoc.* 2006, 106:609-614.
- Ferrer-Miralles N, Domingo-Espín J, Corchero JL, Vázquez E, Villaverde A. Microbial factories for recombinant pharmaceuticals. *Microb Cell Fact.* 2009, 8:17-25.
- Fetih G, Habib F, Okada N, Fujita T, Attia M, Yamamoto A. Colon-specific delivery and enhanced colonic absorption of [Asu 1,7]-eel calcitonin using chitosan capsules containing various additives in rats. *J Drug Target.* 2006, 14:165-172.
- Fetih G, Habib F, Okada N, Fujita T, Attia M, Yamamoto A. Nitric oxide donors can enhance the intestinal transport and absorption of intestinal transport and absorption of insulin and [Asu 1,7]-eel calcitonin in rats. *J Control Release.* 2005, 106:287-297.
- Florea BI, Thanou M, Junginger HE, Borchard G. Enhancement of bronchial octreotide absorption by chitosan shows linear *in vitro/in vivo* correlation. *J Control Release.* 2006, 110:353-361.
- Foss AC, Goto T, Morishita M, Peppas NA. Development of acrylic-based copolymers for oral insulin delivery. *Euro J Pharm Biopharm.* 2004, 57:163-169.
- Fotaki N and Vertzoni M. Biorelevant dissolution methods and their applications in *in vitro-in vivo* correlations for oral formulations. *TODDJ.* 2010, 4:2-13.
- Frokjaer S and Otzen DE. Protein drug stability: a formulation challenge. *Nat Rev Drug Discov.* 2005, 4:298-306.
- Fujita K, Katahira J, Horiguchi Y, Sonoda N, Furuse M, Tsukita S. Clostridium perfringens enterotoxin binds to the second extracellular loop of claudin-3, a tight junction integral membrane protein. *FEBS Lett.* 2000, 476:258-261.
- Furuse M, Hirase T, Itoh M, Nagafuchi A, Yonemura S, Tsukita S, Tsukita S. Occludin: a novel integral membrane protein localizing at tight junctions. *J Cell Biol.* 1993, 123:1777-1788.
- Furuse M, Itoh M, Hirase T, Nagafuchi A, Yonemura S, Tsukita S, Tsukita S. Direct association of occludin with ZO-1 and its possible involvement in the localization of occludin at tight junctions. *J Cell Biol.* 1994, 127:1617-1626.
- Furuse M and Tsukita S. Claudins in occluding junctions of humans and flies. *Trends Cell Biol.* 2006, 16:181-188.

- Gavini E, Hegge AB, Rassu G, Sanna V, Testa C, Pirisino G, Karlsen J, Giunchedi P. Nasal administration of carbamazepine using chitosan microspheres: *in vitro/in vivo* studies. *Int J Pharm.* 2006, 307:9-15.
- George A and Abraham TE. Polyionic hydrocolloids for the intestinal delivery of protein drugs: alginate and chitosan – a review. *J Control Release.* 2006, 114:1-14.
- Giuliani A, Pirri G, Nicoletto SF. Antimicrobial peptides: an overview of a promising class of therapeutics. *Cent Eur J Biol.* 2007, 2:1-33.
- Gómez SM, Cristancho DM, Martínez F. Solubilization thermodynamics of ibuprofen in modified and classical FeSSIF biorelevant media. *J Mol Liq.* 2013, 179:110-117.
- González-Mariscal L, Tapia R, Chamorro D. Crosstalk of tight junction components with signalling pathways. *Biochim Biophys Acta.* 2008, 1778:729-756.
- Goserød O, Jolliffe IG, Hampson FC, Dettmar PW, Skjak-Braek G. The enhancement of the bioadhesive properties of calcium alginate gel beads by coating with chitosan. *Int J Pharm.* 1998, 175:237-246.
- Groschwitz KR and Hogan SP. Intestinal barrier function: molecular regulation and disease pathogenesis. *Clin Rev Allergy Immunol.* 2009, 142:3-20.
- Gu L, Strickley RG, Chi L-H, Chowhan ZT. Drug-excipient incompatibility studies of dipeptide angiotension-converting enzyme inhibitor, moexipril hydrochloride: drug powder vs wet granulation. *Pharm Res.* 1990, 7:379-383.
- Guan P, Lu Y, Qi J, Niu M, Lian R, Hu F, Wu W. Enhanced oral bioavailability of cyclosporine A by liposomes containing a bile salt. *Int J Nanomedicine.* 2011, 6:965-974.
- Guerra A, Etienne-Mesmin L, Livrelli V, Denis S, Blanquet-Diot S, Alric M. Relevance and challenges in modeling human gastric and small intestinal digestion. *Trends Biotechnol.* 2012, 30:591-600.
- Guichard G. Du peptide à ses analogues peptidique: stratégies de stabilisation de la conformation active, amélioration du profil pharmacocinétique (cyclisation, acides amines non naturels, mimes de repliement, modification du squelette); Du peptide naturel...au médicament (Atelier de Formation Inserm 150) Guo X-X, He W, Wang X-Q, Hu X-M (2004) Preparation and efficacy of tumor vascular-targeted doxorubicin cationic liposomes coated by N-trimethyl chitosan. *J Appl Polym Sci.* 2011, 121:2149-2156.
- Guinesi LS and Cavaleiro ÉTG. The use of DSC curves to determine the acetylation degree of chitin/chitosan samples. *Thermochim Acta.* 2006, 444:128-133.
- Guo J, Jin Y-C, Yang X-Q, Yu S-J, Yin S-W, Qi J-R. Computed microtomography and mechanical property analysis of soy protein porous hydrogel prepared by homogenizing and microbial transglutaminase cross-linking. *Food Hydrocolloid.* 2013, 31:220-226.
- Güres S and Kleinebudde P. Dissolution from solid lipid extrudates containing release modifiers. *Int J Pharm.* 2011, 412:77-84.

- Guzmán F, Barberis S, illanes A. Peptide synthesis: Chemical or enzymatic. *Electron J Biotechnol.* 2006, 10:279-314.
- Hagesaether E, Hiorth M, Sande SA. Mucoadhesion and drug permeability of free mixed films of pectin and chitosan: An *in vitro* and *ex vivo* study. *Euro J Pharm Biopharm.* 2009, 71:325-331
- Hamazaki Y, Itoh M, Sasaki J, Furuse M, Tsukita S. Multi-PDZ domain protein 1 (MUPP1) is concentration at tight junctions through its possible interactions with claudin-1 and junctional adhesion molecules. *J Biol Chem.* 2002, 277:455-461.
- Hames BD. Gel electrophoresis of proteins (Hames BD and Rickwood D, Eds). Oxford Univ. Press. New York. 32-38.
- Hamidi M, Azadi A, Rafiei P. Hydrogel nanoparticles in drug delivery. *Adv Drug Delivery Rev.* 60:1638-1649.
- Hamman JH and Kotzé AF. Effect of the type of base and number of reaction steps on the degree of quaternization and molecular weight of N-trimethyl chitosan chloride. *Drug Dev Ind Pharm.* 2001, 27:373-380.
- Hammal JH, Schultz CM, Kotzé AF. N-trimethyl chitosan chloride: optimum degree of quaterinization for drug absorption enhancement across epithelial cells. *Drug Dev Ind Pharm.* 2003, 29:161-172.
- Hammal JH, Stander M, Kotzé AF. Effect of the degree of quaternization of N-trimethyl chitosan chloride on absorption enhancement: *in vivo* evaluation in rat nasal epithelia. *Int J Pharm.* 2002, 232:235-242.
- Hanna PC, Wieckowski EU, Mietzner TA, McClane BA. Mapping of functional regions of clostridium perfringens type A enterotoxin. *Infect Immun.* 1992, 60:2114-2210.
- Hartl D, Hua He C, Koller B, Da Silva CA, Homer R, Lee CG, Elias JA. Acidic mammalian chitinase is secreted via an ADAM17/epidermal growth factor receptor-dependent pathway and stimulates chemokine production by pulmonary epithelial cells. *J Cell Biol.* 2008, 283:33472-33482.
- Haskins J, Gu L, Wittchen ES, Hibbard J, Stevenson BR. ZO-3, a novel member of the MUGUK protein family found at the tight junction, interacts with ZO-1 and occludin. *J Cell Biol.* 1998, 141:199-208.
- Hatsushika S, Tazuma S, Kajiyama G. Nucleation time and fatty acid composition of lecithin in human gallbladder bile. *Scand J Gastroenterol.* 1993, 28:131-136.
- Hayes KC, Livingston A, Trautwein EA. Dietary impact on biliary lipids and gallstones. *Annu Rev Nutr.* 1992, 12:299-326.
- He Q, Shi J, Chen F, Zhu M, Zhang L. An anticancer drug delivery system based on surfactant-templated mesoporous silica nanoparticles. *Biomaterials.* 2010, 31:3335-3346.

- Hickey M, Davis SR, Sturdee DW. Treatment of menopausal symptoms: what shall we do now? *Lancet*. 2005, 366:409-411.
- Hildebrand M. Pharmacokinetics and drug development. *Dtsch Apoth ZTG*. 1994, 134:23-31.
- Hochman J and Artursson P. Mechanisms of absorption enhancement and tight junction regulation. *J Control Release*. 1994, 29:253-267.
- Hofmann AF. The enterohepatic circulation of bile acids in health and disease. In: Sleisenger MH and Fordtran JS (Eds) – *Gastrointestinal disease, pathophysiology, diagnosis, management*, 5th edition. WB Saunders Co., Philadelphia. 1993, pp 127-150.
- Moore F, Okelo G, Colón I, Kushner J. Improving the hardness of dry granulated tablets containing sodium lauryl sulphate. *Int J Pharm*. 2010, 400:37-41.
- Hrabálek A, Doležal P, Vávrová K., Zbytovská J, Holas T, Klimentová J, Novotný J. Synthesis and enhancing effect of transkarbam 12 on the transdermal delivery of theophylline, clotrimazole, flobufen and griseofulvin. *Pharm Res*. 2006, 23:912-919.
- Hrudy VJ. Designing peptide receptor agonists and antagonists. *Nat Rev Drug Discov*. 2002, 1:847-858.
- Hsiao AY. 3D spheroid culture systems for metastatic prostate cancer dormancy studies and anti-cancer therapeutics development. *Biomedical Engineering Events*. <http://www.hme.umich.edu/about/events.php?query=past>. Accessed September 26, 2011.
- Hu Z, Zou Q, Tian J, Sun L, Zhang Z. Simultaneous determination of codeine, ephedrine, guaiphenesin and chlorpheniramine in beagle dog plasma using high performance liquid chromatography coupled with tandem mass spectrometric detection: application to a bioequivalence study. *J Chromatogr B*. 2011, 15:3937-3942.
- Huang A, Makhlof A, Ping Q, Tazuka Y, Takeuchi H. N-trimethyl chitosan-modified liposomes as carriers for oral delivery of salmon calcitonin. *Drug Deliv*. 2011, 18:562-569.
- Hummel G, Reineke U, Reimer U. Translating peptides into small molecules. *Mol BioSyst*. 2006, 2:499-508.
- Hwang M-R, Kim JO, Lee JH, Kim YI, Chang SW, Jin SG, Kim JA, Lyoo WS, Han SS, Ku SK, Yong CS, Choi H-G. Gentamicin-loaded wound dressing with polyvinyl alcohol/dextran hydrogel: gel characterization and *in vivo* healing evaluation. *AAPS PharmSciTech*. 2010, 11:1092-1103.
- Ibekwe VC, Fadda HM, McConnell EL, Khela MK, Evans DF, Basit AW. Interplay between pH, transit time and feed status on the *in vivo* performance of pH responsive ileo-colonic release system. *Pharm Res*. 2008, 25:1828-1835.
- Ibekwe VC, Fadda HM, Parsons GE, Basit AW. A comparative *in vitro* assessment of the drug release performance pH responsive polymers for ileo-colonic drug delivery. *Int J Pharm Sci*. 2006, 308:52-60.

- Islam A, Riaz M, Yasin T. Structural and viscoelastic properties of chitosan-based hydrogel and its drug delivery application. *Int J Biol Macromol*. 2013, 59:119-124.
- Itoh M, Furuse M, Morita K, Kubota K, Saitou M, Tsukita S. Direct binding of three junction-associated MAGUKs, ZO-1, ZO-2, and ZO-3, with the COOH termini of claudins. *J Cell Biol*. 1999, 147:1351-1363.
- Iwao Y, Tanaka S, Uchimoto T, Noguchi S, Itao S. An easy-to-use approach for determining the disintegration ability of disintegrants by analysis of available surface area. *Int J Pharm*. 2013, 448:1-8.
- Jantratid E and Dressman J. Biorelevant dissolution media simulating the proximal human gastrointestinal tract: an update. *Dissolut Technol*. 2009, 16:21-25.
- Jantratid E, Janssen N, Reppas C, Dressman JB. Dissolution media simulating conditions in the proximal human gastrointestinal tract: an update. *Pharm Res*. 2008, 25:1663-1676.
- Jintapattanakit A, Junyaprasert VB, Kissel T. The role of mucoadhesion of trimethyl chitosan and PEGylated trimethyl chitosan nanocomplexes in insulin uptake. *J Pharm Sci*. 2009, 98:4818-4830.
- Jintapattanakit A, Mao S, Kissel T, Junyaprasert VB. Physicochemical properties and biocompatibility of N-trimethyl chitosan: effect of quaternization and dimethylation. *Eur J Pharm Biopharm*. 2008, 70:563-571.
- Jintapattanakit, A, Junyaprasert, VB, Kissel T. The role of mucoadhesion of trimethyl chitosan and PEGylated trimethyl chitosan nanocomplexes in insulin uptake. *J Pharm Sci*. 2009, 98:4818-4830.
- Johnson L. Asymmetry at the molecular level in biology. *Eur Rev*. 2005, 2:77-95.
- Jones CG and Grainger DW. *In vitro* assessments of nanomaterials toxicity. *Adv Drug Deliv Rev*. 2009, 61:438-456.
- Kabiri K, Omidian H, Zohuriaan-Mehr MJ. Novel approach to highly porous superabsorbent hydrogels: synergistic effect of porogens on porosity and swelling rate. *Polym Int*. 2003; 52:1158-1164.
- Karsdal, MA, Henriksen K, Bay-Jensen AC, Molloy B, Arnold M, John MR, Byrjalsen I, Azria M, Riis BJ, Qvist P, Christiansen C. Lessons learned from the development of oral calcitonin: The first tablet formulation of a protein in phase III clinical trials. *J Clin Pharmacol*. 2011, 51:460-471.
- Kasim NA, Whitehouse M, Ramachandran C, Bermejo M, Lennernas H, Hussain AS, Junginger HE, Stavchansky SA, Midha KK, Shah VP, Amidon GL. Molecular properties of WHO essential drugs and provisional biopharmaceutical classification. *Mol Pharm*. 2004 1:85-96.
- Katzung BG, Masters SB, Trevor AJ. *Basic & Clinical Pharmacology* (12th ed). McGraw-Hill Companies, Inc. 2012, pp 592-668, 738-782.

- Kavimandan NJ and Peppas NA. Confocal microscopic analysis of transport mechanisms of insulin across the cell monolayer. *Int J Pharm.* 2008, 354:143-148.
- Kean T, Roth S, Thanou. Trimethylated chitosan as nonviral gene delivery vectors: cytotoxicity and transfection efficiency. *J Control Release.* 2005, 103:643-653.
- Kean T and Thanou M. Biodegradation, biodistribution and toxicity of chitosan. *Adv Drug Deliv Rev.* 2010, 62:3-11.
- Kerss S, Allen A, Garner A. A simple method for measuring the thickness of the mucus gel layer adherent to rat, frog and human gastric mucosa: influence of feeding, prostaglandin, *N*-acetylcysteine and other agents. *Clin Sci.* 1982, 63:187-195.
- Khoshmanesh A, Cook PLM, Wood BR. Quantitative determination of polyphosphate in sediments using attenuated total reflectance-Fourier transform infrared (ATR-FTIR) spectroscopy and partial least square regression. *Analyst.* 2012, 137:3704-3709.
- Kittur FS, Prashanth H, Sankar KU, Tharanathan RN. Characterization of chitin, chitosan and their carboxymethyl derivatives by differential scanning calorimetry. *Carbohydr Polym.* 2002, 49:298-306.
- Klein S. The use of biorelevant dissolution media to forecast the *in vivo* performance of a drug. *AAPS J.* 2010, 12:397-406.
- Kondoh M, Masuyama A, Takahashi A, Asano N, Mizuguchi H, Koizumi N, Fujii M, Hayakawa T, Horiguchi Y, Watanabe Y. A novel strategy for the enhancement of drug absorption using a claudin modulator. *Mol Pharmacol.* 2005, 67:749-756.
- Kondoh M, Yoshida T, Kakutani H, Yagi K. Targeting tight junction proteins-significance for drug development. *Drug Discov Today.* 2008, 13:180-186.
- Kotzé AF, Thanou M, Luessen HL, de Boer AG, Verhoef JC, Junginger HE. Effect of the degree of quaternization of *N*-trimethyl chitosan chloride on the permeability of intestinal epithelial cells (Caco-2). *Eur J Pharm Biopharm.* 1999, 47:269-274.
- Kukreja R and Singh BR. Botulinum Neurotoxins: Structure and mechanism of action. *Microbial ToxinsL Current Research and Future Trends.* Caister Academic Press. 2009. pp 1-192.
- Kulinowski P, Dorożyński P, Jachowicz R, Węglarz WP. An integrated system for dissolution studies and magnetic resonance imaging of controlled release, polymer-based dosage forms- A tool for quantitative assessment of hydrogel formation processes. *J Pharmaceut Biomed.* 2008, 48:685-693.
- Kumar A, Lahiri SS, Singh H. Development of PEGDMA:MAA based hydrogel microparticles for oral insulin delivery. *Int J Pharm.* 2006, 323:117-124.
- Ladner RC, Sato AK, Gorzelany J, De Souza M. Phage display-derived peptides as a therapeutic alternatives to antibodies. *Drug Discov Today.* 2004, 9:525-529.

- Lennernäs H. Intestinal permeability and its relevance for absorption and elimination. *Xenobiotica*. 2007, 37:1015-1051.
- Lennernäs H and Abrahamsson B. The use of biopharmaceutic classification of drugs in drug delivery and development current status and future extension. *J Pharm Pharmacol*. 2005, 57:273-285.
- Lin YH, Mi FL, Chen CT, Chang WC, Peng SF, Liang HF, Sung HW. Preparation and characterization of nanoparticles shelled with chitosan for oral insulin delivery. *Biomacromolecules*. 2007, 8:146-152.
- Lindahl A, Ungel A-L, Knutson L, Lennernaes H. Characterization of fluids from the stomach and proximal jejunum in men and women. *Pharm Res*. 1997, 14:497-502.
- Lindmark T, Kimura Y, Artursson P. Absorption enhancement through intracellular regulation of tight junction permeability by medium chain fatty acids in Caco-2 cells. *J Pharmacol Exp Ther*. 1998, 284:362-369.
- Lindmark T, Nikkilä T, Artursson P. Mechanisms of absorption enhancement by medium chain fatty acids in intestinal epithelial Caco-2 cell monolayers. *J Pharmacol Exp Ther*. 1995, 275:958-964.
- Ling M-H and Chen M-C. Dissolving polymer microneedles patches for rapid and efficient transdermal delivery of insulin to diabetic rats. *Acta Biomaterialia*. 2013, 9:8952-8961.
- Lloyd GR, Craig DQM, Smith A. An investigation into the melting behaviour of binary mixes and solid dispersions of paracetamol and PEG 4000. *J Pharm Sci*. 1997, 86:991-996.
- Loffet A. Peptide as drugs: is there a market? *J Pept Sci*. 2002, 8:1-7.
- Lopes LC, Fajardo AR, Piai JP, Rubira AF, Muniz EC. Incorporation of theophylline in a chitosan/chondroitin sulphate hydrogel matrix: *in vitro* release studies and mechanical properties according to pH changes. *J Appl Polym Sci*. 2013, 128:3417-3424.
- Lowman AM, Morishita M, Kajita M, Nagai T, Peppas NA. Oral delivery of insulin using pH-responsive complexation gels. *ACS*. 1999, 88:933-937.
- Lu Y, Kim S, Park K. *In vitro-in vivo* correlation: perspectives on model development. In *J Pharm*. 2011, 418:142-148.
- Lui J, Zhang L, Hu W, Tian R, Teng Y, Wang C. Preparation of konjac glucomannan-based pulsatile capsule for colonic drug delivery system and its evaluation *in vitro* and *in vivo*. *Carbohydr Polym*. 2012, 87:377-382.
- MacLennan AH. Hormone replacement therapy: a 2008 perspective. *Obstet Gynaecol Reprod Med*. 2008, 19:13-18.
- Makhlof A, Werle M, Tozuka Y, Takeuchi H. A mucoadhesive nanoparticulate system from the simultaneous delivery of macromolecules and permeation enhancers to the intestinal mucosa. *J Control Release*. 2011, 149:81-88.

- Maklof A, Tozuka Y, Takeuchi H. Design and evaluation of novel pH-sensitive chitosan nanoparticles for oral insulin delivery. *Euro J Pharm Sci.* 2011, 42:445-451.
- Mao S, Shuai Xm Unger F, Wittmar M, Xie X, Kissel T. Synthesis, characterization and cytotoxicity of poly(ethylene glycol)-graft-trimethyl chitosan block copolymers. *Biomaterials.* 2005, 26:6343-6356.
- Marais E, Hamman J, du Plessis L, Lemmer R, Steenekamp J. Eudragit® L100/N-trimethyl chitosan chloride microspheres for oral insulin delivery. *Molecules.* 2013, 18:6734-3747.
- Markov AG, Veshnyakova A, Fromm M, Amasheh M, Amasheh S. Segmental exposure of claudin proteins correlates with tight junction barrier properties in rat intestine. *J Comp Physiol B.* 2010, 180:591-598.
- Maroni A, Zema L, Curto MDD, Foppoli A. Oral colon delivery of insulin with aid of functional adjuvants. *Adv Drug Deliver Rev.* 2012, 64:540-556.
- Martins AF, Bueno PVA, Almeida AMS, Rodrigues FHA, Rubira AF, Muniz EC. Characterization of N-trimethyl chitosan/alginate complexes and curcumin release. *Int J Biol Macromol.* 2013, 57:174-184.
- Martins AF, Pereira AGB, Fajardo AR, Rubira AF, Muniz EC. Characterization of polyelectrolytes complexes based on *N,N,N*-trimethyl chitosan/heparin prepared at different pH conditions. *Carbohydr Polym.* 2011, 86:1266-1272.
- Martins AF, Piai JF, Schuquel ITA, Rubira AF, Muniz EC. Polyelectrolyte complexes of chitosan/heparin and *N,N,N*-trimethyl chitosan/heparin obtained at different pH: I. Preparation, characterization, and controlled release of heparin. *Colloid Polym Sci.* 2011, 289:1133-1144.
- Masuyama A, Kondoh M, Seguchi H, Takahashi A, Harada M, Fujii M, Mizuguchi H, Horiguchi Y, Watanabe Y. Role of N-terminal amino acids in the absorption-enhancing effects of N-terminal amino acids in the absorption-enhancing effects of the C-terminal fragments of *Clostridium perfringens* enterotoxin. *J Pharmacol Exp Ther.* 2005, 314:789-795.
- Matricardi P, Meo CD, Coviello T, Hennik WE, Alhaique F. Interpenetrating polymer network polysaccharide hydrogel for drug delivery and tissue engineering. *Adv Drug Delivery Rev.* 2013; 65:1172-1187.
- McCarthy KM, Skare IB, Stankewich MC, Furuse M, Tsukita S, Rogers RA, Lynch RD, Schneeberger EE. Occludin is a functional component of tight junction. *J Cell Sci.* 1996, 109:2287-2298.
- McConnell EL, Fadda HM, Basit AW. Gut instincts: Explorations in intestinal physiology and drug delivery. *Int J Pharm.* 2008, 364:213-226.
- McGregor DP. Discovering and improving novel peptide therapeutics. *Curr Opin Pharmacol.* 2008, 8:616-619.

- Meaney CM and O'Driscoll CM. A comparison of the permeation enhancement potential of simple bile salt and mixed bile salt: fatty acid micellar systems using the Caco-2 cell culture model. *Int J Pharm.* 2000, 207:21-30.
- Mehta S, de Beer T, Remon JP, Vervaet C. Effect of disintegrants on the properties of multiparticulate tablets comprising starch pellets and excipient granules. *Int J Pharm.* 2012, 422:310-317.
- Meng S, Li W, Yim X, Xie J. A comprehensive theoretical study of the hydrogen bonding interactions and microscopic solvation structures of a pyridyl-urea-base hydrogelator in aqueous solution. *Comp Theor Chem.* 2013, 15:76-84.
- Millner RWJ, Lockhart AS, Bird H, Alexiou C. A new hemostatic agent: initial life-saving experience with Celox (chitosan) in cardiothoracic surgery. *Ann Thorac Surg.* 2009, 87:e13-e14.
- Montecucco C and Molgó J. Botulinum neurotoxins: revival of an old killer. *Cur Opin Pharmacol.* 2005, 5:274-279.
- Morishita M and Peppas NA. Is the oral route possible for peptide and protein drug delivery. *Drug Discov Today.* 2006, 11:905-910.
- Morita K, Furuse M, Fujimoto K, Tsukita S. Claudin multigene family encoding four-transmembrane domain protein components of tight junction strands. *Proc Natl Acad Sci USA.* 1999, 96:511-516.
- Mourya VK and Inamda NN. Trimethyl chitosan and its applications in drug delivery. *J. Mater Sci Mater Med.* 2009, 20:1057-1079.
- Mukhopadhyay P, Sarkar K, Bhattacharya S, Bhattacharyya A, Mishra R, Kundu PP. pH sensitive *N*-succinyl chitosan grafted polyacrylamide hydrogel for oral insulin delivery. *Carb Polymer.* 2014, 112: 627-637.
- Muranishi S. Absorption enhancers. *Crit Rev Ther Drug Carrier Syst.* 1990, 7:1-33.
- Murphy DJ, Sankalia MG, Loughlin RG, Donnelly RF, Jenkins MG, McCarron PA. Physical characterization and component release of poly(vinyl alcohol)-tetrahydroxyborate hydrogels and their applicability as potential topical drug delivery systems. *Int J Pharm.* 2012, 423:326-334.
- Nakason C, Wohmang T, Kaesaman A, Kiatkamjornwong S. Preparation of cassava starch-graft-polyacrylamide superabsorbents and associated composites by reactive blending. *Carbohydr Polym* 2010, 81:348-357.
- Nelson EJ, Yoshida S, Kamei N, Iwamae R, Khafagy ES, Olsen J, Rahbek UL, Pedersen BL, Takayama K, Takeda-Morishita M. *In vivo* proof of concept of oral insulin delivery based on a co-administration strategy with the cell-penetration peptide penetratin. *J Control Release.* 2014, 189C: 19-24.

- Naumann M, So Y, Argoff CE, Childers MK, Dykstra DD, Gronseth GS, Jabbari B, Kaufmann HC, Schurch B, Silberstein SD, Simpson DM. Assessment: Botulinum neurotoxin in the treatment of autonomic disorders and pain (an evidence-based review): report of the Therapeutics and Technology Assessment Subcommittee of the American Academy of Neurology. *Neurology*. 2008, 6:1707-1714.
- Nusrat A, Brown GT, Tom J, Drake A, Bui TTT, Quan C, Mrsny RJ. Multiple protein interactions involving proposed extracellular loop domains of the tight junction protein occludin. *Mol Biol Cell*. 2005, 16:1725-1734.
- O'Driscoll CM and Griffin BT. Biopharmaceutical challenges associated with drugs and low aqueous solubility-The potential impact of lipid-based formulations. *Adv Drug Delivery Rev*. 2008, 60:617-624.
- Oberle RL and Das H. Variability in gastric pH and delayed gastric emptying in Yucatan miniature pigs. *Pharm Res*. 1994, 11:592-594.
- Olivera ME, Manzo RH, Junginger HE, Midha KK, Shah VP, Stavchansky S, Dressman JB, Barends DM. Biowaiver monographs for immediate release solid oral dosage forms: ciprofloxacin hydrochloride. *J Pharm Sci*. 2001, 100:22-33.
- Otabe A, Fujieda T, Masuyama T. Chronic oral toxicity of *N*-[*N*-[3-hydroxy-4-methoxyphenyl) propyl]- α -aspartyl]-L-phenylalanine 1-methyl ester, monohydrate (advantame) in the dog. *Food Chem Toxicol*. 2011, 49:S49-S59.
- Oyston PCF, Fox MA, Richards SJ, Clark GC. Novel peptide therapeutics for treatment of infections. *J Med Microbiol*. 2009, 58:977-987.
- Pandey M, Amin MCIM, Ahmed N, Abeer MM. Rapid synthesis of superabsorbent smart-welling bacterial cellulose/acrylamide-based hydrogels for drug delivery. *Int J Polym Sci*. 2013. doi: 10.1155/2013/905471.
- Paranjpe PV and Sinko PJ. Overcoming paracellular tissue barriers for drug delivery. *Pharm News*. 2002, 9:381-395.
- Paris L, Tonutti L, Vannini C, Bazzoni G. Structural organization of tight junctions. *Biochim Biophys Acta*. 2008, 1778:646-659.
- Peppas NA, Kavimandan NJ. Nanoscale analysis of protein and peptide absorption: insulin absorption using complexation and pH-sensitive hydrogels as delivery vehicles. *Eur J Pharm Sci*. 2006, 29:183-197.
- Peri N, Bergman E, Forsell P, Hedeland M, Bondesson U, Knutson L, Lennernäs H. First-pass effects of verapamil on the intestinal absorption and liver disposition of fexofenadine in the porcine model. *Drug Metab Dispos*. 2006, 34:1182-1189.
- Persson EM, Nordgren A, Forsell P, Knutson L, Ohgren C, Forssen S, Lennernäs H, Abrahamsson B. Improved understanding of the effect of food on drug absorption and

- bioavailability for lipophilic compounds using an intestinal pig perfusion model. *Eur J Pharm Sci.* 2008, 34:22-29.
- Pichereau and Allary C. Therapeutic peptides under the spotlight. *EBR (Winter issue).* 2005, 88-91.
- Pillay V, Hibbins AR, Choonara YE, du Toit LC, Kumar P, Ndesendo VMK. Orally administered therapeutic peptide delivery: enhanced absorption through the small intestine using permeation enhancers. *Int J Pept Res Ther.* 2012, 18:259-280.
- Polnok A, Borchard G, Verhoef JC, Sarisuta N, Junginger HE. Influence of methylation process of the degree of quaternization of N-trimethyl chitosan chloride. *Eur J Pharm Biopharm.* 2004, 57:77-83.
- Powell DW. Ion and water transport in the intestine. In: Andreoli TE, Schultz SG (eds) *Physiology of membrane disorders*, 2nd edn, Plenum, New York. 1987, 559-596.
- Pringels E, Verbaet C, Verbeeck R, Foreman P, Remon JP. The addition of calcium ions to starch/Cabopol[®] mixtures enhances the nasal bioavailability of insulin. *Eur J Pharm Biopharm.* 2008, 68:201-206.
- Prodduturi S, Manek RV, Kolling WM, Stodghill SP, Repka MA. Solid-state stability and characterization of hot-melt extruded poly(ethylene oxide) films. *J Pharm Sci.* 2005, 94:2232-2245.
- Qi S, Gryczke A, Belton P, Craig DQM. Characterization of solid dispersions of paracetamol and Eudragit[®] E prepared by hot-melt extrusion using thermal microthermal and spectroscopic analysis. *Int J Pharm.* 2008, 354:158-167.
- Quattrocchi E and Kourlas H. Teriparatide: a review. *Clin Ther.* 2004, 26:841-854.
- Qurrat-ul-Ain A, Sharma S, Khuller GK, Garg SK. Alginate-based oral drug delivery system for tuberculosis: Pharmacokinetics and therapeutic effects. *J Antimicrob Chemother.* 2003, 51:931-938.
- Ranfeild J. Center for devices and radiological health (CDRH)'s approval of Celox topical hemostatic granules as a medical device (K061079). Docstoc. <http://www.docstoc.com/doc/100104805/K090780>. Accessed 10 July 2010.
- Ranoux S, Attal N, Morain F, Bouhassira D. Botulinum toxin type A induces direct analgesic effects in chronic neuropathic pain. *Ann Neurol.* 2008, 64:274-283.
- Reis CP, Veiga FJ, Ribeiro AJ, Neufeld RJ, Damgé C. Nanoparticulate biopolymers deliver insulin orally eliciting pharmacological response. *Pharm Nanotech.* 2008, 97:5290-5305.
- Rekha MR and Sharma CP. Oral delivery of therapeutic protein/peptide for diabetes-Future perspectives. *Int J Pharm.* 2013, 440:48-62.
- Renkema GH, Boot RG, Muijsers AO, Donker-Koopman WE, Aerts JMFG. Purification and characterization of human chitotriosidase, a novel member of the chitinase family of proteins. *J Biol Chem.* 1995, 270:2198-2202.

- Roberts GAF. Chitin chemistry. The MacMillan Press, London. 1992, pp 1-110, 274-315.
- Roeselers G, Bouwman J, Venema K, Montijn R. The human gastrointestinal microbiota-an unexplored frontier for pharmaceutical discovery. *Pharmacol Res.* 2012, 66:443-447.
- Rubas W, Cromwell MEM, Shahrokh Z, Villagran J, Nguyen T-N, Wellton M, Nguyen T-N, Mersny RJ. Flux measurements across Caco-2 monolayers may predict transport in human large intestinal tissue. *J Pharm Sci.* 1996, 85:165-169.
- Rudraraju VS and Wyandt CM. Rheological characterization of microcrystalline cellulose/sodium carboxymethyl cellulose hydrogels using a controlled stress Rheometer: part I. *Int J Pharm.* 2005, 292:53-61.
- Sajeesh S, Bouchemal K, Marsaud V, Vauthier C, Sharma CP. Cyclodextrin complexed insulin encapsulated hydrogel microparticles: An oral delivery system for insulin. *J Control Release.* 2010a, 147:377-384.
- Sajeesh S, Vauthier C, Gueutin C, Ponchel G, Sharma CP. Thiol functionalized polymethacrylic acid-based hydrogel microparticles for oral insulin delivery. *Acta Biomater.* 2010b, 6:3072-3080.
- Sakakibara A, Furuse M, Saitou M, Ando-Akatsuka Y, Tsukita S. Possible involvement of phosphorylation of occludin in tight junction formation. *J Cell Biol.* 1997, 137:1393-1401.
- Salama NN, Eddington ND, Fasano A. Tight junction modulation and its relationship to drug delivery. *Adv Drug Deliv Rev.* 2006, 58:15-28.
- Sandri G, Rossi S, Bonferoni MC, Ferrari F, Zambito Y, Di Colo G, Caramella C. Buccal penetration enhancement properties of N-trimethyl chitosan: influence of quaternization degree on absorption of high molecular weight molecule. *Int J Pharm.* 2005, 297:146-155.
- Sandzen B, Blom H, Dahlgren S. Gastric mucus gel layer thickness measured by direct light microscopy. An experimental study in the rat. *Scand J Gastroenterol.* 1988, 23:1160-1164.
- Sanganwar GP, Salthigarin S, Baby RJ, Gupta RB. Simultaneous production and co-mixing of microparticles of nevirapine and excipients by supercritical antisolvent method for dissolution enhancement. *Euro J Pharm Sci.* 2010, 31:164-174.
- Sangwai M and Vavia P. Amorphous ternary cyclodextrin nanocomposites of telmisartan for oral drug delivery: Improved solubility and reduced pharmacokinetic variability. *Int J Pharm.* 2013, 453:423-432.
- Sarawade PB, Shao GN, Quang DV, Kim HT. Effect of various structure directing agents on the physicochemical properties of the silica aerogels prepared at an ambient pressure. *Appl Surf Sci.* 2013, 287:84-90.
- Sarmento B, Martins S, Ferreira D, Souto E. Oral insulin delivery by means of solid lipid nanoparticles, *Int J Nanomedicine.* 2007, 2:743-749.

- Sarode AL, Sandhu H, Shah N, Malick W, Zia H. Hot melt extrusion (HME) for amorphous solid dispersions; predictive tools for processing and impact of drug-polymer interactions on supersaturation. *Euro J Pharm Sci.* 2013, 48:371-384.
- Sato AK, Viswanathan M, Ket RB, Wood CR. Therapeutic peptides: technological advances driving peptides into development. *Curr Opin Biotechnol.* 2006, 17:638-642.
- Sayin B, Somavarapu S, Li XW, Thanou M, Sesardic D, Alpar HO, Senel S. Mono-N-carboxymethyl chitosan (MCC) and N-trimethyl chitosan (TMC) nanoparticles for non-invasive vaccine delivery. *Int J Pharm.* 2008, 363:139-148.
- Schiller C, Frohlich CP, Geissman T, Siegmund W, Monnikes H, Hosten N, Weitschies W. Intestinal fluid volumes and transit of dosage forms as assessed by magnetic resonance imaging. *Aliment Pharmacol Ther.* 2005, 22:971-979.
- Schipper NGM, Varum KM, Artursson P. Chitosans as absorption enhancers for poorly absorbable drugs. 1: Influence of molecular weight and degree of acetylation on drug transport across human intestinal epithelial (Caco-2) cells. *Pharm Res.* 1996, 13:1686-1692.
- Schipper NGM, Varum KM, Stenberg P, Ocklind G, Lennernas H, Artursson P. Chitosans as absorption enhancers of poorly absorbable drugs 3: influence of mucus on absorption enhancers of poorly absorbable drugs 3: influence of mucus on absorption enhancement. *Eur J Pharm Sci.* 1999, 8:335-343.
- Schoener CA, Hutson HN, Peppas NA. pH-responsive hydrogels with dispersed hydrophobic nanoparticles for the oral delivery of chemotherapeutics. *J Biomed Mater Res A.* 2012, 101A:2229-2238.
- Serra A, Maciá A, Romero M-P, Piñol C, Motilva M-J. Rapid methods to determine procyanidins, anthocyanins, theobromine and caffeine in rat tissues by liquid chromatography-tandem mass spectrometry. *J Chromatogr B.* 2011, 879:1519-1528.
- Serra L, Doménech J, Peppas N. Engineering design and molecular dynamics of mucoadhesive drug delivery system as targeting agents. *Eur J Pharm Biopharm.* 2009, 71:519-528.
- Shah RB and Khan MA. Regional permeability of salmon calcitonin in isolated rat gastrointestinal tracts: transport mechanism using Caco-2 cell monolayer. *APPS J.* 2004, 6:36-40.
- Shao Z, Li Y, Chermak T, Mitra AK. Cyclodextrins as mucosal absorption promoters of insulin. II. Effects of β -cyclodextrin derivatives on α -chymotryptic degradation and enteral absorption of insulin in rats. *Pharmaceut Res.* 1994, 11:1174-1179.
- Shepherd R, Reader S, Falshaw A. Chitosan functional properties. *Glycoconj J.* 1997, 14:535-542.

- Sheth P, Basuroy S, Li C, Naren AP, Rao RK. Role of phosphatidylinositol 3-kinase in oxidative stress-induced disruption of tight junctions. *J Biol Chem*. 2003, 278:49239-49245.
- Shi X-N, Wang W-B, Wang A-Q. Effect of surfactant on porosity and swelling behaviours of guar gum-g-poly(sodium acrylate-co-styrene)/attapulgate superabsorbent hydrogel. *Colloid Surface B*. 2011, 88:279-286.
- Shibayama M, Takata S-I, Norisuye T. Static inhomogeneities and dynamic fluctuations of temperature sensitive polymer gels. *Physica A*. 1999, 249:245-252.
- Shukla HD and Sharma SK. Clostridium botulinum: a bug with beauty and weapon. *Crit Rev Microbiol*. 2005, 31:11-18.
- Silva CM, Ribeiro AJ, Figueiredo IV, Gonçalves RA, Veiga F. Alginate microspheres prepared by internal gelation: Development and effect on insulin stability. *Int J Pharm*. 2006, 311: 1-10.
- Simon DB, Lu Y, Choate KA, Velazquez H, Al-Sabban E, Prage M, Casari G, Bettinelli A, Colussi G, Rodriguez-Soriano J, McCredie, Milford D, Sanjad S, Lifton RP. Paracellin-1, a renal tight junction protein required for paracellular Mg_{2+} resorption. *Science*. 1999, 285:103-106.
- Simonelli C. Parathyroid hormone: a new treatment option for osteoporosis. *Pharm Ther*. 2002, 27:410-413.
- Sing KSW, Everett DH, Haul RAW, Moscou L, Pierotti RA, Rouquerol J, Seimienewska T. Reporting physisorption data for gas-solid systems. *Pure Appl Chem*. 1985, 57:603-619.
- Singh B. Psyllium as therapeutic and drug delivery agent. *Int J Pharm*. 2007, 334:1-14.
- Singh B and Pal L. Sterculia crosslinked PVA and PVA-poly(AAm) hydrogel wound dressings for slow drug delivery: Mechanical, mucoadhesive, biocompatible and permeability properties. *J Mech Behav Biomed*. 2012, 9:9-21.
- Singhal D and Curatolo W. Drug polymorphism and dosage form design: a particle perspective. *Adv Drug Deli Rev*. 2004, 56:335-347.
- Sjodin E, Fritsch H, Eriksson UG, Logren U, Nordgren A, Forsell P, Knutson L, Lennernäs H. Intestinal and hepatobiliary transport of ximelagatran and its metabolites in pigs. *Drug Metab Dispos*. 2008, 36:1519-1528.
- Smales C, Ellis M, Baumber R, Hussain N, Desmond H, Staddon JM. Occludin phosphorylation: identification of an occludin kinase in brain and cell extracts as CK2. *FEBS Lett*. 2003, 545:161-166.
- Snoeck V, Huyghebaert N, Cox E, Vermeire A, Saunders J, Remon JP, Berschooten F, Goddeeris BM. Gastrointestinal transit time of non-disintegrating radio-opaque pellets in suckling and recently weaned piglets. *J Control Release*. 2004, 94:143-153.

- Snyman D, Hamman JH, Kotzé AF. Evaluation of the mucoadhesive properties of N-trimethyl chitosan chloride. *Drug Dev Ind Pharm*. 2003, 29:61-69.
- Snyman D, Hamman JH, Kotzé JS, Rollings JE, Kotzé AF. The relationship between the absolute molecular weight and the degree of quaternization of N-trimethyl chitosan chloride. *Carbohydr Polym*. 2002, 50:145-150.
- Snyman D, Kotzé AF, Walls TH, Govender T, Lachmann G. Conformational characterization of quaternized chitosan polymers. In: *Proceeding of the international symposium on control release of bioactive materials*. 2004, p 211.
- Soderholm JD, Oman H, Blomquist L, Veen J, Lindmard T, Olaison G. Reversible increase in tight junction permeability to macromolecules in rat ileal mucosa *in vitro* by sodium caprate, a constituent of milk fat. *Digest Dis Sci*. 1998, 43:1547-1552.
- Sogias IA, Khutoryanskiy VV, Williams AC. Exploring the factors affecting the solubility of chitosan in water. *Macromol Chem Phys*. 2010, 211:426-433.
- Sonaje K, Lin Y-H, Juang J-H, Wey S-P, Chen C-T, Sung H-W. *In vivo* evaluation of safety and efficacy of self-assembled nanoparticles for oral insulin delivery. *Biomaterials*. 2009, 30:2329-2339.
- Song K-H, Fasano A, Eddington ND. Effect of the six-mer synthetic peptide (AT-1002) fragment of zonula occludens toxin on the intestinal absorption of cyclosporine A. *Int J Pharm*. 2008, 351:8-14.
- Sonoda N, Furuse M, Sasaki H, Yonemura S, Katahira J, Horiguchi Y, Tsukita S. Clostridium perfringens enterotoxin fragment removes specific claudins for tight junction strands: evidence for direct involvement of claudins in tight junction barrier. *J Cell Biol*. 1999, 147:195-204.
- Steed E, Balda MS, Matter K. Dynamics and functions of tight junctions. *Trends Cell Biol*. 2010, 20:142-149.
- Stevenson CL. Advances in peptide pharmaceuticals. *Curr Pharm Biotechnol*. 2009, 10:122-137.
- Strugala V, Allen A, Dettmar PW, Pearson J. Colonic mucin: methods of measuring mucus thickness. *Proc Nutr Soc*. 2003, 62:237-243.
- Sutar PB, Mishra RK, Pal K, Banthia AK. Development of pH sensitive polyacrylamide grafted pectin hydrogel for controlled drug delivery system. *J Mater Sci: Mater Med* 2008, 19:2247-2253.
- Szentkuti L and Lorenz K. The thickness of the mucus layer in different segments of the rat intestine. *Histochem J*. 1995, 27:466-472.
- Tajiri T, Morita S, Sakamoto R, Suzuki M, Yamanashi S, Ozaki Y, Kitamura S. Release mechanisms of acetaminophen from polyethylene oxide/polyethylene glycol matrix tablets utilizing magnetic resonance imaging. *Int J Pharm* 2010, 395:147-153.

- Takács-Novák K, Szőke V, Völgyi G, Horváth P, Ambrus R, Szabó-Révész P. Biorelevant solubility of poorly soluble drugs: Rivaroxaban, furosemide, papaverine and niflumic acid. *J Pharm Biomed Anal.* 2013, 83:279-285.
- Tang B, Cheng G, Gu J-C, Xu C-H. Development of solid self-emulsifying drug delivery systems: preparation techniques and dosage forms. *Drug Discov Today.* 2008, 13:606-612.
- Tavelin S, Hashimoto K, Malkinson J, Lazorova L, Roth I, Artursson P. A new principle for tight junction modulation based on occludin peptides. *Mol Pharm.* 2003, 64:1530-1540.
- Thanou M, Florea BI, Langemeijer MWE, Verhoef JC, Junginger HE. *N*-trimethylated chitosan chloride (TMC) improves the intestinal permeation of peptide drug buserelin *in vitro* (Caco-2 cells) and *in vivo* (rats). *Pharm Res.* 2000a, 17:27-31.
- Thanou M, Verhoef JC, Junginger HE. Chitosan and its derivatives as intestinal absorption enhancers. *Adv Drug Deliv Rev.* 2001a, 50:S91-S101.
- Thanou M, Verhoef JC, Verheijden JHM, Junginger HE. Intestinal absorption of octreotide using trimethyl chitosan chloride: Studies in pigs. *Pharm Res.* 2001b, 18:823-828.
- Thanou MM, Kotze AF, Scharringhausen T, Lueben HL, De Boer AG, Berhoef JC, Junginger HE. Effect of degree of quaterinization of *N*-trimethyl chitosan chloride for enhanced transport of hydrophilic compounds across intestinal Caco-2 cell monolayers. *J Control Release.* 2000b, 64:15-25.
- Thanou MM, Verhoef JC, Romeijn SG, Nagelkerke JF, Merkus FW, Junginger HE. Effects of *N*-trimethyl chitosan chloride, a novel absorption enhancer, on caco-2 intestinal epithelia and the ciliary beat frequency of chicken embryo trachea. *Int J Pharm.* 1999, 185:73-82.
- The USP/The National Formulary (USP 24/NF19). US Pharmacopeial convention, Inc., MD. 2012, pp 856, 874, 1106 and 2236.
- Thörn HA, Hedeland M, Bondesson U, Knutson L, Yasin M, Dickinson P, Lennernäs H. Different effects of ketonconazole on the stereoselective first-pass metabolism of *R/S*-verapamil in the intestine and the liver: important for the mechanistic understanding of first-pass drug-drug interactions. *Drug Metab Dispos.* 2009, 37:2186-2196.
- Thörn HA, Lundahl A, Schrickx JA, Dickinson PA, Lennernäs H. Drug metabolism of CYP3A4, CYP2C9 and CYP2D6 substrates in pigs and humans. *Eur J Pharm Sci.* 2011, 43:89-98.
- Tomita M, Hayashi M, Awazu S. Absorption-enhancing mechanism of EDTA, caprate and decanoylcaritine in Caco-2 cells. *J Pharm Sci.* 1996, 85:608-611.
- Tomita M, Hayashi M, Awazu S. Comparison of absorption enhancing effect between sodium caprate and disodium ethylenediaminetetraacetate in Caco-2 cells. *Biol Pharm Bull.* 1994, 17:753-755.

- Torres-Lugo M, García M, Record R, Peppas NA. Physicochemical behaviour and cytotoxic effects of p(methacrylic acid-g-ethylene glycol) nanospheres for oral delivery of proteins. *J Control Release*. 2002, 80:197-205.
- Tshala-Katumbay D. Peptide-based treatment for neurodegenerative disease. Sumobrain. <http://www.sumobrain.com/patents/wipo/Peptide-based-treatment-neurodegenerative-diseases/WO2011066285.html>. Accessed September 25, 2011.
- Van der Lubben IM, Verhoef JC, Fretz MM, Van O, Mesu I, Kersten G, Junginger HE. Trimethyl chitosan chloride (TMC) as a novel excipient for oral and nasal immunisation against diphtheria. *STP Pharma Sci*. 2002, 12:235-242.
- Van der Merwe M, Verhoeg J, Verheijden J, Kotzé A, Junginger H. Trimethylated chitosan as polymeric absorption enhancer for improved peroral delivery of peptide drugs. *Eur J Pharm Biopharm*. 2004, 58:225-235.
- Varma MV, Gardner I, Steyn SJ, Nkansah P, Rotter CJ, Whitney-Pickett C, Zhang H, Di L, Cram M, Fenner KS, El-Kattan AF. pH-Dependent solubility and permeability criteria for provisional biopharmaceutics classification (BCS and BDDCS) in early drug discovery. *Mol Pharm*. 2012, 9:1199-1212.
- Varum FJO, Veiga F, Sousa JO, Basit AW. An investigation into the role of mucus thickness on mucoadhesion in the gastrointestinal tract of pig. *Euro J Pharm Sci*. 2010, 40:335-341.
- Vázquez JL, Berlanga M, Merino S, Domènech O, Viñas M, Montero MT, Hernández-Borrell J. Determination by fluorimetric titration of the ionization constants of ciprofloxacin in solution and in the presence of liposomes. *Photochem Photobiol*. 2001, 73:14-19.
- Verheul JR, Amidi M, Van der Wal S, Van Riet E, Jiskoot W, Hennink WE. Synthesis, characterization and *in vitro* biological properties of O-methyl free *N,N,N*-trimethylated chitosan. *Biomaterials*. 2008, 29:3642-3649.
- Verheul RJ, Amidi M, van Steenberg MJ, van Riet E, Jiskoot W. Influence of the degree of acetylation of enzymatic degradation and *in vitro* biological properties of trimethylated chitosans. *Biomaterials*. 2009, 30:3129-3135.
- Vertozoni M, Fotaki N, Kostewicz E, Strippler E, Leuner C, Nicolaidis E, Dressman J, Reppas C. Dissolution media simulating the intraluminal composition of the small intestine: physiological issues and practical aspects. *J Pharma Pharmacol*. 2004, 56:453-462.
- Vertzoni M, Dressman J, Butler J, Hempenstall J, Reppas C. Simulation of fasting gastric conditions and its importance for the *in vivo* dissolution of lipophilic compounds. *Eur J Pharm Biopharm*. 2005, 60:413-417.
- Vlieghe P, Lisowski V, Martinez J, Khrestchatsky M. Synthetic therapeutic peptides: science therapeutic peptides: science and market. *Drug Discov Today*. 2010, 15:40-56.

- Vongchan P, Wutti-In Y, Sajomsang W, Gonil P, Kothan S, Linhardt RJ. *N,N,N*-trimethyl chitosan nanoparticles for the delivery of monoclonal antibodies against hepatocellular carcinoma cells. *Carbohydr Polym*. 2011, 85:215-220.
- Wang K, Xu X, Liu T, Fu S, Gou G, Gu Y, Luo F, Zhao X, Wei Y, Qian Z. Synthesis and characterization of biodegradable pH-sensitive hydrogel based on poly(ϵ -caprolactone), methacrylic acid, and Pluronic (L35). *Carb Polym*. 2010, 79:755-761.
- Wang K, Xu X, Wang Y, Yan X, Guo G, Huang M, Luo F, Zhao Z, Wei Y, Qian Z. Synthesis and characterization of poly(methoxyl ethylene glycol-caprolactone-co-methacrylic acid-co-poly(ethylene glycol) methyl ether methacrylate) pH-sensitive hydrogel for delivery of dexamethasone. *Int J Pharm*. 2010, 389:130-138.
- Wang W, Uzzau S, Goldblum SE, Fasano A. Human Zonulin, a potential modulator of intestinal tight junctions. *J Cell Sci*. 2000, 113:4435-4440.
- Ward PD, Tippin TK, Thakker DR. Enhancing paracellular permeability by modulating epithelial tight junctions. *Pharm Sci Technol Today*. 2000, 3:346-358.
- Westberg C, Benkestock K, Fatouros A, Svensson M, Sjöström B. Hexarelin evaluation of factors influencing oral bioavailability and ways to improve absorption. *J Pharm Pharmacol*. 2001, 53:1257-1264.
- Whitehead K and Mltragotri S. Mechanistic analysis of chemical permeation enhancers for oral delivery. *Pharm Res*. 2008, 25:1412-1419.
- Wiedmann TS and Kamel L. Examination of the solubilisation of drugs by bile salts micelles. *J Pharm Sci*. 2002, 91:1743-1764.
- Witzleb R, Müllertz A, Kanikanti V-R, Hamann H-J, Kleinebudde P. Dissolution of solid liquid extrudates in biorelevant media. *Int J Pharm*. 2013, 422:116-124.
- Wong V and Gumbiner BW. A synthetic peptide corresponding to the extracellular domain of occludin perturbs the tight junction permeability barrier. *J Cell Biol*. 1997, 136:399-409.
- Woodley JF. Enzymatic barriers for GI peptide and protein delivery. *Crit Rev Ther Drug*. 1994, 11:61-95.
- Woodley JF, Blanco-Mendez J, Kenworthy S. Cyclodextrins inhibit peptide degradation by intestinal brush border but not luminal enzymes. *Proc Control Release Soc*. 1994, 21:64-65.
- Wu CY and Benet LZ. Predicating drug disposition via application of BCS: Transport/absorption/elimination interplay and development of a biopharmaceutics drug disposition classification system. *Pharm Res*. 2005, 22:11-23.
- Xiong XY, Li QH, Li YP, Guo L, Li ZL, Gong YC. Pluronic P85/poly(lactic acid) vesicles as novel carrier for oral insulin delivery. *Colloids Surf B Biointerfaces*. 2013, doi: 10.1016/j.colsufb.2013.06.019.

- Xu T, Zhang N, Nichols HL, Shi D, Wen X. Modification of nanostructured materials for biomedical applications. *Mater Sci Eng C*. 2007, 27:579-594.
- Yamamoto AM, Tatsumi H, Maruyama M, Uchiyama T, Okada N, Fujita T, Modulation of intestinal delivery of poorly absorbable drugs. *J Pharmacol Exp Ther*. 2001, 296:84-90.
- Yan H, Zhao M, Zheng L. A hydrogel formed by cetylpyrrolidinium bromide and sodium salicylate. *Colloids Surf A:Physicochem Eng Aspects*. 2011, 392:205-212.
- Yang YM, Hu W, Wang XD, Gu XS. The controlled biodegradation of chitosan fibers by N-acetylation *in vitro* and *in vivo*. *J Mater Sci Mater Med*. 2007, 18:2117-2121.
- Yeaman MR and Yount NY. Mechanisms of antimicrobial peptide action and resistance. *Pharmacol Rev*. 2003, 55:27-55.
- Yeh T-H, Hsu L-W, Tseng MT, Lee P-L, Sonjae K, Ho Y-C, Sung H-W. Mechanism and consequence of chitosan-mediated reversible epithelial tight junction opening. *Biomaterials*. 2011, 32:6164-6173.
- Yin L, Ding J, He C, Cui L, Tang C, Yin C. Drug permeability and mucoadhesion properties of thiolated trimethyl chitosan nanoparticles in oral insulin delivery. *Biomaterials*. 2009, 30:5691-5700.
- Yomota C, Yoshii Y, Takahata T, Okada S. Separation of B-3 monodesamidoinulin from human human insulin by high-performance liquid chromatography under alkaline conditions. *J Chromatogr A*. 1996, 721:89-96.
- Yoshii F, Zhanshan Y, Isobe K, Shinozaki K, Makuuchi K. Electron beam cross-linked PEO and PEO/PVA hydrogels for wound dressing. *Radiat Phys Chem*. 1999, 55:133-138.
- Yu AS, Enck AH, Lencer WI, Scheenberger EE. Claudin-8 expression in Madin-Darby canine kidney cells augments the paracellular barrier to cation permeation. *J Biol Chem*. 2003, 278:17350-17359.
- Yushin G, Hoffman EN, Barsoum MW, Gogotsi Y, Howell CA, Sandeman SR, Phillips GJ. Mesoporous carbide-derived carbon with porosity tuned for efficient absorption of cytokines. *Biomaterials*. 2006, 27:5755-5762.
- Zhang N, Qineng P, Huang G, Xu W, Cheng Y, Han X. Lectin-modified solid lipid nanoparticles as carriers for oral administration of insulin. *Int J Pharm*. 2006, 327:153-159.
- Zhang Y, Huo M, Zhou J, Zo A, Li W, Yao, Xie S. DDSolver: an add-in program for modelling and comparison of drug dissolution profiles. *The AAPS journal*. 2010, 12:263-271.
- Zhang Y, Xue C, Li Z, Zhang Y, Fu X. Preparation of half deacetylated chitosan by forced penetration and its properties. *Carbohydr Polym*. 2006, 65:229-234.
- Zhao GH, Kapur N, Carlin B, Selinger E, Guthrie JT. Characterisation of the interactive properties of microcrystalline cellulose-carboxymethyl cellulose hydrogels. *Int J Pharm*. 2011, 415:95-101.

Zhu Q, Deng Y, Vanka P, Brown SJ, Muthusrishnan S, Kramer KJ. Acidic mammalian chitinase in asthmatic Th2 inflammation and IL-13 pathway activation. *Science*. 2006, 304:1678-1682.

Appendix 1

Animal Ethics Certificate

AESC3



STRICTLY CONFIDENTIAL

ANIMAL ETHICS SCREENING COMMITTEE (AESC)

CLEARANCE CERTIFICATE NO. 2011/33/03

APPLICANT: Mr A Hibbins

DEPARTMENT: Pharmacy and Pharmacology

PROJECT TITLE: *In vivo* evaluation of polymeric oral drug delivery systems
in Large White Pigs

Number and Species

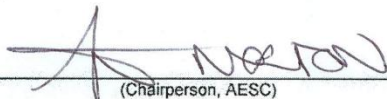
25 White pigs

Approval was given for the use of animals for the project described above at an AESC meeting held on **06 September 2011**. This approval remains valid until **06 September 2013**.

The use of these animals is subject to AESC guidelines for the use and care of animals, is limited to the procedures described in the application form and to the following additional conditions:

Condition 1 - The PI to discuss appropriate anaesthetic combination with CAS Director and provide details of any known side effects.

Signed: _____


(Chairperson, AESC)

Date: _____

19/09/2011

I am satisfied that the persons listed in this application are competent to perform the procedures therein, in terms of Section 23 (1) (c) of the Veterinary and Para-Veterinary Professions Act (19 of 1982)

Signed: _____


(Registered Veterinarian)

Date: _____

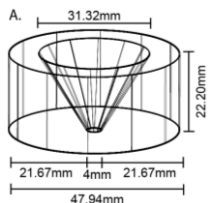
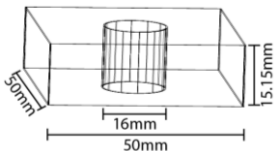
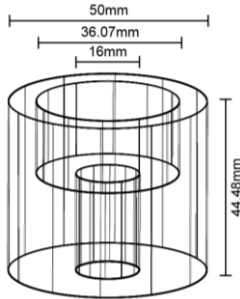
20/09/2011

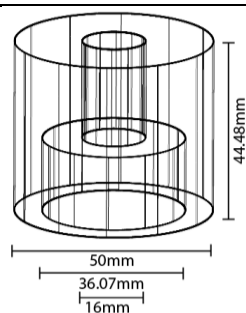
cc: Supervisor:
Director: CAS

Appendix 2

Punch and Die Mechanism Part Schematics

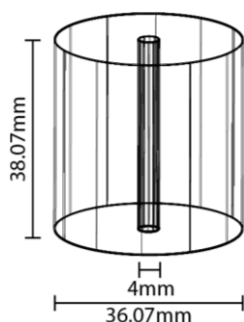
The punch and die mechanism was manufactured as a specialised tooling to produce mini-pellets with a diameter of 4cm and a variable length. In addition, the specialised mini-pellet punch and die mechanism allowed for variable compression force to be applied to the pellets which could be monitored using the hydraulic force gauge which was utilised to generate mini-pellets under a uniform pressure. The punch and die mechanism was manufactured from stainless steel so that the mechanism could be cleaned easily. The punch and die mechanism contains seven parts that assemble into a complete unit that can be used with any table top tableting press. Each part is represented within the schematics below with the appropriate size.

Punch and Die Mechanism	
Part and schematic	Function
<p>Stainless steel funnel</p> 	<p>Stainless steel funnel was designed and manufactured to allow accurately weighted powders to be dispensed within the die.</p>
<p>Stainless steel base plate</p> 	<p>Stainless steel base plate was designed and manufactured to allow stabilisation of the bottom punch after the punch and die mechanism had been assembled</p>
<p>Stainless steel bottom sheath</p> 	<p>Stainless steel bottom sheath was designed and manufactured to allow stabilisation of the bottom punch and die after the punch and die mechanism had been assembled</p>
<p>Stainless steel top sheath</p>	



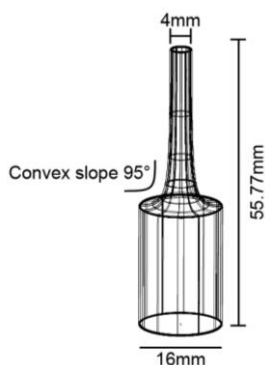
Stainless steel top sheath was designed and manufactured to allow stabilisation of the top punch and die after the punch and die mechanism had been assembled

Stainless steel die



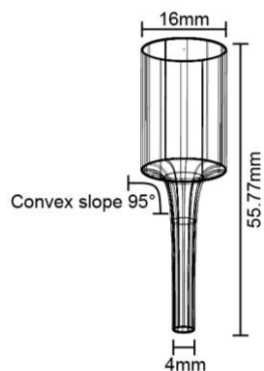
Stainless steel die was designed and manufactured to allow production of mini-pellets at varying lengths.

Stainless steel bottom punch



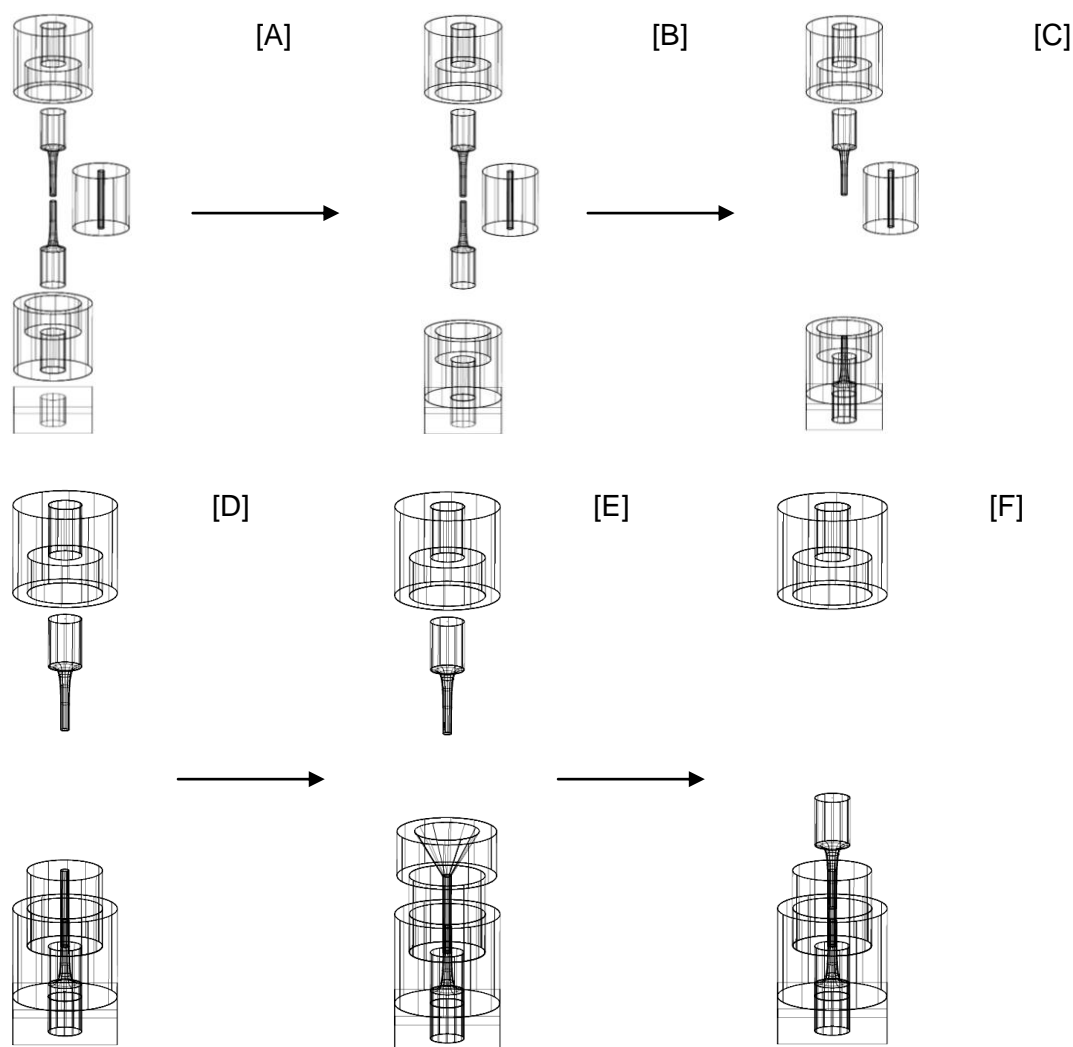
Stainless steel bottom punch was designed and manufactured to allow production of mini-pellets at varying lengths.

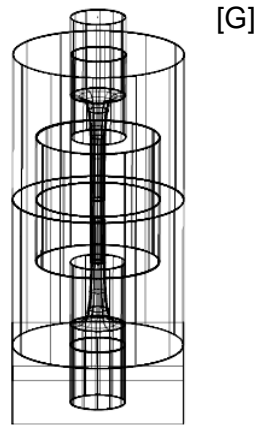
Stainless steel top punch



Stainless steel top punch was designed and manufactured to allow production of mini-pellets at varying lengths.

The punch and die mechanism was assembled as represented in the schematics below. Each part was precisely cut and measured so that each component fitted within the the assembly to generate an air tight seal (prevention of contaminatnes once the punch and die mechanism was assembled). The punch and die parts were first aligned [A]. The bottom sheath was placed on top of the base plate as the structural support for the mechanism [B]. The bottom punch was inserted into the base plate and bottom sheath which effectively “locked” the components together [C]. The die was fitted over the bottom punch and within the bottom sheath [D]. The punch and die at this point would be ready for the addition of a powder formulation that was poured through the funnel to prevent the loss of any powder [E]. The funnel would be removed and the top punch inserted into the die [F]. Finally the top sheath would be fitted over the die to generate an airtight seal and to stabilise the top punch against the compression force exerted by the tableting press [G]. The punch and die mechanism would be placed within a table press, exposed to the desired compression (under 1 metric tonns) and the mini-pellet would thereafter be retrieved by disassembling the punch and die.

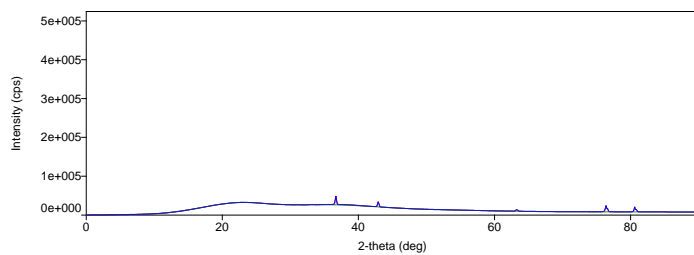




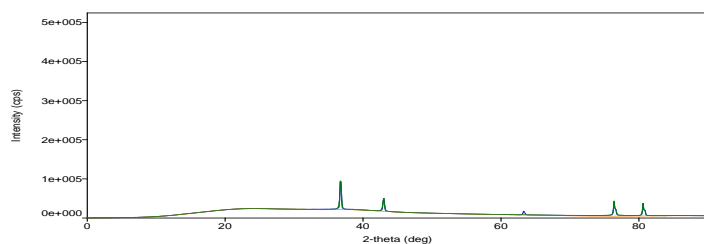
Appendix 3

Powdered X-Ray Diffraction of Hydrogel Formulations

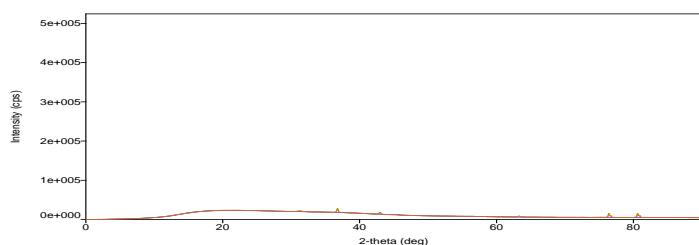
Hydrogel Formulation 1



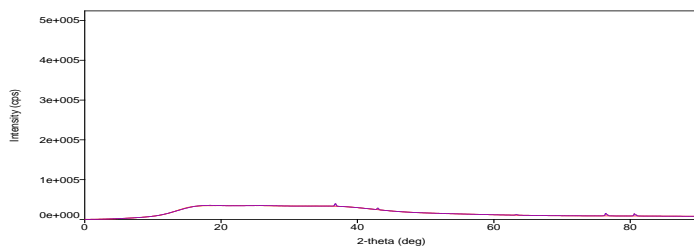
Hydrogel Formulation 2



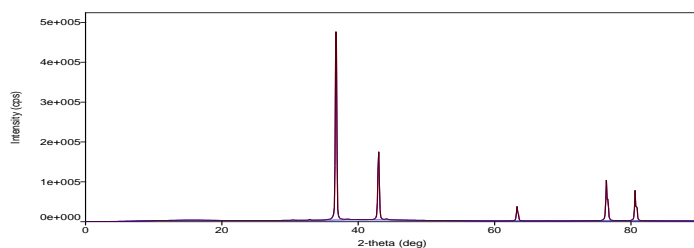
Hydrogel Formulation 3



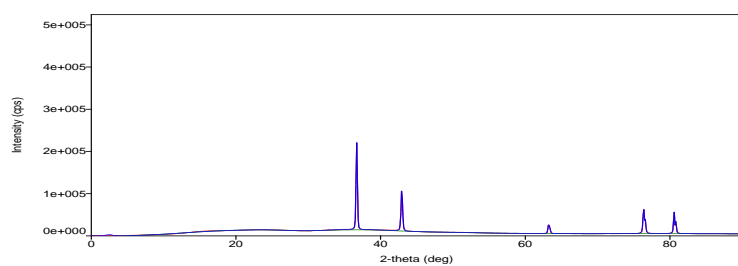
Hydrogel Formulation 4



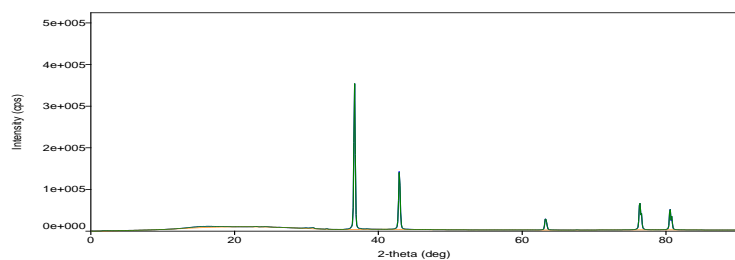
Hydrogel Formulation 5



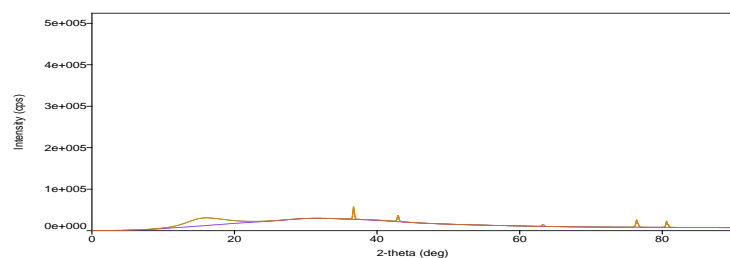
Hydrogel Formulation 6



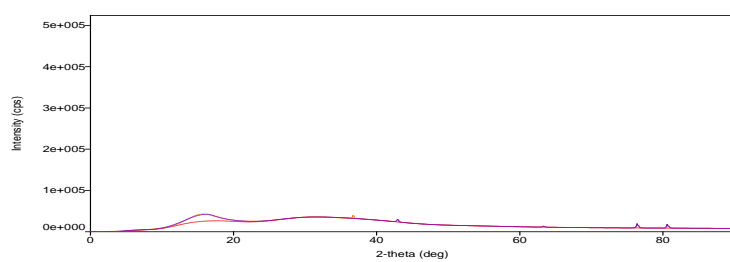
Hydrogel Formulation 7



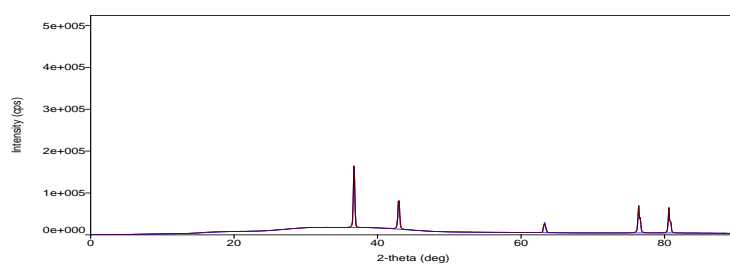
Hydrogel Formulation 8



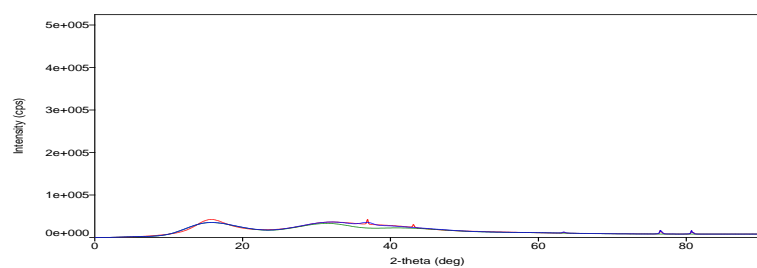
Hydrogel Formulation 9



Hydrogel Formulation 10



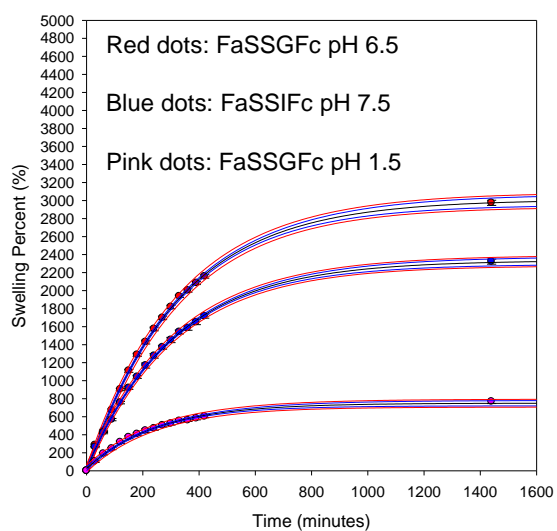
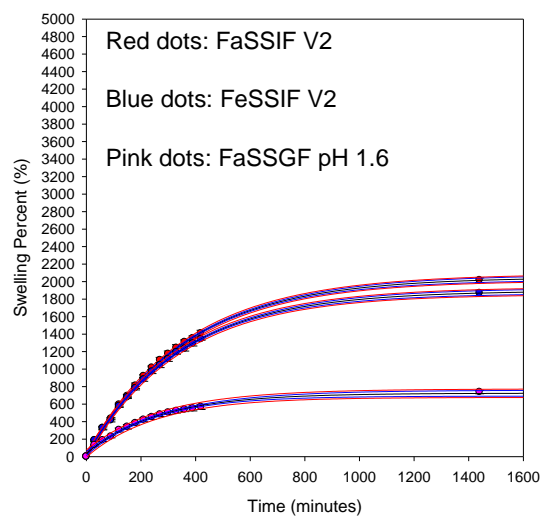
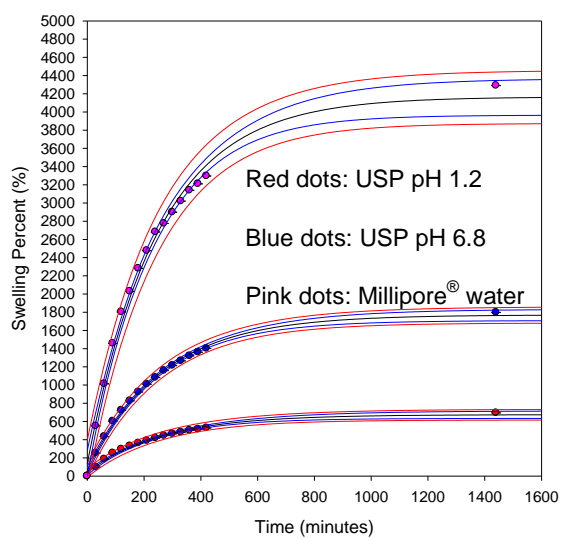
Hydrogel Formulation 11



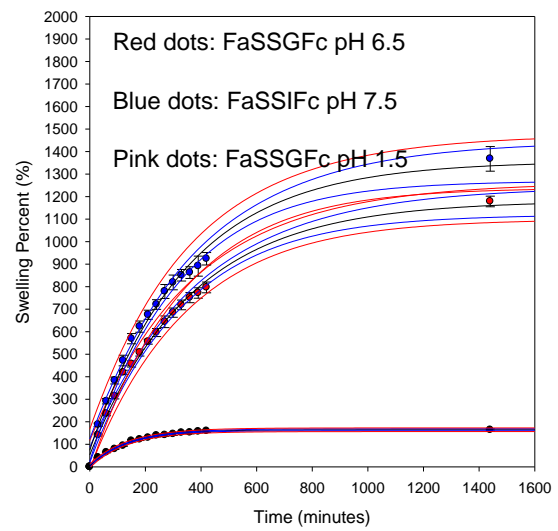
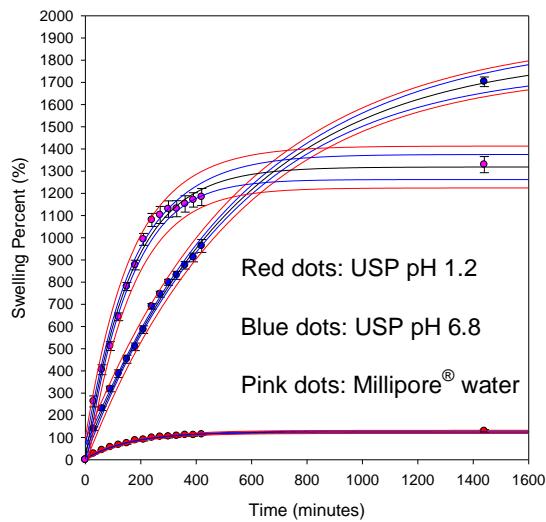
Appendix 4

Gravimetric swelling studies of the stimuli responsive hydrogel in biorelevant media

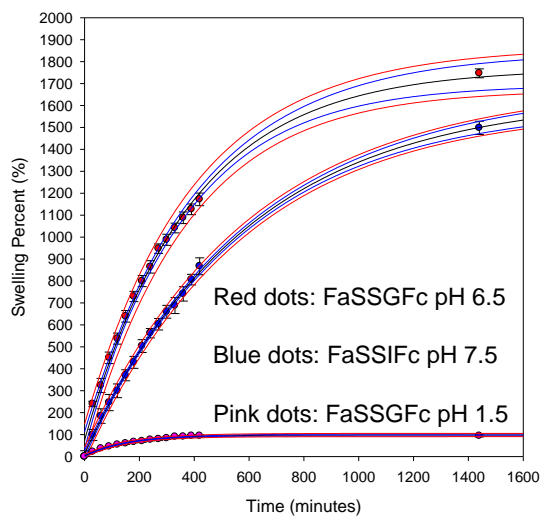
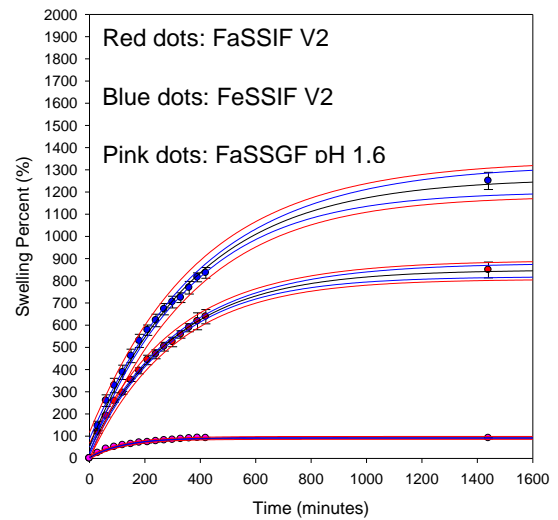
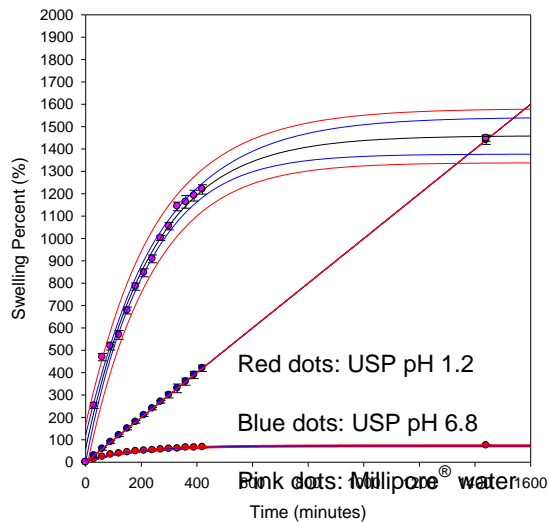
Hydrogel Formulation 2



Hydrogel Formulation 6

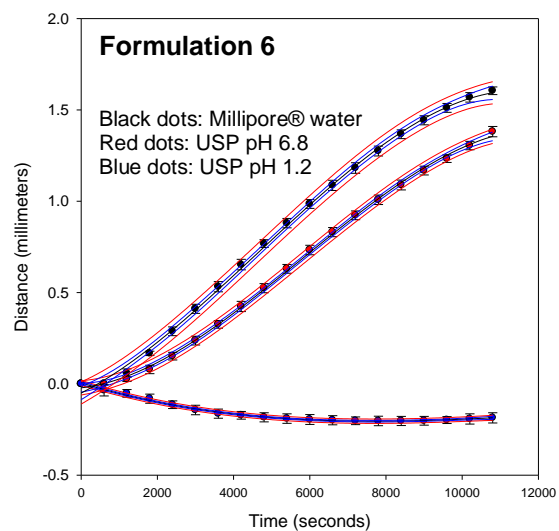
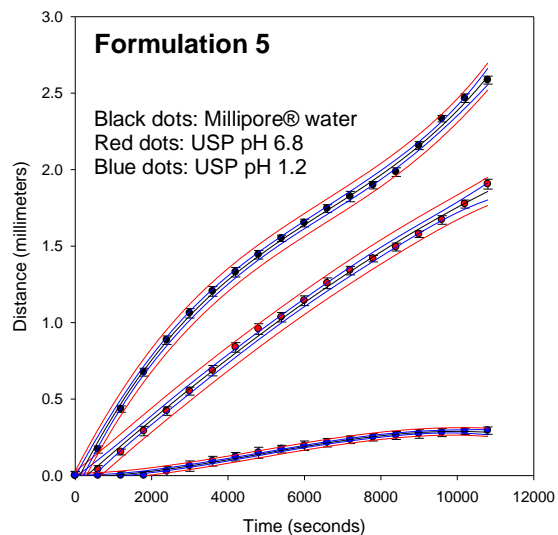
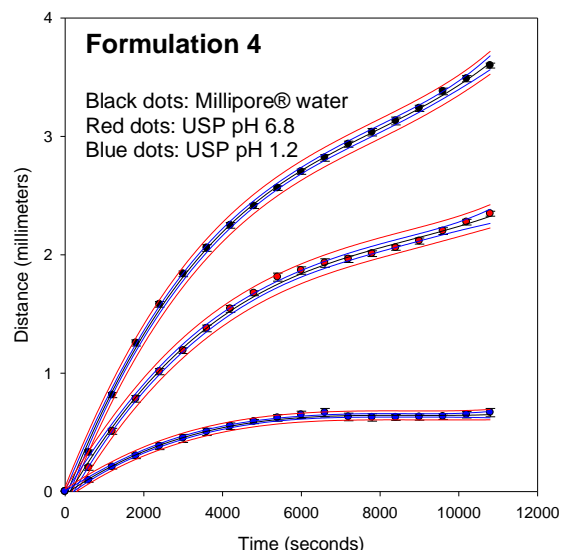
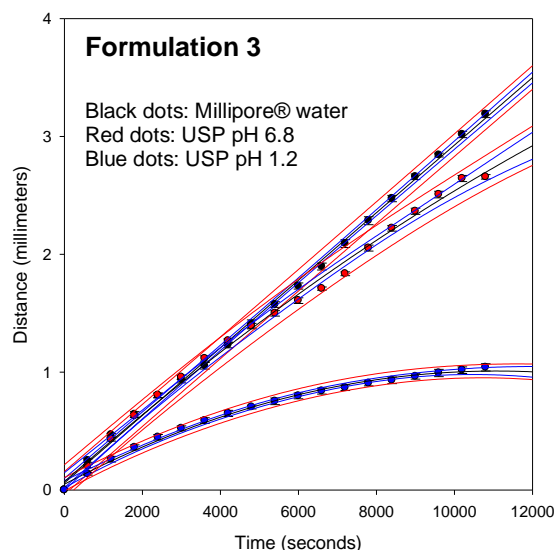
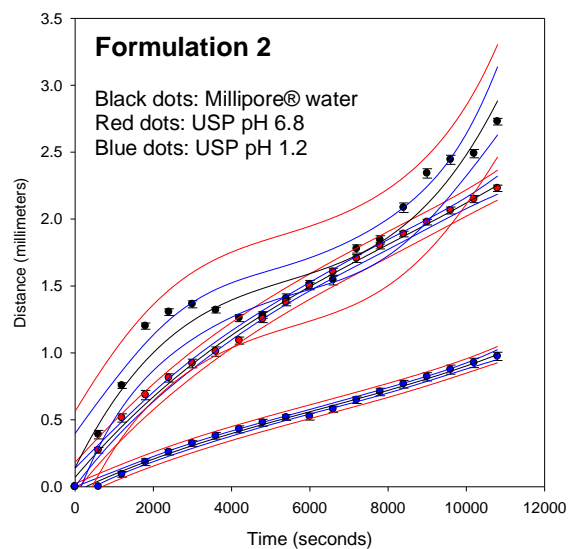
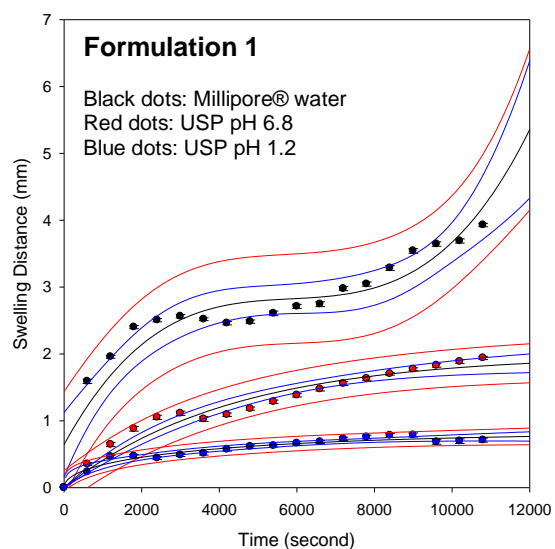


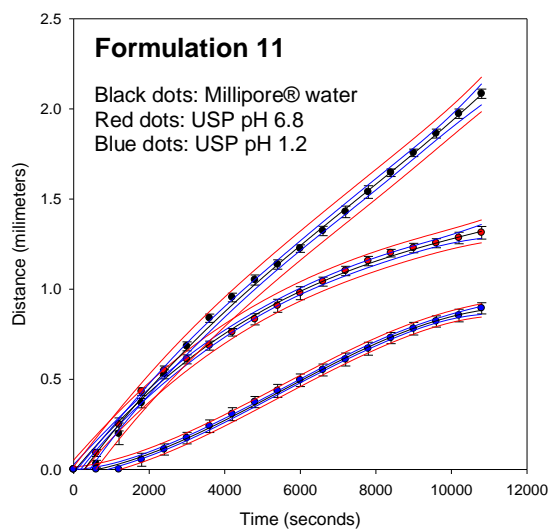
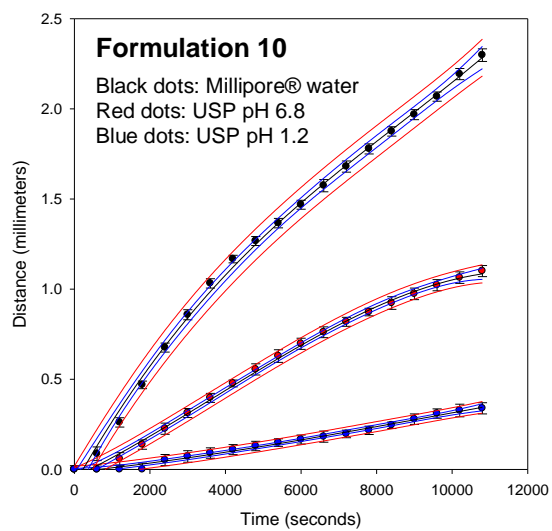
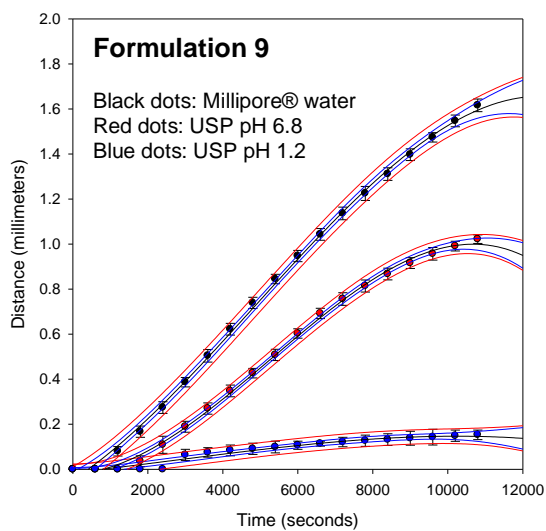
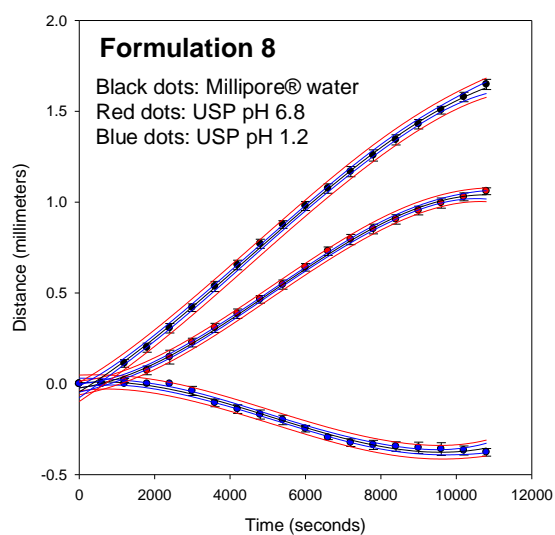
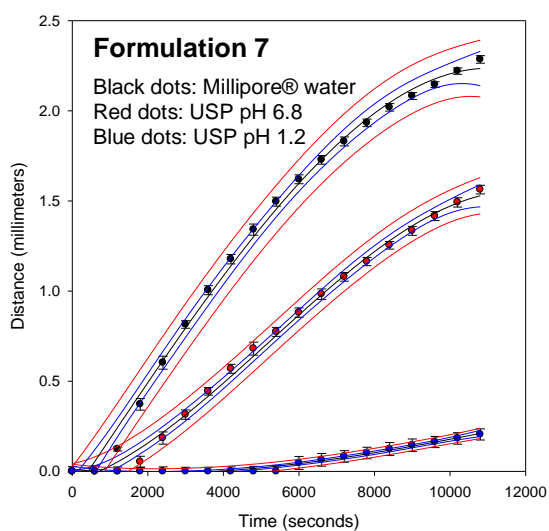
Hydrogel Formulation 8



Appendix 5

Distance-Time Studies of the Stimuli Responsive Hydrogel against a Constant Force of 0.01 N

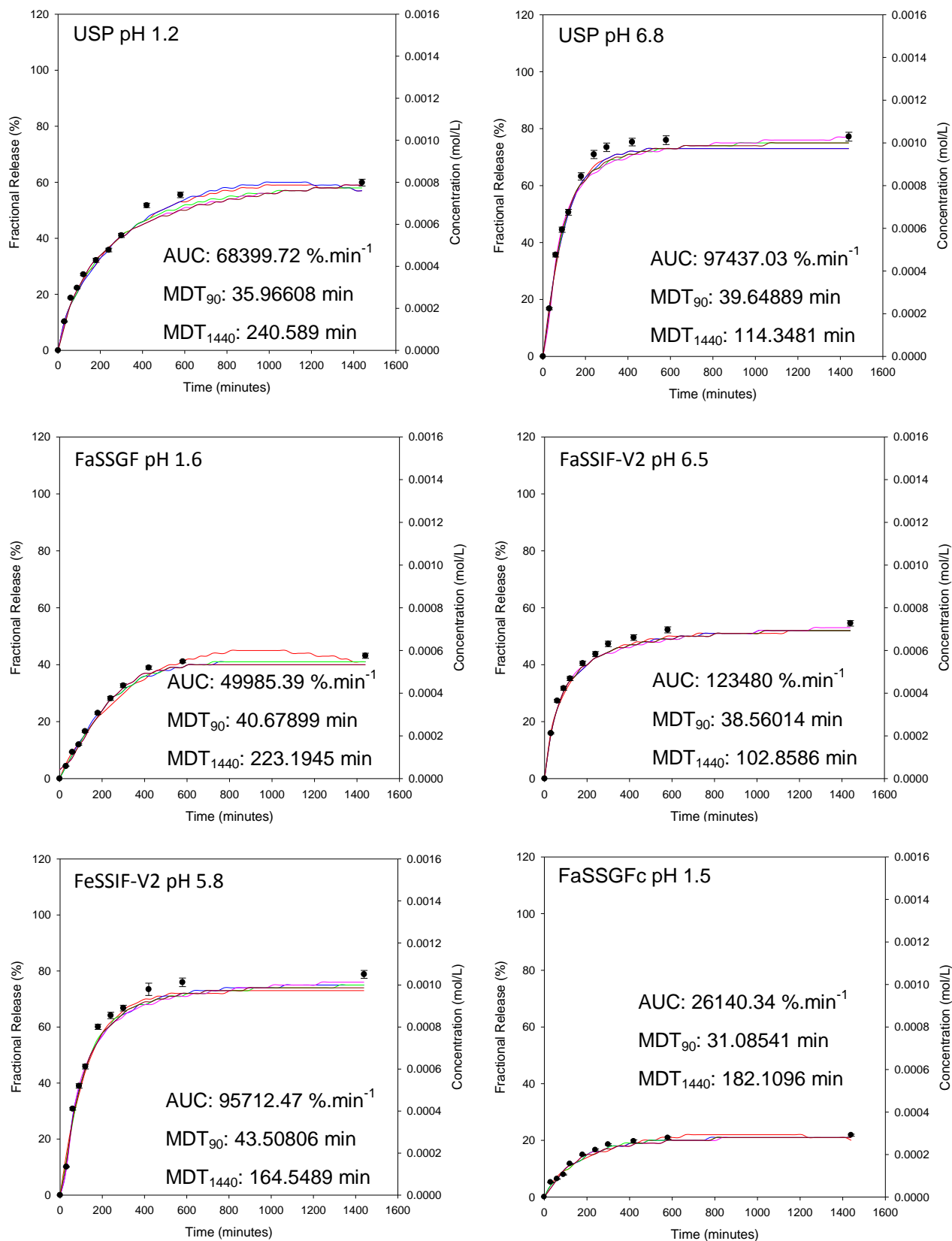


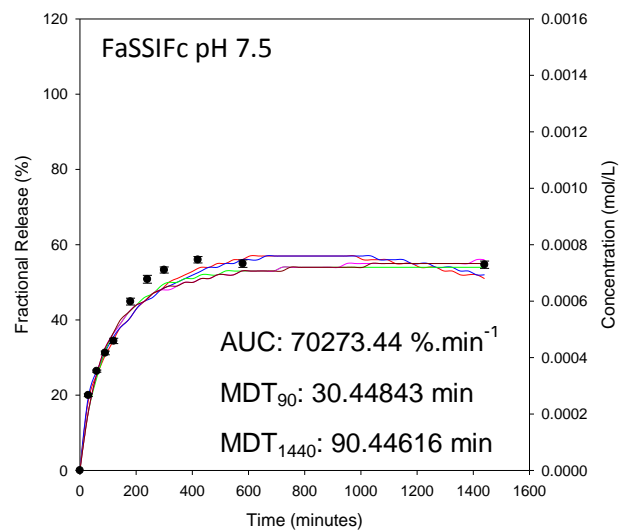
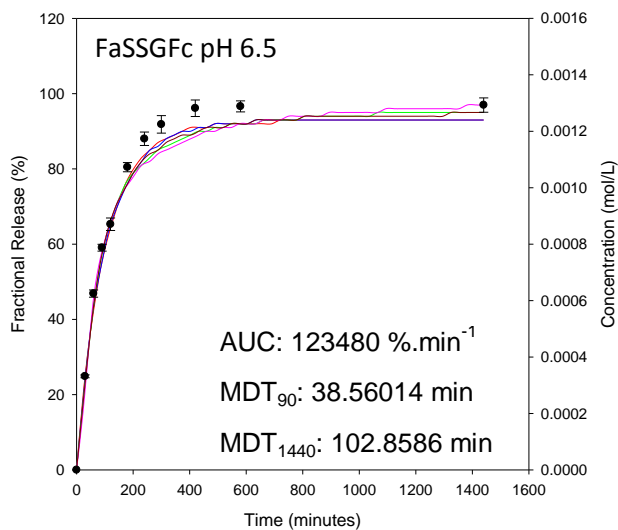


Appendix 6

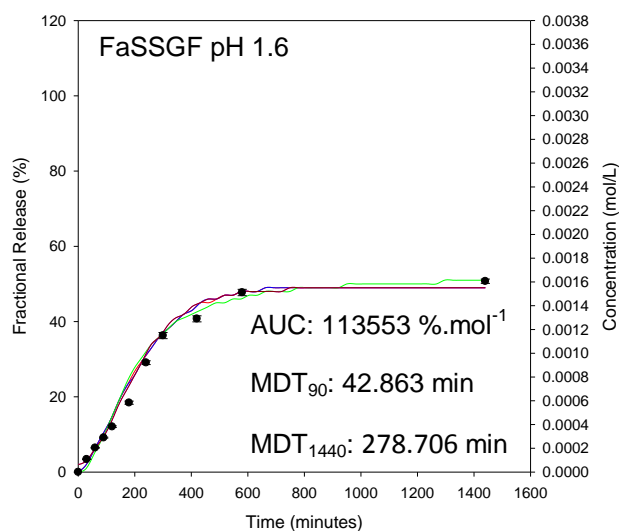
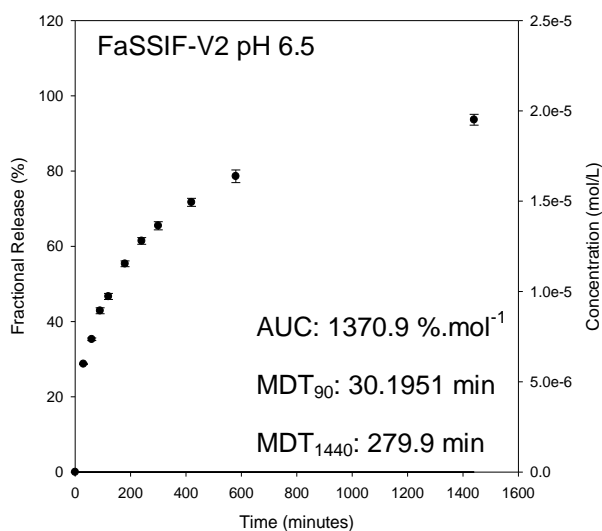
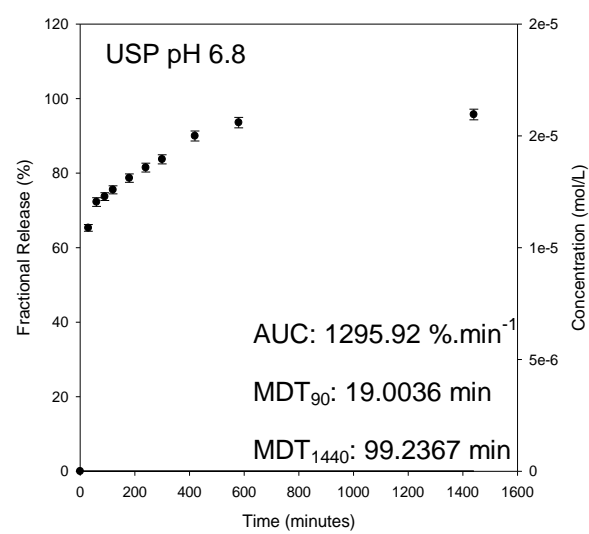
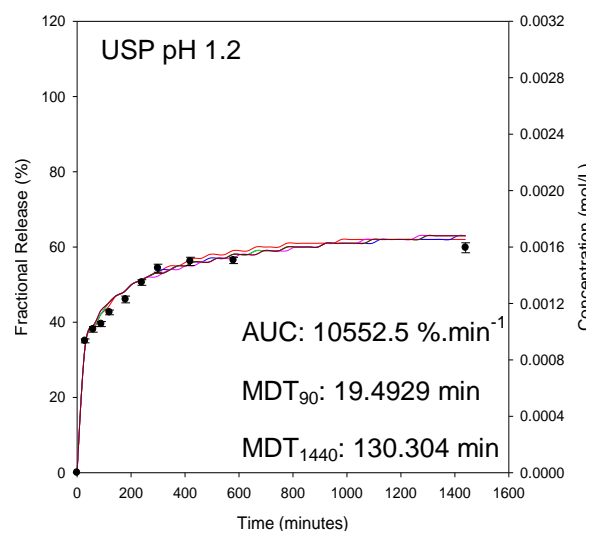
Drug Dissolution of 4-Aminosalicylic Acid within Biorelevant Dissolution Fluid and USP Dissolution Fluid

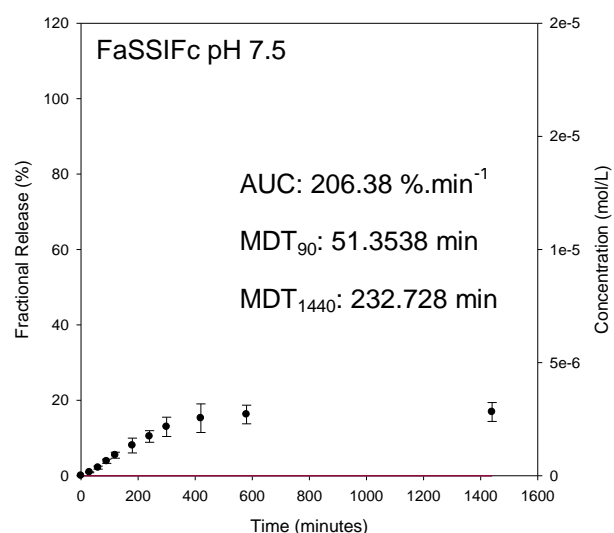
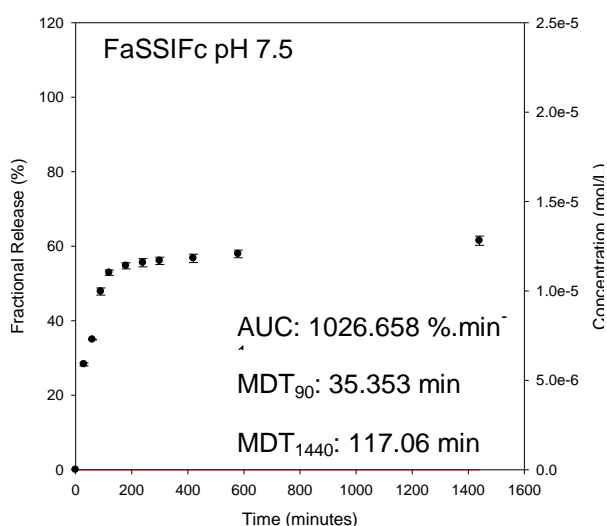
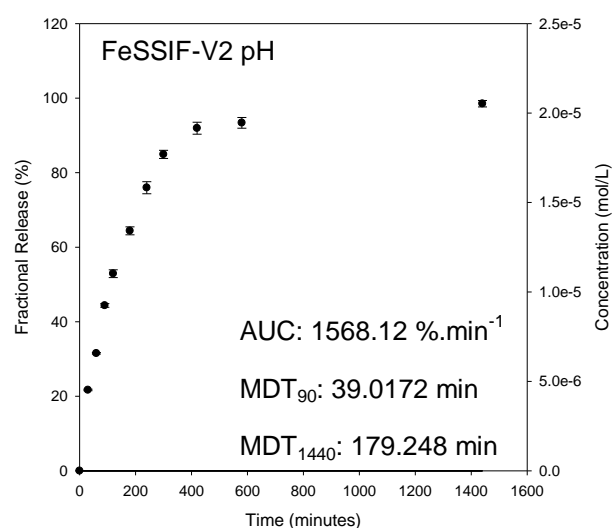
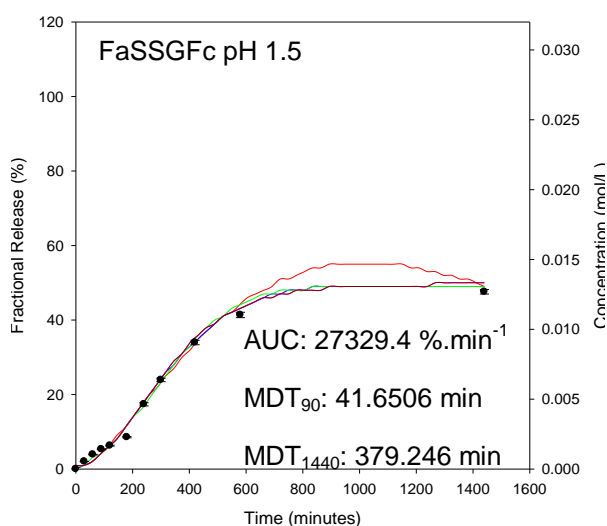
4-Aminosalicylic Acid



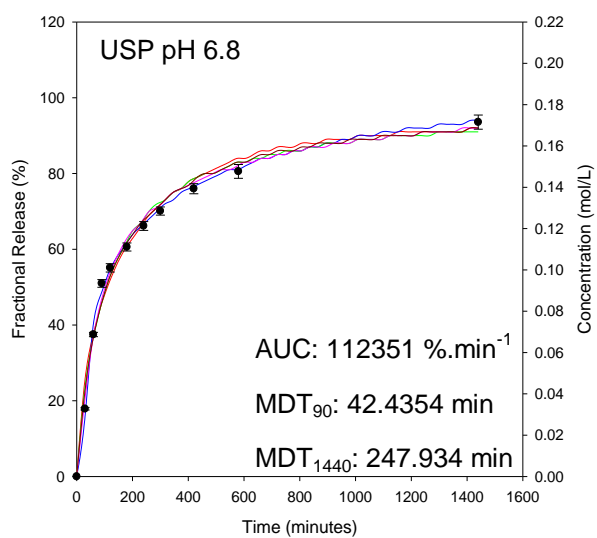
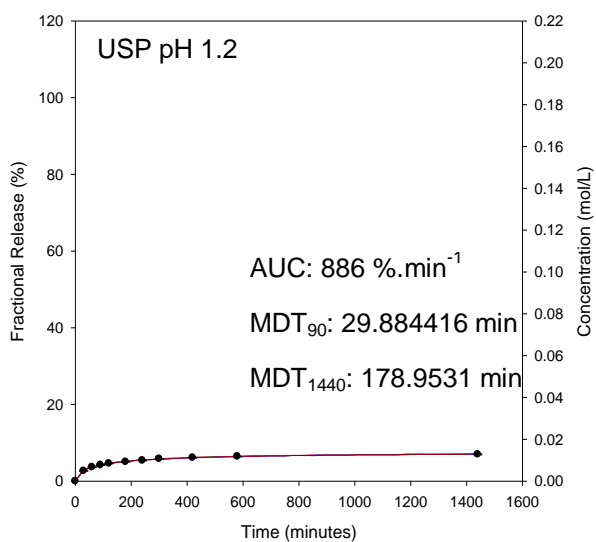


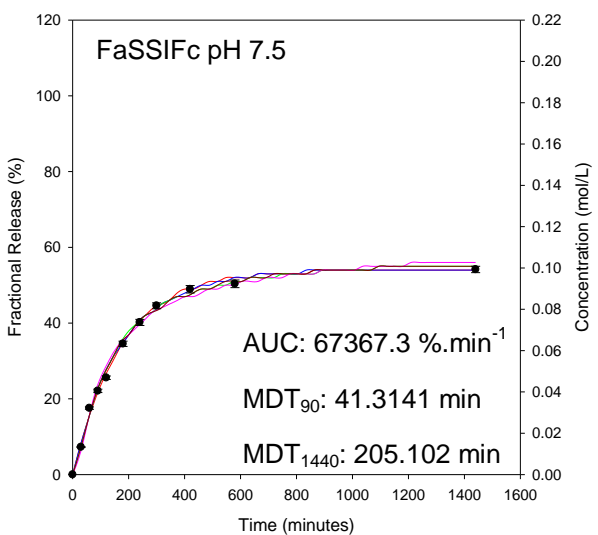
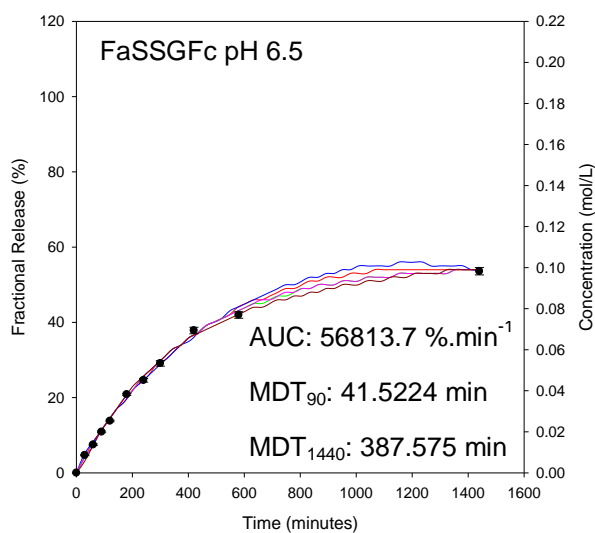
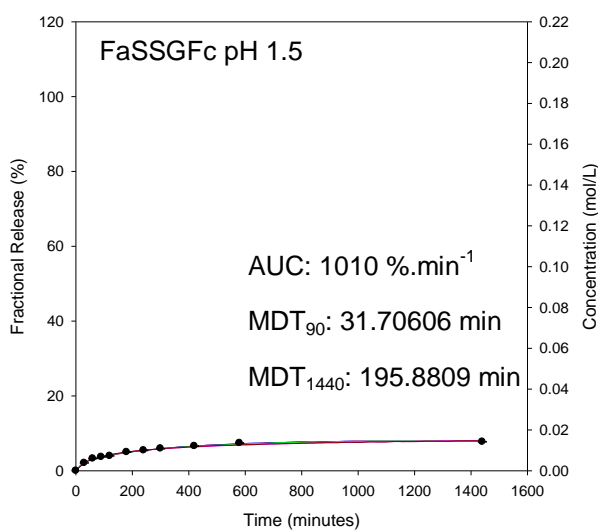
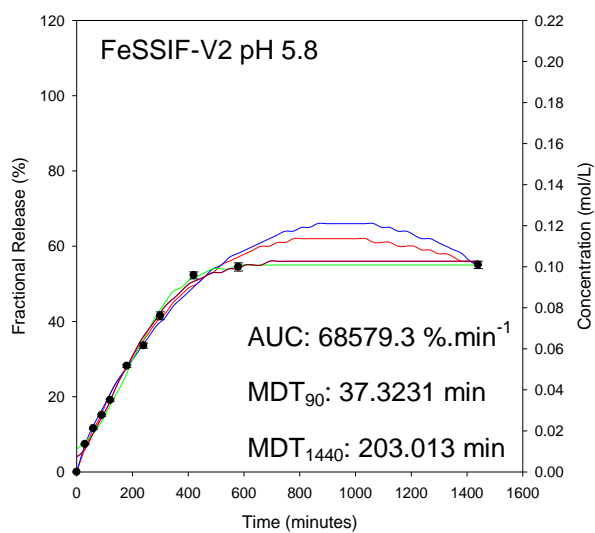
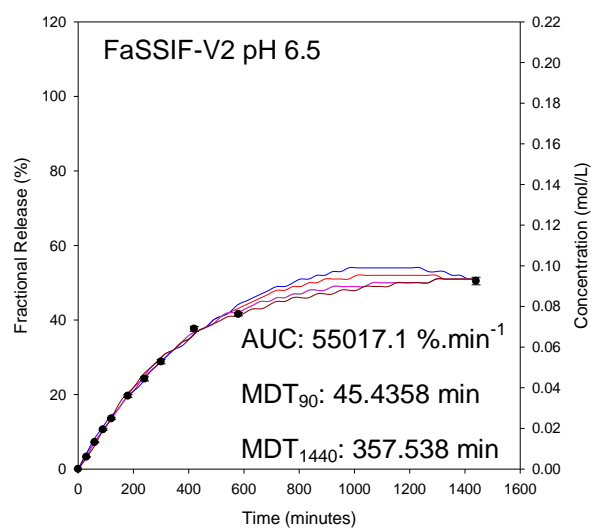
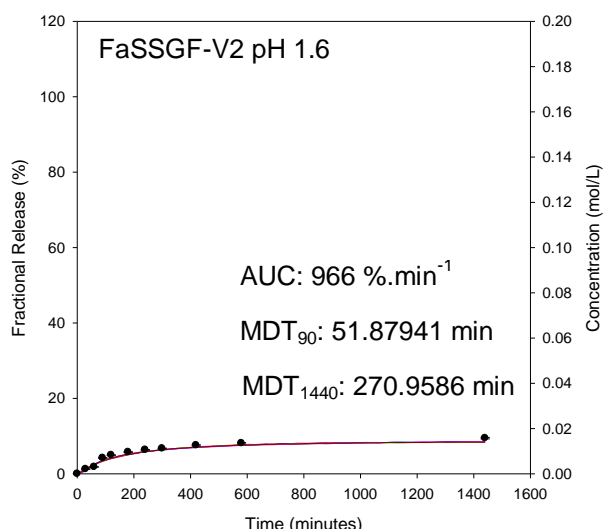
Ciprofloxacin



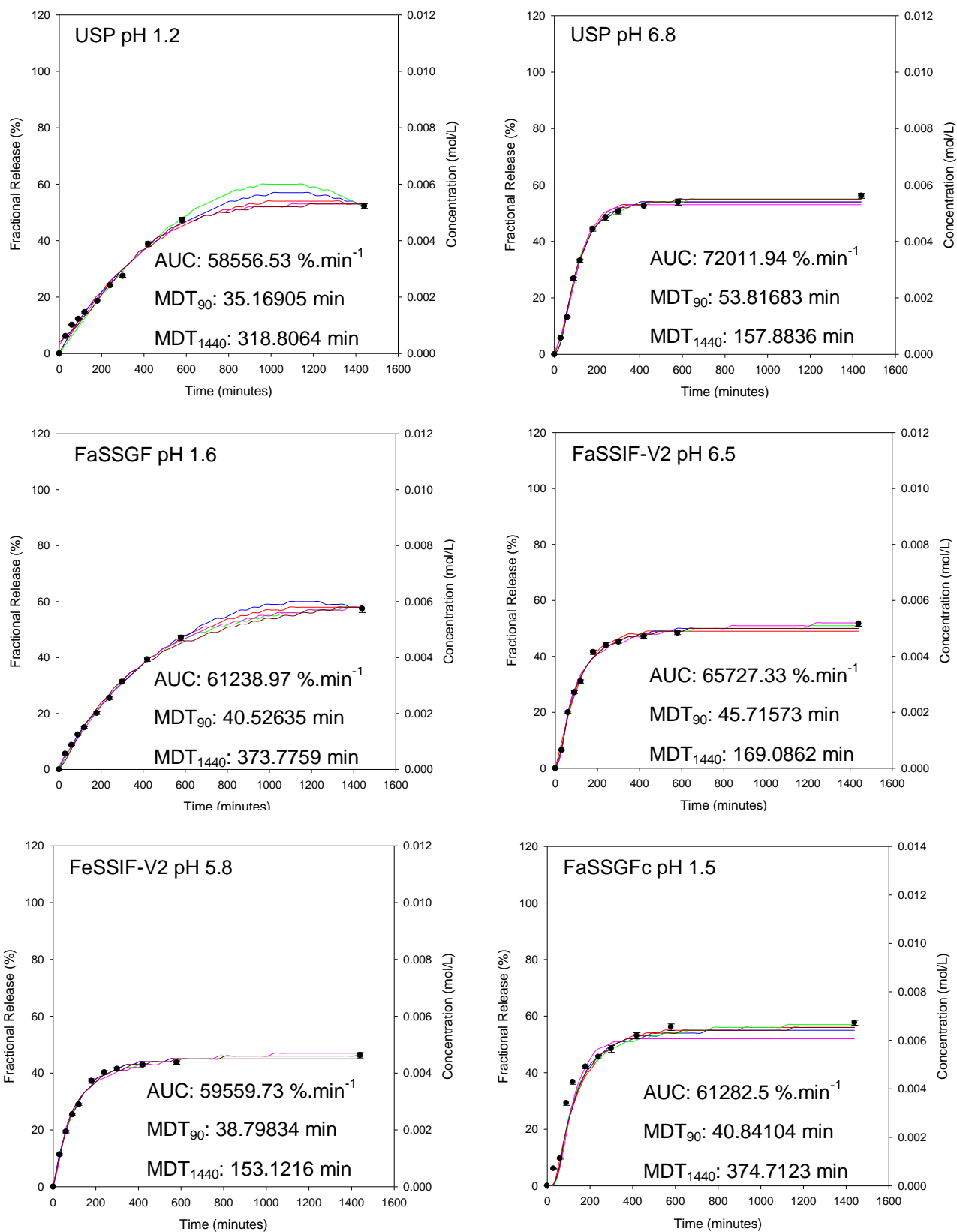


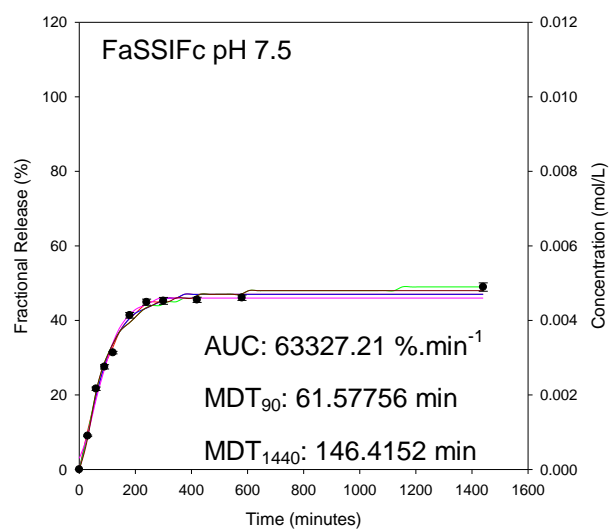
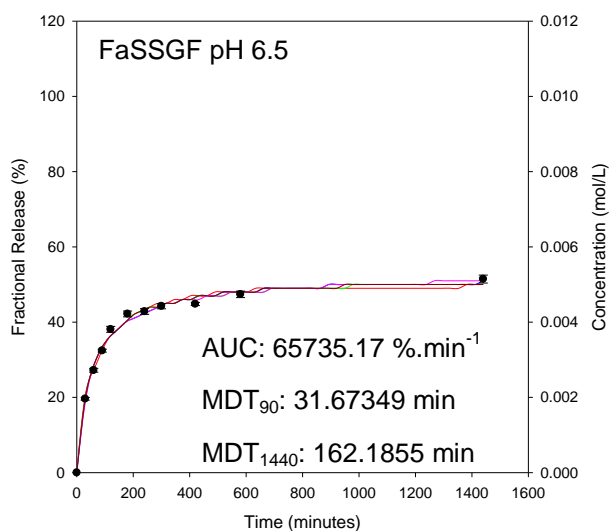
Indomethacin



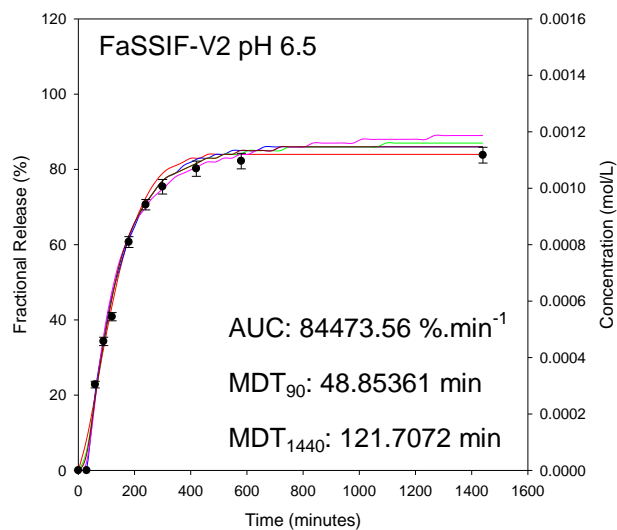
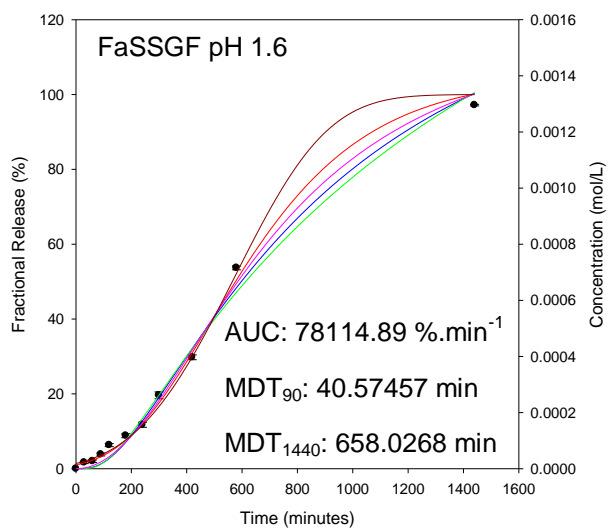
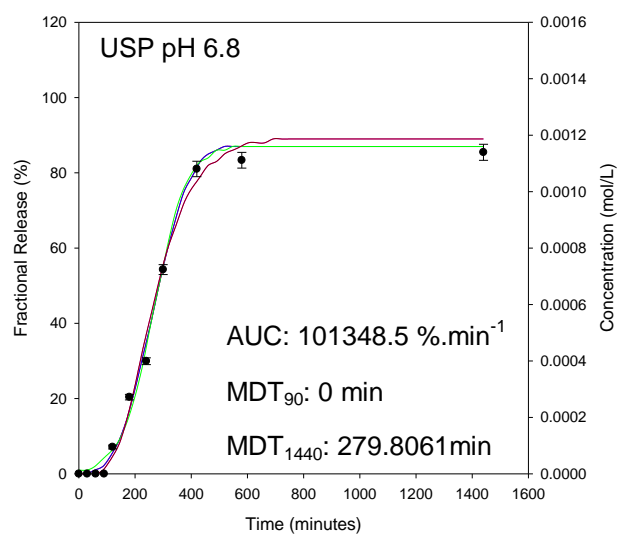
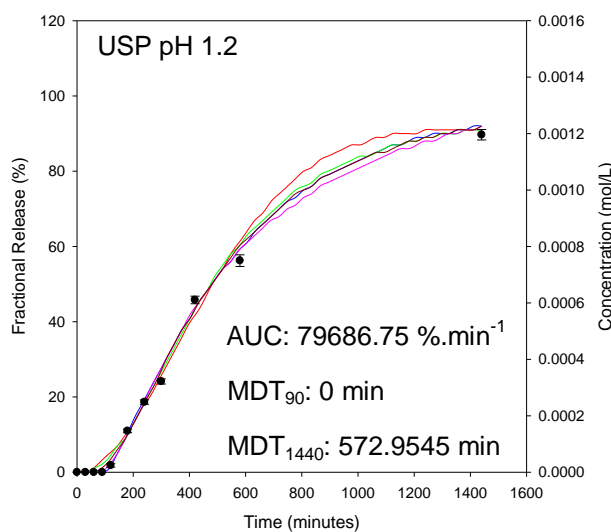


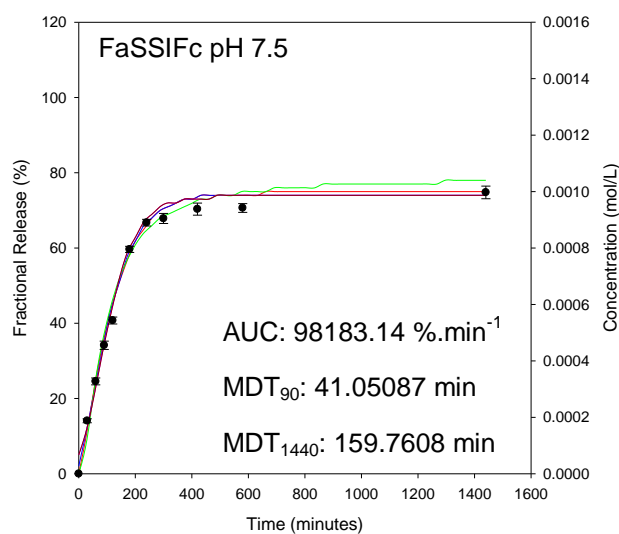
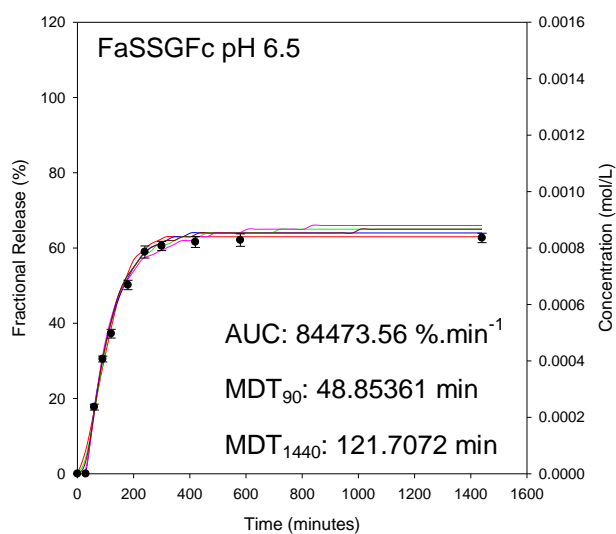
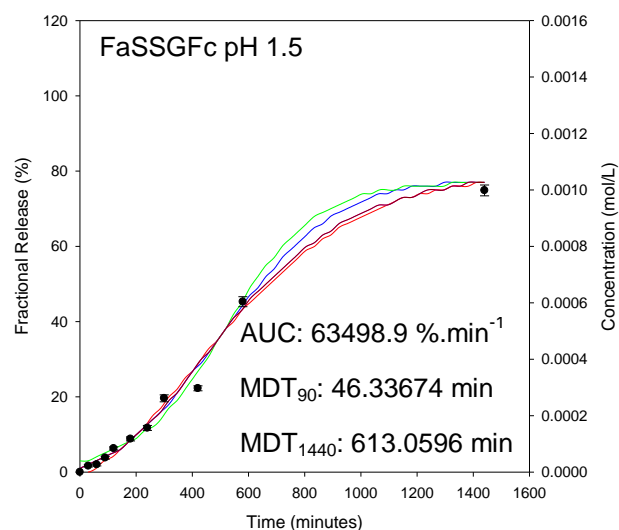
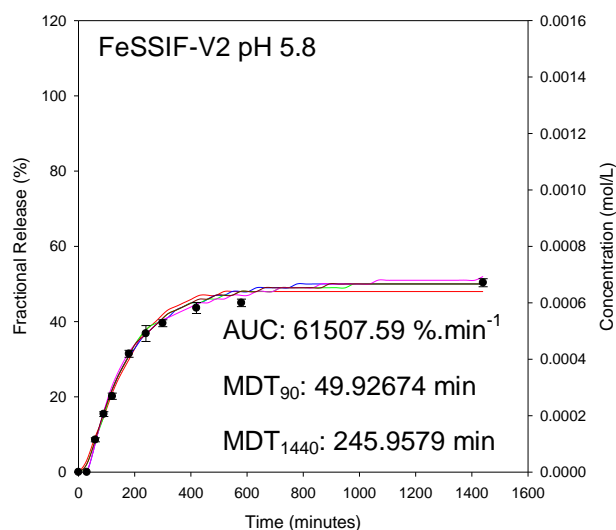
Metronidazole



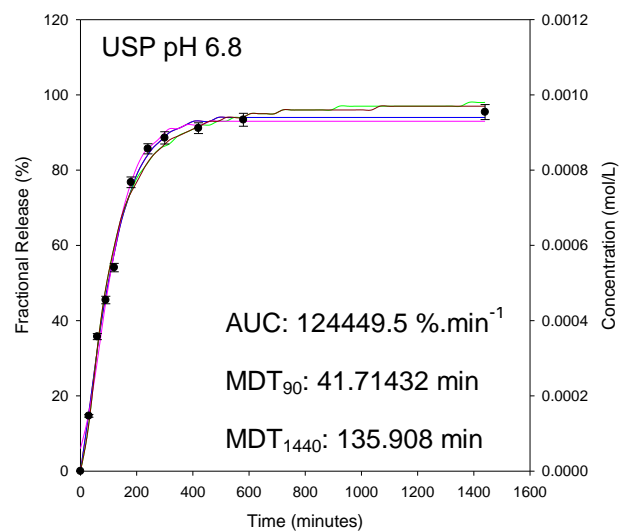
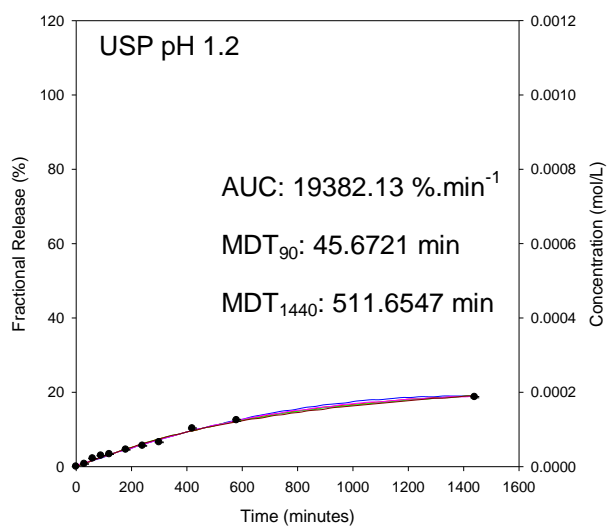


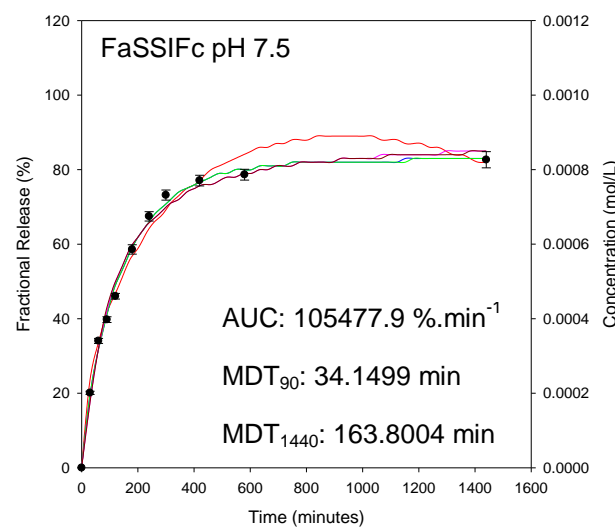
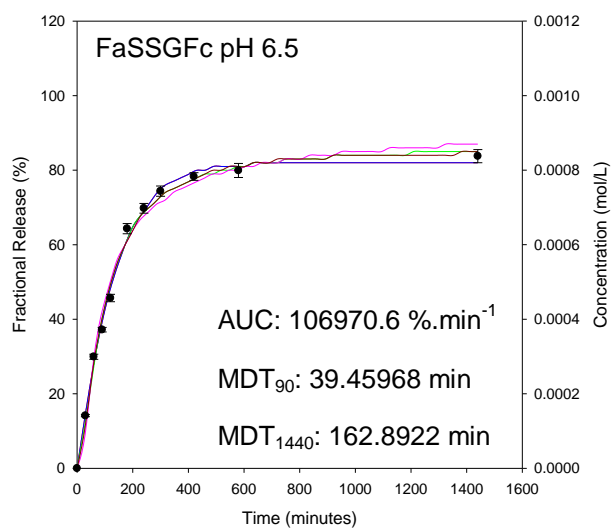
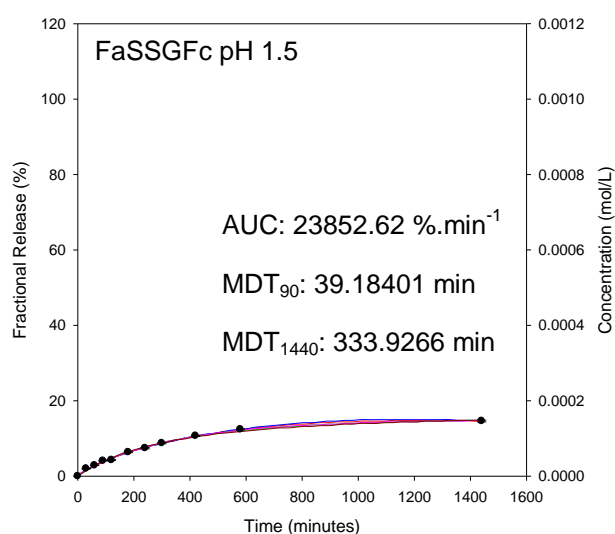
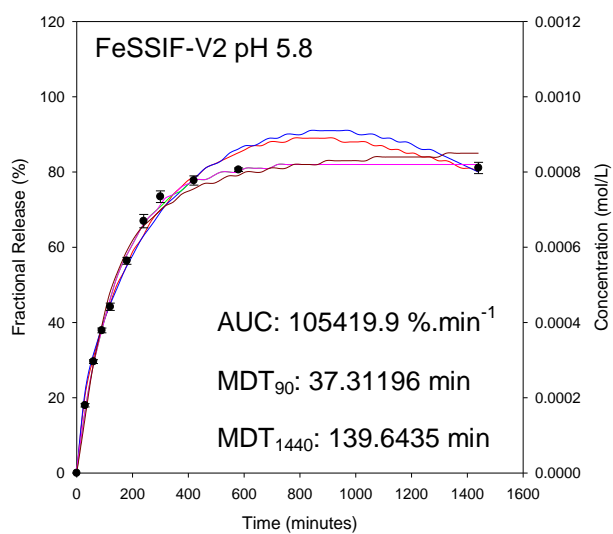
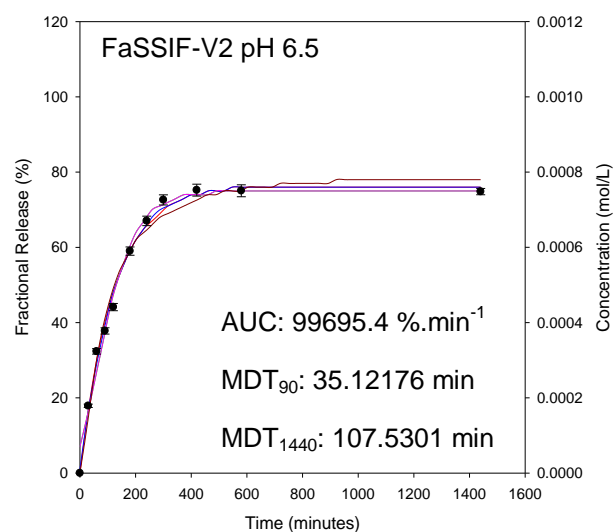
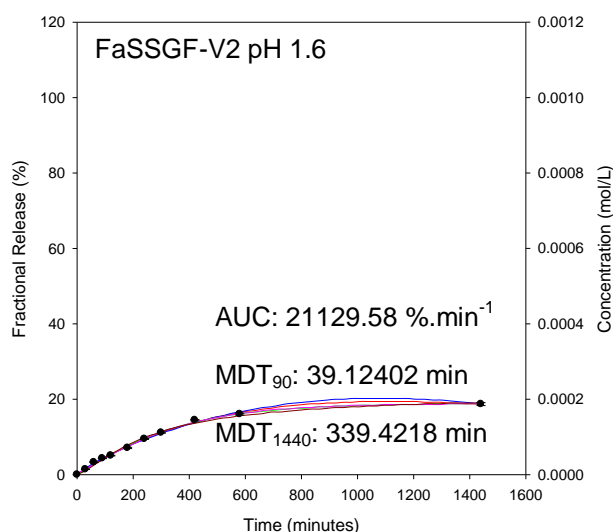
Sulfamethoxazole





Zidovudine





Appendix 7

Dissolution Modeling of the Stimuli Responsive Hydrogel

4-Aminosalicylic acid		
Model	Equation	R ² adjusted
USP pH 1.2		
Peppas-Sahlin	$y = 0.012t^{0.662}$	0.9944
USP pH 6.8		
Weibull	$y = 0.731 \left(1 - e^{\frac{(t^{1.041})}{125.795}} \right)$	0.9971
FaSSGF pH 1.6		
Weibull	$y = 0.412 \left(1 - e^{\left(\frac{-((t+5.85)^{1.222})}{770.803} \right)} \right)$	0.9985
FaSSIF V2		
Weibull	$y = 0.529 \times \left(1 - e^{\left(\frac{-((t-14.945)^{0.567})}{13.543} \right)} \right)$	0.9985
FeSSIF V2		
Weibull	$y = 0.752 \times \left(1 - e^{\left(\frac{-((t-23.537)^{0.702})}{26.698} \right)} \right)$	0.997
FaSSGFc pH 1.5		
Weibull	$y = 0.207 \times \left(1 - e^{\frac{(t^{0.966})}{139.047}} \right)$	0.989
FaSSGFc pH 6.5		
Weibull	$y = 0.927 \times \left(1 - e^{\frac{(t^{0.956})}{81.628}} \right)$	0.9982
FaSSIFc pH 7.5		
Weibull	$y = 0.54 \times \left(1 - e^{\frac{(t^{0.829})}{47.437}} \right)$	0.9844
Ciprofloxacin		
Model	Equation	R ² adjusted
Isolated gastric fluids		
Peppas-Sahlin	$y = 6.215t^{0.5} - 0.098t$	0.9906
Isolated intestinal fluids		
Weibull	$y = 60.822 \times \left(1 - e^{\frac{-(t+21.652)^{1.412}}{3461.141}} \right)$	0.9943
USP pH 1.2		
Weibull	$y = 0.492 \left(1 - e^{\frac{(t^{1.457})}{2949.932}} \right)$	0.9991

FaSSGF		
Gompertz	$y = 0.923e^{(-e^{(-0.008(t-165.375))})}$	0.9943
FaSSGFC pH 1.6		
Logistic	$y = 0.744 \times \frac{e^{(-4.547+2.907 \log(t))}}{(1 + e^{(-4.547+2.907 \log(t))})}$	0.9851
Indomethacin		
Model	Equation	R ² adjusted
USP pH 1.2		
Weibull	$y = 0.736 \times \left(1 - e^{\left(\frac{-((t-9.304)^{0.457})}{8.743}\right)}\right)$	0.9996
USP pH 6.8		
Weibull	$y = 1.080 \times \left(1 - e^{\left(\frac{-((t-27.047)^{0.392})}{8.45}\right)}\right)$	0.9972
FaSSGF pH 1.6		
Gompertz	$y = 0.973 \times e^{(-2.313e^{(-1.708 \log(t))})}$	0.9845
FaSSIF-V2		
Weibull	$y = 0.512 \times \left(1 - e^{\left(\frac{(t^{1.114})}{665.844}\right)}\right)$	0.9987
FeSSIF		
Makoid-Banakar	$y = 0.002 \times t^{0.962} \times e^{(-0.001t)}$	0.9935
FaSSGFC pH 1.5		
Gompertz	$y = 0.973 \times e^{(-29.313e^{(-1.708 \log(t))})}$	0.9845
FaSSGFC pH 6.5		
Weibull	$y = 0.554 \times \left(1 - e^{\left(\frac{(t^{1.024})}{445.089}\right)}\right)$	0.998
FaSSIFc pH 7.5		
Weibull	$y = 0.541 \times \left(1 - e^{\left(\frac{(t^{0.985})}{160.972}\right)}\right)$	0.9966
Metronidazole		
Model	Equation	R ² adjusted
USP pH 1.2		
Peppas-Sahlin	$y = 0.002t^{0.906}$	0.9911
USP pH 6.8		
Logisitic	$y = 0.557 \times \frac{e^{(-9.58+4.819 \log(t))}}{(1 + e^{(-9.58+4.819 \log(t))})}$	0.9974
FaSSGF pH 1.6		

Peppas-Sahlin	$y = 0.002t^{0.874}$	0.999
FaSSIF V2		
Probit	$y = 0.509 \times \Phi(-4.542 + 2.365 \log(t))$	0.996
FeSSIF V2		
Weibull	$y = 0.45 \times \left(1 - e^{\frac{(t^{0.963})}{91.606}}\right)$	0.9967
FaSSGFC pH 1.5		
Gompertz	$y = 0.684 \times e^{(-328.364e^{(-3.079 \log(t))})}$	0.9809
FaSSGFC pH 6.5		
Logistic	$y = 0.524 \times \frac{e^{(-3.948+2.3 \log(t))}}{(1 + e^{(-3.948+2.3 \log(t))})}$	0.9942
FaSSIFc pH 7.5		
Weibull	$y = 0.47 \times \left(1 - e^{\frac{(t^{1.173})}{222.32}}\right)$	0.9927

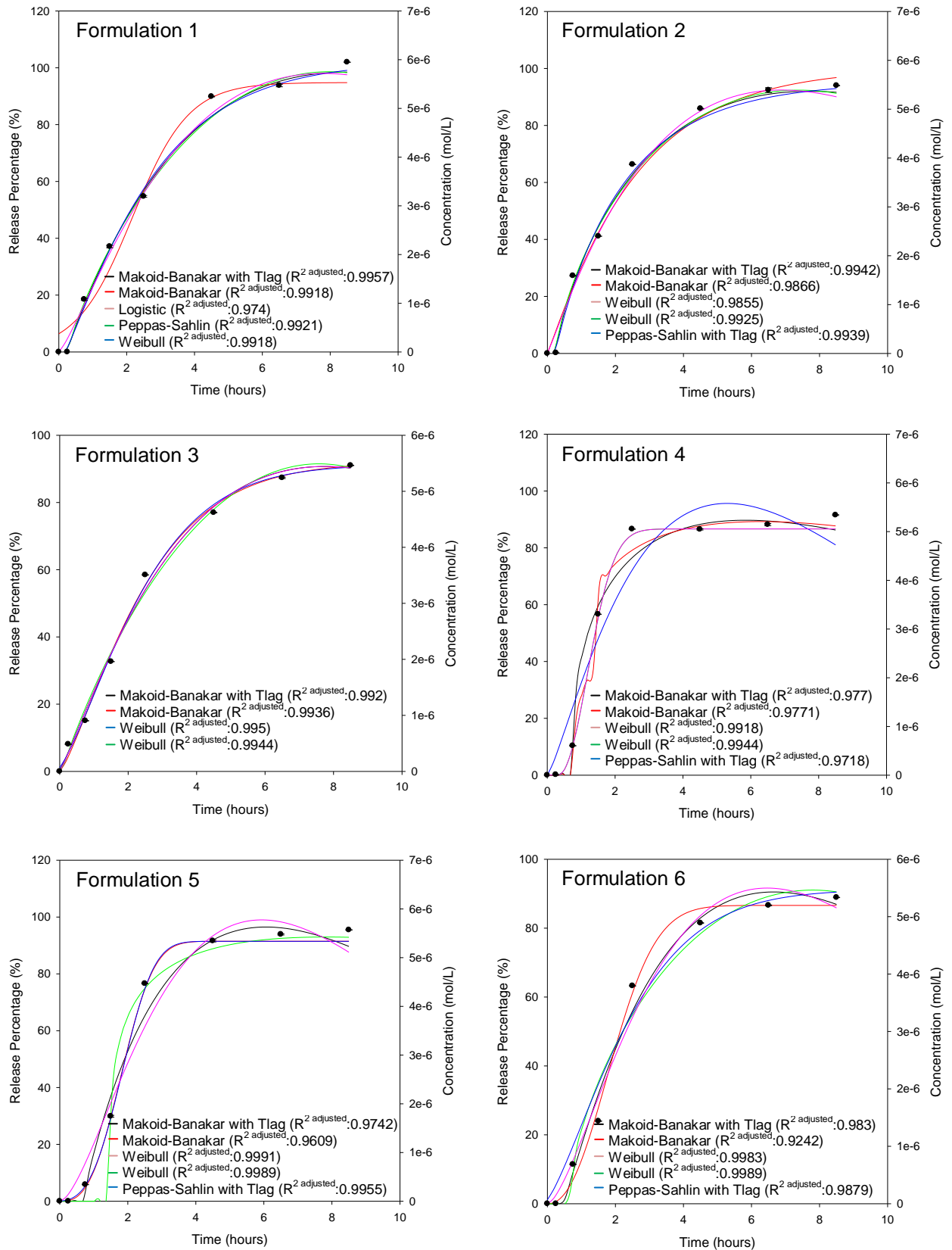
Sulfamethoxazole		
Model	Equation	R² adjusted
USP pH 1.2		
Gompertz	$y = 1.204 \times e^{(-692.461e^{(-2.488 \log(t))})}$	0.9965
USP pH 6.8		
Weibull	$y = 100 \times \left(1 - e^{\left(\frac{(-(t+281.408)^{3.605})}{51046446470.156}\right)}\right)$	0.9893
FaSSGF		
Weibull	$y = 0.872 \times \left(1 - e^{\frac{(t^{2.988})}{25321512.202}}\right)$	0.9957
FaSSIF		
Weibull	$y = 0.861 \times \left(1 - e^{\left(\frac{(-(t-29.037)^{0.964})}{100.481}\right)}\right)$	0.9961
FeSSIF V2		
Gompertz	$y = 0.54 \times e^{(-239.462e^{(-2.702 \log(t))})}$	0.9971
FaSSGFC pH 1.5		
Weibull	$y = 0.769 \times \left(1 - e^{\left(\frac{(-(t+159.589)^{2.593})}{32229639.622}\right)}\right)$	0.9881
FaSSGFC pH 6.5		
Weibull	$y = 0.644 \times \left(1 - e^{\left(\frac{(-(t-29.19)^{1.055})}{118.704}\right)}\right)$	0.9976
FaSSIFc pH 7.5		
Weibull	$y = 0.747 \times \left(1 - e^{\frac{(t^{1.229})}{382.414}}\right)$	0.9917

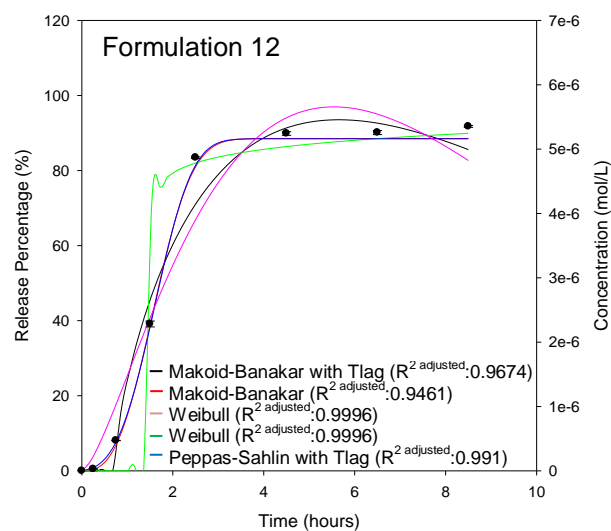
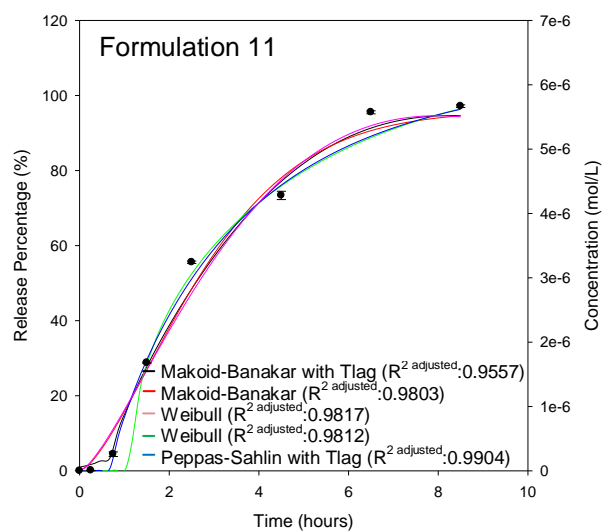
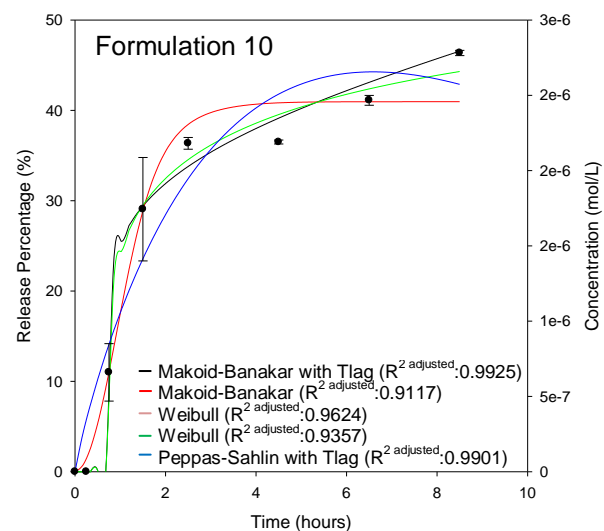
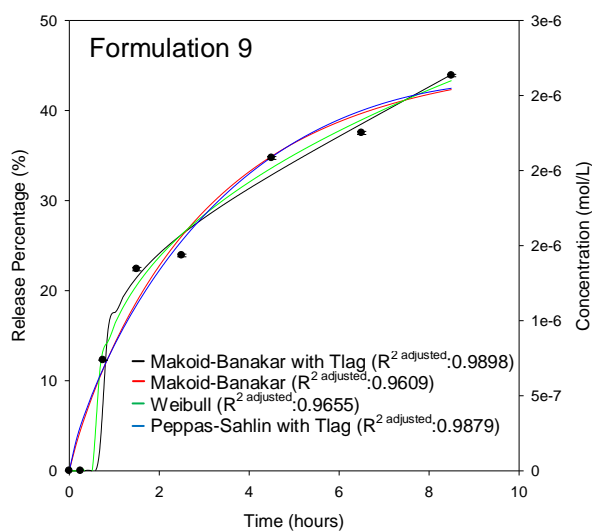
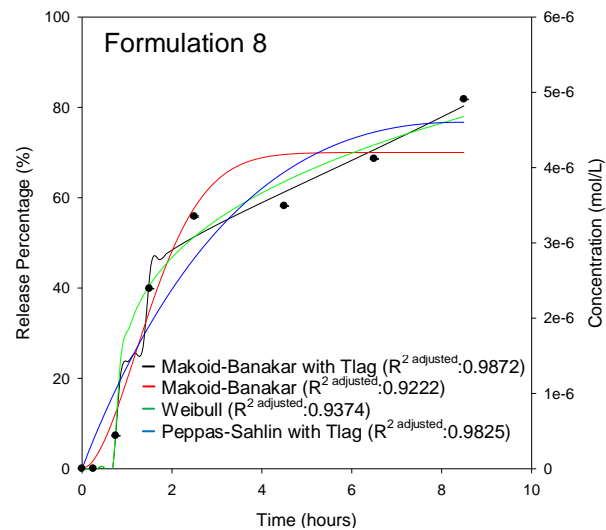
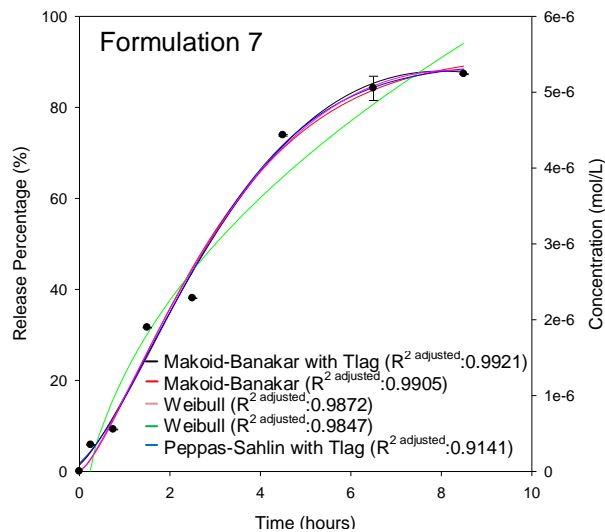
Theophylline		
Model	Equation	R ² adjusted
Isolated gastric fluids		
Peppas-Sahlin	$y = 2.157t^{0.544} - 0.022t^{1.082}$	0.9993
Isolated intestine fluids		
Logistic	$y = 61.586 \times \frac{e^{(-6.688+3.585 \log(t))}}{(1 + e^{(-6.688+3.585 \log(t))})}$	0.9954
USP pH 1.2		
Peppas-Sahlin	$y = 0.01t^{0.714}$	0.9983
USP pH 6.8		
Weibull	$y = 0.597 \left(1 - e^{\frac{(t^{0.93})}{79.549}} \right)$	0.9989
FaSSGF		
Makoid-Banakar	$y = 0.008 \times t^{0.765} \times e^{(-0.001t)}$	0.9949
FaSSIF V2		
Weibull	$y = 0.595 \left(1 - e^{\frac{(t^{1.005})}{90.367}} \right)$	0.9983
FeSSIF V2		
Weibull	$y = 0.643 \times \left(1 - e^{\frac{(t^{0.975})}{117.76}} \right)$	0.9914
FaSSGFc pH 1.5		
Makoid-Banakar	$y = 0.005t^{0.811} \times e^{(-0.001t)}$	0.9873
FaSSGFc pH 6.5		
Probit	$y = 0.766 \times \Phi(-4.971 + 2.451 \log(t))$	0.9967
FaSSIFc pH 7.5		
Peppas-Sahlin	$y = 0.019t^{0.666}$	0.9958
Zidovudine		
Model	Equation	R ² adjusted
USP pH 1.2		
Makoid-Banakar	$y = 0.001t^{1.018} \times e^{(-0.001t)}$	0.9934
USP pH 6.8		
Weibull	$y = 0.942 \left(1 - e^{\frac{(t^{1.207})}{335.13}} \right)$	0.9951
FaSSGF		
Makoid-Banakar	$y = 0.003 \times t^{0.969} \times e^{(-0.001t)}$	0.9967
FaSSIF V2		
Probit	$y = 0.794 \times \Phi(-3.867 + 2.005 \log(t))$	0.9838

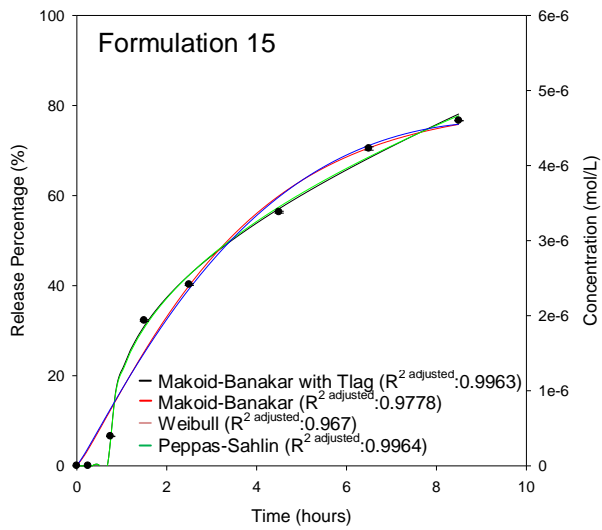
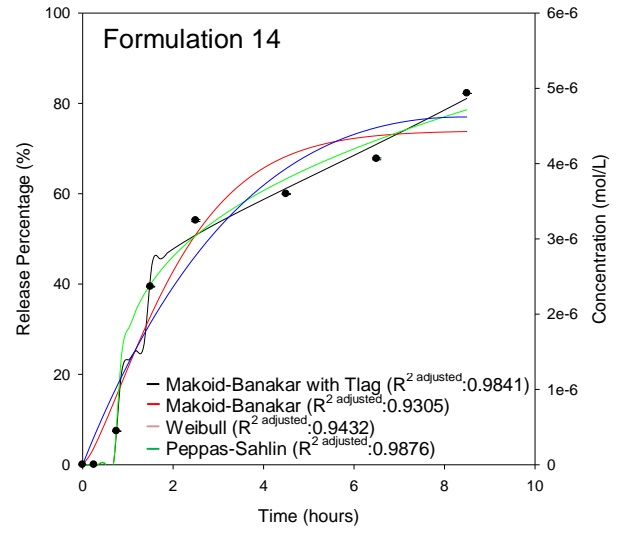
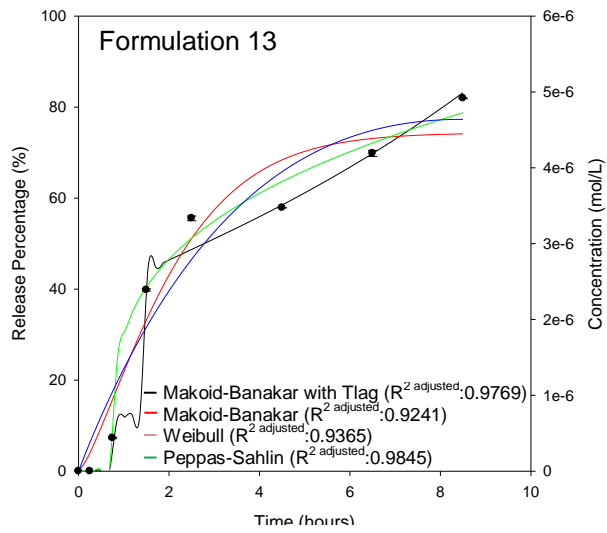
FeSSIF		
Weibull	$y = 0.823 \left(1 - e^{\frac{(t^{0.963})}{121.372}} \right)$	0.9967
FaSSGFc pH 1.5		
Peppas-Sahlin	$y = 0.007t^{0.767}$	0.9976
FaSSGFc pH 6.5		
Weibull	$y = 0.819 \left(1 - e^{\frac{(t^{1.101})}{219.641}} \right)$	0.9956
FaSSIFc pH 7.5		
Weibull	$y = 0.827 \left(1 - e^{\frac{(t^{0.868})}{71.731}} \right)$	0.996

Appendix 8

Fitted Regression Curves of Insulin Formulations Generated From Box-Benkin Design





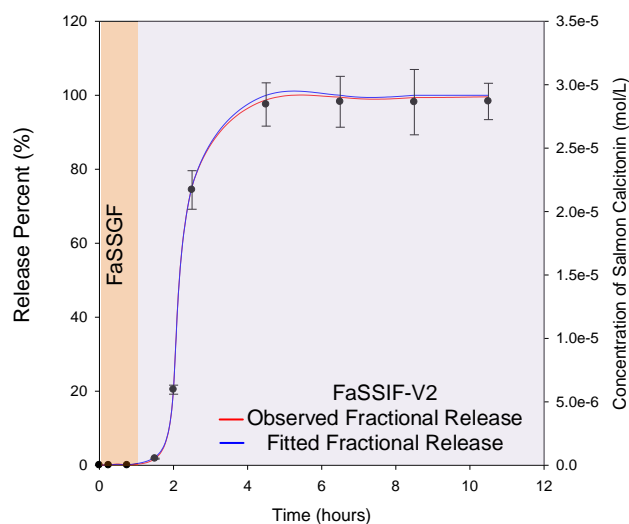


Appendix 9

In vitro-in vivo correlation of salmon calcitonin

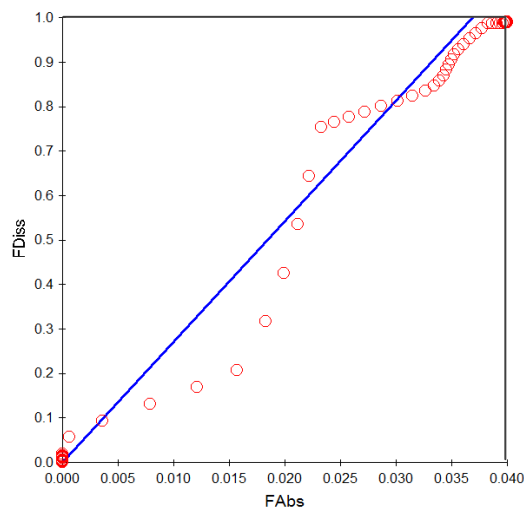
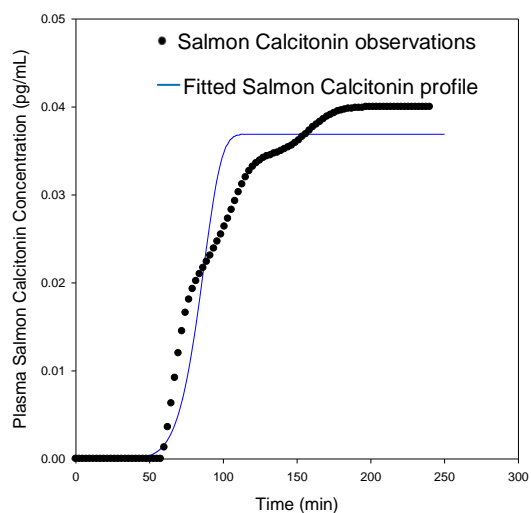
Fasted State Simulated Gastric Fluid to Fasted State Simulated Intestinal Fluid – Version 2

Dissolution fitting



MDT=2.397804 (SE: 0.004302)
 B=8.09257 (SE: 0.15108)
 Corrected Sum of Squared Observations: 2.1045
 Sum of Squared Residuals: 0.256114E-03
 S: 0.565811E-02 with 8 degrees of freedom
 Correlation (Observation, Predicted): 1.00
 AIC Criteria: -78.69889
 SBC: -78.09372
 AUC (0 to last time) by trapezoidal rule: 8.00488

Correlation

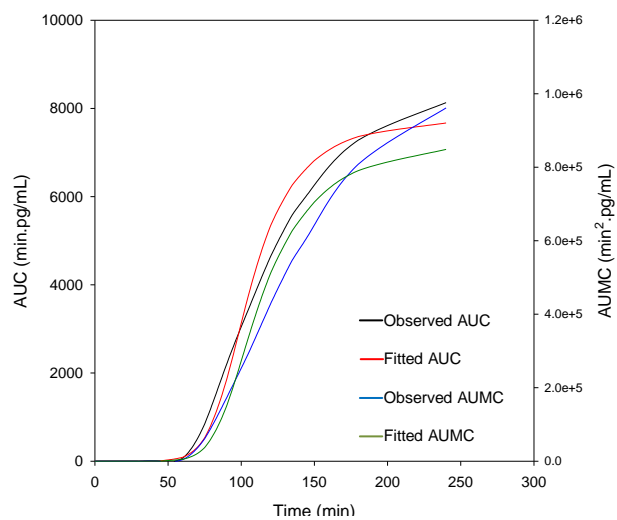
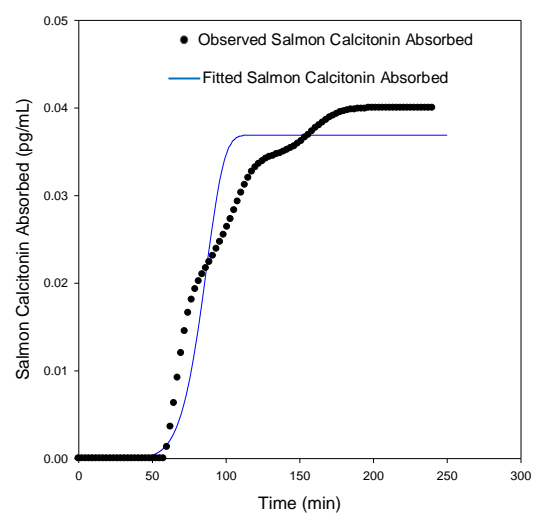
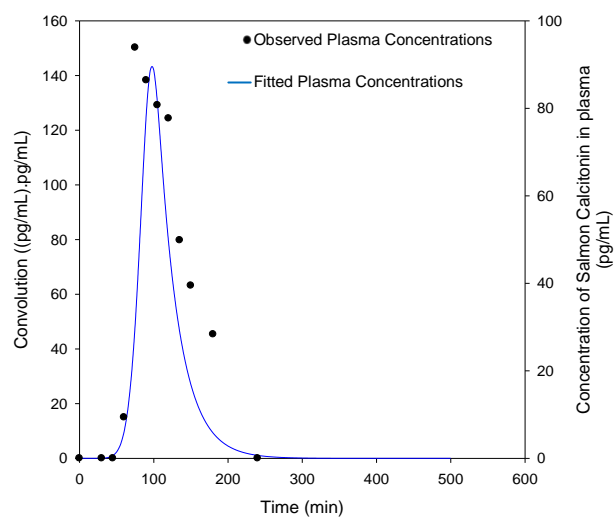


Statistical Analysis of the Predicted Dissolution Profile

Corrected Sum of Squared Observations: 0.269796E-01
 Sum of Squared Residuals: 0.125408E-02
 S=0.355914E-02 with 99 Degrees of Freedom
 Correlation (Observed, Predicted): 0.9771
 AIC criteria: -670.81692
 SBC criteria: -665.58668
 AUC (0 to last time) by trapezoidal rule: 5.87088

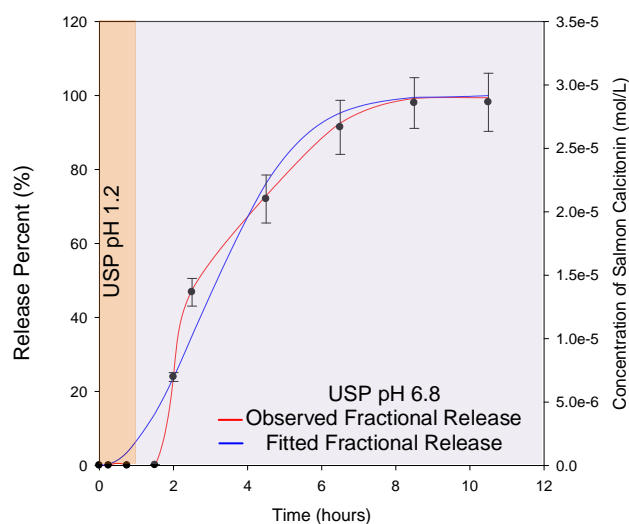
Correlation validation

Noncompartmental Analysis Derived Fasted State Simulated Intestinal Fluid Version 2			
Parameter	human model		
Units		<i>In Vivo</i>	<i>Fitted In Vivo</i>
R^2		0.9919	0.9999
R^2 adjusted		0.9838	0.9999
Correlation (X,Y)		-0.9959	-1
Number points lambda Z		3	6
Lambda Z	1/min	0.0123	0.0356
Lambda Z lower	min	135	105
Lambda Z upper	min	180	240
Half Life Lambda z	min	56.1973	19.4763
Tlag	min	45	0
Tmax	min	75	105
Cmax	pg/mL	93.8674	129.7717
Cmax D	pg/mL/mg	93.8674	129.7717
Tlast	min	180	240
Clast	pg/mL	28.3373	1.0802
AUClast	min*pg/mL	7281.047	7669.539
AUCall	min*pg/mL	8131.166	7669.539
AUCINF observed	min*pg/mL	9578.508	7699.892
AUCINF D observed	min*pg/mL/mg	9578.508	7699.892
AUC %Extrap observed	%	23.9856	0.3942
Vz F observed	mL	8664317	3649184
CL F observed	mL/min	104400.4	129872
AUCINF predicted	min*pg/mL	9556.405	7700.1
AUCINF D predicted	min*pg/mL/mg	9556.405	7700.1
AUC %Extrap predicted	%	23.8098	0.3969
Vz F predicted	mL	8483894	3649086
CL F predicted	mL/min	104641.9	129868.4
AUMClast	min*min*pg/mL	808258.7	848370.1
AUMCINF observed	min*min*pg/mL	1408070	856507.5
AUMC %Extrap observed	%	42.5981	0.9501
AUMCINF predicted	min*min*pg/mL	1402299	856563.3
AUMC %Extrap predicted	%	42.3619	0.9565
MRTlast	min	111.0086	110.6155
MRTINF observed	min	147.003	111.2363
MRTINF predicted	min	146.7392	111.2405



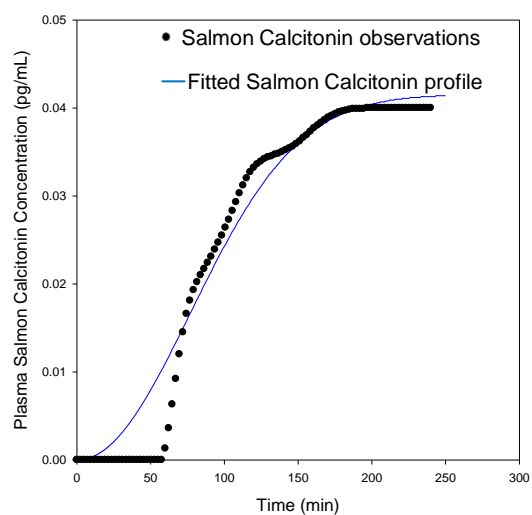
USP Simulated Gastric Fluid (pH 1.2) to USP Simulated Intestinal Fluid (pH 6.8)

Dissolution Fitting

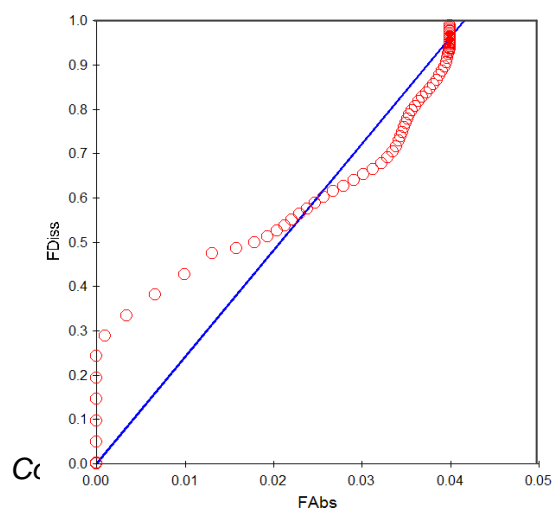


MDT=3.767223 (SE: 0.256742)
 B=2.048134 (SE: 0.303964)
 Corrected Sum of Squared Observations: 1.74497
 Sum of Squared Residuals: 0.379873E-01
 S: 0.689087E-01 with 8 degrees of freedom
 Correlation (Observed, Predicted): 0.9895
 AIC criteria: -28.70503
 SBC criteria: -28.09986
 AUC (0 to last time) by trapezoidal rule: 7.00278

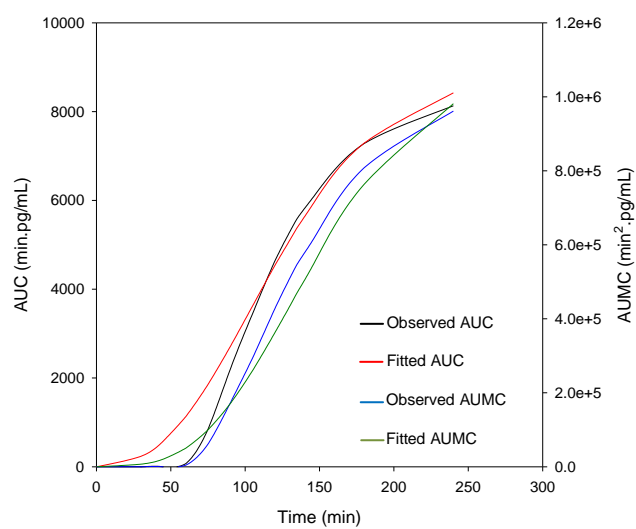
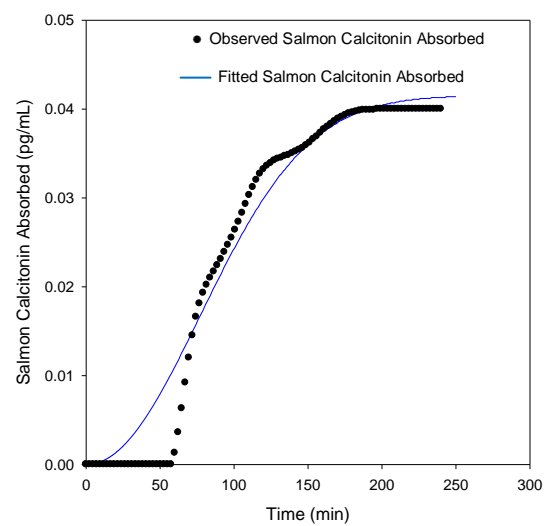
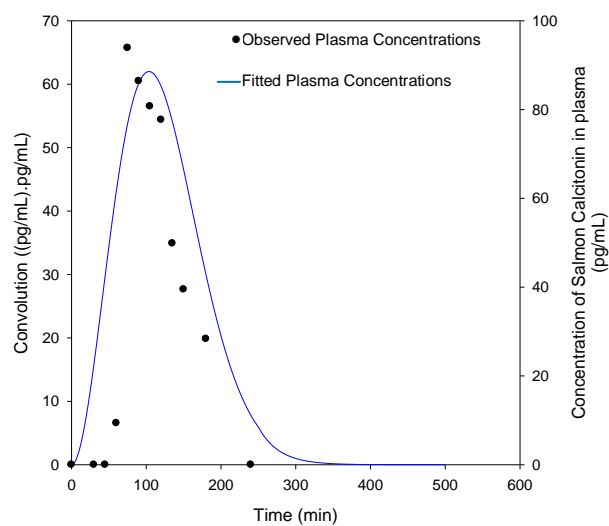
Correlation



Corrected Sum of Squared Observations: 0.269844E-01
 Sum of Squared Residuals: 0.973580E-03
 S=0.313594E-02 with 99 Degrees of Freedom
 Correlation (Observed, Predicted): 0.9861
 AIC criteria: -696.38757
 SBC criteria: -691.15732
 AUC (0 to last time) computed by trapezoidal rule: 5.78141

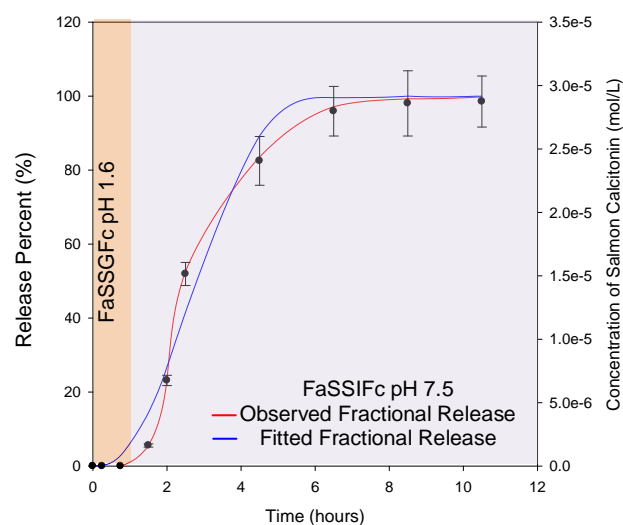


Noncompartmental Analysis of USP Simulated Gastric Fluid to USP Simulated Intestinal Fluid pH 6.8			
Parameter	Units	<i>In Vivo</i>	<i>Fitted In Vivo</i>
R ²		0.9919	0.9912
R ² adjusted		0.9838	0.9823
Correlation (X,Y)		-0.9959	-0.9956
Number points lambda Z		3	3
Lambda Z	1/min	0.0123	0.0202
Lambda Z lower	min	135	150
Lambda Z upper	min	180	240
Half Life Lambda z	min	56.1973	34.2679
Tlag	min	45	0
Tmax	min	75	105
Cmax	pg/mL	93.8674	61.9825
Cmax D	pg/mL/mg	93.8674	61.9825
Tlast	min	180	240
Clast	pg/mL	28.3373	7.7879
AUClast	min*pg/mL	7281.047	8421.629
AUCall	min*pg/mL	8131.166	8421.629
AUCINF observed	min*pg/mL	9578.508	8806.647
AUCINF D observed	min*pg/mL/mg	9578.508	8806.647
AUC %Extrap observed	%	23.9856	4.3719
Vz F observed	mL	8464317	8664317
CL F observed	mL/min	104400.4	113550.6
AUCINF predicted	min*pg/mL	9556.405	8819.605
AUCINF D predicted	min*pg/mL/mg	9556.405	8819.605
AUC %Extrap predicted	%	23.8098	4.5124
Vz F predicted	mL	8483894	5605479
CL F predicted	mL/min	104641.9	113383.8
AUMClast	min*min*pg/mL	808258.7	981275.3
AUMCINF observed	min*min*pg/mL	1408070	1092714
AUMC %Extrap observed	%	42.5981	10.1984
AUMCINF predicted	min*min*pg/mL	1402299	1096465
AUMC %Extrap predicted	%	42.3619	10.5055
MRTlast	min	111.0086	116.5185
MRTINF observed	min	147.003	124.0783
MRTINF predicted	min	146.7392	124.3213



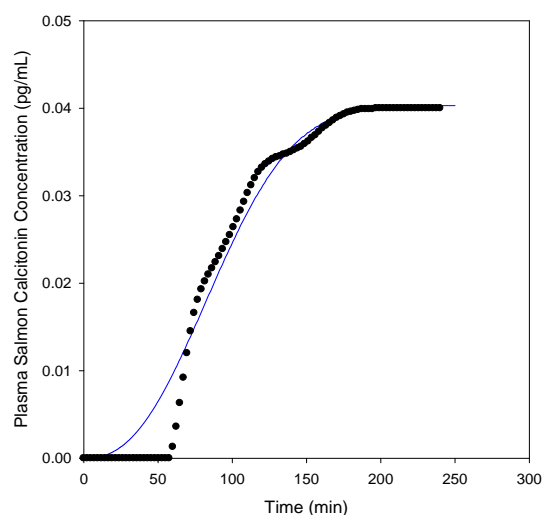
Fasted State Simulated Gastric Fluid Canine Model (pH 1.6) to Fasted State Simulated Intestinal Fluid Canine Model (pH 7.5)

Dissolution Fitting



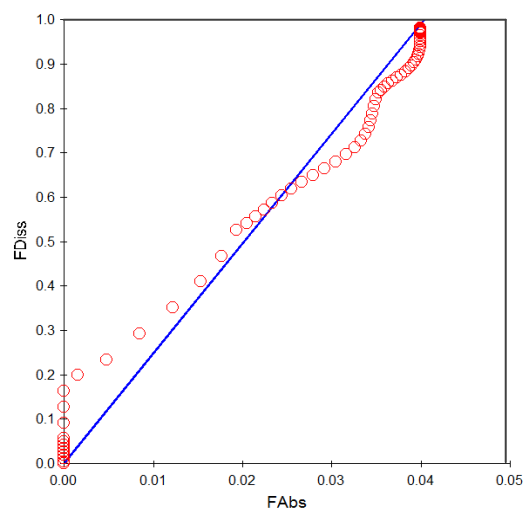
MDT: 3.230728 (SE: 0.183034)
 B: 2.423116 (SE: 0.339031)
 Corrected Sum of Squared Observations: 1.82847
 Sum of Squared Residuals: 0.257965E-01
 S: 0.567852E-01 with 8 Degrees of Freedom
 Correlation (observed, Predicted): 0.9934
 AIC criteria: -32.57516
 SBC criteria: -31.96999
 AUC (0 to last time) by trapezoidal rule: 7.40712

Correlation



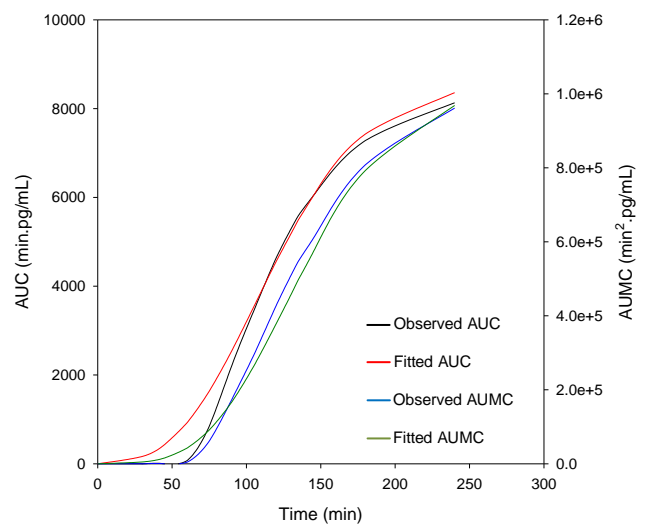
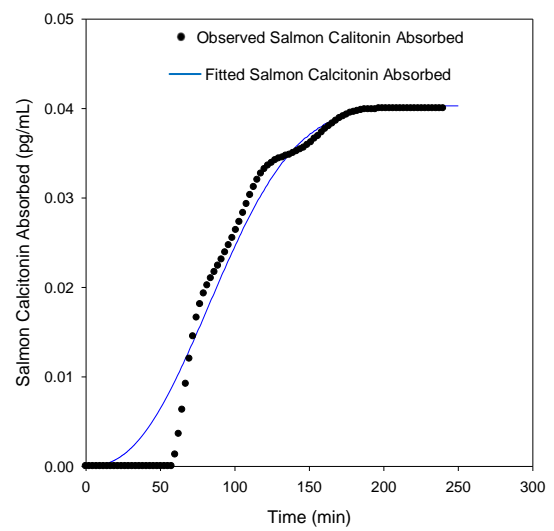
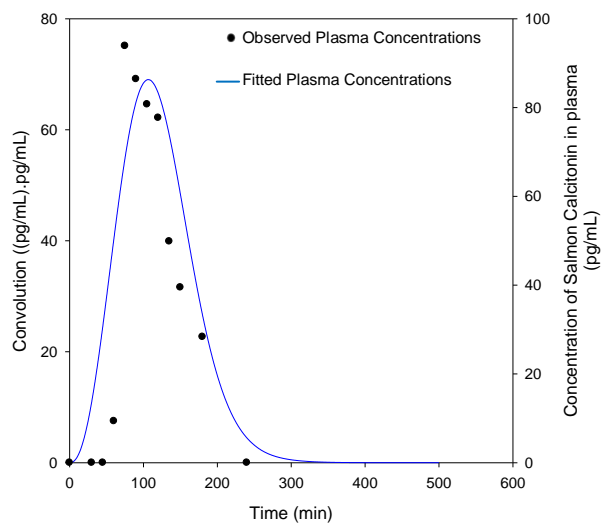
Statistical Analysis of the Predicted Dissolution Profile

Corrected Sum Squared Observations: 0.269851E-01
 Sum of Squared Residuals: 0.638932E-03
 S: 0.254045E-02 with 99 Degrees of Freedom
 Correlation (Observed, Predicted): 0.9906
 AIC criteria: -738.92689
 SBC criteria: -733.69665
 AUC (0 to last time) by trapezoidal rule: 5.87147



Correlation validation

Noncompartmental Analysis of Fasted State Gastric Fluid to Fasted State Simulated Intestinal Fluid Canine Model			
Parameter	Units	<i>In Vivo</i>	<i>Fitted In Vivo</i>
R^2		0.9919	0.9921
R^2 adjusted		0.9838	0.9842
Correlation (X,Y)		-0.9959	-0.9961
Number points lambda Z		3	3
Lambda Z	1/min	0.0123	0.0269
Lambda Z lower	Min	135	150
Lambda Z upper	Min	180	240
Half Life Lambda z	Min	56.1973	25.7408
Tlag	Min	45	0
Tmax	Min	75	105
Cmax	pg/mL	93.8674	69.0159
Cmax D	pg/mL/mg	93.8674	69.0159
Tlast	Min	180	240
Clast	pg/mL	28.3373	4.4692
AUClast	min*pg/mL	7281.047	8359.044
AUCall	min*pg/mL	8131.166	8359.044
AUCINF observed	min*pg/mL	9578.508	8525.014
AUCINF D observed	min*pg/mL/mg	9578.508	8525.014
AUC %Extrap observed	%	23.9856	1.9469
Vz F observed	mL	8664317	4356143
CL F observed	mL/min	104400.4	117301.9
AUCINF predicted	min*pg/mL	9556.405	8532.059
AUCINF D predicted	min*pg/mL/mg	9556.405	8532.059
AUC %Extrap predicted	%	23.8098	2.0278
Vz F predicted	mL	8483894	4352546
CL F predicted	mL/min	104641.9	117205
AUMclast	min*min*pg/mL	808258.7	968563.9
AUMCINF observed	min*min*pg/mL	1408070	1014560
AUMC %Extrap observed	%	42.5981	4.5336
AUMCINF predicted	min*min*pg/mL	1402299	1016513
AUMC %Extrap predicted	%	42.3619	4.717
MRTlast	Min	111.0086	115.8702
MRTINF observed	Min	147.003	119.0098
MRTINF predicted	Min	146.7392	119.1404



Appendix 10

Front Pages of Publications

Int J Pept Res Ther (2012) 18:259–280
DOI 10.1007/s10989-012-9299-7

Orally Administered Therapeutic Peptide Delivery: Enhanced Absorption Through the Small Intestine Using Permeation Enhancers

Vinay Pillay · Angus R. Hibbins ·
Yahya E. Choonara · Lisa C. du Toit ·
Pradeep Kumar · Valence M. K. Ndesendo

Accepted: 2 April 2012 / Published online: 22 April 2012
© Springer Science+Business Media, LLC 2012

Abstract Peptide therapeutics (PTs) is generally regarded as highly effective macromolecule therapeutics at very low concentrations. The main issues surrounding the administration of PTs is guaranteeing that they are bioavailable, reach the desired therapeutic index and distribute throughout the body effectively. The oral administration, a non-invasive route, of PTs is considered a major complication due to inadequate oral absorption through biological membranes such as the small intestine epithelium due to presystemic proteolytic enzymatic activity. PTs bioavailability is further diminished in the systemic circulation due to low stability in the plasma and rapid excretion from the body. Many alternative routes can be considered non-invasive such as transdermal and nasal routes, but this review focuses on the oral route, specifically the small intestine region of the gastrointestinal tract. Although this region has the highest density of proteolytic enzymes, it contains tight junctions which have the lowest trans-epithelial electrical resistance throughout the body; thus paracellular transport of these large PTs can be achieved more readily. The use of a natural polysaccharide polymer, such as trimethyl chitosan (TMC), which enhances the bioavailability of these PTs through the small intestine, will also be discussed in great detail. TMC has been considered because it could potentially solve many of the

mechanistic and chemical problems associated with oral therapeutic peptide administration. The safety of orally administered PTs through the small intestinal epithelium employing a polymer such as TMC is also discussed as this is a significant issue for regulatory bodies.

Keywords Peptide therapeutics · Occludin peptides · Chitosan · Permeation enhancers · Tight junctions · Oral administration

Introduction

Peptide therapeutics (PTs) are relatively small molecules (50 or less amino acids or a maximum molecular weight of 5,000 Da) which may contain a specific sequence of amino acids joined together by peptide bonds resulting in a highly specific secondary structure but absent of tertiary structure that induces a rapid and highly specific beneficial response (Johnson 2005; Sato et al. 2006; Giuliani et al. 2007; Oyston et al. 2009; Tshala-Katumbay 2010). An example of a PT that has demonstrated a significant and unique advantage over traditional small molecule therapeutics is Teriparatide®, also known as recombinant human parathyroid hormone (Quattrocchi and Kourlas 2004). Teriparatide® is a synthetic polypeptide fragment of the parathyroid hormone. Teriparatide® contains amino acids 1–34 of the 84 amino acid sequence that makes up the parathyroid hormone and is the only therapeutics currently approved by the FDA to increase bone formation, as oppose to simply maintaining bone density (Simonelli 2002; Campion and Maricic 2003). This is a significant advantage to patients which suffer from osteoporosis as many patients have lost bone density before diagnosis has been obtained and the specific beneficial response of this

V. Pillay (✉) · A. R. Hibbins · Y. E. Choonara ·
L. C. du Toit · P. Kumar
Department of Pharmacy and Pharmacology, Faculty of Health
Sciences, University of the Witwatersrand, 7 York Road,
Parktown, Johannesburg 2193, South Africa
e-mail: vinay.pillay@wits.ac.za

V. M. K. Ndesendo
School of Pharmacy and Pharmaceutical Sciences,
St. John's University of Tanzania, Dodoma, Tanzania

Research Article

Physicomechanical Characterization and Optimization of EDTA-mPEG and Avicel®-EDTA-mPEG *In Situ* Melt Dispersion Mini-Pellets

Angus R. Hibbins,¹ Yahya E. Choonara,¹ Pradeep Kumar,¹ Lisa C. du Toit,¹ and Viness Pillay^{1,2}

Received 1 February 2013; accepted 8 May 2013; published online 4 June 2013

Abstract. The purpose of this study was to develop a physicomechanically customizable oral metal chelatory *in situ* hot melt dispersion mini-pellet entity which could be utilized within a binary drug delivery system. Avicel® RC/CL type R-591 was included within the *in situ* hot melt dispersion mini-pellet formulations to determine the physicomechanical effect this compound would have on the mini-pellet formulations. The physicomechanical properties of the hot melt *in situ* mini-pellet formulations were mathematically fitted to regression curves. Physicomechanical adjustment of the *in situ* hot melt dispersion mini-pellet formulations could be mathematically predicted with the derived regression curve equations. The addition of Avicel® RC/CL type R-591 increased the physicomechanical properties such as matrix hardness and increased total disintegration of the *in situ* hot melt dispersion mini-pellet formulations. The utilization of a physicomechanically customizable oral metal chelatory *in situ* hot melt dispersion mini-pellet entity within a binary drug delivery system would to achieve a synergistically enhance the activity of a drug-carrying entity or a permeation enhancing entity within a single drug delivery unit. The experimental results indicated that weights of the pellets that achieved optimal hardness ranged between 35 and 45 mg. The melt-dispersion formulations disintegrated within shorter time periods and maintained higher ethylenediaminetetraacetic acid (EDTA) concentrations whereas melt-dispersion formulations which included Avicel® had superior physicomechanical properties. Disintegration times ranged between 1,000 s for melt-dispersions containing EDTA and methoxy polyethylene glycol 2000 (mPEG) only, to >6,000 s for melt-dispersions comprising EDTA, mPEG, and Avicel®.

KEY WORDS: chelation therapy; disintegration studies; mini-pellets; oral drug delivery; polymer melts; solid dosage forms; textual analysis.

INTRODUCTION

A binary drug delivery system is a single dosage form that contains two distinct entities and is administered as a single unit. Each distinct entity performs a unique function that will synergistically enhance the *in vivo* bioavailability of a therapeutic compound. Each entity within the drug delivery system has to be optimized in order to obtain a maximal synergistic effect. The development of an oral binary drug delivery system for drug compounds that will allow patients to avoid the parenteral route of administration will result in increased patient compliance (1–4). An example of this is the inclusion of a metal chelator containing entity and a permeation enhancer entity within a single dosage form for the oral delivery of peptide therapeutics. The metal chelator entity would exist

to facilitate the accelerated liberation of the metal chelator from the dosage form, before the release of the peptide therapeutic within a localized small intestine lumen environment. This study evaluates the physicomechanical properties of the *in situ* melt dispersion of ethylenediaminetetraacetic acid (EDTA) and the effect of including Avicel® RC/CL type R-591 (Avicel®) has on these *in situ* melt dispersions to facilitate the development of a predictably customizable metal chelatory containing entity.

Hot melt dispersion is a process whereby a drug entity is homogeneously incorporated within a polymeric matrix without the use of solvents. This methodology requires two elements, a polymeric material that can undergo stable melting and a drug entity that is thermostable at the melting point of the polymeric material. A hot melt dispersion procedure has advantages which pertain specifically within an industrial setting. These advantages primarily rest in that a hot melt dispersion is a single-step process (polymeric material is melted at required temperature and drug mass is added to the molten polymeric material under constant aggregation) and no solvents are required which is an economical and environmental advantage (5).

A metal chelator such as EDTA has been utilized for oral delivery of peptide therapeutics because it has been indicated that EDTA decreases the localized ionic concentration load

Electronic supplementary material The online version of this article (doi:10.1208/s12249-013-9979-4) contains supplementary material, which is available to authorized users.

¹ Faculty of Health Sciences, Department of Pharmacy and Pharmacology, University of the Witwatersrand, 7 York Road, Parktown, 2193, Johannesburg, South Africa.

² To whom correspondence should be addressed. (e-mail: Viness.Pillay@wits.ac.za)